DEVELOPMENT OF BIOFABRICATION TECHNIQUES TO ENGINEER 3D *IN VITRO* AVATARS OF TISSUES

DEVELOPMENT OF BIOFABRICATION TECHNIQUES TO ENGINEER 3D *IN VITRO* AVATARS OF TISSUES

By ALIREZA SHAHIN-SHAMSABADI, M.Sc.

A Thesis Submitted to the School of Graduate Studies

in Partial Fulfilment of the Requirements for the Degree of

Doctor of Philosophy in Biomedical Engineering

DOCTOR OF PHILOSOPHY (2020)

Graduate Program in

McMaster University, Hamilton, Ontario, Canada

TITLE: Development of Biofabrication Techniques to Engineer 3D *in vitro* Avatars of Tissues

AUTHOR: Alireza Shahin-Shamsabadi

M.Sc. (Amirkabir University of Technology, Tehran Polytechnique)

SUPERVISOR: Dr. P. Ravi Selvaganapathy

PAGES: xxi, 274

LAY ABSTRACT

Experimentation on humans is unethical, therefore in order to understand how human body works and test new therapeutic drugs researchers have used animals and cells isolated from animals or humans. Animals are inherently different from humans and isolated cells are culture in conditions different than human body, therefore a huge gap exists between the knowledge derived from these models and what happens in human body. Since there is no one-size-fits-all technique to model all of the human tissues, the objective of current study was set to build a *toolbox of techniques* that each could create better environment in the lab for cells isolated from different tissues and organs with more similarity to original tissues, to bridge the gap and eliminate the need to use animal models entirely. During the course of this PhD studies, three different techniques that can be used to make such models for different tissues and organs, as well as different diseases, were developed and characterized. These techniques were also used to shed light on some of the cellular behavior that are already observed in human body but either are not explained or aren't re-created in the lab for mechanistic studies. Certain questions regarding selected tissues were chosen and the technique most compatible with that tissue was used for the modeling purposes. For example, one investigated niche was the origin of the bone sensory cells which could be important to heal damaged bones or prevent osteoporosis. The first technique was deemed most suitable for this question while for the next question, how the fat and muscle cells are affecting each other that can be useful to better understand conditions such as diabetes and obesity, the second technique was the best option. Overall, a variety of tools were developed that can be used by biologists to create better models of

human tissues in the lab as platforms to study human physiology and as media for developing treatments for different diseases.

ABSTRACT

Two-dimensional (2D) *in vitro* models of tissues and organs have long been used as one of the main tools to understand human physiology and for applications such as drug discovery. But there is a huge disparity between *in vivo* conditions and these models which has created the need for better models. It has been shown that making three-dimensional models with dynamic environments that provide proper physical and chemical cues for cells, can bridge this gap between 2D models and *in vivo* conditions but the toolbox for creating such models has been imperfect and rudimentary. Introduction of tissue engineering concept and advent of biofabrication tools to meet its demands has provided new possible avenues for *in vitro* modeling but many of these tools are specifically designed to create tissue and organ replacements and lack features such as the ability to investigate cellular behavior with ease that are necessary for *in vitro* modeling purposes. The objective of this doctoral thesis was to introduce a novel toolbox of biofabrication techniques, based on bioprinting and bioassembly, that together are capable of recapitulating anatomical and physiological requirements of different tissue in *in vitro* setups in a more relevant way while creating the possibility of investigating cellular behavior. A bioprinting technique was developed that allowed formation of large constructs with proper mechanical stability, perfusion, and direct access to cells in different locations. The second technique was based on bioassembly of collagenous grafts in micro-molds and cells from different tissues with the ability to control cell positioning and create tissue-relevant cell densities with higher degree of similarity to human tissues compared to previous techniques. The third technique was based on bioassembled stand alone and dense cell-sheets for cells capable of fusion. These

techniques were subsequently used for modeling a few chosen biological phenomenon to showcase the advantages of the techniques over previously developed ones and to further shed light on possible shortcomings of each of the techniques in their application for those specific tissues. In conclusion, our techniques may serve as valuable and easy to use tools for researchers, specifically biologists to investigate different aspects of human biology and disease mechanism in more details.

ACKNOWLEDGEMENT

To my supervisor, Dr. Ravi Selvaganapathy; thank you for your mentorship, for the freedom you provided me to follow my ideas, collaborate with the groups that my interests were aligned with, attend conferences, and spend time abroad as a visiting scholar. These activities helped shape my personality as a researcher. I am grateful for your willingness to listen to all of my concerns and opinions, although I know it might have been difficult and overwhelming for you. Thank you for your caring and understanding. I wish you the best as you dive into new research territories.

To my committee, Dr. Kim Jones and Dr. Raja Ghosh; thank you for taking the time to provide me with advice and guidance on my research. Your input has made a huge impact on how I think about different aspects of my research.

To my family, thank you for your unwavering love and support throughout my life. You sacrificed your lives so that I could grow up to live and to pursue what I desired.

To my friends and collaborators, Bryan, Rana, Crystal, Michael, and Priyanka, thank you for your wisdom, patience, and more importantly your friendship. You made this journey more enjoyable and fruitful. I have no doubt that our friendship will last forever and you will continue to change my life for the better.

TABLE OF CONTENTS

LIST OF FIGURES AND TABLES

LIST OF ALL ABBREVIATIONS AND SYMBOLS

2D - Two dimensional

3D - Three dimensional

3T3 - 3 day transfer, inoculum 3×10^5 cells (mouse embryonic fibroblasts)

ABA - Alamar blue assay

ANOVA - Analysis of variance

ATCC - American Type Culture Collection

BCA - Bicinchoninic acid

Ca - Calcium

CHO - Chinese Hamster ovary

CMR - Collagen to medium ratio

DAPI - 4’,6-Diamidino-2-Phenylindole

DI - Deionized

DM - Differentiation medium

DMEM - Dulbecco's Modified Eagle Medium

DMSO - Dimethyl sulfoxide

EBM-2 - Endothelial basal medium 2

ECM - Extracellular matrices

EDS - Energy-dispersive x-ray spectroscopy

Em - Emission

Ex - Excitation

ExCeL - Combining extrusion printing on cellulose scaffolds with lamination to create in vitro biological models

FBS - Fetal bovine serum

FITC - Fluorescein isothiocyanate

GFP - Green fluorescent protein

GM - Growth medium

HUVEC - Human umbilical vein endothelial cell

ID - Inner diameter

LAT-A - Latrunculin A

LDA - Live/dead assay

LDH - Lactate dehydrogenase

MCF-7 - Michigan Cancer Foundation-7, a breast cancer cell line

MTT - 3-(4,5- dimethylthiazole-yl)-,5-diphenyltetrazolium bromide

NaOH - Sodium hydroxide

PBS- Phosphate buffered saline

PDGF - Platelet-derived growth factor

PDMS - Poly dimethyl siloxane

PIPAAm - N-isopropylacrylamide

PVC - Polyvinyl chloride

qRT-PCR - quantitative reverse transcription polymerase chain reaction

RFP - Red fluorescent protein

RGD - Arginylglycylaspartic acid

Saos-2 - Sarcoma osteogenic

SD - Standard Deviation

SLA - Stereolithography

TGF-β - Transforming growth factor-β

UV - Ultraviolet

VEGF - Vascular endothelial growth factor

π-SACS - pH Induced Self-Assembled Cell Sheets Without the Need for Modified Surfaces

DECLARATION OF ACADEMIC ACHIEVEMENT

Alireza Shahin-Shamsabadi contributed to the writing, experimental design, conducting of experiments, literature research, data analysis, interpretation of results, and figure generation for all chapters of this thesis.

Ponnambalam R. Selvaganapathy contributed to experimental design, interpretation of results, and revision of the manuscripts for all chapters of this thesis.

Kathrine Grandfield contributed to experimental design, interpretation of results, and revision of the manuscript for chapter 3.

Sandeep Raha contributed to interpretation of results for Part 2 of chapter 3.

Alireza Shahin-Shamsabadi and Bryan E.J. Lee equally contributed to the writing, experimental design, conducting of experiments, literature research, data analysis, interpretation of results, and figure generation for Chapter 3.

Michael K. Wong contributed in experiments and data analysis of Chapter 3.

Chapter 1: INTRODUCTION

Chapter Preface

Monolayer cell culture on plastic or glass surfaces as well as animal models have long been traditional tools used to understand human physiology and pathology, as well as to test safety and efficiency of drug candidates. Although most of our knowledge has come from experiments involving one or both of these tools, the need for more sophisticated models with better resemblance to human body has become more evident as these models are not accurate. 2D *in vitro* models provide cells with microenvironments that are entirely different than *in vivo* conditions while animals have inherently different physiologies and their high cost and ethical concerns make them less attractive. Research has been going on for a long time to recreate tissues and organs *in vitro* as models that can be manipulated and studied in the lab. It is now evident that for these models to be accurate representatives of their *in vivo* counterparts, only certain aspects of their native state needs to be recreated rather than their whole complex structure which not only is impossible considering current state of our technology, but also makes it impractical to interpret their behavior.

The features that need to be recreated for a model to be faithful to its *in vivo* condition and suitable for applications such as drug testing, are three-dimensional structure of the tissue, proper cell density and tissue interfaces that promote the cross-talk between different cell types, as well as appropriate dynamic features including mechanical and electrical activities. Although our understanding of importance of such factors is improving at a rapid pace, the toolbox available to properly implement them in the models is lagging behind. It is becoming more evident that there is no single tool that can be used for all tissues and conditions and new techniques inspired by the characteristics of different tissues need to be developed. Among all the different techniques that are capable of implementing one or a few of these features, biofabrication-based techniques,

originally devised for tissue engineering applications to aid the *in vivo* regeneration of damaged tissues and organs, are most promising. However, there is still room for improvement and a toolbox of techniques capable of forming tissue avatars in a simple and fast manner, with precise control over cell positioning and tissue interface creation, structural stability and proper mass transfer to support cell viability, and the ability to implement necessary dynamic factors at the same time, is needed. Such techniques need to have high degree of repeatability and be suitable for high throughput applications.

Here in this chapter current state of the different *in vitro* modeling techniques is discussed. Then different biofabrication-based models with their strengths and shortcomings are reviewed to shed light on the status quo of the field that helps to understand the requirements of next generation techniques. Ultimately in the chapters that follow, a variety of novel biofabrication-based techniques, both bioprinting and bioassembly, are devised solely for *in vitro* modeling purposes to meet the requirements of different tissues based on the structural and functional requirements of those target tissues.

1. *in vitro* modeling

Many of the investigations regarding human health research and drug discovery and development cannot use humans as subjects due to ethical issues. Currently animal models and 2D *in vitro* models are being used for this purpose but it has become evident that better models are needed as many of the drugs are facing post-approval withdrawal. On the other hand, many acute injuries in organs such as kidney, heart, or liver are considered drug-induced that are not predicted by current models. Such models cannot predict personalized sensitivities and effect of drugs on prenatal

conditions are not understood either [1]. Chances for success of a drug that has entered phase I trials and moving it to bedside is less than 8% [2].

2D culture models, made preferably using human-derived cells, are often preferred to animal studies. Besides from the fact that these 2D cell culture studies are less cost-intensive, they have more reproducibility, and are fast and versatile [3]. There are also several other driving factors to create models based on human cells as animal models can only predict some of the important facets of human physiology and pathophysiology and have different genomics and proteomics. For example, pathogens are often species-specific and liver toxicity of some drugs cannot be properly predicted in animal models. Humanizing animals is also difficult and expensive and observations regarding the fundamental differences between transgenic rodents and humans such as telomerase regulation has raised questions regarding validity of these models. Human and rodent cytokines are also incompatible and in some cases have different roles therefore animal models cannot be used for modeling behaviors involving such factors [4-6].

Although 2D cell cultures are considered the gold standard of *in vitro* modeling, culturing mammalian cells in three-dimensional (3D) has a long history as well. Initial investigations for *in vitro* cell cultures were made using 3D systems rather than 2D ones [7]. Such studies were reported as early as 1912 where 3D *in vitro* cell culture of chick embryo was performed for cells derived from explants [8] but a major milestone study was performed in 1952 where 3D cellular aggregates of disrupted cells of explanted tissues were developed *in vitro* in a repeatable manner [9]. These 3D models have shown critical differences with 2D ones, for instance only 3D systems show drug responses and gene/protein expressions that are comparable to *in vivo* systems [10]. This is because 3D systems better recreate tissue topography and cell-cell interactions [11].

In addition to the features that are replicated in 3D models such as cell-cell and cell-ECM interactions and paracrine activities, addition of biophysical signals such as mechanical or electrical stimulation plays an important role in recreating the *in vivo*-like microenvironments that determine the cellular behavior and function, both for 2D and 3D systems [12, 13]. Including relevant stimuli in these models, specifically in 3D systems, plays an important role in recreating the physiologically- and anatomically-relevant models that can potentially replace animal models and all of the *in vitro* models.

1.1. Importance of third dimension in *in vitro* modeling

A large portion of our understanding of biological processes has been made possible by using reductionist 2D culture systems where a monolayers of homogenous cell population grown on a plastic or glass surfaces are investigated but a huge disparity is observed between these models and human body since an over simplification has been made in their creation compared to *in vivo* conditions where information rich and complex 3D environment of the human body that has multiple ECM components, cell cross-talks and tissue interfaces, and secreted-factors, are taken away [14]. One of the undesired features of 2D cell culture systems is their forced apical-basal polarity which is only applicable to limited cell types including epithelial cells while most cells assume stellate morphology *in vivo* [14]. This changes the surface to volume ratio of cells (membrane to cytoplasm ratio) and intracellular signal propagation [15] or even cells' sensitivity to apoptosis [16]. Adopting and changing the cells' morphology in their native 3D environment takes longer times compared to 2D as they have to adopt themselves to the complex and dynamic structure of their ECM [14, 17].

Different cell types change their morphology and behavior once isolated from their natural niche and cultured on 2D surfaces by becoming more stretched, showing uncontrolled proliferation and

losing their differentiated states, but some of them can regain their natural state once embedded in proper 3D environments [14] for example in case of chondrocytes [18]. Many cell types show reduced and more controlled proliferation in 3D compared to 2D [19]. Aside from these, certain behavior of cells are intrinsic to 3D environments such as higher cell order, blood vessels and their sprouting in angiogenesis, and cancer cell migration (Figure 1) [14]. ECM and its physical properties also affect cellular response to a drug in a tissue specific way by promoting drug resistance or enhancing drug efficacy, as well as changing the mechanism of action of the drug [3, 20]. Such observations have led to development of 3D *in vitro* models that are better representatives of *in vivo* conditions. Some of the differences between 2D and 3D cell culture environments are shown in Figure 2 and summarized in Table 1.

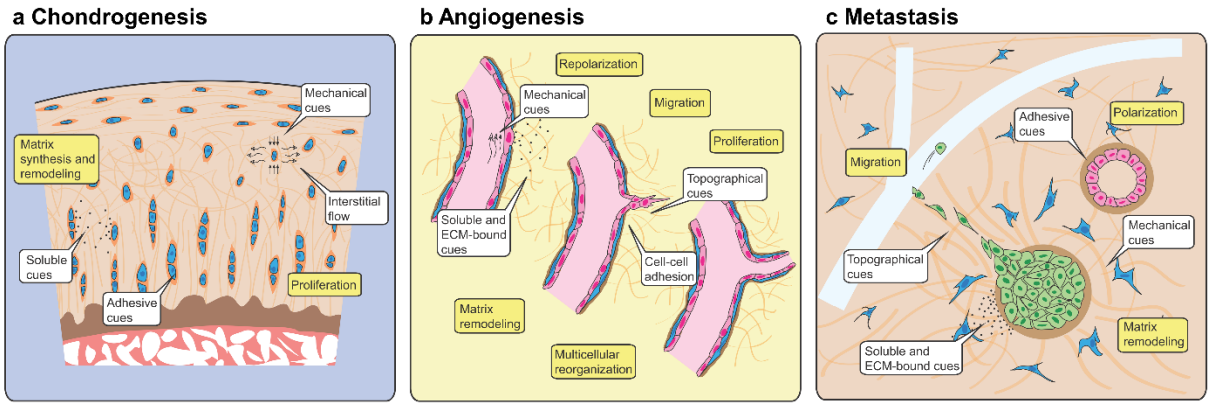

Figure 1. Conduction of cellular behavior in 3D environment through biophysical and biochemical cues as well as cellular crosstalk on **a)** chondrogenesis, **b)** angiogenesis, and **c)** cancer cell metastasis [14].

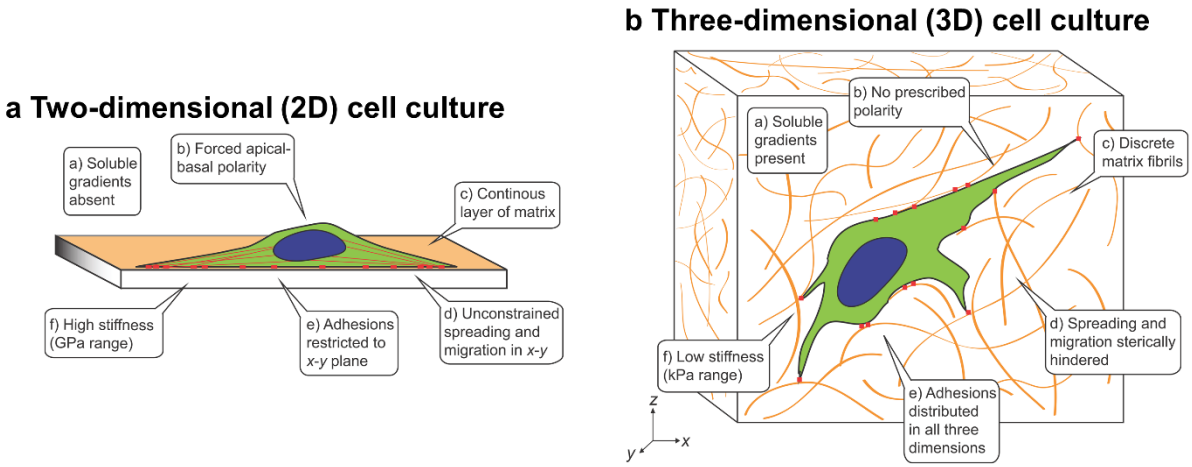

Figure 2. Differences between **a)** 2D and **b)** 3D cell culture environments [14].

Table 1. 2D vs. 3D cell culture environments. Biophysical and biochemical environments differ in 2D and 3D culture systems through the effect of adhesive, topographical, mechanical, and soluble factor distributions [14, 21].

2D	**3D**
High stiffness surface	Tunable stiffness of the environment (usually lower than 2D tissue culture surfaces)
Flat surface with no restrictions for cell adhesion, spreading, proliferation, and migration	Nano- and micro-scale 3D environments limiting cellular mobility through adhesion moieties and porosities of the matrix
No gradients for soluble factors	Gradients of soluble elements through matrix or cells
2D cell-surface interactions and limited cell-cell junctions	Frequent cell-cell and cell-matrix interactions with the ability to self-organize
Predefined apical-basal polarization	Self-organized apical-basal polarization
Lose\s of cell maturity with different gene and protein expression levels compared to *in vivo* conditions	Preserving cells' differentiated state as well as their gene and protein expression patterns
Drug toxicity in much lower concentration of drugs	Higher resistance to drugs
Cheaper processes, easier to interpret, and suitable for longer time cultures	More expensive and require more time to process

One of the important features of 3D environments is presence of mass transfer patterns that does not exist in 2D culture systems. Presence of ECM components and compartmentalization of tissues that create tissue interfaces create transport properties and diffusion gradients in 3D systems while

in 2D only a rapidly equilibrating convection exists [14]. ECM structural properties that define these gradients are pore size, connectivity, and distribution of its components. Solutes size and charge as well as cell density and distribution are also important factors in defining the mass transfer properties [14]. Spatial distribution of soluble factors such as nutrients, metabolism byproducts, and gases such as oxygen and carbon dioxide can also be affected by macroscopic deformation of the construct and pressure gradients created during body movements or by interstitial flow [6]. Storage and binding of soluble factors to ECM is also a factor in creating these gradients [14]. Many growth factors can bind to ECM proteins and mechanical forces or enzymatic cleavage are needed to cleave them to define their presentation or availability [22] as compared to 2D cultures that they can freely move into the supernatant [23]. Different production and consumption rates of cells can also affect these gradients. Cellular behavior in different locations can change due to different local concentrations or a chemotactic response such as cell migration elicited by large enough concentration differences that are understandable for cells. The mass transfer limit for oxygen and nutrient diffusion *in vivo* and in 3D models is 100-200 μm while in 2D culture conditions, many factors such as glucose and amino acids don't show a gradient while oxygen that has a very low solubility in culture medium, depletes rapidly [6].

Another important factor is the mechanical cue that only exists in 3D environments and *in vivo* conditions. Cell deformation and active response to forces in 2D happens in a predictable and homogenous way but in 3D the deformation and response is heterogenous and anisotropic due to the fibrous structure of ECM [14, 24]. A 3D culture system can also provide cues for cellular behavior through ECM stiffness and number of integrin-ligand bonds that are formed to define how much cells can contract the ECM, how much tension they can create, and to what extent migration can be done. 3D environment can also create a gradient of material properties but such

features are lacking in 2D models. Natural ECM hydrogels can provide a milieu of such biophysical and biochemical cues that exist *in vivo* and are needed for proper function of cells. Some of these roles are summarized in Table 2.

Table 2. Roles of ECM components *in vivo* [6].

ECM component	**Function**
Fibrillar collagen	Structural material Defining the stiffness Binding to adhesion factors and growth factors Controling porosity and molecular transfer
Non-fibrillar collagen	Binding to other ECM components to stabilize and organize construct and control cell behavior including proliferation and migration
Fibrin	Abundant in wound healing and actively participate in ECM remodeling Defining the stiffness Binding to adhesion factors and growth factors
Elastin	Providing elasticity to ECM
Proteoglycans	Resisting compression Hindering water and molecular transport Binding to growth factors and chemokines Defining electrokinetics of the ECM

Besides from features of a 3D environment, dynamic features of the *in vivo* conditions are also detrimental in recreating proper cellular behavior and need to be considered in the models. In the next section, the dynamic features that need to be considered as well as different 2D and 3D models considering such stimulations are briefly discussed.

1.2. Dynamicity of *in vitro* models

Another feature that traditional models lack is the dynamic cues of the niche biological environments. Cells are known to understand and be influenced by such dynamic cues *in vivo*. It has been shown that proper development of heart in zebrafish requires large shear forces applied by blood flow that acts as an essential epigenetic factor [25]. In case of chick embryo, position and fate of individual cells rely not only on gene expression but on other factors such as mechanical

forces [11, 26]. Similar phenomenon has been observed in *in vitro*. Cells cultured without constraints, without proper physical boundaries and exposed to isotropic signals, show limited organization abilities but once proper boundaries and cues are provided, they respond to these geometrical and physical cues and organize themselves [27]. This creates the possibility of organizing cells into structures with higher orders of organization [28].

Cells are sensitive to mechanical cues such as fluid flow, compression and stretching which can be implemented in both 2D and 3D models (Figure 3). Effect of tension on the cells can be modeled by stretching the flexible membrane that they have cultured on to study cell behavior in lung and airway tract, gastrointestinal tract, or cardiac tissue, endothelial and smooth muscle cells in blood vessels in uni- or multi-directional ways [29]. Effect of compression on cellular behavior has also been shown on osteogenic differentiation of stem cells [30] and wound healing [31]. Mode of mechanical stimulation has been shown to be important. For examples it has been previously shown that not only cyclic mechanical strain that is more biomimetic affects cardiac cells in 3D [32], even static stretching affects differentiation of mesenchymal stem cells into cardiac cells in a strain-dependent manner [33]. Similarly, bone marrow derived progenitor cells showed different behaviors in their differentiation towards smooth muscle lineage in fibrin once in free floating hydrogels compared to statically confined ones and constructs under dynamic cyclic deformation [34].

Fluid flow is another mechanical cue that can influence cells for example in the case of interstitial fluid flow. Interstitial flow is the very slow fluid flow around cells through the 3D structure of ECM that moves in different directions around the cell-ECM interactions and faces very high resistance. It defines the pericellular protein gradients, especially the matrix-binding ones. The primary driver of this flow is plasma leaving the blood capillaries and draining into lymphatic

vessels, or sometimes its reabsorption in post-capillary venules. It can be affected by skeletal motion (such as muscle movements and cartilage and bone compression) and tissue and organ movements (such as respiration and arterial pulsation) [35]. Effect of interstitial flow on cellular behavior such as angiogenesis [36] and lymphatogenesis [37] can only be modeled in 3D as presence of ECM is necessary. Effect of interstitial flow on morphology and behavior of cardiomyocytes, bone, neuronal, endothelial, and epithelial cells has been shown [29, 38]. For example in bone tissue the hydrostatic and osmotic pressure differences between blood vessels, interstitium, and lymphatics, drive the slow and constant interstitial flow and this pressure gradient affects and defines cellular function in lacunar-canalicular system [39].

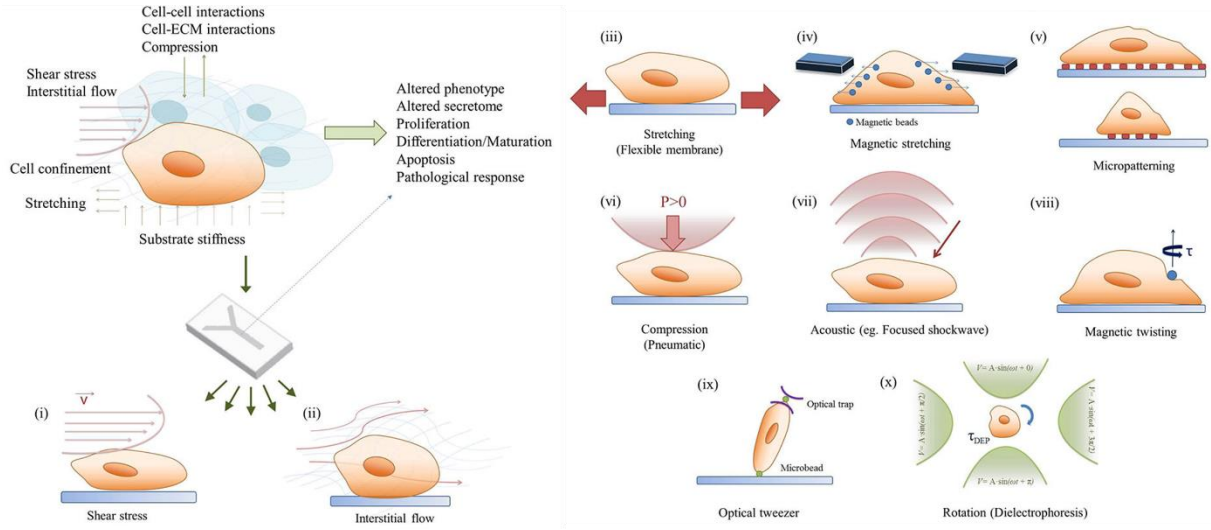

Figure 3. Different mechanobiological cues implemented in *in vitro* models [29].

Electrical signals can affect cells too. Effect of endogenous electrical signals are well understood not only in tissues with electrical activity such as nerves and muscles but also in development, maintenance, and repair of other tissues and in pathophysiological situations such as cancer and during wound healing [40]. Electrical current and potential as well as piezoelectricity of collagen in the ECM of the bone tissue has been shown to guide osteocytes during remodeling and healing

of bone [41, 42]. *In vitro*, electrical stimulation can be delivered directly to the cell culture environment which is very simple but pH change, reduction in soluble oxygen levels, and production of Faradic byproducts close to electrodes limits its application. Capacitive coupling can be created using two parallel conductive plates with gaps between them and culture environment to create the electric field which will form uniform fields but requires very high voltages (as high as 100 V). Similarly, inductive coupling can be used to create the electric field through the coil that is positioned around the culture (Figure 4). Alternatively, electrically conductive biomaterials such as polypyrrole can also be used to deliver the electrical signal directly to cells [40].

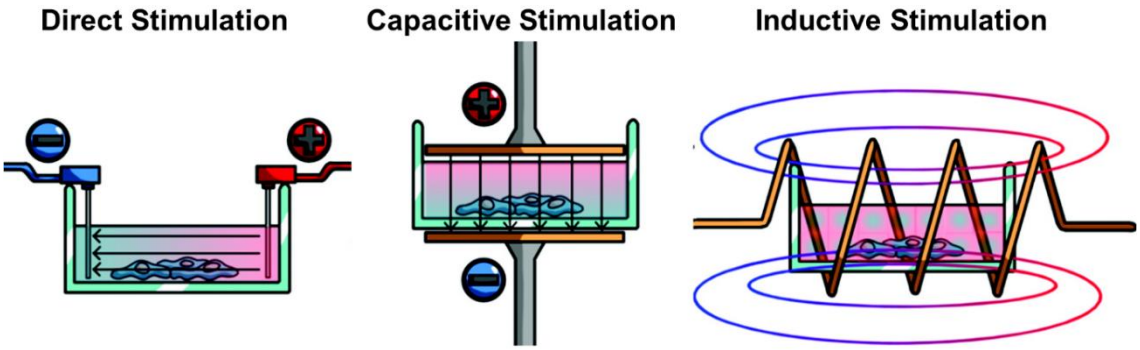

Figure 4. Different delivery routes for electrical signals used in in vitro studies [40].

In order to include previously discussed features of the *in vivo* conditions in the *in vitro* models, 3D culture systems can be combined with microfluidics and microdevices that offer certain features necessary for promoting *in vivo* like behaviors. These features include recreating co-culture of cells with controlled spatial patterning, spatiotemporal control of gradients, and integration of flow and perfusion and other types of stimuli. Spatial control of cells and ECMs in 3D models is important to create tissue interfaces as well as implementing gradients and perfusion in the construct [43] which requires specific equipment and are labor intensive. Creating such dynamic environments in microdevices allows the use of lower amounts of precious materials and

lower cell numbers as well as better control over spatiotemporal distribution of the biophysical and biochemical cues [43]. Such microdevices are also compatible with actuating mechanisms as well as observation systems to trigger certain behaviors and observe them in the system [29]. Number of studies following such approaches have been increased during the last decade which shows its importance (Figure 5) [43].

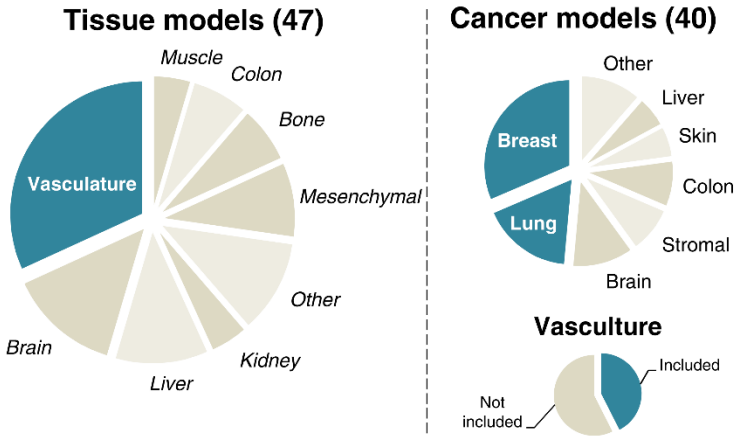

Figure 5. Overview of publications combining 3D cell culture with microfluidics and microdevices published between 2012-2015 [43]. Abundance of vasculature modeling could be related to the fact that microdevices are best suited to model such behavior. Abundance of studies on breast and lung cancer is a result of their high incidence in humans.

Although importance of 3D culture environment regulated with dynamic cues has been recognized for more than a century, introduction of tissue engineering concepts created a big momentum in creation of such models. Originally meant to recreate damaged tissues or organs using a combination of cells, scaffolds, and signaling factors, tissue engineering had the ability to recreate some of the structural and functional properties of the target tissue followed by remodeling in the human body. Different scaffold fabrication techniques and scaffolding materials were developed to make these constructs as close as possible to the natural physiological conditions in order to make it easier for the body to remodel it. The initial fabrication techniques required two separate steps, first fabrication of the scaffold followed by implantation and migration of cells into its bulk.

Later, biofabrication techniques were introduced that incorporated cells within the bulk of the scaffold during the fabrication phase which not only accelerated the process by eliminating the need for proliferation and migration of cells to the scaffold, but also had the added ability of precisely controlling the distribution and positioning of the cells to recreate the tissue interfaces naturally observed *in vivo*. Such biofabricated constructs could also be preconditioned in bioreactors to further adjust cellular behavior or construct properties before implantation. Although great progress has been made during the last three decades, these techniques are still limited in their ability to completely recreate a tissue or organ with all of the features necessary to the meet the requirements for replacing an organ. Despite these shortcomings, these techniques can be used to create 3D dynamic *in vitro* models with much higher complexity and similarity to the target physiological or pathological condition as compared to other preexisting techniques. Currently, many of the biofabrication techniques are repurposed for *in vitro* modeling applications but since structural and physiological requirements of different tissues for modeling purposes are different compared to implantation requirements, these techniques lack certain features that an effective *in vitro* model requires. For example, unlike *in vivo* implantation of organ surrogates that function of the structure will be monitored after implantation in an undisruptive manner, in *in vitro* modeling structures will be scrutinized and their behavior will be studied down to single cell level and it should be possible to provide direct access to the cells in different positions. This highlights the need for development of techniques specifically designed for modeling purposes and since different tissues have different requirements, a single omnipotent technique does not exist. In the following chapter different biofabrication strategies are discussed in order to recognize strengths and shortcomings of each of them that could help develop new and better techniques.

2. Biofabrication toolbox for *in vitro* modeling

Biofabrication is termed as “the automated generation of biologically functional products with structural organization from living cells, bioactive molecules, biomaterials, cell aggregates such as micro-tissues, or hybrid cell-material constructs, through bioprinting or bioassembly and subsequent tissue maturation processes” [44, 45].

During the past three decades scaffold-based tissue engineering approaches have been improved and proven promising in recreating small and simple tissues in a high throughput top-down approach but creating more complex tissues that are larger and more complex becomes challenging as creating vasculature, spatial organization of cells in high and tissue relevant densities, aligning cells, as well as creating tissue interfaces and gradients of ECM materials, cells, and signaling factors has been proven to be challenging using these techniques [28, 46]. Alternatively, biofabrication-based techniques follow bottom-up modular tissue engineering approaches, unlike previous top-down tissue engineering methods, and create the opportunity to create more complex constructs in a scalable fashion by assembling living and nonliving building blocks. This approach establishes a precise control over both micro- and macro-scales [46, 47]. Another advantage of these biofabrication-based techniques over traditional engineered scaffolds is their higher resolution and the ability to simultaneously incorporate cells and biological signals during the fabrication phase [48].

Bioassembly is the fabrication of 2D/3D constructs with hierarchical organization using preformed units via cell-driven self-organization either with biomaterial-free cell solutions or cell-biomaterial hybrids with the help of enabling technologies such as microfluidics or microfabricated molds. In **bioprinting** such constructs are created using computer-aided transfer processes in an automated and layer-by-layer fashion. The combination of biomaterials and biological elements including cells and molecules that are used in these techniques is called the

bioink [44, 45]. **Additive biomanufacturing** as a subfield of biofabrication with more industrial focus is defined as "a type of manufacturing that utilizes biological systems (e.g., living microorganisms, resting cells, plants, animals, tissues, enzymes, or *in vitro* synthetic (enzymatic) systems) to produce commercially important value-added biomolecules for use in the agricultural, food, energy, material, and pharmaceutical industries" [45, 49]. An example of additive biomanufacturing application is the newly emerging field of artificial meat manufacturing.

One of the features of biofabrication techniques that determines their widespread acceptance and can be used to quantitatively compare them is their spatial resolution and manufacturing time (RTM) (Equation 1):

$$RTM = \frac{spatial\ resolution}{manufacturing\ time} \cong R.P = \frac{1}{d}.\frac{V}{t} \quad \textbf{(1)}$$

Where R is the best spatial resolution (inverse of minimum feature dimension d) and P is the delivery rate of the bioink with the physical dimensions of RTM being square-length/time, 10^{-3} m^2/minute for most biofabrication techniques [45]. Minimum feature size of different biofabrication based techniques are summarized in Table 3.

Table 3. Comparison of minimum feature size of different Biofabrication-based techniques [45].

Technique	**Minimum feature size (μm)**	**RTM ratio (10^{-3} m^2/minute)**
Extrusion bioprinting (Bioplotting)	~100	Medium (~0.5)
Ink-jet bioprinting	~50-100	Medium (~0.1)
Laser-induced forward transfer	~300	Low (~0.04)
Spheroid-based approaches	~300	Low to very low (<0.001)

Biofabrication-based techniques can be powerful tools to create 3D *in vitro* models. Most of the current 3D *in vitro* models cannot properly mimic spatial and functional complexities of tissues and organs as well as their multicellular dynamic microenvironments [48, 50]. Hierarchy of complex tissues and organs includes highly ordered components (signaling molecules, proteins,

and cells) that enables their functions and biofabrication strategies can be applied to recreate these 3D spatiotemporal orders through accurate deposition and assembly of cells and bioinks in predefined patterns to recreate tissue-relevant cell-cell and cell-matrix communications and interfaces [48]. Figure 6 summarizes different techniques that have been used to create higher order *in vitro* models. Understanding requirements of 3D *in vitro* models that are necessary to make them faithful to their *in vivo* counterparts is necessary. Ideal 3D culture systems properly mimic the physiological or pathophysiological microenvironment with cell-cell, cell-ECM, ECM stiffness, gradients, and cell population relevant to the tissues [6]. These systems can be ECM-free (mostly used to study cellular/physiological gradients), ECM-based (mostly used to study cell-ECM interactions), or hybrid culture where ECM-free constructs are embedded into the ECM material after fabrication [3, 51]. On the other hand, dynamic environments can be included in *in vitro* models using microfluidic or microfabricated systems, initially created through the application of organ-on-a-chip devices [1]. Biofabrication-based techniques are well suited for these purposes and will be discussed in the following sections.

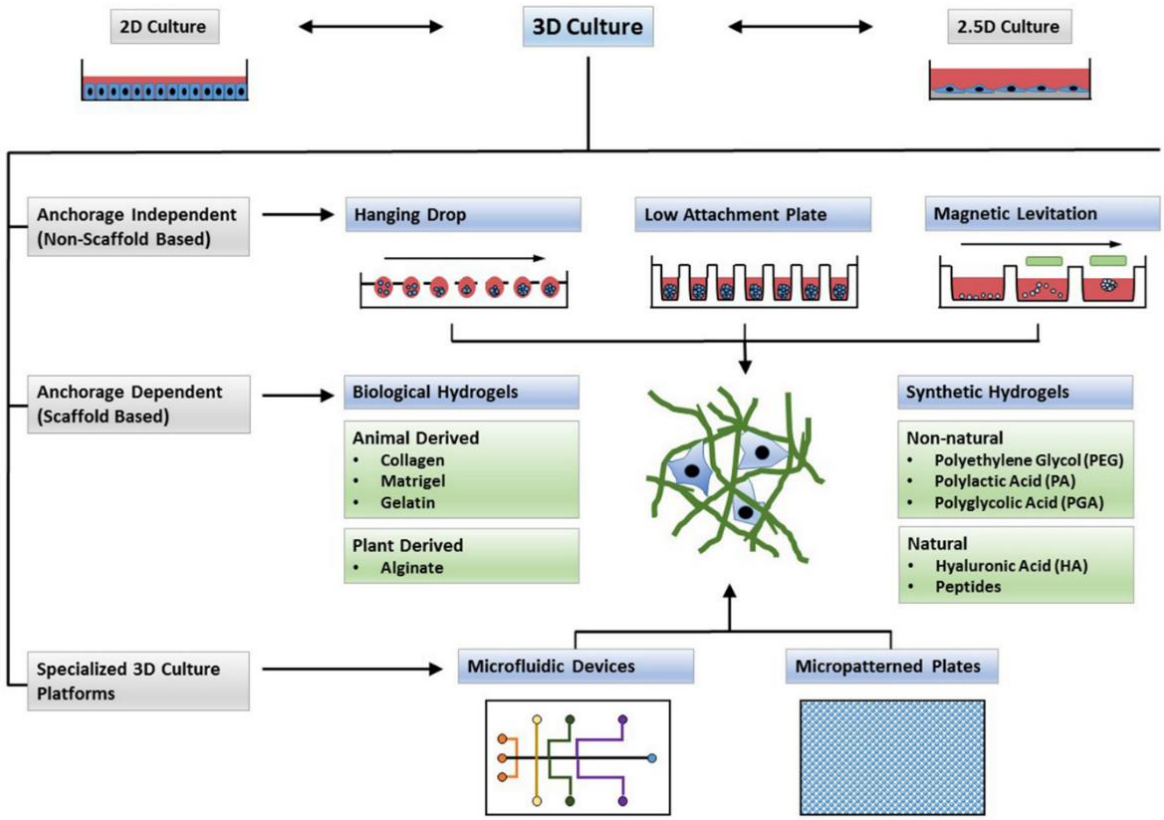

Figure 6. Different 3D culture systems. A 2.5D culture system is where cells are cultured on a thick layer of ECM [3].

2.1. Bioprinting

3D printing was first introduced in 1986 in the form of stereolithography that used UV-cured thin layers of materials to create 3D solid structures [52]. This approach was later adopted to create the solid structures using biomaterials to be transplanted *in vivo* with or without post-fabrication cell seeding [53]. Solid materials were later replaced with bioinks to fabricate structures with biological resemblance and function and since the whole process was automated, the created structures showed more reproducibility in terms of structure and function compared to previous techniques [54]. Bioprinting can be performed using three different approaches. **Inkjet bioprinting** creates droplets of bioink by using piezoelectric actuations or by creating localized heating and 3D objects

are created by moving the bioink-containing stage in z direction. Although this technique is fast and has low cost, it requires low viscosity bioinks (3.5–12 mPa/s) and low cell densities (< 10^6 cells/mL) to generate droplets that can achieve a resolution of ~50 μm. **Extrusion bioprinting** controls the flow of bioink using pneumatic systems or mechanical compressions/movements which are suitable for high cell densities (very high cell densities, even compact spheroids can be used) and can be used with a wide range of viscosities (30 mPa/s to > 6×10^7 mPa/s) but is slow (as low as 10-50 μm/s) and has medium cost. In **laser-assisted bioprinting** a laser beam is illuminated to the bioink layer through a photo-absorbing layer that causes localized heat and bubble formation that subsequently propels bioink towards the stage. The cell densities in this technique are medium to high (10^8 cells/mL), can be used with medium range viscosities (1-300 mPa/s), is fast (200-1600 mm/s) but very expensive [54, 55]. One advantage of inkjet bioprinting technique is its precise control over the number of cells in each droplet and since there are no nozzles involved in the process, damage due to shear stress to cells is not a concern [45]. On the other hand, extrusion bioprinting is the most commonly used technique due to its simplicity, high cell density and wide range of bioink chemistries and viscosities that can be used [48] however its most important limitation is the resolution of the process that is defined by the fiber size which is normally >100 μm [46]. These technologies are summarized in Figure 7.

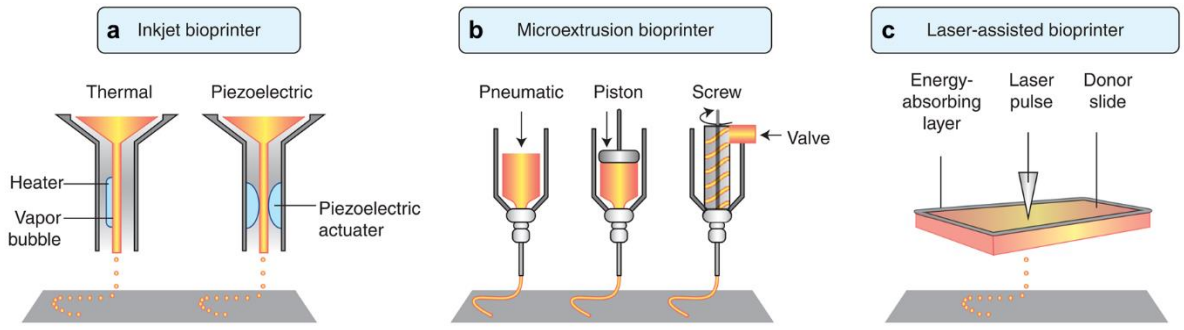

Figure 7. Different bioprinting technologies [55].

Although extrusion bioprinting lacks the resolution required for organ printing purposes by itself, use of microfluidic-based nozzles increases the control over cell and molecule deposition, and helps with creation of required gradients and formation of different structures [56]. There are four different general strategies for performing extrusion bioprinting, direct ink writing, coaxial printing, coagulation bath, and free-form reversible embedding (Figure 8). The driving force for development of different techniques is the need for biocompatible materials with suitable crosslinking mechanisms that allow high resolution bioprinting of complex patterns with proper structural integrity in different formats [56].

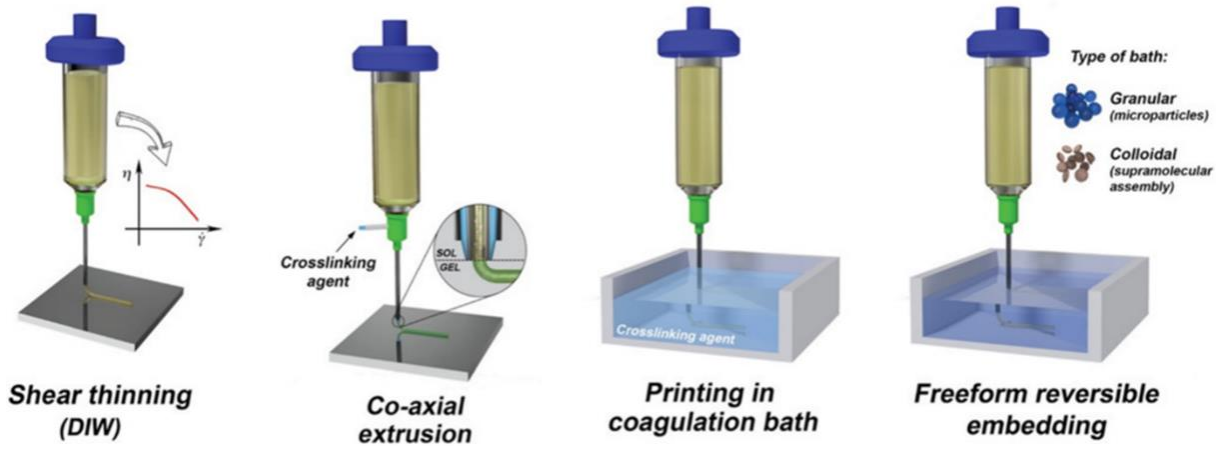

Figure 8. Different strategies of extrusion bioprinting [56].

Direct ink writing is one of the first extrusion bioprinting techniques developed that usually uses shear thinning hydrogels as bioink. Tuning the rheological properties of the bioink for high resolution bioprinting while preserving cell viability and function is a challenge. Co-axial bioprinting decouples the rheological properties of the bioink from printing resolution and has higher resolution with the ability to make more complicated structures. Printing in a coagulation bath allows for applicability of different materials but nozzle clogging and lack of structural

integrity due to improper adhesion between layers are its disadvantages. Free-form reversible embedding in a pseudoplastic or granular bath is a more sophisticated technique where rheological properties of the bath become more important which offers more freedom in the choice of bioink and tunability of the construct but removing the bath after printing has proven to be challenging [56].

The major challenge in clinical translation of any engineering artificial tissue, especially bioprinted ones that are larger in dimensions, is vascularization. This becomes a challenge for *in vitro* models as well that are considering tissue relevant sizes. Blood vessels create the environment for exchange of nutrients and gasses as well as metabolic wastes through a monolayer of endothelial cells that also prevent thrombogenesis. Although vasculogenesis is crucial to preserve cell viability and function, in the proper conditions it happens at a rate of a few millimeters per day and it will take several months to finish a human-size tissue by which necrotic regions are formed. Bioprinting has a great potential to pre-form such complex networks that increases the vascularization rate and supports cellular needs during this process. Alternatively incorporating oxygen-generating materials or reducing cells' metabolism to reduce their needs can prevent cell death while vasculogenesis is being performed. Incorporating growth factors such as vascular endothelial growth factor (VEGF), platelet-derived growth factor (PDGF), and transforming growth factor-β (TGF-β) as well as coculture with other cell types including fibroblasts, smooth muscle cells, and mesenchymal stem cells can also promote angiogenesis and vasculogenesis [57].

In the context of vasculogenesis, bioprinting techniques can be divided into direct and indirect techniques. Direct bioprinting uses techniques such as extrusion bioprinting with multiaxial nozzles to directly print blood vessel like constructs but it is limited in the complexity of the network that can be printed, diversity in the bioinks, and low cell viability. Indirect techniques

however create channels indirectly by removing fugitive materials that were printed in the form of vascular network. These techniques are better suited to create branched networks with a wide range of bioinks and higher resolution can be achieved. The major drawback however is the difficulty of removing fugitive bioinks particularly in larger constructs [57].

Indirect bioprinting is also known as sacrificial bioprinting and involves four steps: 1) 3D printing of the sacrificial material in the form of intended vascular network, 2) casting the bioink, 3) removing the sacrificial template, and 4) endothelialisation of network. Not only the sacrificial material itself should be biocompatible, the removing conditions shouldn't expose cells to cytotoxic conditions either [54]. To create such multidirectional networks embedded bioprinting (otherwise known as free-form reversible embedding) can be used to form complex discrete 3D constructs [54]. Despite the improvements made through development of new techniques, engineering vasculature with capillary sizes (5-10 μm) is still challenging since it is smaller than the needle diameter [58]. Lack of proper mechanical stability, especially in constructs with blood vessel networks, is another major concern for bioprinted samples but nevertheless bioprinting has been largely adopted for *in vitro* model development purposes which will be discussed in the following section.

2.2. Bioprinted *in vitro* models

Among different techniques, bioprinting has a unique ability in recreating certain feature of different tissues and pathophysiological conditions. Bioprinting is probably one of the most suited techniques to recreate the complex tumor microenvironment, including the effect of stromal population and cancer metastasis, mechanical, biochemical, and geometrical cues and tissue architecture [59]. One of the other aspects of tumor microenvironment that bioprinting-based techniques can and other techniques such as spheroid models cannot consider is their complex

vascular or neural network [48]. The same is true for any other tissue that is highly vascularized or has high metabolic activity and requires higher mass transfer and perfusion to maintain viability of the cells. The most commonly used technique to recreate such interconnected vasculature is 3D printing of sacrificial materials, casting cell embedded hydrogels, and eventually endothelialization of the channels after sacrificial material is removed [60, 61]. Coaxial bioprinting is also another commonly used approach for this purpose [62, 63]. Using such techniques, thick (>1cm) vascularized constructs that can be perfused for long times have been created [60].

Bioprinting has been used for *in vitro* modeling of other tissues in physiological or pathophysiological states as well. In order to properly mimic liver's structure and function with proper molecular metabolism, relevant hexagonal units of liver containing heterogenous population of parenchymal cells and supporting stromal cells, as well as gradients of molecules and cellular functions need to be recreated. This has been done by direct bioprinting of UV crosslinkable hydrogels [64] and further by bioprinting hepatic spheroid and recreating these functional units within a microfluidic device for fluid perfusion [65]. Left ventricular myocardium of the heart tissue is the main pumping chamber of the heart and the main site for pathological conditions of the heart. This tissue has a 3D multilayer microstructure which makes bioprinting an ideal technique for its *in vitro* modeling. Bioprinting is also capable of tuning the cell alignment, varying mechanical properties, and increased dimensionality that is needed for heart tissue [59]. Bioprinting techniques combined with patient derived cells have been used for applications in personalized medicine [66]. Other examples of bioprinted *in vitro* models are applications in tissue and disease modeling including but not limited to cardiovascular tissue [67, 68], skin [69, 70], cancer models [71, 72], and neuronal system [73, 74].

Extrusion bioprinting in specific has been used to print different tissues for a variety of *in vitro* modeling applications. This bioprinting method is well suited to recreate anisotropic structure of skeletal muscle tissue for applications such as drug screening [75]. The shear force applied to the cells in direct writing extrusion bioprinting can further align the skeletal muscle cells [76]. Native-like cardiac tissue composed of branched fibers, high cell densities, and rich vasculature with synchronized contraction using different bioinks and bioprinting approaches such as coaxial extrusion printing has been created [77, 78]. Vascularized 3D constructs with different sizes and wall thicknesses have been bioprinted using a combination of different cell-responsive bioinks to achieve proper cell behavior [79, 80]. 3D bioprinting of highly vascularized and stiff bone tissue, avascular chondral tissue, as well as the transition between the two has been shown [81]. The layer-by-layer structure of skin, a highly vascularized and innervated tissue composed of three distinct layers, makes bioprinting one of the best techniques available for example for drug screening applications [82] or as grafts for wound healing [83] for this tissue.

Despite the advantages of the extrusion bioprinting, several shortcomings have hindered its application for *in vitro* modeling applications. The major drawback is lack of biomaterials that support *in vivo*-like cellular behavior and are appropriate for printing stable constructs with proper resolution that can handle rigorous processes required for evaluating cellular behavior *in vitro*. These materials often lack biomimicry of natural ECM which affects cellular behavior and their ability to remodel the bioink. Fabrication of complex and heterogeneous structures using multiple cell types or bioinks to create structural organization of the target tissues is another challenge. The speed of these techniques is also lower than other bioprinting techniques which limits their high throughputness. Creating functional vessels and connecting them to fluid flow source is also a challenge especially in case of micro-vascularized systems [56].

Developing new bioprinting methods or improving previously established techniques to resolve these shortcomings could further advance application of bioprinting for development of *in vitro* models. One of the limitations of bioprinting techniques is their inability in recreating conditions such as initial stage of tumor development where there is a very dense avascular tissue that is usually smaller than 1 mm in diameter. Bioprinting might not be the best option for modeling conditions like this while other *in vitro* models such as multicellular spheroids fabricated using bioassembly-based methods are much better representatives of this stage of the tumor development. Another example where techniques such as bioassembly-based techniques are superior to bioprinting, is the use of cell sheet engineering technique to recreate tissues such as retina that are inherently 2D. Such tissues with 2D structures have a very dense cellular structure that can be formed with higher accuracy using such techniques rather than bioprinting. Here bioassembly-based techniques and their applications in *in vitro* modeling are briefly discussed.

2.3. Bioassembly

Bioassembly-based techniques can be used to create 1D (line-shaped), 2D (plane-shaped), and 3D (point-shaped) building blocks for biofabricating macroscopic tissues and tissue avatars. 1D (fibers) and 2D (sheets) modules have one or two dimensions with high aspect ratios (≥20) while 3D modules have low aspect ratios in all dimensions. Each of these modules can be formed with or without presence of biomaterials [46]. These bioassembly-based approaches are summarized in **Error! Reference source not found.**.

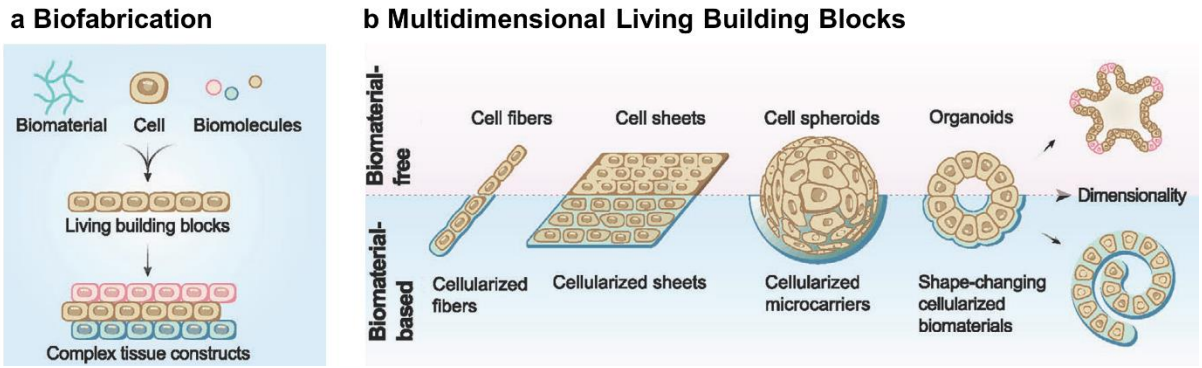

Figure 9. a) Bottom-up bioassembly strategies, **b)** different multidimensional living building blocks formed using bioassembly-based strategies [46].

1D fibers, building blocks with aspect ratios of larger than 20 in two dimensions, can be formed using microfluidic systems [84, 85], patterning substrates for cell culture and subsequently releasing them as fibers [86, 87], or bioprinting techniques [88, 89]. In such constructs, cells can be aligned with the main axis of the fiber to create constructs such as muscle or neuronal fibers. Although bioprinting techniques have also been used for formation of such 1D constructs by extruding the bioinks and further crosslinking them, bioinks used in the process usually contain hydrogels with low cell densities, less than a few million cells/mL [90-92] and have difficulties in creating branching networks. Some of the newer bioprinting techniques provide control over axial and radial cellular patterning of these fibers that combined with bioassembly techniques show higher abilities in creating constructs that are more *in vivo*-like but they require specialized equipment [93, 94]. Microfluidic systems use similar concepts for creating such fibers. Alternatively, methods solely based on bioassembly such as hanging drop, an ECM-free bioassembly technique originally used for fabrication of spheroids in a non-adhesive environment, has been modified with patterned substrates in rectangularly designed hydrophilic regions to

confine cells in a semi-cylindrical fashion in order to assemble ECM-free fibers with much higher cell densities [95].

2D sheets, building blocks with aspect ratios of larger than 20 in only one dimension, have been fabricated using several techniques. One of the first techniques for this purpose, assembled the cells to sheets using poly N-isopropylacrylamid (PIPAAm)-grafted surfaces as cell culture platform. Once cells cover the surface and secret their ECM, decreasing the temperature below 32°C causes hydrophobic to hydrophilic transition of the surface and as a result it no longer will be suitable for attachment of cells and their secreted ECMs which results in their delamination as a continuous sheet. The cells in these constructs show high viability as the secreted proteins, such as E-cadherin and Laminin 5 are preserved [96] which gives the continuous sheets adhesive properties such that they can be stacked on top of each other or other tissues without using glue or suture [97]. Other mechanisms such as enzymatic treatment, pH change, and electrochemical polarization have been developed to make similar sheet-like building blocks [46, 98]. Formation of continuous cell sheets by growing cells on a feeder layer has been done as well where detaching the cell sheet is performed using treatment with dispase that digests some of the ECM proteins and not cell-cell junctions. Alternatively growing cells on amniotic membrane as a carrier and then using them with this membrane is another option to make 2D sheets [98]. In order to handle these 2D building blocks that are often fragile, customized equipment has been developed to maintain the delaminated sheets as flat blocks and stack them into thicker constructs in an automated process [99-101].

One of the first instances to fabricate 3D modules was in the form of multicellular spheroids originally by aggregating cells in suspension cultures using different techniques such as non-adherent surfaces, hanging drop method, as well as spinning and rotating flasks [46]. These

spheroid fabrication techniques promote cell-cell interactions by creating environments to resist cell-surface adhesion in the air-liquid interface of droplets, in the bottom of concave surfaces or in other non-adherent surfaces, or alternatively through continuous agitation of cell suspensions. More homogenous spheroids can be formed by proliferation of single cells to a spheroid in order to eliminate the heterogeneity of the initial cell population [46]. Micromolds formed with microfabrication techniques are another possible method that provide the advantage of precise replication and high repeatability [102]. Polyethylene glycol (PEG) that resists protein and cell adhesion can be used to make these molds [103] but PDMS with the same property and compatibility with soft-lithography is another option [104]. These techniques and many of the other ECM-free techniques are capable of forming only spherical constructs, while only a few ECM-free techniques have been developed to fabricate complex shapes [105, 106]. Despite advantages that these techniques possess such as simplicity and independence from exogenous ECM materials, the constructs formed with these techniques, spherical and non-spherical ones, have low reproducibility, are limited in size due to nutrient and gas transfer limitations, and lack controlled cell/ECM positioning and they offer no control over ECM composition as it is secreted by the cells.

Alternatively, ECM-based techniques can be used that provide more control over porosity and stiffness of the matrix, its chemical structure and electrical charges, binding sites, and the ability to trap growth factors [107]. The ECM material can be a natural hydrogel with proper adhesion sites that supports natural behavior of cells including controlled proliferation and differentiation as well as proper phenotype of cells, or a synthetic hydrogel with well-defined physical and chemical properties such as stiffness and porosity as well as controlled degradation rate. Incorporating proper adhesion moieties, proteolytic cites, and growth factor binding domains to

synthetic hydrogels have been used to elicit proper cellular functions in these bioassembled 3D building blocks [3]. ECM-based techniques that use micro-molds are more efficient for *in vitro* modeling purposes as they can preserve valuable bioinks by reducing the amount of reagents that they use and show higher viability of cells because of the lower amount of shear stress that is applied to the cells during initial deposition. Such techniques can be used to form spherical shapes and other predefined complex geometries like rods and honeycombs for high-throughput screening [108, 109]. The ECM could be collagen [110], Matrigel™ [111], or UV curable hydrogels such as methacrylated hyaluronic acid or poly(ethylene glycol) [112, 113]. The use of molds also allows to scale up (up to 822 spheroids can be formed in a single mold with a microwell array) and standardize the spheroid generation [114, 115]. Despite these advantages the current ECM-based techniques have some limitations too. They are limited in the cell types and densities, fabrication speed, control over positioning of different cell types, and creation of tissue/organ interfaces. More importantly, formation of necrotic cores and the inability to grow them beyond a certain size due to mass transport limitations is one of the key limitations, especially for applications other than modeling avascular stage of the cancerous tissues. Finally, it is also difficult to incorporate biophysical cues such as electrical and mechanical stimulation that is increasingly being considered important to recreate the *in vivo* environments, due to their form factors

Organoids are a subset of bioassmebled 3D building blocks that have gained attention recently. These constructs are formed using primary tissue cells or stem cells (embryonic, pluripotent, multipotent, or induced pluripotent stem cells) and by having the dynamic self-renewal and self-organization of stem cells they are capable of recreating more of the functions and structural details of the target tissues [3, 46]. Organoids comprise multiple cell types and mimic near-physiological structure and function of the native tissues. These constructs show genomic stability which makes

them suitable for long term preservation (biobanking) and high throughput studies. Despite these advantages, formation of such building blocks is time consuming and resource intensive, they show low reproducibility [28]. Although some organoids have shown vascularization upon implantation, they naturally lack vascularization and innervation which hinders their ability in maintaining tissue homeostasis and repair. The organoid formation is dependent on ECM properties and variability in the sources of these materials could decrease their reproducibility. Organoid structure formation is highly dependent on proper temporal and spatial delivery of different signals and currently proper signal delivery and monitoring systems for organoids such as organ-on-a-chip systems are lacking [116]. Organoids limited size further hinders their application. Although stem cells have shown high degree of self-organization and self-patterning *in vitro*, certain degree of microengineering seems to be necessary to control their organogenesis [28]. Organoids also suffer from variability and lack of control over size, shape, and cell distribution, and are not compatible with implementing biomechanical stimuli [117, 118]. On the other hand, since organoids usually self-organize, prescribed positioning of cells and ECM materials is not possible.

Bioassembled constructs can be used as bioinks for the bioprinting or other automated processes to reduce the exogenous biomaterial content and make more native-like architecture with denser cell populations and higher degrees of complexity [48], for example through the use of cell-sheet bioinks [119]. These building blocks can be assembled as a diverse library to create macrostructures in a bottom-up approach and in an automated manner which gives bioassembly more freedom in creating complex macrostructures [48]. 1D fibers (line-shaped building blocks) can be assembled using reeling or weaving with or without support material to create centimeter-sized constructs with precise alignment of cells and ECM materials. They can also be used to

promote vascularized tissue formation. 2D sheets (plane-shaped blocks) can be stacked to create thicker structures or rolled to form tubular tissues for example for vasculogenesis applications. Cell patterning can also be done inside each sheet separately to create more precise control over microstructure of the macro-tissues. 3D building blocks (point-shaped) can be assembled to larger constructs using molding to create constructs that are several millimeters large. They can also be manipulated using microfluidic and dielectrophoretic forces (Figure 10) [48].

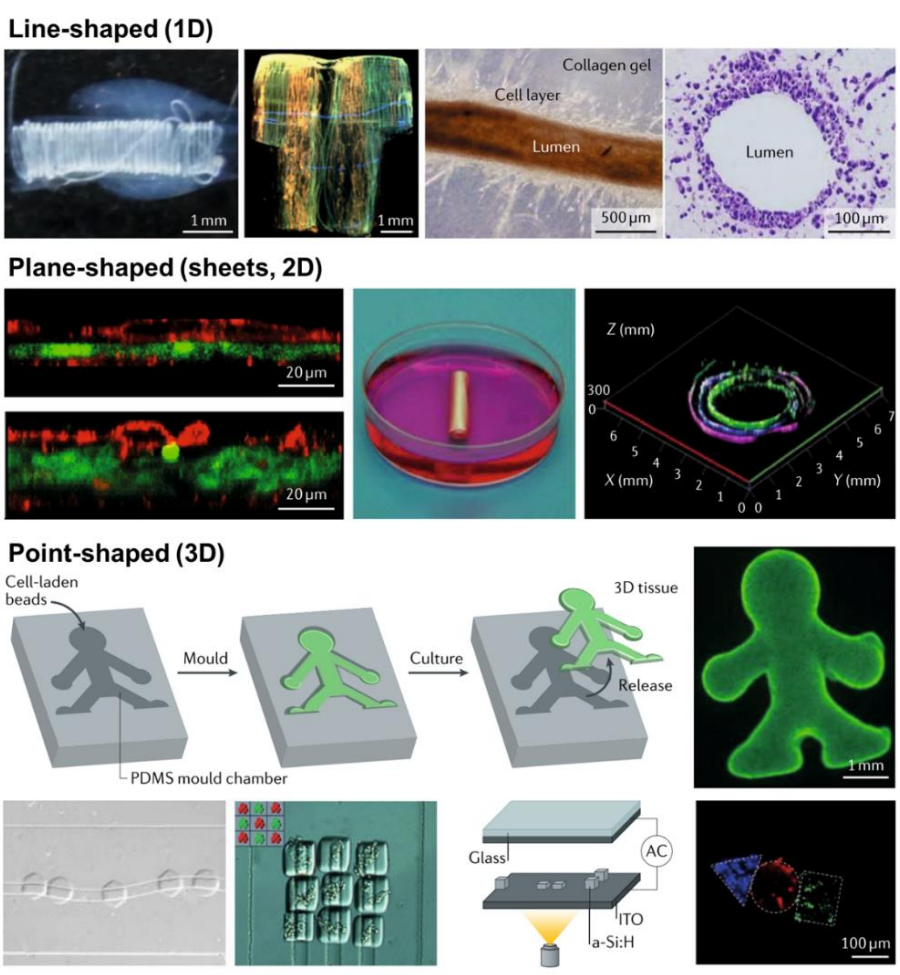

Figure 10. Bioassembly of 1D, 2D, and 3D self-assembled building blocks into more complex macrostructures with precise control over its microstructure [48].

2.4. Bioassembled *in vitro* models

Bioassembled *in vitro* models involve the use of point-, line-, and plane-shaped building blocks to recreate macroscopic organo-mimetic tissue avatars [120]. Some of the important and most widely used bioassembled building blocks are multicellular spheroids, cell sheets, and organoids [121, 122]. Multicellular spheroids are capable of recreating histomorphological as well as functional features of tissues such as microenvironmental factors including cell-cell and cell-ECM interactions and oxygen and pH gradients (Figure 11). It has been shown that 3D spheroids better resemble solid tumors and show comparable drug resistance patterns compared to *in vivo* conditions, as well as appropriate gene and protein expressions [123, 124]. Spheroids formed using bioassembly techniques with diameters less than 150 μm show the major behaviors observed in *in vivo* conditions that are lacking in 2D culture systems on some of the other 3D models such as heterogeneity of cells in their metabolism and drug sensitivity that can only be seen in the spheroids [102]. Although multicellular spheroids are mostly used to study cancer cell behavior [125], they have been used for other applications such as testing potential anti- or pro-angiogenic drugs using spheroids of endothelial cells [126] as well as cellular behavior in different tissues and organs. A combination of endothelial, fibroblasts, and iPSC-derived cardiomyocytes have been used in a spheroid format that mimics the cellular and ECM organization as well as microvascular network of human heart tissue [127]. Toxicity studies using hepatocyte spheroids were performed in long-term cultures while transcript markers were more or less similar to the freshly isolated hepatocytes during the whole time [128]. Neurospheres that were able to imitate most of the basic processes of brain development *in vitro* were used for CNS drug studies [129]. An ECM-based technique was used to embed prostate cells between two Matrigel® layers and form their spheroids in order to study prostate epithelial cells in normal and cancer states [130]. Similarly cells embedded in fibrinogen-modified poly(ethylene glycol)-diacrylate hydrogel formed spheroids of liver-like cells

in a three-week time span and were used to study effect of mechanical properties of environment on cellular behavior [131].

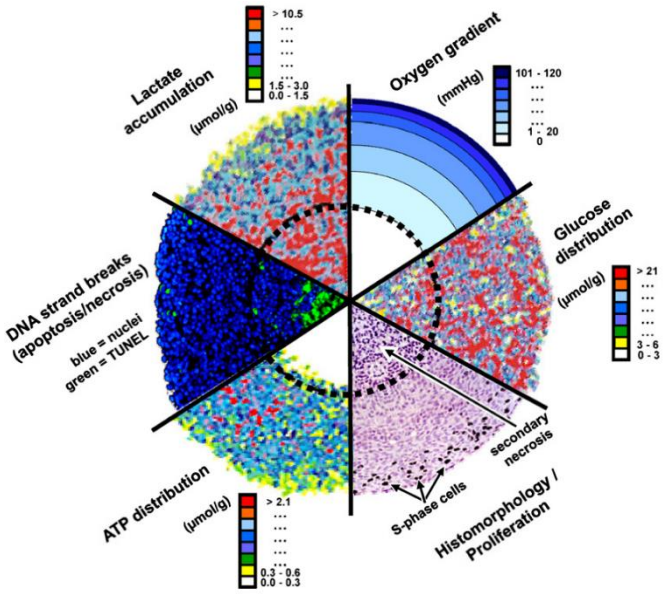

Figure 11. Characteristics of spheroids' microenvironment [102].

Organoids provide another 3D bioassembled *in vitro* modeling technique, that compared to traditional 2D models and other 3D models, provide more insight into organ development and tissues homeostasis and create better media for drug development [28]. Besides from applications of organoids in regenerative medicine, they can be used to study tissue development and different diseases as well as for therapeutics and drug development, specifically diseases that are difficult to model in animals such as those involving human brain development [117]. Intestinal organoids have been extensively used to study pathways influencing recurrent mutations in colon cancer [132] and the role of bacterial pathogens in development of gastric adenocarcinoma during intestinal infection [133]. Patient derived organoids have been used for personalized medicine applications for example to study liver toxicity of experimental drug combinations [134]. Similarly development of brain has been studied using brain organoids formed with pluripotent stem cell by

recreating various brain regions that could be used to create phenotypes of different diseases as part of the *in vitro* models [135].

Cell sheet engineering techniques have been mostly used for transplantation purposes. Transplantation of cell sheets in animal models has been done for corneal, cardiac, cartilage, esophageal, hepatic tissue, thoracic, periodontal, retinal, pancreatic islet, and thyroid regeneration by using autologous and allogenic-based tissue engineering techniques and with primary, progenitor, and stem cells including pluripotent stem cells such as embryonic and induced pluripotent stem cells as well as adult stem cells including mesenchymal stem cells from different tissues. These regenerative strategies are being followed in clinical trials for different tissues [136]. Cell sheets can also be assembled by stacking [137] or rolling [138] to create macrostructures with higher order of complexity. Besides from *in vivo* implantation applications, cell sheets have been used in a few cases for *in vitro* modeling. For example skin cell sheets formed with keratinocytes were used with melanoma spheroids formed using hanging drop method and the effect of different chemotherapy agents on the assembled constructs were studied [139]. Cell sheets have also been used as *in vitro* models to study different behaviors of endothelial cells such as changes in their morphology and their migratory behavior during blood vessel formation by coculturing endothelial cells within a stack of myoblast cell sheets [140, 141].

Although these biofabricated models contain many structural details of human tissues, in order to make constructs that are more faithful to the *in vivo* conditions, introduction of biophysical signals such as electrical and mechanical stimuli, or perfusion that normally exist in physiological conditions is necessary as they provide cues to guide cellular behavior and function. Studies that have attempted to create such dynamic 3D environments are discussed here.

2.5. Biofabricated dynamic models

Cells are constantly exposed to different mechanical, electrical, and chemical stimulations in their natural environments and therefore recreating relevant dynamic *in vitro* models of human tissues can further advance the performance of the models and bridge the gap between the *in vitro* models and *in vivo* conditions. Effect of mechanical deformation in static or dynamic modes have been shown on a variety of cell types. For example, cardiomyocyte cultured in bioassembled 3D constructs exposed to a periodic stretch showed more mature phenotypes. Even when only pneumatic pressure was used to create the cyclic deformation and other biophysical stimulus such as electrical signals that normally exist *in vivo* weren't considered, such effects on cell maturation were observed [142]. A few millimeters long 3D skeletal muscle constructs fabricated using self-assembly around anchoring pins, either using rigid pins without application of external mechanical deformation or compliant pins capable of measuring the self generated traction forces but not providing stimulus have been used to study skeletal muscle cells in dynamic environments [143, 144]. These models were able to form functional muscle constructs capable of showing contraction and where used for applications such as studying effect of different drugs on muscle contraction or shedding light on muscle cell behavior during injury and healing process. Some models have created more sophisticated environments by incorporating more than one cell type and positioning them in predefined patterns for example to create neuromuscular interfaces. A lengthy microfabrication process was used to create pillars that acted as anchors for muscle cells and confine neuronal cells to create motor units *in vitro* and study mechanisms of neurodegenerative diseases such as spinal muscle atrophy and amyotrophic lateral sclerosis by using pillars as sensors that provided quantitative readouts of muscle force generation [145, 146].

Effect of electrical stimulation on cellular behavior in *in vitro* models has also been shown. Like mechanical deformation, it was shown that similar effects on cardiac muscle cells maturation and

function, could be observed when cardiac tissue constructs were exposed to electrical stimulation. Constructs fabricated by self-assembly of the bioinks around suture wires [147] or hollow fibers [148] were exposed to external electrical stimulation through electrodes incorporated in the culture system. These constructs were formed using human pluripotent stem cell derived cardiomyocytes and were used for applications such as pre-clinical testing of different drug candidates while cells were evaluated through studying their myofibrillar structure and organization as well as their electrophysiological response to external stimulation.

Unlike previous studies that only one kind of stimulation is applied to the cells, a few studies have incorporated multiple biophysical stimuli such as mechanical and electrical stimuli, simultaneously. Rat cardiomyocytes subjected to electromechanical stimulation had improved structural organization compared to cells exposed only to one of the stimulation types [149]. On the other hand, although most dynamic *in vitro* models are formed using bioassembly-based techniques, bioprinting has also been used for creation of such models. For example a combination of 3D printing and bioprinting has been used to fabricate cardiac microphysiological devices with integrated sensors that were used to perform non-invasive readouts of tissue contraction and study effect of different parameters such as surface topography on maturation of cardiomyocytes [150]. Although many of the studies creating dynamic microenvironments using electrical or mechanical stimulation have considered such effects either on skeletal muscle cells or cardiac muscle cells, similar effects have been shown to affect other cell types such as bone cells. External stimulation of bone cells has been shown to affect their alkaline phosphatase activity or even create an influence on osteogenic differentiation of stem cells [151, 152].

In summary, although superior to static 3D models, currently developed dynamic models do not combine all the features expected from 3D models that properly represent physiological or

pathological conditions. These models also lack features required for their practicality including rapid processes, ability to precisely position different cell types in larger size constructs in order to recreate tissue and organ interfaces, and possibility of incorporating different biophysical stimuli, simultaneously. Many of these studies often include only one cell type and show limited or no control over cell or ECM positioning. More importantly, fabrication of these models involves specific equipment that makes it difficult to adopt their techniques. Therefore, development of easy to implement and universally acceptable biofabrication-based techniques coupled with bioreactors for delivering different types of stimuli could further advance our knowledge of biological processes, decrease cost of drug development, and in case of personalized medicine, increase the quality of life for patients.

3. Summary

2D *in vitro* and animal models are currently considered as the gold standard models for studying physiological and pathological conditions of different tissues as well as medium to test new therapeutics. Increasing evidence has shown that there is a huge disparity between *in vivo* conditions and these models and the demand for more accurate models has ramped up. Advent of tissue engineering introduced biofabrication tools based on bioprinting and bioassembly that not only can be used for development of organ replacements for implantation purposes, but also provide a toolbox for development of 3D models that are better representatives of *in vivo* conditions, and might one day replace other models entirely. More sophisticated biofabrication techniques are being introduced, even techniques capable of delivering different modes of stimulation, but we are still in the era of overpromising and under delivering for the use of biofabrication-based techniques in regenerating damaged tissues and organs as part of the tissue engineering and regenerative medicine fields. These techniques however can very well be used for

development of highly sophisticated dynamic 3D *in vitro* models. Biofabrication tools have the potential to recreate such tissue avatars but since on one hand many of these techniques are originally designed for organ replacement fabrication purposes and on the other hand the requirements of different tissues are different, no single technique can be used universally for this purpose and a toolbox of techniques specifically designed for modeling purposes need to be created and evaluated. Such techniques need to be able to faithfully create characteristics of tissues such as their morphology and form factors, their cell and ECM positioning to create proper tissue interfaces, and features of dynamic microenvironment that cells experience *in vivo*. Such models should be high throughput and compatible with different biological and functional assays that are needed to be performed.

4. Objectives of the thesis

The objective of this doctoral thesis was to introduce a novel toolbox of biofabrication techniques, based on bioprinting and bioassembly, that together are capable of recapitulating anatomical and physiological requirements of different tissue in *in vitro* setups in a more relevant way while creating the possibility of investigating cellular behavior. This objective is met by performing smaller projects in each of them a different technique is developed and characterized. These techniques are then used for certain biological applications, in order to gain firsthand experience from users' perspective on the possible shortcomings of each of them, and either improve upon the initial version of the technique or devise a completely different one to meet these drawbacks.

5. Thesis organization

This thesis is comprised of 7 main chapters and two appendices in a "sandwich" thesis format. Chapters 1 and 7 encompass relevant introductory and concluding information, respectively. Chapters 2 and 3 include two published papers regarding the development and application of a bioprinting technique while chapters 4 to 6 contain three published papers regarding development, application, and improvement of a micro-molding technique. Two manuscripts discussing a cell sheet engineering technique and its application in lab-grown meat development, both currently under review, are presented in Appendices 1 and 2. Contents of these chapters are provided here.

Chapter 1: This chapter reviews relevant introductory and background information with respect to *in vitro* modeling, specifically biofabrication-based techniques and 3D dynamic models that have been used for this purpose. The motivation behind development of such state-of-the-art techniques is thoroughly discussed and studies using them are briefly reviewed. Various

biofabrication technologies used for *in vitro* modeling, are assessed in terms of their advantages and shortcomings in order to identify a clear path for invention of newer and better suited techniques.

Chapter 2: This chapter encompasses the development of an extrusion-based bioprinting technique using an open source 3D printer to print cell embedded hydrogels on paper that provides mechanical stability and direct access to cells in different locations for examination of cellular behavior with acceptable resolution for *in vitro* modeling purposes. Xurography technique is implemented to create blood vessel like patterns in the paper acting as a perfusion network necessary to maintain cell viability in the large constructs in long term cultures necessary for such studies.

Chapter 3: This chapter show-cases advantages of the previous technique and provides an example for many other possible applications of the technique by modeling trans-differentiation of osteoblasts to osteocytes *in vitro*, a phenomenon that was hypothesized to happen *in vivo* due to entrapment of osteoblasts during bone deposition but no *in vitro* model was developed for this behavior at the time.

Chapter 4: Development of a micro-molding bioassembly technique capable of forming grafts using collagen type I as ECM with complex shapes is presented in this chapter. This technique has a variety of favorable features never before offered in a single technique including very high and tissue relevant cell densities, with the ability to precisely control cell positioning and creating clear tissue interfaces in a tissue relevant manner, compatible with different cell types in a fast and easy to implement process that results in high cell viabilities.

Chapter 5: The main motivation behind this chapter is to show-case advantages and possible applications of the technique introduced in chapter 4 by modeling the crosstalk between adipocytes and skeletal muscle cells in order to show importance of cell positioning by showing effect of cells on each other in different coculture conditions. This study not only further proves the strengths of the original technique, also provides new information that can be used for studying conditions and diseases such as obesity and diabetes.

Chapter 6: Further advancing the original technique in chapter 4, the improved technique included in this chapter implements elements necessary for creating dynamic environment of different tissues by including mechanical deformation, electrical stimulation, and perfusion while preserves other capabilities of the technique. Such conditions are necessary for modeling a wide range of physiological and pathological conditions and the technique can be easily adopted by other researchers.

Chapter 7: This chapter includes the conclusions of the thesis and suggested future works.

Appendix 1: A cell sheet engineering technique developed to form standalone sheets without the need for specific equipment or modified surfaces is discussed here. This easy to implement technique provides a platform to model tissues that are 2D in nature and show cell fusion.

Appendix 2: Application of the cell sheet technique for creation of lab-grown meat consisting of fully mature adipocytes and skeletal muscle cells with the ability to tune fat and protein content of the constructs is the main topic of this chapter. Final product of this study can be used as environment friendly replacement for meat as a food source.

6. Research Contributions

The principle objective of this thesis is to develop a toolbox of biofabrication-based techniques for development of *in vitro* models to meet requirements of different tissues and organs as well as pathological conditions in a more relevant manner. These techniques are designed to be fast, simple, and easy to implement by individuals that don't necessarily have the engineering background, biologists in particular that are end users and beneficiaries of this toolbox. Parallel to development phase of each technique that includes characterization of their working parameters, a trial phase is considered to implement that technique for a certain biological application and identify the possible shortcomings that can be used to develop the next generation of the technique or an alternative technique that can cover those applications. Contributions made in different projects, included as chapters 2-6 and appendices 1 and 2, are discussed here.

Chapter 2: This chapter contains a new bioprinting technique called ExCeL (combining extrusion printing on cellulose scaffolds with lamination to create in vitro biological models). Current bioprinted models only allow access to fixed cells after sectioning is performed or only provide an average of the cellular behavior after the whole construct is dissolved but this new technique that is specifically aimed for *in vitro* modeling, provides direct access to cells in different locations of the model to assess their function as respect to their position. This technique involves bioprinting of the bioink on papers and stacking of these impregnated papers. These layers can be detached at the end of the culture time to provide access to live cells in each layer separately. The method also provides mechanical stability to create thicker constructs that can be maintained in culture for longer culture times. Combining technique with xurography allows to form blood vessel like networks that can be used for perfusion of media.

Chapter 3: This chapter is an application of the technique introduced in the previous one in bone biology. In this study bone osteoblast cells are cultured in an environment with control over its

mechanical properties through changing the defining parameters of the technique, concentration of the hydrogel and the amount of crosslinker. Effect of different mechanical properties on trans-differentiation of osteoblasts to osteocytes is studied while only a thin layer of hydrogel on paper is used. Formation of a thin and uniform layer that can be handled without damaging it is not easily doable with most of the other bioprinting techniques and provides easy and constant monitoring of cells that have proper viability. Similar approaches can be taken to model other biological phenomenon.

Chapter 4: This chapter introduces a technique based on bioassembled collagenous grafts formed using PDMS molds. It meets the requirements of *in vitro* modeling of tissues and conditions that require much higher cell densities that cannot be achieved using bioprinting techniques. It is also more suitable for applications where smaller sizes of the constructs are needed to recreate the specific functions of cells that are meant to be studied. This technique can control positioning of the cells compared to each other to make complicated structures and shapes with clear tissue interfaces. Cells with different sources can be used with this technique while mechanical properties and compactness of the construct can be controlled. The process is very short and yields high viability.

Chapter 5: Here, technique in the previous chapter is used to study importance of cell positioning and controlled cross-talk between adipocyte and skeletal muscle cells in a coculture system. It is shown that cell positioning and physical contact between different cell types causes different effects as compared to when they only have paracrine effects on each other. Similar to the application of bioprinting technique, the same approach can be used to model many other biological phenomena.

Chapter 6: A more advanced version of the molding technique with the ability to provide cells with a dynamic environment is presented in this chapter. This technique uses the same concept but instead of PDMS molds, silicone tubing is used with stainless steel pins as anchors for the grafts form around them. They are also used to apply electrical and mechanical stimuli to the grafts. This improved version of the technique maintains all of the features of the original technique and adds the possibility of dynamicity.

Appendix 1: A new cell sheet engineering technique is introduced that creates 2D building blocks for cells that are fusogenic in an easy to implement setup that does not require specific equipment. These sheets are fully functional, preserve cell secreted ECM, and can be stacked to form thicker 3D structures for different applications

Appendix 2: The protocol introduced for the new cell sheet engineering is adopted and modified to create sheets with a coculture of skeletal muscle and adipocytes and by stacking them meat like structures that can potentially be used as a food source (lab-grown meat) are formed and evaluated.

7. Note to the reader

Images in Chapter 1 that are reused from other works have been adapted with permission from their publications. Chapters 2 to 6 are published with permission from their respective journals.

8. References

1. Zhang, B., et al., *Advances in organ-on-a-chip engineering.* Nature Reviews Materials, 2018. **3**(8): p. 257-278.
2. U. S. Food, D., Administration. *Innovation or Stagnation : Challenge and Opportunity on the Critical Path to New Medical Products*. http://www.fda.gov/ScienceResearch/SpecialTopics/CriticalPathInitiative/default.htm 2004 2004; Available from: https://ci.nii.ac.jp/naid/10029432449/en/.
3. Langhans, S.A., *Three-Dimensional in Vitro Cell Culture Models in Drug Discovery and Drug Repositioning.* Front Pharmacol, 2018. **9**: p. 6.
4. Sivaraman, A., et al., *A microscale in vitro physiological model of the liver: predictive screens for drug metabolism and enzyme induction.* Curr Drug Metab, 2005. **6**(6): p. 569-91.
5. Rangarajan, A., et al., *Species- and cell type-specific requirements for cellular transformation.* Cancer Cell, 2004. **6**(2): p. 171-83.
6. Griffith, L.G. and M.A. Swartz, *Capturing complex 3D tissue physiology in vitro.* Nat Rev Mol Cell Biol, 2006. **7**(3): p. 211-24.
7. Benien, P. and A. Swami, *3D tumor models: history, advances and future perspectives.* Future Oncol, 2014. **10**(7): p. 1311-27.
8. Carrel, A., *On the Permanent Life of Tissues Outside of the Organism.* J Exp Med, 1912. **15**(5): p. 516-28.
9. Moscona, A. and H. Moscona, *The dissociation and aggregation of cells from organ rudiments of the early chick embryo.* J Anat, 1952. **86**(3): p. 287-301.
10. Hoffman, R.M., *To do tissue culture in two or three dimensions? That is the question.* Stem Cells, 1993. **11**(2): p. 105-11.
11. Pampaloni, F., E.G. Reynaud, and E.H. Stelzer, *The third dimension bridges the gap between cell culture and live tissue.* Nat Rev Mol Cell Biol, 2007. **8**(10): p. 839-45.
12. Caddeo, S., M. Boffito, and S. Sartori, *Tissue Engineering Approaches in the Design of Healthy and Pathological In Vitro Tissue Models.* Front Bioeng Biotechnol, 2017. **5**: p. 40.
13. Wiesmann, H.P., et al., *Biophysical Stimulation of Cells and Tissues in Bioreactors*, in *Fundamentals of Tissue Engineering and Regenerative Medicine*, U. Meyer, et al., Editors. 2009, Springer Berlin Heidelberg: Berlin, Heidelberg. p. 633-646.
14. Baker, B.M. and C.S. Chen, *Deconstructing the third dimension: how 3D culture microenvironments alter cellular cues.* J Cell Sci, 2012. **125**(Pt 13): p. 3015-24.
15. Meyers, J., J. Craig, and D.J. Odde, *Potential for control of signaling pathways via cell size and shape.* Curr Biol, 2006. **16**(17): p. 1685-93.
16. Weaver, V.M., et al., *beta4 integrin-dependent formation of polarized three-dimensional architecture confers resistance to apoptosis in normal and malignant mammary epithelium.* Cancer Cell, 2002. **2**(3): p. 205-16.
17. Khetan, S. and J.A. Burdick, *Patterning network structure to spatially control cellular remodeling and stem cell fate within 3-dimensional hydrogels.* Biomaterials, 2010. **31**(32): p. 8228-34.
18. Benya, P.D. and J.D. Shaffer, *Dedifferentiated chondrocytes reexpress the differentiated collagen phenotype when cultured in agarose gels.* Cell, 1982. **30**(1): p. 215-24.
19. Edmondson, R., et al., *Three-dimensional cell culture systems and their applications in drug discovery and cell-based biosensors.* Assay Drug Dev Technol, 2014. **12**(4): p. 207-18.
20. Sebens, S. and H. Schafer, *The tumor stroma as mediator of drug resistance--a potential target to improve cancer therapy?* Curr Pharm Biotechnol, 2012. **13**(11): p. 2259-72.

21. Jensen, C. and Y. Teng, *Is It Time to Start Transitioning From 2D to 3D Cell Culture?* Front Mol Biosci, 2020. **7**: p. 33.
22. Muncie, J.M. and V.M. Weaver, *The Physical and Biochemical Properties of the Extracellular Matrix Regulate Cell Fate.* Curr Top Dev Biol, 2018. **130**: p. 1-37.
23. Jain, R.K., et al., *Engineering vascularized tissue.* Nat Biotechnol, 2005. **23**(7): p. 821-3.
24. Pathak, A. and S. Kumar, *Biophysical regulation of tumor cell invasion: moving beyond matrix stiffness.* Integr Biol (Camb), 2011. **3**(4): p. 267-78.
25. Hove, J.R., et al., *Intracardiac fluid forces are an essential epigenetic factor for embryonic cardiogenesis.* Nature, 2003. **421**(6919): p. 172-7.
26. Kulesa, P.M. and S.E. Fraser, *Cell dynamics during somite boundary formation revealed by time-lapse analysis.* Science, 2002. **298**(5595): p. 991-5.
27. Thery, M., *Micropatterning as a tool to decipher cell morphogenesis and functions.* J Cell Sci, 2010. **123**(Pt 24): p. 4201-13.
28. Laurent, J., et al., *Convergence of microengineering and cellular self-organization towards functional tissue manufacturing.* Nat Biomed Eng, 2017. **1**(12): p. 939-956.
29. Ergir, E., et al., *Small Force, Big Impact: Next Generation Organ-on-a-Chip Systems Incorporating Biomechanical Cues.* Front Physiol, 2018. **9**: p. 1417.
30. Park, S.H., et al., *Chip-based comparison of the osteogenesis of human bone marrow- and adipose tissue-derived mesenchymal stem cells under mechanical stimulation.* PLoS One, 2012. **7**(9): p. e46689.
31. Sticker, D., et al., *Microfluidic Migration and Wound Healing Assay Based on Mechanically Induced Injuries of Defined and Highly Reproducible Areas.* Anal Chem, 2017. **89**(4): p. 2326-2333.
32. Tobita, K., et al., *Engineered early embryonic cardiac tissue retains proliferative and contractile properties of developing embryonic myocardium.* Am J Physiol Heart Circ Physiol, 2006. **291**(4): p. H1829-37.
33. Guan, J., et al., *The stimulation of the cardiac differentiation of mesenchymal stem cells in tissue constructs that mimic myocardium structure and biomechanics.* Biomaterials, 2011. **32**(24): p. 5568-80.
34. Nieponice, A., et al., *Mechanical stimulation induces morphological and phenotypic changes in bone marrow-derived progenitor cells within a three-dimensional fibrin matrix.* J Biomed Mater Res A, 2007. **81**(3): p. 523-30.
35. Rutkowski, J.M. and M.A. Swartz, *A driving force for change: interstitial flow as a morphoregulator.* Trends Cell Biol, 2007. **17**(1): p. 44-50.
36. Jeon, J.S., et al., *Generation of 3D functional microvascular networks with human mesenchymal stem cells in microfluidic systems.* Integr Biol (Camb), 2014. **6**(5): p. 555-63.
37. Kim, S., M. Chung, and N.L. Jeon, *Three-dimensional biomimetic model to reconstitute sprouting lymphangiogenesis in vitro.* Biomaterials, 2016. **78**: p. 115-28.
38. Rothbauer, M., H. Zirath, and P. Ertl, *Recent advances in microfluidic technologies for cell-to-cell interaction studies.* Lab Chip, 2018. **18**(2): p. 249-270.
39. Xing, J., et al., *Surface chemistry modulates osteoblasts sensitivity to low fluid shear stress.* J Biomed Mater Res A, 2014. **102**(11): p. 4151-60.
40. Balint, R., N.J. Cassidy, and S.H. Cartmell, *Electrical stimulation: a novel tool for tissue engineering.* Tissue Eng Part B Rev, 2013. **19**(1): p. 48-57.
41. MacGinitie, L.A., D.D. Wu, and G.V. Cochran, *Streaming potentials in healing, remodeling, and intact cortical bone.* J Bone Miner Res, 1993. **8**(11): p. 1323-35.
42. Huang, C.P., X.M. Chen, and Z.Q. Chen, *Osteocyte: the impresario in the electrical stimulation for bone fracture healing.* Med Hypotheses, 2008. **70**(2): p. 287-90.

43. van Duinen, V., et al., *Microfluidic 3D cell culture: from tools to tissue models.* Curr Opin Biotechnol, 2015. **35**: p. 118-26.
44. Groll, J., et al., *Biofabrication: reappraising the definition of an evolving field.* Biofabrication, 2016. **8**(1): p. 013001.
45. Moroni, L., et al., *Biofabrication: A Guide to Technology and Terminology.* Trends Biotechnol, 2018. **36**(4): p. 384-402.
46. Ouyang, L., et al., *Assembling Living Building Blocks to Engineer Complex Tissues.* Advanced Functional Materials, 2020. **n/a**(n/a): p. 1909009.
47. Nichol, J.W. and A. Khademhosseini, *Modular Tissue Engineering: Engineering Biological Tissues from the Bottom Up.* Soft Matter, 2009. **5**(7): p. 1312-1319.
48. Moroni, L., et al., *Biofabrication strategies for 3D in vitro models and regenerative medicine.* Nat Rev Mater, 2018. **3**(5): p. 21-37.
49. Zhang, Y.P., J. Sun, and Y. Ma, *Biomanufacturing: history and perspective.* J Ind Microbiol Biotechnol, 2017. **44**(4-5): p. 773-784.
50. Pati, F., J. Gantelius, and H.A. Svahn, *3D Bioprinting of Tissue/Organ Models.* Angew Chem Int Ed Engl, 2016. **55**(15): p. 4650-65.
51. Ho, W.J., et al., *Incorporation of multicellular spheroids into 3-D polymeric scaffolds provides an improved tumor model for screening anticancer drugs.* Cancer Sci, 2010. **101**(12): p. 2637-43.
52. Hull Charles, W., *Apparatus For Production Of Three-dimensional Objects By Stereolithography*. 1986, UVP INC: US.
53. Nakamura, M., et al., *Biomatrices and biomaterials for future developments of bioprinting and biofabrication.* Biofabrication, 2010. **2**(1): p. 014110.
54. Zhang, Y.S., et al., *Three-Dimensional Bioprinting Strategies for Tissue Engineering.* Cold Spring Harb Perspect Med, 2018. **8**(2).
55. Murphy, S.V. and A. Atala, *3D bioprinting of tissues and organs.* Nat Biotechnol, 2014. **32**(8): p. 773-85.
56. Davoodi, E., et al., *Extrusion and Microfluidic-Based Bioprinting to Fabricate Biomimetic Tissues and Organs.* Advanced Materials Technologies, 2020. **n/a**(n/a): p. 1901044.
57. Ke, D. and S.V. Murphy, *Current Challenges of Bioprinted Tissues Toward Clinical Translation.* Tissue Eng Part B Rev, 2019. **25**(1): p. 1-13.
58. Lee, A., et al., *3D bioprinting of collagen to rebuild components of the human heart.* Science, 2019. **365**(6452): p. 482-487.
59. Ma, X., et al., *3D bioprinting of functional tissue models for personalized drug screening and in vitro disease modeling.* Adv Drug Deliv Rev, 2018. **132**: p. 235-251.
60. Kolesky, D.B., et al., *Three-dimensional bioprinting of thick vascularized tissues.* Proc Natl Acad Sci U S A, 2016. **113**(12): p. 3179-84.
61. Miller, J.S., et al., *Rapid casting of patterned vascular networks for perfusable engineered three-dimensional tissues.* Nat Mater, 2012. **11**(9): p. 768-74.
62. Gao, Q., et al., *Coaxial nozzle-assisted 3D bioprinting with built-in microchannels for nutrients delivery.* Biomaterials, 2015. **61**: p. 203-15.
63. Attalla, R., et al., *3D bioprinting of heterogeneous bi- and tri-layered hollow channels within gel scaffolds using scalable multi-axial microfluidic extrusion nozzle.* Biofabrication, 2018. **11**(1): p. 015012.
64. Ma, X., et al., *Deterministically patterned biomimetic human iPSC-derived hepatic model via rapid 3D bioprinting.* Proc Natl Acad Sci U S A, 2016. **113**(8): p. 2206-11.
65. Bhise, N.S., et al., *A liver-on-a-chip platform with bioprinted hepatic spheroids.* Biofabrication, 2016. **8**(1): p. 014101.

66. Park, J.H., et al., *Current advances in three-dimensional tissue/organ printing.* Tissue Engineering and Regenerative Medicine, 2016. **13**(6): p. 612-621.
67. Mosadegh, B., et al., *Three-dimensional paper-based model for cardiac ischemia.* Adv Healthc Mater, 2014. **3**(7): p. 1036-43.
68. Ma, Z., et al., *Three-dimensional filamentous human diseased cardiac tissue model.* Biomaterials, 2014. **35**(5): p. 1367-77.
69. Koch, L., et al., *Skin tissue generation by laser cell printing.* Biotechnol Bioeng, 2012. **109**(7): p. 1855-63.
70. Kim, B.S., et al., *3D cell printing of in vitro stabilized skin model and in vivo pre-vascularized skin patch using tissue-specific extracellular matrix bioink: A step towards advanced skin tissue engineering.* Biomaterials, 2018. **168**: p. 38-53.
71. Ling, K., et al., *Bioprinting-Based High-Throughput Fabrication of Three-Dimensional MCF-7 Human Breast Cancer Cellular Spheroids.* Engineering, 2015. **1**(2): p. 269-274.
72. Xu, F., et al., *A three-dimensional in vitro ovarian cancer coculture model using a high-throughput cell patterning platform.* Biotechnol J, 2011. **6**(2): p. 204-212.
73. Lee, W.G., U. Demirci, and A. Khademhosseini, *Microscale electroporation: challenges and perspectives for clinical applications.* Integr Biol (Camb), 2009. **1**(3): p. 242-51.
74. Lozano, R., et al., *3D printing of layered brain-like structures using peptide modified gellan gum substrates.* Biomaterials, 2015. **67**: p. 264-73.
75. Mohammadi, M.H., et al., *Engineered Muscle Tissues for Disease Modeling and Drug Screening Applications.* Curr Pharm Des, 2017. **23**(20): p. 2991-3004.
76. Mozetic, P., et al., *Engineering muscle cell alignment through 3D bioprinting.* J Biomed Mater Res A, 2017. **105**(9): p. 2582-2588.
77. Zhu, K., et al., *Gold Nanocomposite Bioink for Printing 3D Cardiac Constructs.* Adv Funct Mater, 2017. **27**(12).
78. Jang, J., et al., *3D printed complex tissue construct using stem cell-laden decellularized extracellular matrix bioinks for cardiac repair.* Biomaterials, 2017. **112**: p. 264-274.
79. Skardal, A., J. Zhang, and G.D. Prestwich, *Bioprinting vessel-like constructs using hyaluronan hydrogels crosslinked with tetrahedral polyethylene glycol tetracrylates.* Biomaterials, 2010. **31**(24): p. 6173-81.
80. Zhang, Y., et al., *Characterization of printable cellular micro-fluidic channels for tissue engineering.* Biofabrication, 2013. **5**(2): p. 025004.
81. Shim, J.-H., et al., *Bioprinting of a mechanically enhanced three-dimensional dual cell-laden construct for osteochondral tissue engineering using a multi-head tissue/organ building system.* Journal of Micromechanics and Microengineering, 2012. **22**(8): p. 085014.
82. Admane, P., et al., *Direct 3D bioprinted full-thickness skin constructs recapitulate regulatory signaling pathways and physiology of human skin.* Bioprinting, 2019. **15**: p. e00051.
83. Jorgensen, A.M., et al., *Bioprinted Skin Recapitulates Normal Collagen Remodeling in Full-Thickness Wounds.* Tissue Eng Part A, 2020. **26**(9-10): p. 512-526.
84. Kato-Negishi, M., et al., *Rod-Shaped Neural Units for Aligned 3D Neural Network Connection.* Adv Healthc Mater, 2017. **6**(15).
85. Onoe, H., et al., *Metre-long cell-laden microfibres exhibit tissue morphologies and functions.* Nat Mater, 2013. **12**(6): p. 584-90.
86. Gantumur, E., et al., *Inkjet micropatterning through horseradish peroxidase-mediated hydrogelation for controlled cell immobilization and microtissue fabrication.* Biofabrication, 2019. **12**(1): p. 011001.
87. Mubyana, K. and D.T. Corr, *Cyclic Uniaxial Tensile Strain Enhances the Mechanical Properties of Engineered, Scaffold-Free Tendon Fibers.* Tissue Eng Part A, 2018.

88. Akkouch, A., Y. Yu, and I.T. Ozbolat, *Microfabrication of scaffold-free tissue strands for three-dimensional tissue engineering.* Biofabrication, 2015. **7**(3): p. 031002.
89. Yu, Y., et al., *Three-dimensional bioprinting using self-assembling scalable scaffold-free "tissue strands" as a new bioink.* Sci Rep, 2016. **6**: p. 28714.
90. Lee, J.M. and W.Y. Yeong, *Design and Printing Strategies in 3D Bioprinting of Cell-Hydrogels: A Review.* Adv Healthc Mater, 2016. **5**(22): p. 2856-2865.
91. Liu, W., et al., *Rapid Continuous Multimaterial Extrusion Bioprinting.* Adv Mater, 2017. **29**(3).
92. Holzl, K., et al., *Bioink properties before, during and after 3D bioprinting.* Biofabrication, 2016. **8**(3): p. 032002.
93. Goyanes, A., et al., *3D Printing of Medicines: Engineering Novel Oral Devices with Unique Design and Drug Release Characteristics.* Mol Pharm, 2015. **12**(11): p. 4077-84.
94. Trujillo-de Santiago, G., et al., *Chaotic printing: using chaos to fabricate densely packed micro- and nanostructures at high resolution and speed.* Materials Horizons, 2018. **5**(5): p. 813-822.
95. Sousa, A.R., et al., *One-Step Rapid Fabrication of Cell-Only Living Fibers.* Adv Mater, 2020. **32**(2): p. e1906305.
96. Yamato, M., et al., *Thermo-responsive culture dishes allow the intact harvest of multilayered keratinocyte sheets without dispase by reducing temperature.* Tissue Eng, 2001. **7**(4): p. 473-80.
97. Iwata, T., M. Yamato, and T. Okano, *Chapter 29 - Intelligent Surfaces for Cell-Sheet Engineering*, in *Principles of Regenerative Medicine (Second Edition)*, A. Atala, et al., Editors. 2011, Academic Press: San Diego. p. 517-527.
98. Owaki, T., et al., *Cell sheet engineering for regenerative medicine: current challenges and strategies.* Biotechnol J, 2014. **9**(7): p. 904-14.
99. Haraguchi, Y., et al., *Fabrication of functional three-dimensional tissues by stacking cell sheets in vitro.* Nat Protoc, 2012. **7**(5): p. 850-8.
100. Tadakuma, K., et al., *A device for the rapid transfer/transplantation of living cell sheets with the absence of cell damage.* Biomaterials, 2013. **34**(36): p. 9018-25.
101. Hirose, M., et al., *Creation of designed shape cell sheets that are noninvasively harvested and moved onto another surface.* Biomacromolecules, 2000. **1**(3): p. 377-81.
102. Hirschhaeuser, F., et al., *Multicellular tumor spheroids: an underestimated tool is catching up again.* J Biotechnol, 2010. **148**(1): p. 3-15.
103. Frimat, J.P., et al., *Plasma stencilling methods for cell patterning.* Anal Bioanal Chem, 2009. **395**(3): p. 601-9.
104. Nakazawa, K., Y. Izumi, and R. Mori, *Morphological and functional studies of rat hepatocytes on a hydrophobic or hydrophilic polydimethylsiloxane surface.* Acta Biomater, 2009. **5**(2): p. 613-20.
105. Rago, A.P., D.M. Dean, and J.R. Morgan, *Controlling cell position in complex heterotypic 3D microtissues by tissue fusion.* Biotechnol Bioeng, 2009. **102**(4): p. 1231-41.
106. Livoti, C.M. and J.R. Morgan, *Self-assembly and tissue fusion of toroid-shaped minimal building units.* Tissue Eng Part A, 2010. **16**(6): p. 2051-61.
107. Caliari, S.R. and J.A. Burdick, *A practical guide to hydrogels for cell culture.* Nat Methods, 2016. **13**(5): p. 405-14.
108. Cui, X., Y. Hartanto, and H. Zhang, *Advances in multicellular spheroids formation.* J R Soc Interface, 2017. **14**(127).
109. Lin, R.Z. and H.Y. Chang, *Recent advances in three-dimensional multicellular spheroid culture for biomedical research.* Biotechnol J, 2008. **3**(9-10): p. 1172-84.
110. McGuigan, A.P., et al., *Cell Encapsulation in Sub-mm Sized Gel Modules Using Replica Molding.* PloS one, 2008. **3**(7).
111. Sodunke, T.R., et al., *Micropatterns of Matrigel for three-dimensional epithelial cultures.* Biomaterials, 2007. **28**(27): p. 4006-16.

112. Khademhosseini, A., et al., *Micromolding of photocrosslinkable hyaluronic acid for cell encapsulation and entrapment.* J Biomed Mater Res A, 2006. **79**(3): p. 522-32.
113. Yeh, J., et al., *Micromolding of shape-controlled, harvestable cell-laden hydrogels.* Biomaterials, 2006. **27**(31): p. 5391-8.
114. Achilli, T.M., J. Meyer, and J.R. Morgan, *Advances in the formation, use and understanding of multi-cellular spheroids.* Expert Opin Biol Ther, 2012. **12**(10): p. 1347-60.
115. Napolitano, A.P., et al., *Dynamics of the self-assembly of complex cellular aggregates on micromolded nonadhesive hydrogels.* Tissue Eng, 2007. **13**(8): p. 2087-94.
116. Li, M. and J.C. Izpisua Belmonte, *Organoids - Preclinical Models of Human Disease.* N Engl J Med, 2019. **380**(6): p. 569-579.
117. Fatehullah, A., S.H. Tan, and N. Barker, *Organoids as an in vitro model of human development and disease.* Nature Cell Biology, 2016. **18**(3): p. 246-254.
118. Yin, X., et al., *Engineering Stem Cell Organoids.* Cell Stem Cell, 2016. **18**(1): p. 25-38.
119. Bakirci, E., et al., *Cell sheet based bioink for 3D bioprinting applications.* Biofabrication, 2017. **9**(2): p. 024105.
120. Morimoto, Y., A.Y. Hsiao, and S. Takeuchi, *Point-, line-, and plane-shaped cellular constructs for 3D tissue assembly.* Adv Drug Deliv Rev, 2015. **95**: p. 29-39.
121. Matsunaga, Y.T., Y. Morimoto, and S. Takeuchi, *Molding cell beads for rapid construction of macroscopic 3D tissue architecture.* Adv Mater, 2011. **23**(12): p. H90-4.
122. Luo, H., et al., *Fabrication of viable centimeter-sized 3D tissue constructs with microchannel conduits for improved tissue properties through assembly of cell-laden microbeads.* J Tissue Eng Regen Med, 2014. **8**(6): p. 493-504.
123. Sutherland, R.M., *Cell and environment interactions in tumor microregions: the multicell spheroid model.* Science, 1988. **240**(4849): p. 177-84.
124. van den Brand, D., et al., *Mimicking Tumors: Toward More Predictive In Vitro Models for Peptide- and Protein-Conjugated Drugs.* Bioconjug Chem, 2017. **28**(3): p. 846-856.
125. Nath, S. and G.R. Devi, *Three-dimensional culture systems in cancer research: Focus on tumor spheroid model.* Pharmacol Ther, 2016. **163**: p. 94-108.
126. Kern, J., et al., *Vasohibin inhibits angiogenic sprouting in vitro and supports vascular maturation processes in vivo.* BMC Cancer, 2009. **9**: p. 284.
127. Polonchuk, L., et al., *Cardiac spheroids as promising in vitro models to study the human heart microenvironment.* Sci Rep, 2017. **7**(1): p. 7005.
128. Shri, M., et al., *Hanging Drop, A Best Three-Dimensional (3D) Culture Method for Primary Buffalo and Sheep Hepatocytes.* Sci Rep, 2017. **7**(1): p. 1203.
129. Moors, M., et al., *Human neurospheres as three-dimensional cellular systems for developmental neurotoxicity testing.* Environ Health Perspect, 2009. **117**(7): p. 1131-8.
130. Harma, V., et al., *A comprehensive panel of three-dimensional models for studies of prostate cancer growth, invasion and drug responses.* PLoS One, 2010. **5**(5): p. e10431.
131. Lee, B.H., et al., *Modulation of Huh7.5 spheroid formation and functionality using modified PEG-based hydrogels of different stiffness.* PLoS One, 2015. **10**(2): p. e0118123.
132. Matano, M., et al., *Modeling colorectal cancer using CRISPR-Cas9-mediated engineering of human intestinal organoids.* Nat Med, 2015. **21**(3): p. 256-62.
133. Schlaermann, P., et al., *A novel human gastric primary cell culture system for modelling Helicobacter pylori infection in vitro.* Gut, 2016. **65**(2): p. 202-213.
134. Meng, Q., *Three-dimensional culture of hepatocytes for prediction of drug-induced hepatotoxicity.* Expert Opin Drug Metab Toxicol, 2010. **6**(6): p. 733-46.
135. Lancaster, M.A., et al., *Cerebral organoids model human brain development and microcephaly.* Nature, 2013. **501**(7467): p. 373-9.

136. Takahashi, H., T. Shimizu, and T. Okano, *Chapter 28 - Intelligent Surfaces for Cell Sheet Engineering*, in *Principles of Regenerative Medicine (Third Edition)*, A. Atala, et al., Editors. 2019, Academic Press: Boston. p. 469-484.
137. Kim, K., et al., *Fabrication of functional 3D hepatic tissues with polarized hepatocytes by stacking endothelial cell sheets in vitro.* J Tissue Eng Regen Med, 2017. **11**(7): p. 2071-2080.
138. Ito, A., et al., *Novel methodology for fabrication of tissue-engineered tubular constructs using magnetite nanoparticles and magnetic force.* Tissue Eng, 2005. **11**(9-10): p. 1553-61.
139. Bourland, J., J. Fradette, and F.A. Auger, *Tissue-engineered 3D melanoma model with blood and lymphatic capillaries for drug development.* Scientific Reports, 2018. **8**(1): p. 13191.
140. Ngo, T.X., et al., *Endothelial cell behavior inside myoblast sheets with different thickness.* Biotechnol Lett, 2013. **35**(7): p. 1001-8.
141. Nagamori, E., et al., *Network formation through active migration of human vascular endothelial cells in a multilayered skeletal myoblast sheet.* Biomaterials, 2013. **34**(3): p. 662-8.
142. Rogers, A.J., et al., *Hemodynamic Stimulation Using the Biomimetic Cardiac Tissue Model (BCTM) Enhances Maturation of Human Induced Pluripotent Stem Cell-Derived Cardiomyocytes.* Cells Tissues Organs, 2018. **206**(1-2): p. 82-94.
143. Agrawal, G., A. Aung, and S. Varghese, *Skeletal muscle-on-a-chip: an in vitro model to evaluate tissue formation and injury.* Lab Chip, 2017. **17**(20): p. 3447-3461.
144. Vandenburgh, H., et al., *Drug-screening platform based on the contractility of tissue-engineered muscle.* Muscle Nerve, 2008. **37**(4): p. 438-47.
145. Uzel, S.G., et al., *Microfluidic device for the formation of optically excitable, three-dimensional, compartmentalized motor units.* Sci Adv, 2016. **2**(8): p. e1501429.
146. Osaki, T., S.G.M. Uzel, and R.D. Kamm, *Microphysiological 3D model of amyotrophic lateral sclerosis (ALS) from human iPS-derived muscle cells and optogenetic motor neurons.* Sci Adv, 2018. **4**(10): p. eaat5847.
147. Nunes, S.S., et al., *Biowire: a platform for maturation of human pluripotent stem cell-derived cardiomyocytes.* Nat Methods, 2013. **10**(8): p. 781-7.
148. Xiao, Y., et al., *Microfabricated perfusable cardiac biowire: a platform that mimics native cardiac bundle.* Lab Chip, 2014. **14**(5): p. 869-82.
149. Miklas, J.W., et al., *Bioreactor for modulation of cardiac microtissue phenotype by combined static stretch and electrical stimulation.* Biofabrication, 2014. **6**(2): p. 024113.
150. Lind, J.U., et al., *Instrumented cardiac microphysiological devices via multimaterial three-dimensional printing.* Nat Mater, 2017. **16**(3): p. 303-308.
151. Portan, D.V., et al., *Combined Optimized Effect of a Highly Self-Organized Nanosubstrate and an Electric Field on Osteoblast Bone Cells Activity.* Biomed Res Int, 2019. **2019**: p. 7574635.
152. Qi, Z., et al., *Combined treatment with electrical stimulation and insulin-like growth factor-1 promotes bone regeneration in vitro.* PLoS One, 2018. **13**(5): p. e0197006.

Chapter 2: BIOPRINTING TECHNIQUE

ExCeL: Combining Extrusion Printing on Cellulose Scaffolds with Lamination to Create *In Vitro* Biological Models

Alireza Shahin-Shamsabadi[1], P. Ravi Selvaganapathy [1,2,*]

[1] School of Biomedical Engineering, McMaster University, Canada

[2] Department of Mechanical Engineering, McMaster University, Canada

[*] Corresponding Author: P. Ravi Selvaganapathy, Department of Mechanical Engineering, McMaster University, Canada

Status: Published

Full Citation:

Shahin-Shamsabadi, Alireza, and P. Ravi Selvaganapathy. "ExCeL: combining extrusion printing on cellulose scaffolds with lamination to create in vitro biological models." Biofabrication 11.3 (2019): 035002.

Abstract

Bioprinting is rapidly developing to be a powerful tool in tissue engineering for both whole tissue printing and development of *in vitro* models that can be used in drug discovery, toxicology and as *in vitro* bioreactors. Nevertheless, the ability to create complex 3D culture systems with different types of cells and extracellular matrices integrated with perfusable channels has been a challenge. Here we develop an approach that combines xurography of a scaffold material (cellulose) with extrusion printing of bioinks on it, followed by assembly in a layer by layer fashion to create complex 3D culture systems that could be used as *in vitro* models of biological processes. This new method, termed as **ExCeL** can recapitulate the complexities of natural tissues with proper 3D distribution of cells, ECMs, and different molecules while providing the whole structure with mechanical stability, direct and easy access to the cells, even the ones that are positioned deep in to the bulk of the structure, without the need to fix or section the samples. Briefly, bioprinting of predefined patterns with feature size of ~1 mm has been made possible by treating paper with the hydrogel's crosslinker and printing cell embedded hydrogel that will solidify immediately upon contact with the paper. These impregnated layers can be used as single layers or in a layer-by-layer approach by stacking them (here up to 4 layers) for applications such as cell migration and proliferation in 3D structures composed of collagen or alginate. The cells response to exposure to different FBS amounts was also assessed. By cutting the paper in certain patterns, printing hydrogel on the rest of it, and stacking them, features like embedded channels could be formed that will provide cells will better mass transfer in thick structures. This technique provides biologists with a unique tool to perform sophisticated *in vitro* assays.

Keywords: 3D Bioprinting; Chromatography Paper; Xurography; Layer-by-layer Approach; 3D *In Vitro* Model

1. Introduction

Although the ultimate goal of tissue engineering is to create functional tissues and organs using cells and natural scaffolds, considerable effort has been directed towards the development of tissue mimics that are not meant to be implanted inside the body but rather used *in vitro* to facilitate understanding human physiology or disease processes for applications such as basic or diagnostic research [1, 2]. The ability to model normal or diseased tissues made of human cells and expose them to different conditions like drug candidates has the potential to make medical investigations like drug discovery faster and more efficient [3]. Although flat, 2D culture systems are dominant and have been used for over a century, growing evidence suggests that under some conditions their results do not represent *in vivo* responses accurately [4]. This is mostly because of the dimensional limitations of these systems and lack of environmental cues that cells receive in physiological environment [5]. For example, there isn't any nutrient and oxygen gradient in these systems and cells cannot grow on top of each other which changes their morphology and inter-cellular contact [6]. As a result of these differences, when 2D systems are used as models of drug development, a significant failure rate is reported [7].

Recently, 3D systems have been developed that can recapitulate some of the cellular and compositional distribution of ECMs in 3D and therefore yield more accurate responses akin to natural tissues [3]. Compared to 2D cell culture systems, these 3D models can maintain the phenotype of cells [8] by controlling the polarity of cell-cell and cell-matrix contacts [9, 10], as well as mechanical properties of their environment [11, 12] and transport characteristics of important soluble growth factors [1]. The various 3D cell culture systems can be categorized into scaffold-based, which use a wide variety of synthetic or natural biomaterials as ECM, as well as scaffold-free techniques that rely on the cells forming their own ECM [13, 14]. Despite these

improvements, many of the methods used to fabricate the 3D models are time consuming, require specialized instruments and are still incapable of mimicking natural conditions accurately [15]. Some of these techniques have limitations in accurately recreating complex 3D geometries and compositions, scaling up, ability to handle samples after printing, or to extract cells from them for further analysis post culture [6]. For a 3D model to be accurate it should exhibit the architectural complexities of native tissues and bioprinting has emerged as a promising technique [16, 17] for this purpose. Bioprinting evolved from additive manufacturing methods which were developed more than 40 years ago as a rapid prototyping method to physically recreate shape and structure of a 3D computer model and initially used plastics, metals or ceramics [18, 19]. Later, these techniques were adapted for use with soft materials, gels and extracellular matrices which could support growth of cells and formation of tissue like constructs [20, 21]. Bioprinting, has enabled researchers to manufacture complex structures and constructs with biomaterials containing extracellular matrices and cells, sometimes with integrated perfusion networks for the purposes of drug discovery [22, 23] and tissue engineering [21, 24].

Among all of the 3D cell culture techniques, bioprinting is most suited to recapitulate biophysical and biochemical microenvironments in physiological or pathological conditions in a well-defined manner with high accuracy [16, 25, 26]. These multicellular environments together with realistic architectural features can be used in disease studies and drug screening [16] and if combined with patient derived cells they can have applications in personalized medicine [27]. Examples of applications of bioprinting in tissue and disease models includes but not limited to cardiovascular tissue [28, 29], skin [30, 31], cancer models [32, 33], and neuronal system [34, 35].

A variety of bioprinting approaches including inkjet printing, extrusion, layer by layer lamination, or stereolithography have been developed. Among them, extrusion-based techniques are

considered as the simplest and most convenient method with homogenous cell distribution and suitable cell viability [36, 37]. Despite their potential, bioprinting techniques still suffer from limitations including, inability to print thicker structures as in the case of ink-jet printing [36, 38] or are limited to a single bio-ink such as in stereolithography [36, 39]. Moreover, the lack of structural strength of many natural ECMs make construction of 3D structures solely from them difficult. Often a structural scaffolding material is added. For instance, a simple approach where stacked paper scaffolds (as structural scaffold) soaked in cell laden hydrogels have been used as to create oxygen concentration gradient is one example [15, 40]. Nevertheless, this method still does not have the ability to incorporate multiple ECMs or cell types with predefined patterns nor does it allow integration of perfusion channels that are critical in maintaining appropriate conditions for cell growth in the bulk. However, by using paper as a structural scaffold and combining it with bioprinting for precise distribution of ECMs and cells on it, one could create complex biomaterial patterns that could mimic the natural tissue compositions.

In the current study, we combine extrusion printing with layer by layer lamination to develop a new technique (termed ExCeL) to create complex 3D architectures that are difficult or expensive to create otherwise, using simple tools. The extrusion printing on a paper scaffold is used to create any designed pattern of cell and ECM loading on a single layer. Xurographic cutting of the scaffold is used to create perfusion channels in these layers. Finally, layer by layer lamination is used to extend the geometry to 3D. Using this approach and combining different cell types, hydrogels as ECMs, and xurographic patterns, and any configuration of 3D construct that mimic complex geometries and perfusion networks of natural tissues could potentially be constructed.

2. Design of the ExCeL process

The **ExCeL** process (shown in Figure 1) starts by pretreating the paper (Whatman® cellulose chromatography papers, Grade 1 Chr) with the hydrogel's crosslinker (in this case calcium (Ca) as the crosslinker of the sodium alginate) (Figure 1a). In order to create 2D patterned structures, hydrogel precursors (such as alginate) are then printed (Figure 1b) which leads to rapid crosslinking once the precursor wicks into the crosslinker soaked paper. Using an extrusion printer various spatial patterns such as a pixelated one or a ring shaped one as shown in Figure 1c with different type of cells embedded in them is printed. In order to create 3D structures, the pretreated cellulose sheets are cut using automated cutters in the desired patterns that constitute the perfusion channels, inlets, outlets and other features in the 3D structure. Next, hydrogels with different type of cells embedded in them are printed on paper in predefined patterns that reconstitute the biological complexity of a single layer of the final desired 3D structure. Finally, the individually printed layers are stacked one on top of another and allowed to bond with each other to create the final 3D structure. By cutting the paper with different patterns and stacking them properly, perfusable channels will form that provide the proper nutrient and oxygen distribution. Since the hydrogel is crosslinked immediately upon touching the paper that has its crosslinker on it and won't spread uncontrollably the need for other steps such as wax printing to confine the hydrogel is eliminated. By printing cells in different patterns and then stacking layers containing different patterns with proper aligning, 3D structures with higher thicknesses and proper support of cellular viability can be formed and used as *in vitro* models. These layers can also be destacked to have direct access to live cells on each layer. Hydrogels printed on only one layer of the paper could also allow easier handling of thin layers of hydrogel that aren't mechanically stable.

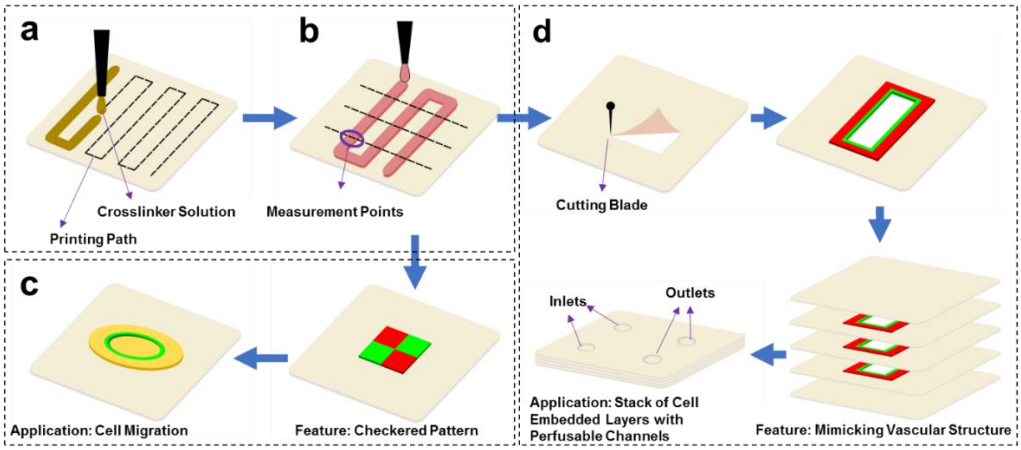

Figure 1. a) Printing calcium solution on paper that allows its uniform distribution (lines in the depicted path are 5 mm apart); **b)** Evaluation of printing resolution by printing 10 mm apart hydrogel lines and measuring thickness in different locations; **c)** Printing thin layers of hydrogel with different types of cells embedded in them with high resolution for applications such as cell migration assays; d) fabrication of 3d structures by cutting the paper, printing different hydrogels with different cells surrounding cut area, and stacking layers. This allows to mimic blood vessel like structures that are perfusable.

3. Materials and Methods

3.1. ExCeL Bioprinting

For bioprinting purposes an open source plastic 3D printer (MK2S, Prusa Inc) was modified. A holder was designed to replace the printhead with a stainless-steel needle as the printing nozzle. The needle was connected using tubing to a syringe attached to a syringe pump that enabled extrusion of its contents. The print bed had a vacuum port and appropriate holes that kept the paper on the stage by applying vacuum from below (Supplementary Figure 1). To pre-treat the chromatography paper (Whatman® 1 Chr, 0.180) with Ca as the crosslinker of the chosen hydrogel (Alginic Acid Sodium Salt-Sigma), two different calcium concentrations (0.1 and 1 M) were printed with different printing speeds (2000, 3000, and 4000 mm/min) on paper in a certain pattern with the flow rate of 0.5 mL/min (Figure 1a). After printing, sufficient time was given so that the Ca solution could penetrate to the whole paper and distribute uniformly. The printed paper was

kept at room temperature overnight in the sterile environment so that the excess water evaporated and then it was cut to desired patterns for further use. To find out the amount of calcium for each condition and to make sure they have uniform distributions, Energy-dispersive X-ray Spectroscopy (EDS) analysis was performed in each case in map mode. Based on the initial concentration of the used solution and the speed rates used, 4 different quantified concentrations (called High (H) (1 M and 2000 mm/min), Medium (M) (1 M and 3000 mm/min), Low (L) (1 M and 4000 mm/min), and very Low (vL) (0.1 M and 2000 mm/min)) were prepared for further use.

Different parameters effective on the printing resolution were studied: Ca content of the paper, gauge number of the needle, flow rate of the hydrogel from nozzle, and speed of the nozzle movement (feed rate). In all cases 2 wt% alginate was used. For the characterization purposes, a zigzag pattern was printed and immediately after printing pictures of three different locations of each line (top, middle, and bottom) were taken using a stereo microscope and thickness of the line was measured using ImageJ (Figure 1b). To study effect of printing layers of hydrogel on top of each other on the resolution, in the next step the same pattern was printed twice (double layer format) and characterization was performed the same as before. The distance between the tip of the nozzle and the paper for the first layer was kept constant at 0.5 mm and for printing more than one layer it was increase by 0.5 mm for each additional layer. Using these information three different situations were defined, “uniform” condition where the line had uniform thickness (less than 10% variation in thickness), “unstable” condition where the line wasn’t continuous, and “nonuniform” where the line wasn’t steady.

3.2.Viability Assessment

Effect of different steps in the process including the stress applied to the cells during the process and Ca concentration on cell viability was studied using designed protocols based on Alamar Blue

and Live/Dead assays (called ABA and LDA, respectively). Briefly, alginate was dissolved in DMEM culture media to reach the concentration of 2 wt%. 3T3 Fibroblast cells were cultured in DMEM supplemented with 10 wt% FBS. After reaching 90% confluence cells were trypsinized, counted, and gently mixed with alginate solution to create final concentration of 1×10^6 cells/mL. All 4 types of paper were cut using a Xurographic cutting machine (Silhouette®, Cameo) to the size of 6 well plates (diameter of 34 mm). A circle with diameter of 28 mm was printed with optimal printing condition found in previous section (0.5 mL/min, 1000 mm/min, gauge #18) on the center part of the paper in a double layer format. After printing, each sample was kept on the printing bed for 5 min to complete the crosslinking process, transferred to the wells, washed with phosphate buffered saline (PBS) solution to get rid of extra calcium on the paper, 2 mL of culture media was added to each well, and transferred to an incubator. Viability assays were performed 16 hrs later.

For ABA, culture media was replaced with 2 mL of new culture media supplemented with 0.1 M sodium tricitrate to help dissolve the alginate solution. The samples were transferred to incubator once again for 2 hours to allow citrate to dissolve alginate and the cells to attach to the paper. Culture media was changed with normal media to avoid any toxicity caused by excess citrate following by another 4 hours of incubation. Alamar Blue solution was added (10% V/V) to each well and incubated for 1.5 hrs. At the end, 100 µL samples of culture media in each well were transferred to a black 96 well-plate and reading was done at excitation and emission of 560 and 590 nm. Hydrogel samples printed without cells were used as control in each case and the same dissolving process was performed. Finally difference between fluorescence activity of each case with its control was reported.

For LDA, after 16 hrs of incubation culture media was aspirated and samples were washed with PBS twice. Because of the inherent auto-fluorescence of the paper, florescent reading was performed before staining using a plate reader at excitations and emissions of 485 and 530 nm for live and 530 and 645 for dead cells as control in multiple regions of the sample. Live/Dead staining of the samples were performed using Calcein/Ethidium homodimer kit following the instructions. After staining, samples were washed with PBS again and the same reading was performed. Pre-staining amounts were subtracted from post-staining readings and reported as final values.

3.3. Fabrication and Application in 2D and 3D

The ExCeL bioprinting technique was used to fabricate different features on a single layer or by cutting paper, printing patterns on multiple layers, and stacking them to fabricate multilayer features.

3.3.1. 2D Structures: Patterning of Cells and ECMs on Paper

To show the ability of the technique to print complex cellular structures on paper with acceptable accuracy without mixing and contamination of adjacent regions with each other, checkered patterns of cells were printed on paper. Solutions of 2 wt% alginate embedded with green fluorescent protein tagged 3T3s (gfp-3T3) and red fluorescent protein tagged human umbilical vein endothelial cells (rfp-HUVEC) were printed in a checkered pattern and images were taken using a ChemiDoc™ MP imaging system (Bio-Rad) and an upright microscope. Printing was performed using previously defined optimal conditions. Squares of 6 mm were printed that were 0.5 mm apart from each other (Figure 1c).

3.3.2. 2D Application: Cell Migration Evaluation

The 2D patterning feature of this bioprinting technique was used to study *in vitro* cell migration in 3D (thick gel layer) environment by printing on only one layer. vL paper was used; hydrogel with 10×10^6 cells/mL of gfp-3T3 cells were printed in a ring like structure with diameter of 6 mm. This ring was then embedded in a bigger circular area of alginate without any cells in it that filled both inside and outside area of the ring. The printed samples were transferred to 6 well-plates and culture media was replaced every 3 days. Images of the whole structure were taken every 3 days using ChemiDoc system and analyzed using MatLab image processing toolbox to measure migration of the cells toward inside and outside of the ring (MatLab code in Supplementary Information). To further study the effect of ECM type on cell migration, the same assay was performed but instead of embedding the ring in a circle of alginate, it was embedded in bovine collagen type I (Life Technologies) with concentration of 5 mg/mL and the same process was performed to measure cell migration. Effect of fetal bovine serum (FBS) content of media on migration speed was also studied by adding 5 %V/V and 10 %V/V FBS containing DMEM to samples of ring embedded in collagen.

3.3.3. 3D Structures: Layer by Layer Assembly of 2D Patterned Scaffolds

In order to demonstrate the ability to construct 3D structures, a perfusion channel with multicellular patterning was designed (Figure 1d). Channel designs with 2 mm width attached to inlet and outlet regions were cut into the Ca loaded paper layers to serve as the scaffold. Next, hydrogel was printed on paper but not inside the channels and layers of paper were stack to create a 3D structure in which channels were parallel to each other or crossed each other on different layers. To show these channels were perfusable without leaking, different solutions with different colors were perfused in each of the channels using a syringe pump. Patterned multicellular constructs were created by printing a layer of hydrogel with rfp-HUVEC cells in the regions of the

paper scaffold surrounding the channel structure and gfp-3T3 cells in the surrounding regions around to HUVEC cells. By stacking and aligning these bioprinted papers a 3D structure with channels were fabricated that resembled the natural distribution of the cells. To verify proper distribution of hydrogels and cells with distinguishable borders of cells without unintended mixing, images of fluorescent cells were taken using ChemiDoc system. To show the paper was able to support the hydrogel and prevent it from filling the channels, printed and stacked samples were flash-frozen and broken in half and images of the cross-section were taken.

3.3.4. 3D Application: Cell Viability in Stacked Layers and Effect of Channels

Importance of perfusable channels in a 3D structure on cell viability was studied by fabricating multilayer stacked structure of cells. Two parallel channels were cut on the paper scaffold. Then, hydrogel with 2×10^6 cells/mL (gfp-3T3 cells) was printed on the paper and these layers were stacked by proper aligning of the channels (called With Channel (WC) samples). The same hydrogel patterns were also made on scaffolds without channels (called Without Channel (WoC) samples) and were used for comparison. In each case, three layers of paper with channel structures and printed hydrogel on top of them were stacked and finally a last layer of paper, with inlets and outlets for WC samples, added on top to seal the whole structure. Samples were transferred to 6 well-plates and 2 mL culture media was added to each well and changed every two days. Culture media was also pipetted into the channels every 12 hrs in order to replace the media present inside them. To measure the proliferation of cells in each case, fluorescence intensity of the cells was measured every two days using a plate-reader in the center part of each sample and the change in their fluorescent intensity was compared to each other over time. To study effect of having channels on cell distribution, images of the samples were taken using ChemiDoc system and the number of cell clusters were measured using ImageJ. Live/Dead staining was also performed to

study the effect of channels on cellular viability. After staining was done, each layer with the hydrogel on top of it was carefully detached by applying a slight shear force and images of the middle layer that had the least access to the surrounding environment were taken using an upright microscope.

4. Results and Discussion

4.1. ExCeL Technique

The first step in the extrusion printing process on a single layer is the uniform printing of the cross-linking agent. This step is done to ensure that there are uniform amounts of cross-linking agent absorbed on the paper scaffold. The absorbed cross-linking agent was then used to instantaneously cross-link any subsequent gel precursor that is printed on top of it and prevent it from spreading within the paper scaffold. In the case of printing alginate gels, calcium chloride is used as the crosslinking agent. Although methods such as dip coating and soaking could be used, we found that extrusion printing of the cross-linking agent provided a robust method to uniformly deliver defined quantities of crosslinking agent across the entire paper scaffold. Using different molarities of Ca solutions (0.1 and 1 M) and different feed rates (2000, 3000, and 4000 mm/min) 4 different amounts of Ca was deposited on the paper.

In the next step alginate hydrogel was printed on paper which started crosslinking immediately upon contact due to the presence of the crosslinker on paper. This instantaneous crosslinking was crucial to preventing excessive spreading of the gel on the hydrophilic scaffold allowing high resolution of printing which is crucial for fabricating patterns with high complexities. When there was no crosslinker on the paper, the hydrogel spread quickly in either direction from the printed line due to the capillary forces from the paper matrix and a much broader feature size with diffused edges was obtained.

The amount of crosslinker on paper and its distribution could affect the resolution of printing and the viability of the cells. Therefore, paper scaffolds were printed with Ca inks at four different concentrations in a back and forth pattern as shown in Figure 1a. Elemental analysis on the printed paper scaffold was performed using EDS which showed that the Ca distribution was uniform in all cases and the amount of Ca immobilized on the paper increased with increasing concentration in the ink (Figure 2a). Next, extrusion printing the alginate on top of the Ca loaded paper scaffold produced a good definition of the defined zig zag pattern as shown in Figures 2b and c. The width of the crosslinked gel line that was formed was found to be significantly dependent on the number of times a line is printed with an ~40% increase in line width when line was printed twice compared to printing only once. When another line of gel is printed on top of previously printed one, it is not in immediate contact the Ca loaded paper scaffold and won't be exposed to as much Ca as the first line. Therefore, it spreads more until it reaches a region of enough Ca concentration to crosslink and immobilize. Surprisingly, the effect of nozzle size wasn't found to be significant as extrusion from 18 gauge (838 μm inner diameter) and 22 gauge (603 μm inner diameter) produced similar line thicknesses indicating that the capillary process in the paper substrate dominates over the extrusion process in determining the dimensions of the printing.

The effect of flow rate and the feed rate of the extrusion printing process on the dimensions of the printed line was also determined. Alginate (2 wt% solution) was printed on top of H Ca (high calcium content) paper at various feed rates between 250 and 4000 mm/min and flow rates between 0.25 and 2 mL/min with 18 gauge needle. Interestingly, when feed rate to flow rate ratio (R) was between 1000 and 2000 mm/mL, a uniform line was printed on the paper with a linewidth of 1.08±0.07 mm and 1.59±0.13 mm for ratios of 2000 and 1000 mm/mL respectively, as shown in Figure 2d. At higher ratios, the linewidth is non-uniform while at lower ratios the printing was

intermittent. Such optimal ratios are often seen in extrusion of non-Newtonian fluids where the flow rate and feed rate are well matched to produce printed lines with well-defined and uniform edges. Alginate lines were also printed with the printhead moving in different directions (top to bottom and bottom to top) to determine if the direction of printing has any effect on the thickness and uniformity of the printed line (Figure 1b). Images at three different locations along each line (top, middle, and bottom) were taken. In all the samples printed within the "stable" region, width of the line was measured at various locations along the printed zig zag pattern and it was found to be nearly the same. Although the printed lines demonstrated here are ~1 mm in width, thinner lines could be printed by extruding through smaller nozzles and onto papers that are thinner.

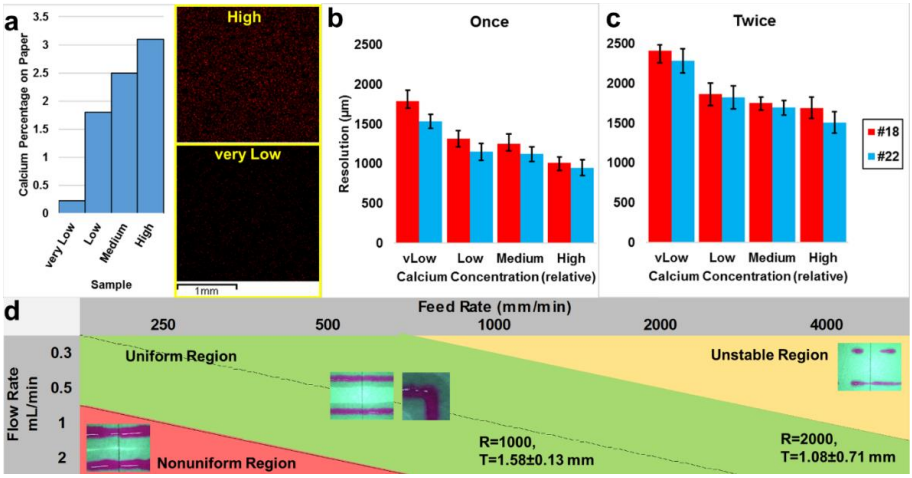

Figure 2. a) Amount of Ca deposited on paper printed with various solution concentrations and print speeds and measured using EDS. The distribution shows that Ca is deposited uniformly; **b, c)** Linewidth of the printed gel line with various amount of Ca preloaded on paper. Printing resolution is lower in lower Ca content or when two layers are printed on top of each other but the effect of nozzle size (between gauge size of 18 and 22) is not meaningful; **c)** Effect of flow and feed rate on printed patterns. Optimal conditions produce uniform line printing.

4.2.Viability Assessment

After determining the conditions for stable printing of alginate gels, a bioink was prepared by mixing 2 wt% alginate with 3T3 mouse fibroblasts with the concentration of 1×10^6 cells/mL and

used for printing. To study effect of printing process and Ca concentration on paper on the cells' viability, two different assays were performed on printed lines that were fabricated with the optimized "stable" printing conditions. Metabolic assays such as MTT ((3-(4,5-dimethylthiazol-2-yl)-2,5-diphenyltetrazolium bromide)) assay or Alamar blue assay (ABA) that are typically used for assessing cell viability in plate based assays are not suitable in our case as the printed patterns that were compared had varying amounts of crosslinking due to the different amounts of Ca loaded on the paper substrate. Consequently, the amount of cross linking and therefore the mass transfer through these gels could potentially be different which could affect the results obtained. Therefore, the traditional ABA assay was modified with an additional step where 0.1 M sodium tricitrate solution in DMEM, which is known to dissolve Ca crosslinked alginate, was added to the samples after printing so that the matrix was dissolved and the cells precipitated on the surface of the paper. ABA assay was performed on the precipitated cells after a few hours to allow complete cell attachment. To further study the number of live and dead cells in each case, Live/Dead staining was also performed and the amount of fluorescence corresponding to the live and dead cells was measured using a plate reader. The autofluorescence background of chromatography paper was also measured prior to staining and subtracted from the measurement for normalization. It was clear, as shown in Figure 3, that there was no meaningful difference between metabolic activity and number of live and dead cells of all the conditions of calcium loading on paper chosen in this study indicating that the conditions of printing were benign and did not affect cell viability. Images of the Live/Dead stained cells also show acceptable number of live cells in these samples.

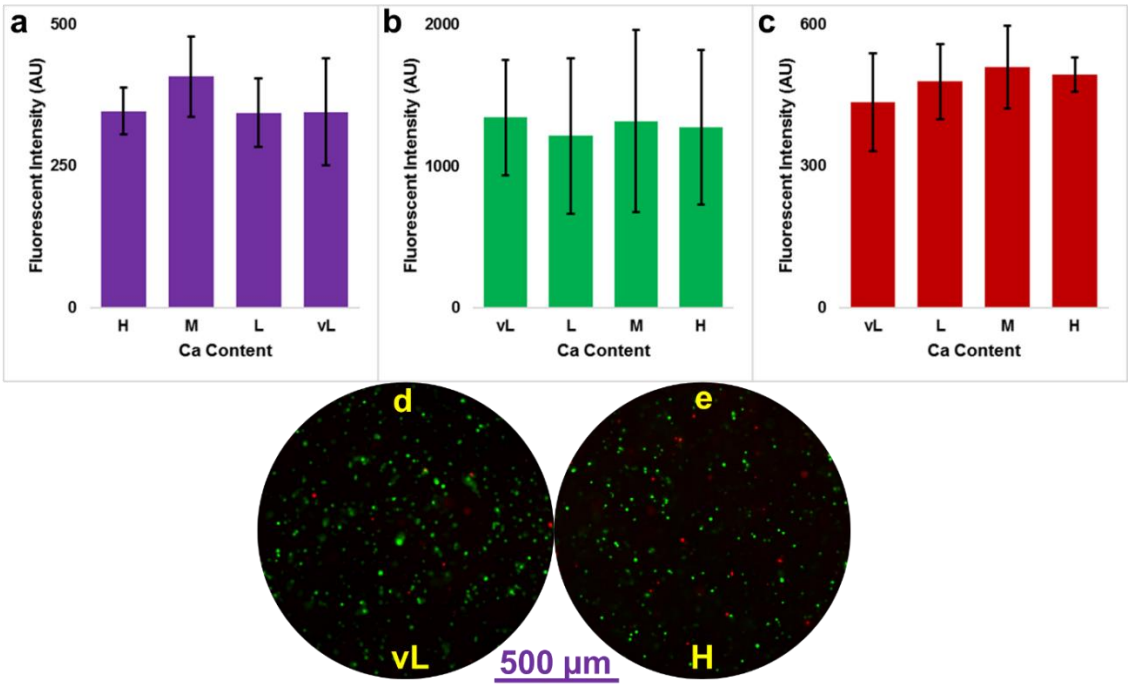

Figure 3. a) Measurement from Alamar blue viability assay; **b)** Intensity of fluorescent light from stained live cells; **c)** Intensity of fluorescent light from stained dead cells; live/dead images of **d)** vL and **e)** H Ca samples.

4.3. Fabrication and Application in 2D and 3D

This technique uses paper as a scaffold in the bioprinting process to enable the mechanical stability of the 2D patterns of gels and ECMs formed by extrusion printing as well as a suitable handle to assemble 3D structures. For instance, it creates mechanically robust thin layer 2D hydrogel patterns that are either not possible or challenging to create and handle through other means. The ability to handle and move individual 2D layers of patterned hydrogels enables creation of complex 3D structures. The structures thus formed enable assays that require indirect contact of cells to each other by having them printed on different layers, mimicking paracrine signaling in natural tissues. Furthermore, this method also provides a means to access live cells in different locations of the thick structure without the need to fix and section samples. Here, we demonstrate the ability

to print complex patterns with precise and sharply defined interfaces between regions printed close to each other both in 2D and 3D.

4.3.1. 2D Structures: Patterning of Cells and ECMs on Paper

In order to demonstrate the ability of extrusion printing of gels on crosslinker loaded scaffolds, we designed a checkerboard pattern (Figure 4a) consisting of alternate regions of gels containing two different types of cells. Each of the square regions was designed to be 6×6 mm in size and represent a pixel element. Each pixel element was filled by the parallel hatching style shown in Figure 4a with a spacing of 0.5 mm. Figure 4b shows the checkered pattern printed with gfp-3T3 and rfp-HUVEC cells in alternate squares of the checkerboard pattern. The definition of the squares was found to be accurate and the borders between the regions containing alginate loaded with different cells were sharply defined as shown in Figure 4c without any mixing. By combining various patterns of these pixel elements complex designs could be printed in 2D. Interestingly, since the paper is prepatterned with the crosslinker of the hydrogel, it is possible to accurately control the amount of crosslinking spatially as well.

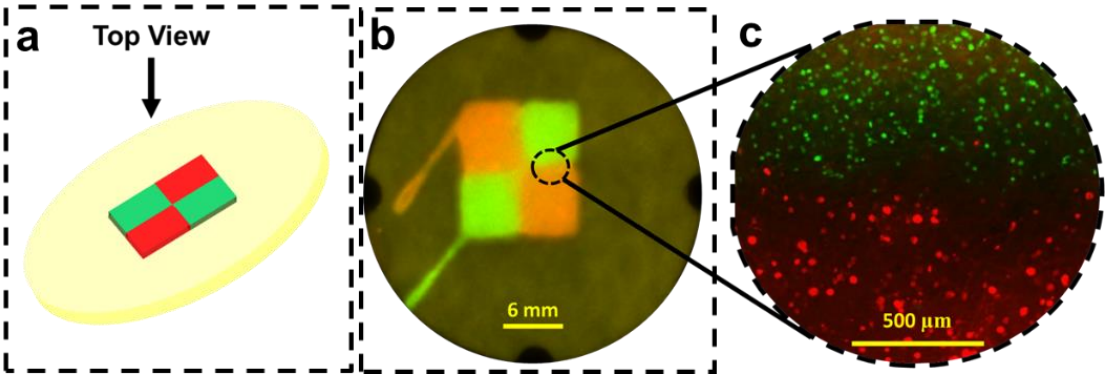

Figure 4. a) Schematic of checkered pattern printing of HUVECs and 3T3 cells printed using optimal printing condition on H Ca paper (2 wt% alginate in DMEM, flow rate of 0.5 mL/min and feed rate of 1000 mm/min); **b)** Images of printed hydrogel checkered pattern; **c)** A close up image showing sharply defined borders between regions containing different cells.

4.3.2. 2D Application: Cell Migration Evaluation

The ability to define sharp boundaries between different hydrogels can be used to perform cell migration studies under different conditions. Cell migration is an important step in different physiological processes such as embryonic development, immune response and healing, as well as in pathological conditions such as cancer metastasis that can be studied using 2D techniques such as wound closure and transwell migration assays [41]. Although these assays provide us with valuable information, they are 2D *in vitro* models (single layer of cells on a plastic substrate) and cannot accurately recapitulate 3D *in vivo* environments. There have been a few attempts to develop 3D *in vitro* migration models to address this issue. For example, in another study 3D rings of cells were formed by adding magnetic nanoparticles and applying magnetic force using a ring-like magnet [42]. They measured the change in outer diameter of the ring with time as an indicator of cell migration speed. Although promising, some limitations include the use of nanoparticles and magnetic field that could alter the cellular response and behaviour as well as the difficulty to pattern 3D multimaterial features consisting of different types of cells and/or ECMs in different locations.

In order to demonstrate the versatility of the ExCeL process in constructing suitable multimaterial 3D structures for this assay, cells were printed in a ring like structure (cells were embedded in alginate and with its crosslinking the structure of the ring was preserved). The printed ring was then embedded in either alginate or collagen and their migration was tracked over time by measuring the change in area inside and outside of the initially printed ring. Not only this technique can be used to study the effect of ECM on cell migration, but by changing the composition in culture media (such as the amount of nutrients or drugs) it could also be used to study effect of chemicals in the environment on cell migration as well. Figure 5a shows the images taken by

ChemiDoc system and analyzed using a Matlab image processing of cells embedded in collagen provided with 5 %V/V FBS supplemented culture media. It also shows the inward and outward migration pattern for cells in collagen with both 5 and 10 %V/V FBS (Figure 5b). As it is shown in Figures 5b and c, cells migrate faster when the concentration of FBS in the surrounding media is increased which sets up a concentration gradient of this nutrient in the 3D ring that promotes migration. Interestingly, they migrate faster toward the center of the ring rather than outwards. It could be because cells prefer to maintain their cell-cell connections rather than losing them. While cells were able to migrate in a certain pattern in collagen, when they were embedded in alginate they were unable to migrate (Figures 5d and e). Various scenarios were then investigated for alginate embedded cells by printing a ring of alginate loaded with cells where some of the cells were in close proximity to the culture media and contrasting its behavior to when another layer of cell free alginate was present on the top. In case where the cells in the 3D printed ring were printed close to the surrounding media, the cells escaped from the alginate gel after a few days. However, when the 3D ring was embedded underneath another layer of crosslinked alginate, the cells quickly became unviable and the fluorescent intensity decreased dramatically. It could have been because of the lack of ligands like RGD on alginate that cells could attach to and migrate [43].

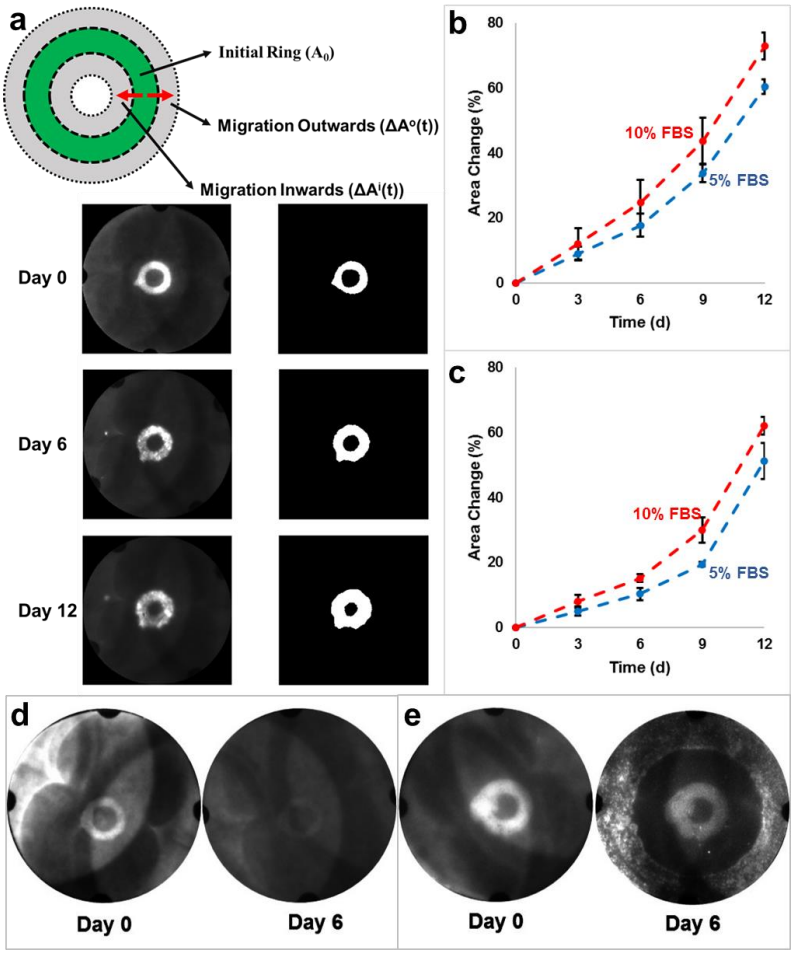

Figure 5. a) Images of 3T3s migration in collagen type I; **b)** Effect of FBS content on outwards migration of the cells embedded in collagen; **c)** Effect of FBS content on inwards migration of the cells embedded in collagen; **d)** Cells become unviable instead of migrating when the ring is printed deep in alginate; **e)** Cells escaping the environment instead of migrating when the ring is printed deep.

4.3.3. 3D Structures: Layer by Layer Assembly of 2D Patterned Scaffolds

In order to demonstrate the ability of this approach to create complex multicellular 3D constructs, we designed a perfusable 3D structure that contains hollow channels that were extrusion printed layer by layer and then assembled with alignment. The hollow channels could be used to perfuse cell culture media to keep the cells in the bulk of the structure alive. The construct consisted of several layers (as shown in Figure 6a) some of which were xurographically cut to have empty

channel structures in the paper scaffold. The xurographically cut layers consisted of alginate loaded with HUVEC cells that were extrusion printed at the borders close to the cut channel regions. They also had alginate loaded with 3T3s printed elsewhere. Lamination of these layers together lead to formation of a 3D bioink printed and loaded scaffold that had hollow perfusion channels inbuilt. During the lamination process, the top part of the gel on each layer is not completely crosslinked and when another layer of paper is placed on top of it, it comes to direct contact with a new layer of paper with Ca on it that helps it to crosslink faster and bond to the top layer. With the extrusion printing, an inner lining of HUVEC loaded gel layer was created surrounded by fibroblasts as shown in Figures 6b and c. These channels that were formed can be easily perfused without leaking when they are parallel on the same layer or crossing each other on different layers.

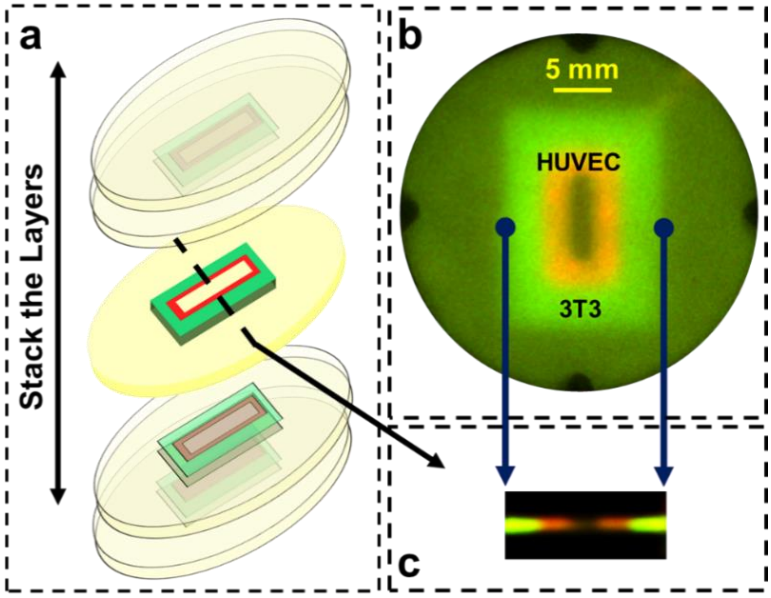

Figure 6. a) Schematic of the fabrication and assembly process to create multicellular patterned 3D structures with perfusion channels integrated; **b)** Top view of printed samples; c) Cross-section of printed samples.

4.3.4. 3D Application: Cell Viability in Stacked Layers and Effect of Channels

To show the effect of perfusion channels in 3D *in vitro* models, 3D structures fabricated by stacking three layers of paper with hydrogel printed on them was prepared in which one of them had two parallel 2 mm wide channels that were placed 9 mm apart embedded in it. Using the plate-reader the amount of fluorescent intensity in the center part of each of the samples were measured every 2 days (Figure 7a). To mimic the perfusion in the channels culture media was pipetted into each of the channels every 12 hrs. As shown in Figure 7a, after 12 days, fluorescence intensity of cells was higher in the WC samples. The cells form clusters and the number of cell aggregates (Figure 7b) at day 12 was higher in WC samples and they were located mostly close to the channels (Figures 7c and d). The same formation of clusters for other cells in alginate has been previously reported [44] and has been attributed to lack of cell-adhesivity ligands such as arginine-glycine-aspartic acid (RGD) sequence [45]. Live/Dead stained images of samples (Figure 7e) also indicated lower live cells and higher dead cells in the center part of WoC samples as opposed to WC channels. Although cells started to die in both samples after a few days but presence of channels, although far from each other, helped retain the viability of cells closer to them as seen from the distribution of clusters. Increasing the density of perfusion channels by reducing the spacing between them is likely to improve the access to nutrients further and ensure cell growth throughout the 3D structure. Therefore, the ExCeL process is versatile in forming hydrogel structures with various cell types embedded in them and integrated with perfusion channels.

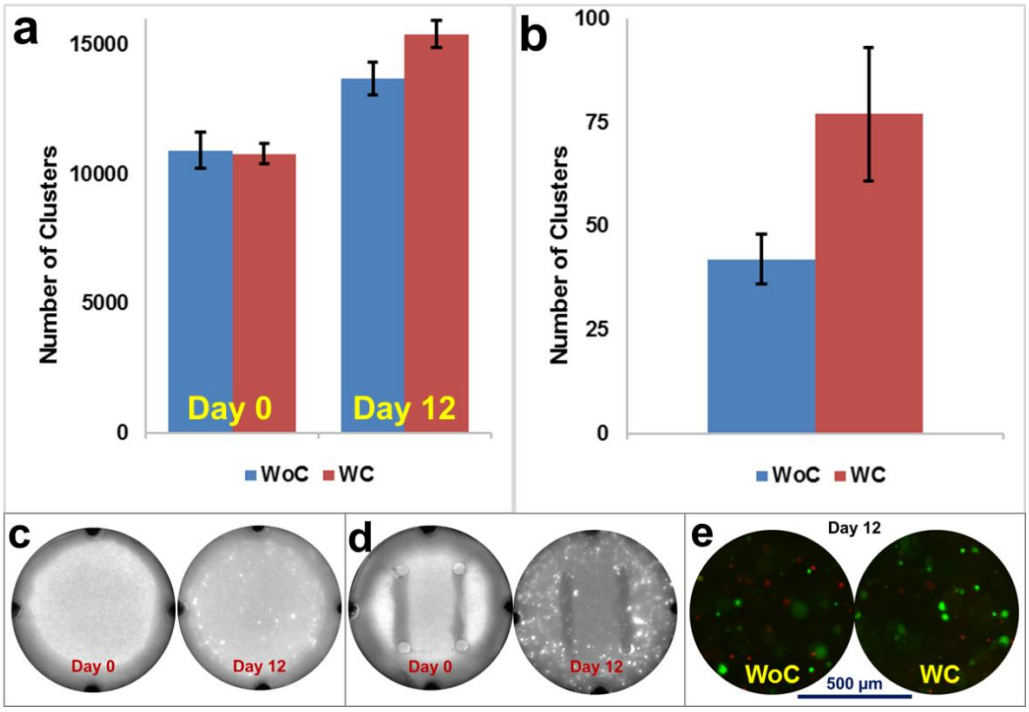

Figure 7. a) Change in fluorescent activity of samples at the center; **b)** Number of clusters in each condition after 12 days; **c, d)** Low magnification image of printed samples; **e)** Live/Dead stained samples at day 12.

5. Conclusions

In summary, a new bioprinting technique has been developed that is based on printing hydrogel on paper and *in situ* crosslinking it with pretreating the paper with hydrogel's crosslinker. Paper provides mechanical stability that thin hydrogel layers lack and allows for patterned printing of complex structures out of soft materials. This bioprinting method together with cutting the paper layers and stacking them has the capability to fabricate structures that recapitulate some of the biological complexity of tissues *in vitro* and can be used as a powerful biological model for drug discovery. In the proof of the concept demonstrated in this study, its ability to fabricate checkered patterns on one layer of paper and fabrication of perfusion channels embedded in the bulk of the structure with co-axial structure of endothelial cells and fibroblast was shown. Further optimization of this process like replacing the paper with a completely transparent membrane that

allows better microscopy will enable production of *in vitro* models with a wide range of applications. Furthermore, improving the resolution of cutting and patterning to allow closely spaced channels can allow the entire bulk of the structure to access nutrients sufficiently.

References:

1. Griffith, L.G. and M.A. Swartz, *Capturing complex 3D tissue physiology in vitro.* Nat Rev Mol Cell Biol, 2006. **7**(3): p. 211-24.
2. Caddeo, S., M. Boffito, and S. Sartori, *Tissue Engineering Approaches in the Design of Healthy and Pathological In Vitro Tissue Models.* Front Bioeng Biotechnol, 2017. **5**: p. 40.
3. Nelson, C.M., J.L. Inman, and M.J. Bissell, *Three-dimensional lithographically defined organotypic tissue arrays for quantitative analysis of morphogenesis and neoplastic progression.* Nat Protoc, 2008. **3**(4): p. 674-8.
4. Duval, K., et al., *Modeling Physiological Events in 2D vs. 3D Cell Culture.* Physiology (Bethesda), 2017. **32**(4): p. 266-277.
5. Baker, B.M. and C.S. Chen, *Deconstructing the third dimension: how 3D culture microenvironments alter cellular cues.* J Cell Sci, 2012. **125**(Pt 13): p. 3015-24.
6. Antoni, D., et al., *Three-dimensional cell culture: a breakthrough in vivo.* Int J Mol Sci, 2015. **16**(3): p. 5517-27.
7. Hutchinson, L. and R. Kirk, *High drug attrition rates--where are we going wrong?* Nat Rev Clin Oncol, 2011. **8**(4): p. 189-90.
8. Abbott, A., *Cell culture: biology's new dimension.* Nature, 2003. **424**(6951): p. 870-2.
9. Wodarz, A. and I. Nathke, *Cell polarity in development and cancer.* Nat Cell Biol, 2007. **9**(9): p. 1016-24.
10. Morrison, S.J. and J. Kimble, *Asymmetric and symmetric stem-cell divisions in development and cancer.* Nature, 2006. **441**(7097): p. 1068-74.
11. Legant, W.R., et al., *Measurement of mechanical tractions exerted by cells in three-dimensional matrices.* Nat Methods, 2010. **7**(12): p. 969-71.
12. Huang, S. and D.E. Ingber, *The structural and mechanical complexity of cell-growth control.* Nat Cell Biol, 1999. **1**(5): p. E131-8.
13. Larson, B., *3D Cell Culture: A Review of Current Techniques.*
14. Knight, E. and S. Przyborski, *Advances in 3D cell culture technologies enabling tissue-like structures to be created in vitro.* J Anat, 2015. **227**(6): p. 746-56.
15. Derda, R., et al., *Paper-supported 3D cell culture for tissue-based bioassays.* Proc Natl Acad Sci U S A, 2009. **106**(44): p. 18457-62.
16. Ozbolat, I.T., W. Peng, and V. Ozbolat, *Application areas of 3D bioprinting.* Drug Discov Today, 2016. **21**(8): p. 1257-71.
17. Peng, W., D. Unutmaz, and I.T. Ozbolat, *Bioprinting towards Physiologically Relevant Tissue Models for Pharmaceutics.* Trends Biotechnol, 2016. **34**(9): p. 722-32.
18. Hull, C.W., *Apparatus for production of three-dimensional objects by stereolithography*, 1986, Google Patents: US.
19. Ashley, S., *Rapid prototyping systems.* Mechanical Engineering, 1991. **113**(4): p. 34.

20. Gao, G., et al., *Organ Bioprinting: Are We There Yet?* Adv Healthc Mater, 2018. **7**(1).
21. Zhang, Y.S., et al., *Three-Dimensional Bioprinting Strategies for Tissue Engineering.* Cold Spring Harb Perspect Med, 2017.
22. Peng, W., et al., *3D bioprinting for drug discovery and development in pharmaceutics.* Acta Biomater, 2017. **57**: p. 26-46.
23. Park, J., et al., *3D Miniaturization of Human Organs for Drug Discovery.* Adv Healthc Mater, 2018. **7**(2).
24. Noh, S., et al., *3D Bioprinting for Tissue Engineering*, in *Clinical Regenerative Medicine in Urology*, B.W. Kim, Editor. 2018, Springer Singapore: Singapore. p. 105-123.
25. Kang, H.W., et al., *A 3D bioprinting system to produce human-scale tissue constructs with structural integrity.* Nat Biotechnol, 2016. **34**(3): p. 312-9.
26. Jang, J., H.G. Yi, and D.W. Cho, *3D Printed Tissue Models: Present and Future.* ACS Biomaterials Science & Engineering, 2016. **2**(10): p. 1722-1731.
27. Park, J.H., et al., *Current advances in three-dimensional tissue/organ printing.* Tissue Engineering and Regenerative Medicine, 2016. **13**(6): p. 612-621.
28. Mosadegh, B., et al., *Three-dimensional paper-based model for cardiac ischemia.* Adv Healthc Mater, 2014. **3**(7): p. 1036-43.
29. Ma, Z., et al., *Three-dimensional filamentous human diseased cardiac tissue model.* Biomaterials, 2014. **35**(5): p. 1367-77.
30. Koch, L., et al., *Skin tissue generation by laser cell printing.* Biotechnol Bioeng, 2012. **109**(7): p. 1855-63.
31. Kim, B.S., et al., *3D cell printing of in vitro stabilized skin model and in vivo pre-vascularized skin patch using tissue-specific extracellular matrix bioink: A step towards advanced skin tissue engineering.* Biomaterials, 2018. **168**: p. 38-53.
32. Ling, K., et al., *Bioprinting-Based High-Throughput Fabrication of Three-Dimensional MCF-7 Human Breast Cancer Cellular Spheroids.* Engineering, 2015. **1**(2): p. 269-274.
33. Xu, F., et al., *A three-dimensional in vitro ovarian cancer coculture model using a high-throughput cell patterning platform.* Biotechnol J, 2011. **6**(2): p. 204-212.
34. Lee, W.G., U. Demirci, and A. Khademhosseini, *Microscale electroporation: challenges and perspectives for clinical applications.* Integr Biol (Camb), 2009. **1**(3): p. 242-51.
35. Lozano, R., et al., *3D printing of layered brain-like structures using peptide modified gellan gum substrates.* Biomaterials, 2015. **67**: p. 264-73.
36. Dababneh, A.B. and I.T. Ozbolat, *Bioprinting Technology: A Current State-of-the-Art Review.* Journal of Manufacturing Science and Engineering, 2014. **136**(6): p. 061016-061016-11.
37. Li, J., et al., *Recent advances in bioprinting techniques: approaches, applications and future prospects.* J Transl Med, 2016. **14**: p. 271.
38. Kolesky, D.B., et al., *Three-dimensional bioprinting of thick vascularized tissues.* Proc Natl Acad Sci U S A, 2016. **113**(12): p. 3179-84.
39. Liu, W., et al., *Rapid Continuous Multimaterial Extrusion Bioprinting.* Adv Mater, 2017. **29**(3).
40. Derda, R., et al., *Multizone paper platform for 3D cell cultures.* PLoS One, 2011. **6**(5): p. e18940.
41. Justus, C.R., et al., *In vitro cell migration and invasion assays.* J Vis Exp, 2014(88).

42. Timm, D.M., et al., *A high-throughput three-dimensional cell migration assay for toxicity screening with mobile device-based macroscopic image analysis.* Sci Rep, 2013. **3**: p. 3000.
43. Ho, S.S., et al., *Cell Migration and Bone Formation from Mesenchymal Stem Cell Spheroids in Alginate Hydrogels Are Regulated by Adhesive Ligand Density.* Biomacromolecules, 2017. **18**(12): p. 4331-4340.
44. Guillaume, O., et al., *Enhancing cell migration in shape-memory alginate-collagen composite scaffolds: In vitro and ex vivo assessment for intervertebral disc repair.* J Biomater Appl, 2015. **29**(9): p. 1230-46.
45. Koo, L.Y., et al., *Co-regulation of cell adhesion by nanoscale RGD organization and mechanical stimulus.* J Cell Sci, 2002. **115**(Pt 7): p. 1423-33.

Supplementary Information

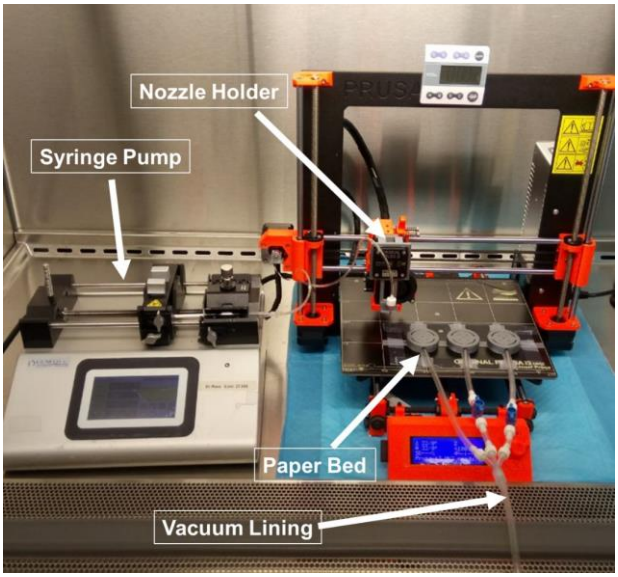

Supplementary Figure 1. Devised setup for ExCeL process

Supplementary Information - MatLab Codes

```
A = imread('*.jpg'); %read image
subplot(1,2,1)
imshow(A) %plot the figure
subplot(1,2,2)
A=rgb2gray(A); %turn it into gray scale
A1 = imsharpen(A,'Radius',*,'Amount',1); %sharpen edges %* was optimized for each sample separately
A2 = im2bw(A1,*); %turn it into binary image %* was optimized for each sample separately
A3 = bwareaopen(A2, 10000); %reduce noise
imshow(A3) %plot the final image
S1=regionprops(A3,'Area'); %measure the ring area
S1.Area
A4=imcomplement(A3);
S2=regionprops(A4,'Area'); %measure the center area
S2.Area
```

Chapter 3: BIOPRINTING APPLICATION

A Bioprinted in vitro Model for Osteoblast to Osteocyte Transformation by Changing Mechanical Properties of the ECM

Bryan E.J. Lee [1], ‡, Alireza Shahin-Shamsabadi [1], ‡, Michael K. Wong [4], Sandeep Raha [4], [5], P Ravi Selvaganapathy [1],[2],*, Kathryn Grandfield [1],[3],*

[1]School of Biomedical Engineering, McMaster University, Canada

[2]Department of Mechanical Engineering, McMaster University, Canada

[3]Department of Material Science and Engineering, McMaster University, Canada

[4]Graduate Program of Medical Science, McMaster University, Hamilton, Ontario, Canada.

[5]Department of Pediatrics, McMaster University, Hamilton, Ontario, Canada.

‡ Equal Contribution

* Corresponding authors

Status: Published

Full Citation:

Lee, B. E., Shahin-Shamsabadi, A., Wong, M. K., Raha, S., Selvaganapathy, P. R., & Grandfield, K. (2019). A Bioprinted In Vitro Model for Osteoblast to Osteocyte Transformation by Changing Mechanical Properties of the ECM. Advanced Biosystems, 3(10), 1900126.

Abstract

Osteocytes are key contributors to bone remodeling. During the remodeling process, trapped osteoblasts undergo a phenotypic change to become osteocytes. The specific mechanisms by which osteocytes work are still debatable and models that exist to study them are sparse. This work presents an *in vitro*, bioprinted model based on the previously developed technique, ExCeL, in which we print and immediately crosslink a cell-embedded hydrogel using paper as a crosslinker-storing substrate. This process mimics the phenotypical change of osteoblast to osteocyte by altering the mechanical properties of the hydrogel. By printing Saos-2, osteosarcoma cells, embedded in alginate hydrogel with differing mechanical properties, we were able to change their morphology, protein, and gene expression from osteoblast-like to osteocyte-like. The stiffer gel was 30 times stiffer and resulted in significantly smaller cells with reduced alkaline phosphatase activity and expression of osteoblast-marker genes such as MMP9 and TIMP2. There was no change in viability between cells despite encapsulation in gels with different mechanical properties. Our results show that the phenomenon of osteoblasts becoming encapsulated during the bone remodeling process can be replicated using the ExCeL bioprinting technique. This model has potential for studying how osteocytes can interact with external mechanical stimuli or drugs.

Keywords: Bioprinting; *In vitro* model; Bone; Osteoblast; Osteocyte

1. Introduction

Bone is a dynamic, hierarchical material that actively remodels itself in response to mechanical signals. One of the major constituents of the bone remodeling process are osteocytes, which come from osteoblasts that were entrapped during the bone remodeling [1, 2]. During the remodeling process, osteoblasts are slowly buried by bone matrix which is a combination of collagenous fibers and mineral deposits, otherwise known as osteoid. Over time this osteoid becomes mineralized leading to the formation of new bone tissue with embedded osteoblasts which have now been differentiated into osteocytes. The expression of many proteins differs greatly between osteoblasts and osteocytes despite their shared lineage [3, 4]. One of the primary characteristics of osteocytes is that they translate external mechanical cues into biochemical actions which fuels the bone remodeling process, a process termed mechanotransduction [5]. Despite this important role in bone biology, there is a lack of available models or cell lines for *in vitro* studies of osteocytes role in bone remodeling or their response to stimuli. This is compounded by the fact that most *in vitro* systems are two-dimensional (2D) in nature and incapable of entrapping osteocytes. 2D culture systems are dominant and have been used extensively but often do not accurately represent the in vivo response [6]. This is predominantly due to their dimensional limitations and lack of environmental cues that cells would otherwise receive in the physiological environment such as mechanical properties of the extracellular matrix (ECM), nutrient and oxygen gradients, and inter-cellular and cell-matrix interactions [7, 8]. Different 3D systems have been developed that yield more accurate responses similar to natural tissues by recapitulating some of these features [9]. Compared to 2D cell culture systems, these 3D models can maintain the phenotype of cells [10] by controlling the polarity of cell-cell and cell-matrix contacts [11, 12], as well as mechanical

properties of their environment [11, 12] and transport characteristics of important soluble growth factors [13].

The MLO-Y4 mouse cell line has been most commonly used to study osteocyte behavior with success but they are primarily utilized in 2D *in vitro* culture methods [14, 15]. Other researchers have created a three-dimensional (3D) model of osteocytes by embedding human osteoblasts in a mineral matrix comprised of biphasic calcium phosphate similar in composition to that of natural bone but this work has not considered the organic phase [16]. However, the specific mechanical entrapment required to initiate phenotypical changes of osteoblasts to osteocytes has yet to be determined. Many studies involving 3D models for bone or osteocyte-behavior do not consider the specific mechanical properties required to entrap and influence differentiation from osteoblast to osteocyte [16, 17]. For a 3D model to be accurate it should exhibit the architectural complexities of native tissue and bioprinting has emerged as a promising technique [18, 19] for this purpose. Bioprinting evolved from additive manufacturing methods to use soft materials like gels and extracellular matrices which could support growth of cells and formation of tissue-like constructs [20, 21]. Bioprinting has enabled researchers to manufacture complex structures and constructs with biomaterials containing extracellular matrices and cells [21, 22] and to reproduce biophysical and biochemical microenvironment in physiological or pathological conditions in a well-defined manner with high accuracy [18, 23, 24].

This work investigates how changes in mechanical properties of non-mineralized bone matrix can influence the osteoblast to osteocyte phenotype transformation in a 3D environment using a bioprinting based technique named Combing Extrusion printing on Cellulose scaffolds with Lamination (ExCeL).

2. Methods Summary

A 3D *in vitro* model was developed using the ExCeL bioprinting technique [25] to study effect of mechanical properties of ECM on osteoblast to osteocyte phenotype transformation. Figure 1 summarizes this process. First, two different calcium chloride solutions (0.1 M and 1 M) were printed, with printing speeds of 1000 and 2000 mm/sec respectively, on chromatography paper. The first condition is referred to further as the low calcium (Low-Ca) content paper, and the second the high calcium (High-Ca) content paper. The papers were allowed to dry overnight. Subsequently, two different concentrations of alginate (2 and 3 wt% in McCoy's culture medium) embedded with bone cells from the Saos-2 cell line were printed on each of them (2 wt% on Low-Ca (2L) and 3 wt% on High-Ca papers (3H)). Alginate as a material lends itself well to the ExCeL process, which allows for tuning of the gel stiffness, compared to collagen or gelatin [25]. Additionally, it is also the most commonly used hydrogel in bioprinting processes and has seen success printing with Saos-2 cells [39, 40]. These hydrogels crosslink immediately upon contact with the paper and reside on top of it thus giving it mechanical properties independent of the paper. The 300 μm tall cylinder shape, calculated from volume of printed hydrogel and covered area, was chosen such that the scaffold would be a homogeneous shape and thus prevent mass transfer induced gas or nutrient gradients which could alter the morphology or phenotype of the cells. It was assumed that 2L condition would yield lower stiffness compared to the 3H condition and hence cells would change to more osteocyte like phenotype in the 3H samples with higher stiffness. Other conditions were experimented with but did not generate sufficient differences in preliminary protein expression experiment to warrant further investigation (Supplementary Figure 1).

Mechanical properties of the two condition were evaluated and compared using a Microsquisher mechanical tester. Viability of the cells in these conditions was compared using Alamar blue assay

(ABA) and live/dead staining kit. Total protein synthesized by cells in each condition, as well as amount of alkaline phosphatase activity, a biomarker of osteoblast cells, was studied using pierce BCA protein and alkaline phosphatase kits. Using Quantitative Reverse Transcription Polymerase Chain Reaction (qRT-PCR) several genes that are highly expressed in either osteoblasts or osteocytes were investigated to further study the phenotype change. SEM of these 3D printed samples was performed to compare morphology of cells in each of these conditions. Fluorescent microscopy of samples stained with DAPI and Nile Red was performed, and cell sizes were compared in different conditions.

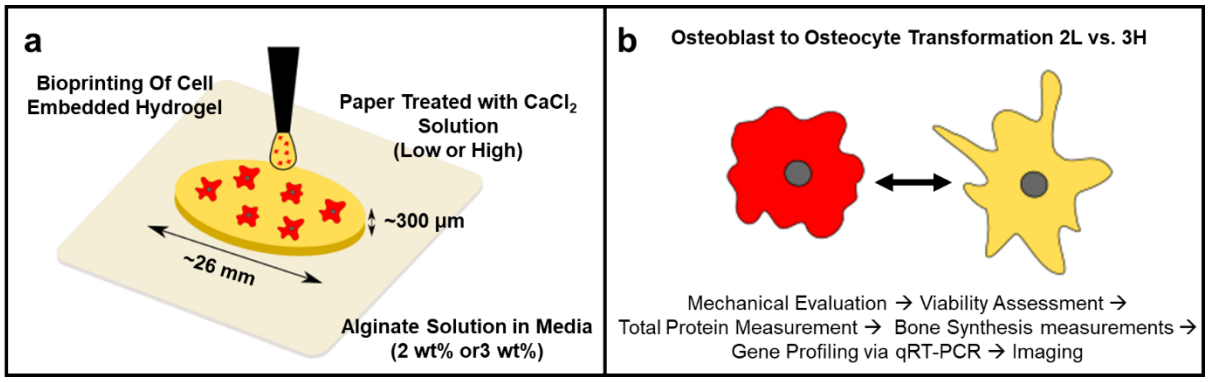

Figure 1. Design of experiment, a) Bioprinting procedure, b) Phenotype change confirmation through series of experiments. Using the ExCeL process, Saos-2 cells are encapsulated in an alginate hydrogel using different amounts of crosslinker and wt% to create scaffolds with differing stiffnesses. The encapsulated cells in these scaffolds are subsequently evaluated based on their phenotype.

3. Materials and Methods

3.1. Bioprinting Setup

Development of the 3D *in vitro* model was performed using the ExCeL process [26]. It starts by pretreating the paper (Whatman® cellulose chromatography papers, Grade 3 MMCHR) with the alginate crosslinker (calcium chloride solution, Sigma Aldrich). In order to create the required 3D

structures, alginic acid sodium salt (Sigma-Aldrich) solutions were printed in concentric circles that are 1.5 mm apart with the printing speed of 500 mm/min and hydrogel flow rate of 0.5 mL/min to form a circle with diameter of 26 mm. Because of the presence of calcium (Ca) on paper, the hydrogel crosslinks rapidly upon touching the paper and maintains the desired pattern. After printing is complete, samples were kept on the printing stage for 10 more minutes to allow complete crosslinking of the hydrogel and then they were transferred to a 6 well plate, where they were washed with PBS to remove excess amounts of Ca. Eventually samples were soaked in 2 mL culture medium that was changed every 2 days.

3.2. Mechanical testing

Mechanical properties of the printed structures were evaluated using a MicroSquisher machine (Cell Scale Biomaterials Testing, model). A 2×2 mm stainless steel platen connected to a 0.5 mm diameter cantilever was pressed towards the center part of the hydrogel at a defined rate (10% of the total thickness of the hydrogel per minute) in a displacement-controlled setup. Displacement of the platen was tracked by analyzing images taken by a camera while a load cell connected to the other end of cantilever measured the amount of force exerted by the hydrogel. The force-displacement data were then translated to stress-strain curves and the Young's modulus was defined as the slope of the initial linear range of the diagram. The ratio of Young's modulus of 3H to 2L was reported to compare difference between mechanical properties of the chosen conditions. Five samples were tested for each condition.

3.3. Viability

Saos-2 (ATCC®), osteosarcoma, cells were cultured in McCoy's 5A modified medium (Life Technologies Inc) with 15% fetal bovine serum (FBS) (Life Technologies Inc) and 1% penicillin/streptomycin (Life Technologies Inc). Cells were detached when confluent and mixed

with alginate (2 or 3 wt% in McCoy's medium) before printing at a concentration of 2×10^6 cells/mL alginate solution.

Viability of the cells was assessed using a live/dead assay kit (Molecular Probes, Oregon, USA) where the concentration was 2 µM Calcein AM and 4 µM ethidium homodimer-1 for live and dead respectively. Media was removed from wells following one day of the cells being embedded in the hydrogel matrix and the stain was added for 1 hour. Following incubation at 37°C, the samples were observed using an Olympus BX53F upright light microscope (Olympus, USA) using 475-485/485-536 nm (FITC) and 542-582/582-644 nm (TXRED) filters for the live and dead stains respectively. Samples were also examined for cell metabolism using an Alamar blue® (Life Technologies Inc.) assay following one day of incubation. Media was removed from the samples and replaced with a 5% Alamar blue® solution (in McCoy's 5A medium). Samples were incubated for 1 hour in the dark at 37°C before measuring fluorescence using an Infinite® M200 (Tecan, Männedorf, Switzerland) at 540-580 nm (excitation-emission).

In order to measure the effect of chosen conditions on cell morphology, 7-day old samples were fixed and stained using Nile Red and DAPI. First 10 µL of Nile Red stock solution (10 mg/mL in acetone) was diluted in 10 mL PBS and 3 mL of this solution was added to each sample followed by 10 min incubation. Then samples were counterstained with 3 mL of working solution of DAPI that was prepared by dissolving 2.9 µL of its stock solution (5 mg/mL in PBS) in 10 mL PBS. Incubation time for this step was also 10 min. Finally, samples were washed with PBS and imaged using an upright microscope and 10X magnification.

3.4. Protein Assays

Following 4, 7, and 14 days of incubation, hydrogel samples were rinsed with PBS before being dissolved using 3 mL of sodium citrate (0.1 M) on a shaker. 2 mL of the suspended cell solution was aliquoted for PCR while the remaining 1 mL was used for protein assays.

For the protein assays, 1 mL of a 0.1% triton lysis solution (in PBS) was added to each well to lyse the cells. 25 µL from each well was taken (in triplicate) and placed in two different 96 well plates to determine total protein content and alkaline phosphatase activity. A Pierce™ BCA Protein assay was performed using provided protocol (Thermo Scientific) to determine total protein content. Samples in the BCA 96 well plate were incubated for 30 minutes with 200 µL of BCA solution. Absorbance readings were taken on an Infinite ® M200 (Tecan, Männedorf, Switzerland) at 562 nm. The alkaline phosphatase assay was performed using the ALP assay (Abcam®). Samples in the ALP 96 well plate were incubated for 20 minutes with 100 µL of p-nitrophenol phosphate in assay buffer. Absorbance readings were taken on an Infinite® M200 (Tecan, Männedorf, Switzerland) at 405 nm. Blank readings were subtracted from each data point of each assay and via the standard curve absorbance values were converted to total protein content and ALP activity for the BCA and ALP assays, respectively.

3.5. qRT-PCR

2 mL aliquots were centrifuged at 200 g for 6 minutes. Supernatant was removed and aliquots were flash frozen in liquid nitrogen. Total RNA (250 ng) was isolated and reserve-transcribed to cDNA as previously described [27]. Primer sets directed against gene targets of interest were designed through National Center for Biotechnology Information's Primer-BLAST primer designing tool and synthesized at McMaster's Mobix Labs (Table 1). Quantitative analysis of mRNA expression was performed via qPCR using SsoAdvanced™ Universal SYBR® Green Supermix (BioRad) and CFX384 Touch Real-Time PCR Detection System (BioRad). The cycling conditions were 95°C

for 10 min, followed by 40 cycles of 95°C for 10 secs and 60°C for 10 secs and 72°C for 15 secs. Relative fold changes were calculated using the comparative cycle times (Ct) method, normalizing all values to the geometric mean of three endogenous control genes (18S, ACTB, GAPDH). The endogenous control gene was selected based on experimentally-determined Ct stability across all treatment groups. Given that all primer sets had equal priming efficiency, the ΔCt values for each primer set were calibrated to the average of all control Ct values, and the relative abundance of each primer set compared with calibrator was determined by the formula 2ΔΔCt, in which ΔΔCt was the normalized value.

Table 1. Forward and reverse sequences for the primers used for qPCR.

Gene	Forward	Reverse	GenBank
18S (RNA18S5)	CACGCCAGTACAAGATCCCA	AAGTGACGCAGCCCTCTATG	NR_003286.2
ACTB	TTACAGGAAGTCCCTTGCCATC	GCAATGCTATCACCTCCCCTG	NM_001101.5
GAPDH	TCACCATCTTCCAGGAGCGA	ATGACGAACATGGGGGCATC	NM_001357943.1
ALPL	AGGACGCTGGGAAATCTGTG	CATGAGCTGGTAGGCGATGT	AH005272.2
MMP9	CCGGCATTCAGGGAGACGCC	TGGAACCACGACGCCCTTGC	NM_004994.2
TIMP1	GGGCTTCACCAAGACCTACA	TGCAGGGGATGGATAAACAG	NM_003254.3
TIMP2	GAAGAGCCTGAACCACAGGT	GGGGGAGGAGATGTAGCAC	NM_003255.4

3.6. Scanning Electron Microscopy

Bioprinted samples were prepared and allowed to incubate for 1 day. Samples were then fixed with 0.25% glutaraldehyde in a sodium cacodylate buffer. Following this, the samples were stained

with osmium tetraoxide before being sequentially dehydrated with ethanol starting at 25% (in Milli-Q water) to 100%. Samples were critically point dried (Leica Microsystems, Wetzlar, Germany) and coated with 5 nm of platinum before being examined under SEM (TESCAN VP. SEM at 10kV). Samples were cut in half using a scalpel blade and imaged in cross-section.

3.7. Statistics

Statistical analysis for cell viability, protein assays, PCR and SEM image analysis was performed using the programming language, R (R Core Team, New Zealand). Protein assays used two-way ANOVA at a significance of $\alpha = 0.05$ and Tukey's HSD test was used to evaluate contrasts. All other methods were evaluated using the student's t-test with an accepted statistical significance of $p<0.05$.

4. Results

4.1. Mechanical testing

The mechanical properties of the samples were evaluated to determine the difference in Young's modulus between the 2L and 3H conditions using the initial linear region (Figure 2). Using Microsquisher testing machine, a platen was pressed against surface of the hydrogel and force applied to the platen and its displacement was measured. Figure 2 shows the stress vs. strain diagram for each of the samples. As expected, 3H samples had greater Young's modulus compared to 2L samples (35.8 ± 1.98 MPa vs. 1.08 ± 0.56 MPa for 3H and 2L respectively).

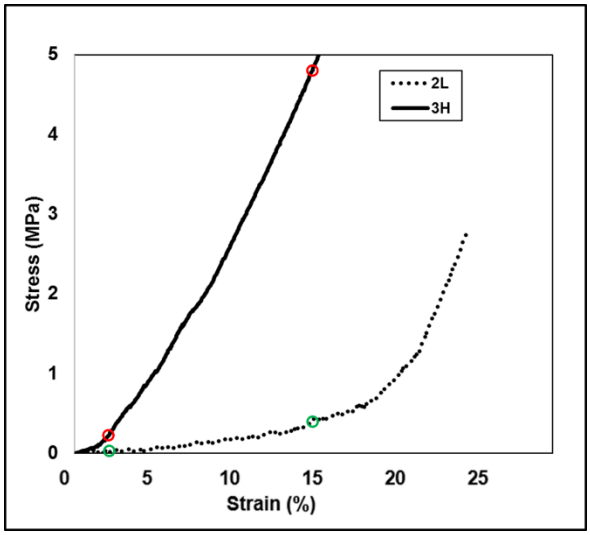

Figure 2. Stress vs. Strain diagram of 2L and 3H bioprinted samples demonstrating the improved mechanical properties of the 3H compared to 2L samples. The 2L and 3H samples both deform elastically with the 3H (35.8 MPa) being considerably stiffer ($p < 0.05$) than 2L (1.08 MPa) for 4 samples. The red circles indicate the start and end points for determining the modulus of the 3H samples while the green circles do the same for the 2L samples.

4.2. Viability

The viability of cells bioprinted within 2L and 3H hydrogels was evaluated using a live/dead stain kit after 1 day of incubation following printing (Figure 3). There were numerous live cells in both 2L and 3H samples, indicating that the printing process has a minimal effect on the cell viability. This is confirmed by Figure 3E which shows that there is no difference in the ratio of live to dead cells ($p<0.05$) between 2L and 3H samples. There is noticeable autofluorescence in the images which is a consequence of the printing process as the cellulose-based paper fluoresces significantly. As a control, cells were cultured on paper alone and evaluated in terms of cell metabolism after one day of incubation. The results indicate that there is no statistically significant change in metabolism between cells cultured on paper or traditional cell culture polystyrene ($p<0.05$) (Supplementary Figure 2). Cells embedded in the 2L and 3H samples were stained with Nile Red and DAPI and imaged under an upright microscope (Figure 4). The cells in the 3H

samples were found to be statistically significantly smaller than the cells in the 2L samples ($p<0.05$ over 3 samples). The average diameter, with the cells being modelled as circles, for the 2L and 3H samples were 40.1 and 21.3 µm, respectively. With 10 different focal planes being considered in the analysis for each sample, the cells in the 3H samples were found to be 70-80% smaller by area compared to the cells in the 2L samples.

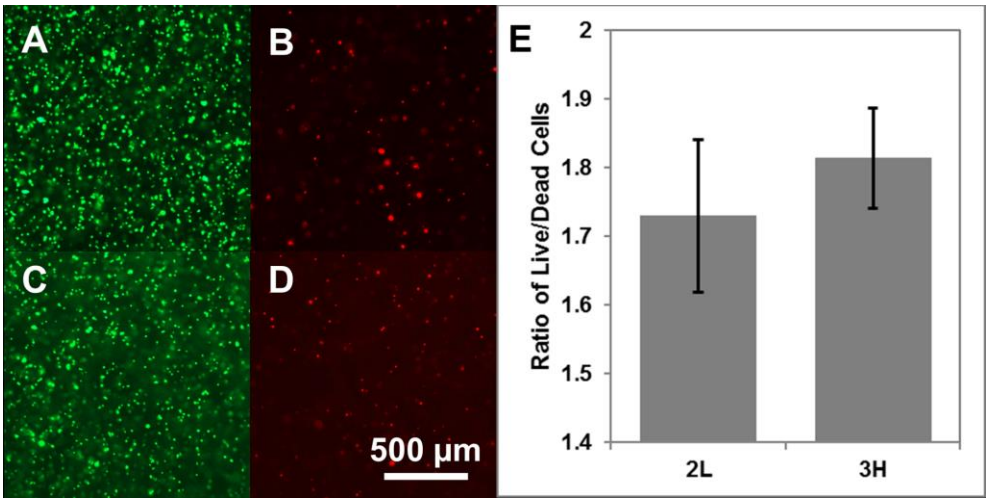

Figure 3. Live/dead stained fluorescent images taken for 2L (A/B) and 3H (C/D) after 1 day of incubation following bioprinting (n=3). Qualitatively, there are numerous live cells in both 2L and 3H samples and relatively few dead cells. The ratio of live to dead cells through fluorescent readings was determined to be statistically the same for 2L and 3H samples.

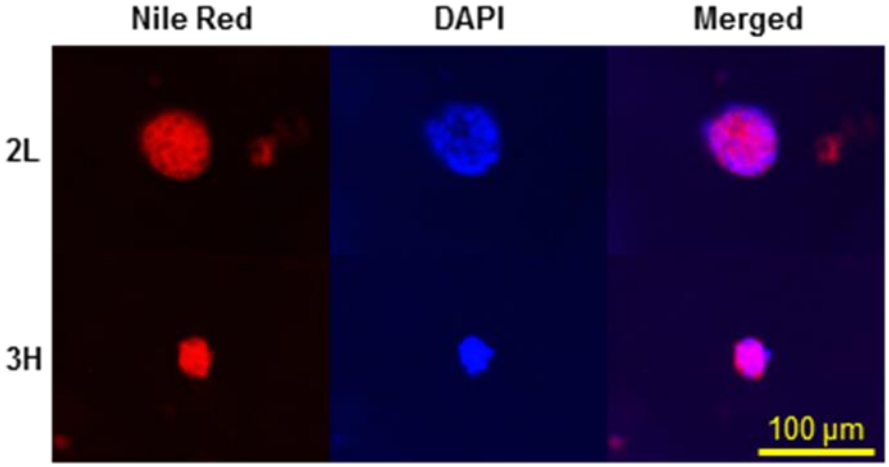

Figure 4. Nile Red and DAPI stained A) 2L and B) 3H samples. Saos-2 cells are multinucleated resulting in significant staining of membranes from both Nile Red and DAPI. Cells are visibly and quantifiably smaller in size (20.3 vs. 40.1 µm by diameter) in the 3H hydrogel compared to 2L hydrogel.

4.3. Protein Assays

2L and 3H samples with cells were evaluated *in vitro* for alkaline phosphatase (ALP) activity and total protein content (Figure 5). Over time, ALP activity showed statistically significant increases from 1 to 4 to 7 to 14 days for 3H ($p<0.05$). This effect was not observed for the 2L samples where ALP activity was statistically the same across all time points. When comparing between the groups, at the 4, 7, and 14 time points, the 3H samples showed statistically significantly less ALP activity compared to 2L samples ($p<0.05$). For total protein content, there were no significant differences between 2L and 3H sample groups. When normalizing ALP activity with respect to total protein content, the same statistical effects were observed as were seen in ALP activity alone. This provides additional evidence that comparable amounts of cells were successfully embedded, and viability was the same within the different printed hydrogel samples.

Confirmation that the embedding effect is influencing the change in ALP activity was achieved by comparing ALP activity and total protein content between cells embedded and cells simply cultured on paper for 4 days (Supplementary Figure 3). There was no statistically significant difference in ALP activity or total protein content between cells cultured only on the two different calcium treated papers ($p<0.05$).

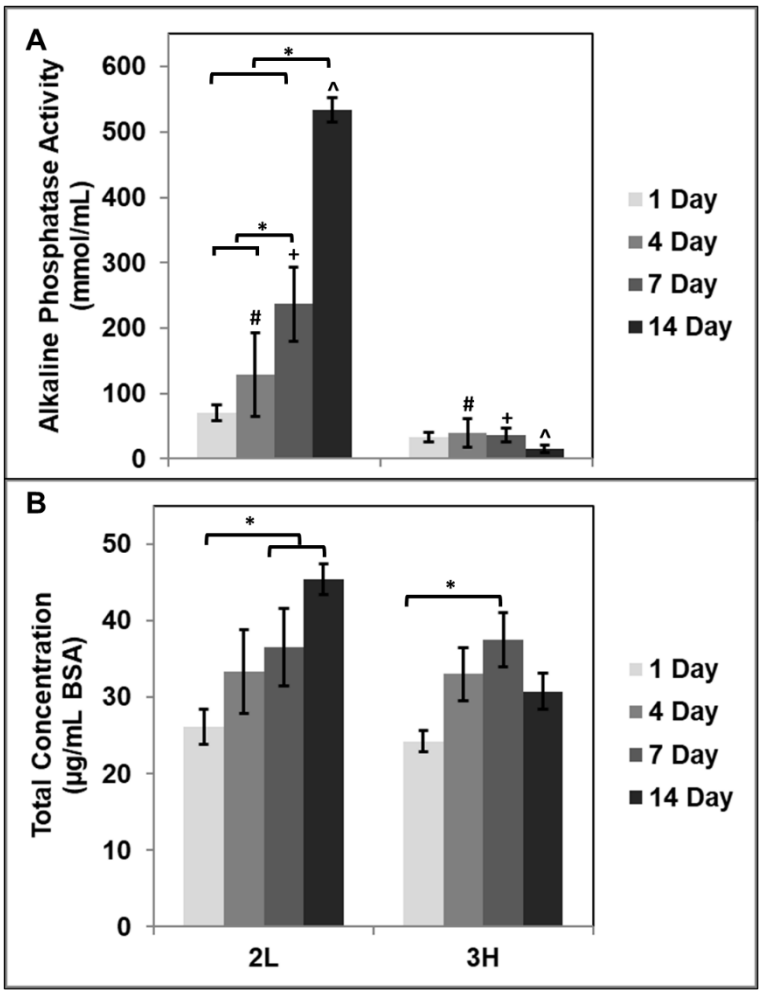

Figure 5. Alkaline phosphatase (ALP) activity, normalized by volume, (A) and total protein content (B) for 2L and 3H samples after 1, 4, 7, and 14 days of incubation (n = 5). ALP activity increases over time for 2L samples but remains statistically constant in 3H samples. ALP activity was significantly less in 3H samples at 4, 7, and 14 time points ($p<0.05$). There are no statistically significant differences in total protein content between samples at each time point.

4.4. PCR

qRT-PCR was performed on 2L and 3H samples after 4 days of incubation. mRNA levels of ALPL, MMP9 and TIMP2 were significantly decreased in 3H samples compared to 2L samples ($p<0.05$; Figure 6A, B, D). mRNA levels of TIMP1 remained unchanged (Figure 6C).

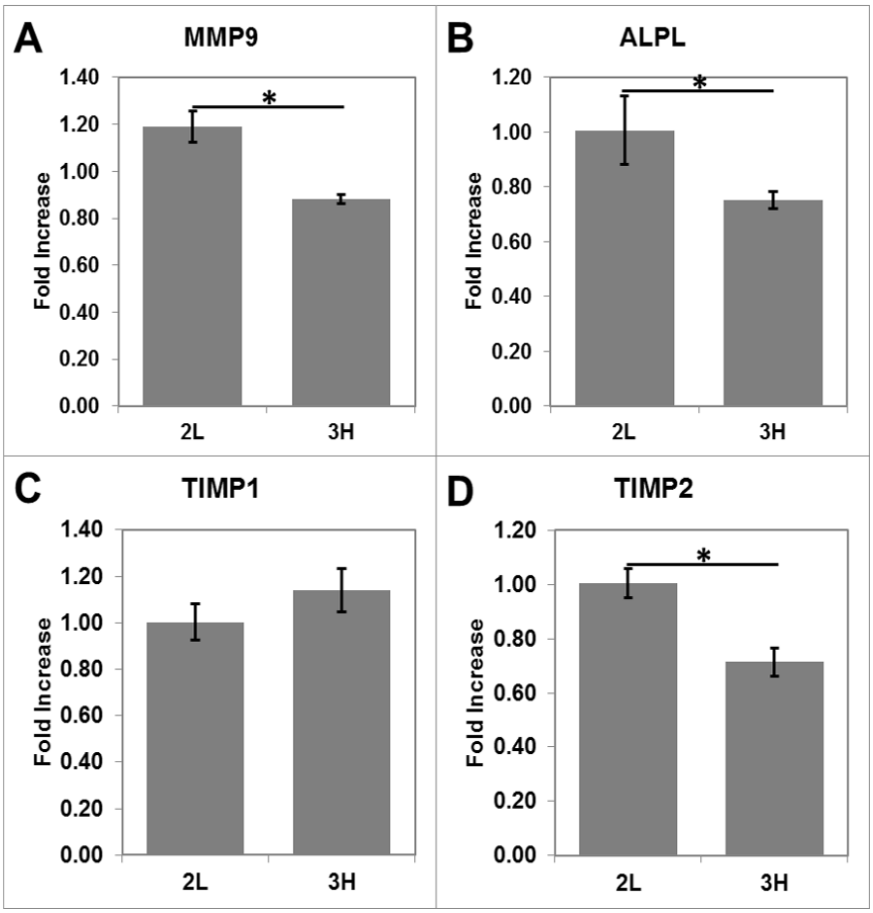

Figure 6. Normalized fold increases of (A) ALPL, (B) MMP9, (C) TIMP1 and (D) TIMP2 genes from qRT-PCR of 2L and 3H samples. There were statistically significant decreases ($p<0.05$, *) in expression of ALPL, MMP9, and TIMP2 genes in the 3H samples compared to 2L samples.

4.5. SEM

2L and 3H bioprinted samples were examined under SEM to observe how cells were embedded within the hydrogel matrix (Figure 7). Numerous cells can be identified in cross-section and top-down SEM images (Figures 7A, B). The cells appear as nodules on the surface and pores are not visible due to the hydrogel thickness being reduced during the dehydration steps required to image in SEM. The cells appear well distributed throughout the matrix and there are cellular processes that appear to extend within the hydrogel matrix (Figure 7C).

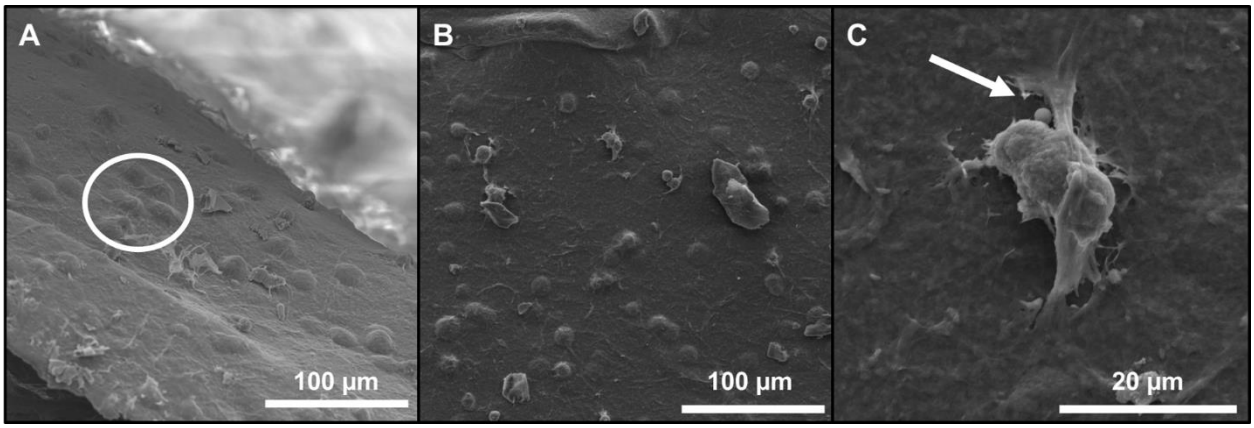

Figure 7. SEM images demonstrating how embedded cells are organized within the hydrogel matrix. Cells embedded (white circle) in 2L samples can be viewed in cross-section (A) and top-down (B) and are well-distributed. Cellular processes (white arrow) from the cells that extend into and within the matrix can also be observed (C).

5. Discussion

Osteoblast-like cells were successfully encapsulated in hydrogel using an ExCeL bioprinting setup to alter their phenotype to that similar to osteocytes. This change in phenotype was induced by differing hydrogel stiffness as a result of altering the amount of crosslinking agent and hydrogel solution. Two distinct hydrogels, 2L and 3H, were printed with notable differences in Young's modulus under compression. By increasing the stiffness of the matrix, it was hypothesized that osteoblasts would be entrapped and less capable of migration and that this system would encourage a change in phenotype from osteoblast to osteocyte.

The different printing conditions were determined to have no statistically significant effect on the viability of the cells. Other work has identified that materials with differing stiffness can effect cell function, viability and in some cases induce apoptosis [28, 29], however, this was not the case for the 2L and 3H hydrogels used in this work. It was further confirmed by SEM images which demonstrate that cells were distributed across the entirety of the hydrogel matrix with cellular processes extended within the matrix. In natural bone, these extended cellular processes enable

osteocytes to communicate with other cells through the lacunar-canalicular network. As such, it is promising that these cellular processes have been preserved and that the osteogenic cells embedded in hydrogel are expressing an osteocyte-like phenotype.

The change in phenotype of osteoblast-like, Saos-2, cells towards that of osteocytes was confirmed via Nile red/DAPI staining, protein assays, and qRT-PCR. Fluorescent staining showed the cells were 70-80% smaller in 3H samples compared to 2L samples. This provides evidence that an osteocyte-like phenotype was induced as other work has shown that mature osteocytes are approximately 70% smaller than osteoblasts [30, 31]. Alkaline phosphatase (ALP) is an enzyme primarily produced at sites of bone growth and is considered a marker for osteoblastic activity [32]. ALP is also typically not expressed, or weakly expressed, in osteocytes [16]. Protein assays demonstrated that ALP activity was significantly decreased for cells printed in the 3H hydrogels without any change in total protein content. This effect, both for ALP activity and total protein content, was observed over time up to 14 days suggesting that the cells maintain their altered phenotype in the designed system. qRT-PCR confirmed this change in expression as the ALPL gene was significantly down-regulated at the mRNA level for cells encapsulated in the 3H hydrogel. mRNA levels of MMP9 and TIMP2 were also significantly down-regulated in 3H samples, which suggests a reduction in cell migration [28, 29] and further supports that the Saos-2 cells are encapsulated by the hydrogel matrix. MMP9 and TIMP2 are known to be markers of bone remodeling [26, 33, 34], as increased expression of both genes have been observed at sites of bone remodeling or high osteoblastic activity [33, [34]. Mouse in vivo studies conducted by others indicate that TIMP2 may inhibit osteoblastic differentiation into osteocytes [35], while emphasizing the importance of the MMP family for proper transformation of osteoblasts into osteocytes [36]. These studies are in agreement with the decreased TIMP2 expression observed in

3H samples compared to 2L samples. Similarly, the balance of expression between the two is important as an imbalance of MMP to TIMP genes has been suggested to lead to bone loss [34]. These changes in expression, at the protein and gene level, indicate that the different mechanical properties between the 2L and 3H hydrogel are capable of inducing osteoblast-like to osteocyte-like differentiation.

This work used Saos-2 cells, an immortalized cell line considered a good model for osteoblast activity [32]. These cells are generally considered incapable of differentiating into other types of cells, osteocytes included [32], and as such, this work represents the first step towards the development of a model for osteocyte differentiation. Future iterations would require either bone mesenchymal stem cells or primary human osteoblasts to identify how the phenotype of these cells could be adjusted by modulating the mechanical properties of the printed hydrogels. Mesenchymal stem cells could be differentiated into osteoblasts using known methods, such as dexamethasone treatment, and subsequently encapsulated in the process described in this work [37]. The modulus of the scaffolds, while noticeable different from each other, does not approach the known modulus of bone which is typically estimated to be between 7-30 GPa [38]. The current scaffolds do not have any mineral present beyond what is produced by the cells, so future work could see the addition of hydroxyapatite to simulate the mineral presence in bone and subsequently stiffen the material [16]. Additionally, a more physiologically relevant model could be constructed using a co-culture system to characterize the interactions between the various cell types present during bone remodeling.

6. Conclusion

An *in vitro* model to study osteoblast entrapment was created using a paper-based bioprinting technique. By altering the amount of crosslinking in an alginate hydrogel, two gels with drastically

different Young's moduli were generated. When osteoblast-like cells were bioprinted, the stiffer gels resulted in smaller cells without any decrease in overall cell viability. The alkaline phosphatase activity was greatly reduced in the stiffer hydrogel while the total protein content remained the same. Similarly, expression levels of osteoblast relevant genes were all reduced in the stiffer hydrogel, which along with the reduced size and protein expression demonstrates that an osteocyte-like behavior has been induced. This *in vitro* model is a stepping stone towards larger studies of osteocyte-osteoblast behavior that could be explored by interfacing this *in vitro* model with mechanical stimuli, or by using it as a platform for drug discovery, or biomaterials testing to observe complex bone cell behavior.

ASSOCIATED CONTENT

AUTHOR INFORMATION

Corresponding Author

*To whom correspondence should be addressed:
Email: kgrandfield@mcmaster.ca, selvaga@mcmaster.ca

Present Addresses

†If an author's address is different than the one given in the affiliation line, this information may be included here.

Author Contributions

The manuscript was written through contributions of all authors. All authors have given approval to the final version of the manuscript. ‡B.E.J. L and A.S contributed equally.

Funding Sources

We would like to acknowledge the support of the Natural Sciences and Engineering Research Council of Canada (NSERC) and the Discovery Grant Program (RGPIN 2014-06053). PRS acknowledges support from the Canada Research Chairs Program and the NSERC Discovery Accelerator Supplement.

ACKNOWLEDGMENTS

We would like to acknowledge the support of the Natural Sciences and Engineering Research Council of Canada (NSERC) and the Discovery Grant Program (RGPIN 2014-06053). PRS acknowledges support from the Canada Research Chairs Program and the NSERC Discovery Accelerator Supplement. Microscopy was carried out at the Faculty of Health Sciences Electron Microscopy Facility at McMaster University. *In vitro* studies were performed at the Biointerfaces Institute at McMaster University.

References:

1. T. A. Franz-Odendaal, B. K. Hall, and P. E. Witten, "Buried alive: How osteoblasts become osteocytes," Dev. Dyn., vol. 235, no. 1, pp. 176–190, 2006.

2. S. L. Dallas and L. F. Bonewald, "Dynamics of the transition from osteoblast to osteocyte," Ann. N. Y. Acad. Sci., vol. 1192, pp. 437–443, 2010.

3. F. Paic et al., "Identification of differentially expressed genes between osteoblasts and osteocytes," Bone, vol. 45, no. 4, pp. 682–692, 2009.

4. M. Capulli, R. Paone, and N. Rucci, "Osteoblast and osteocyte : Games without frontiers," Arch. Biochem. Biophys., vol. 561, pp. 3–12, 2014.

5. R. Civitelli, "Cell-cell communication in the osteoblast/osteocyte lineage," Arch. Biochem. Biophys., vol. 473, no. 2, pp. 188–192, 2008.

6. K. Duval et al., "Modeling Physiological Events in 2D vs. 3D Cell Culture," Physiology, vol. 32, no. 4, pp. 266–277, 2017.

7. B. M. Baker and C. S. Chen, "Deconstructing the third dimension – how 3D culture microenvironments alter cellular cues," J. Cell Sci., vol. 125, no. 13, pp. 3015–3024, 2012.

8. D. Anton, H. Burckel, E. Josset, and G. Noel, "Three-dimensional cell culture: A breakthrough in vivo," Int. J. Mol. Sci., vol. 16, no. 3, pp. 5517–5527, 2015.

9. C. M. Nelson, J. L. Inman, and M. J. Bissell, "Three-dimensional lithographically defined organotypic tissue arrays for quantitative analysis of morphogenesis and neoplastic progression," Nat. Protoc., vol. 3, no. 4, pp. 674–678, 2008.

10. A. Abbott, "Cell culture: biology's new dimension," vol. 424, no. August, 2003.

11. A. Wodarz and I. Näthke, "Cell polarity in development and cancer," Nat. Cell Biol., vol. 9, no. 9, pp. 1016–1024, 2007.

12. S. J. Morrison and J. Kimble, "Asymmetric and symmetric stem-cell divisions in development and cancer," Nature, vol. 441, no. 7097, pp. 1068–1074, 2006.

13. F. Coşkun and C. R. Parks, "A molecular phylogeny of Cercis L. (fabaceae) using the chloroplast trnl-F DNA sequences," Pakistan J. Bot., vol. 41, no. 4, pp. 1587–1592, 2009.

14. Y. Kato, J. J. Windle, B. A. Koop, G. R. Mundy, and L. F. Bonewald, "Establishment of an Osteocyte-like Cell Line, MLO-Y4," J. Bone Miner. Res., vol. 12, no. 12, pp. 2014–2023, 2010.

15. D. Nicolella, V. Dusevich, M. R. Dallas, J. D. Eick, and L. F. Bonewald, "Mechanism by which MLO-A5 Late Osteoblasts / Early Osteocytes Mineralize in Culture : Similarities with Mineralization of Lamellar Bone," pp. 340–353, 2006.

16. F. Boukhechba et al., "Human primary osteocyte differentiation in a 3D culture system," J. Bone Miner. Res., vol. 24, no. 11, pp. 1927–1935, 2009.

17. K. Uchihashi, S. Aoki, A. Matsunobu, and S. Toda, "Osteoblast migration into type I collagen gel and differentiation to osteocyte-like cells within a self-produced mineralized matrix :

A novel system for analyzing differentiation from osteoblast to osteocyte," Bone, vol. 52, no. 1, pp. 102–110, 2013.

18. I. T. Ozbolat, W. Peng, and V. Ozbolat, "Application areas of 3D bioprinting," Drug Discov. Today, vol. 21, no. 8, pp. 1257–1271, 2016.

19. W. Peng, D. Unutmaz, and I. T. Ozbolat, "Bioprinting towards Physiologically Relevant Tissue Models for Pharmaceutics," Trends Biotechnol., vol. 34, no. 9, pp. 722–732, 2016.

20. G. Gao, Y. Huang, A. F. Schilling, K. Hubbell, and X. Cui, "Organ Bioprinting: Are We There Yet?," Adv. Healthc. Mater., vol. 7, no. 1, pp. 1–8, 2018.

21. Y. S. Zhang, Three-Dimensional Bioprinting Strategies for Tissue Engineering. Cold Spring Harbor Perspectives, 2017.

22. S. Noh, 3D Bioprinting for Tissue Engineering. Springer Singapore, 2018.

23. H. W. Kang, S. J. Lee, I. K. Ko, C. Kengla, J. J. Yoo, and A. Atala, "A 3D bioprinting system to produce human-scale tissue constructs with structural integrity," Nat. Biotechnol., vol. 34, no. 3, pp. 312–319, 2016.

24. J. Jang, H. G. Yi, and D. W. Cho, "3D Printed Tissue Models: Present and Future," ACS Biomater. Sci. Eng., vol. 2, no. 10, pp. 1722–1731, 2016.

25. A. Shahin-Shamsabadi and P. R. Selvaganapathy, "ExCel: Combing Extrusion printing on Cellulose scaffolds with Lamination to create in vitro biological models," Biofabrication, vol. 11, no. 3, 2019.

26. E. Kostovski, N. Hjeltnes, E. F. Eriksen, S. O. Kolset, and P. O. Iversen, "Differences in Bone Mineral Density , Markers of Bone Turnover and Extracellular Matrix and Daily Life Muscular Activity Among Patients with Recent Motor-Incomplete Versus Motor- Complete Spinal Cord Injury," Calcif. Tissue Int., vol. 96, no. 2, pp. 145–154, 2015.

27. M. K. Wong et al., "Extracellular matrix surface regulates self- assembly of three-dimensional placental trophoblast spheroids," pp. 1–18, 2018.

28. J. D. Hood and D. A. Cheresh, "Role of integrins in cell invasion and migration," Nat. Rev. Cancer, vol. 2, no. 2, pp. 91–100, 2002.

29. G. Murphy and J. Gavrilovic, "Proteolysis and cell migration: Creating a path?," Curr. Opin. Cell Biol., vol. 11, no. 5, pp. 614–621, 1999.

30. C. Palumbo, "A three-dimensional ultrastructural study of osteoid-osteocytes in the tibia of chick embryos," Cell Tissue Res., vol. 246, no. 1, pp. 125–131, 1986.

31. Y. Sugawara, H. Kamioka, T. Honjo, K. I. Tezuka, and T. Takano-Yamamoto, "Three-dimensional reconstruction of chick calvarial osteocytes and their cell processes using confocal microscopy," Bone, vol. 36, no. 5, pp. 877–883, 2005.

32. C. Pautke et al., "Characterization of Osteosarcoma Cell Lines MG-63 , Saos-2 and U-2 OS in Comparison to Human Osteoblasts," Anticancer Res., vol. 24, no. 6, pp. 3743–3748, 2004.

33. G. Dew et al., “Localisation of matrix metalloproteinases and TIMP-2 in resorbing mouse bone,” Cell Tissue Res., vol. 299, no. 3, pp. 385–394, 2000.

34. P. A. Hill and J. J. Reynolds, “Inhibition of stimulated bone resorption in vitro by TIMP-1 and TIMP-2,” Biochim. Biophys. Acta (BBA)-Molecular Cell Res., vol. 1177, no. 1, pp. 71–74, 1993.

35. M. A. Karsdal, T. A. Andersen, L. Bonewald, and C. Christiansen, “Matrix Metalloproteinases (MMPs) Safeguard Osteoblasts from Apoptosis during Transdifferentiation into Osteocytes: MT1-MMP Maintains Osteocyte Viability,” DNA Cell Biol., vol. 23, no. 3, pp. 155–165, 2004.

36. K. Holmbeck et al., “MT1-MMP-Deficient Mice Develop Dwarfism, Osteopenia, Arthritis, and Connective Tissue Disease due to Inadequate Collagen Turnover MMP Unit cellular tools in embryonic development, in growth, in mammary involution, and in a number of diseases such,” Cell, vol. 99, pp. 81–92, 1999.

37. A. Khojasteh et al., “The Effect of Deproteinized Bovine Bone Mineral on Saos-2 Cell Proliferation,” Iran. Endod. J., vol. 8, no. 3, pp. 118–122, 2013.

38. Q. Chen, C. Zhu, and G. A. Thouas, “Progress and challenges in biomaterials used for bone tissue engineering : bioactive glasses and elastomeric composites,” Prog. Biomater., vol. 1, no. 2, pp. 1–22, 2012.

39. E. Axpe and M. L. Oyen, “Applications of Alginate-Based Bioinks in 3D Bioprinting,” Int. J. Mol. Sci., vol. 17, no. 12, 2016.

40. Q. Feng et al., “Engineering a morphogenetically active hydrogel for bioprinting of bioarti fi cial tissue derived from human osteoblast-like SaOS-2 cells,” Biomaterials, vol. 35, pp. 8810–8819, 2014.

Supplementary Information

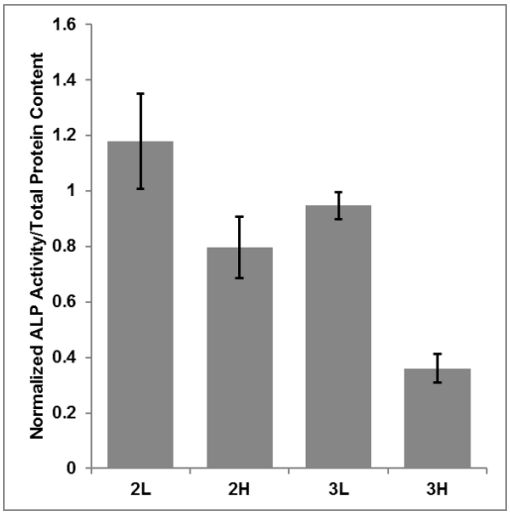

Figure S1. Alkaline phosphatase activity for 2L, 2H, 3L, and 3H bioprinted samples. 2L and 3H conditions were chosen for further examination as the 2H and 3L ALP activity was statistically equivalent.

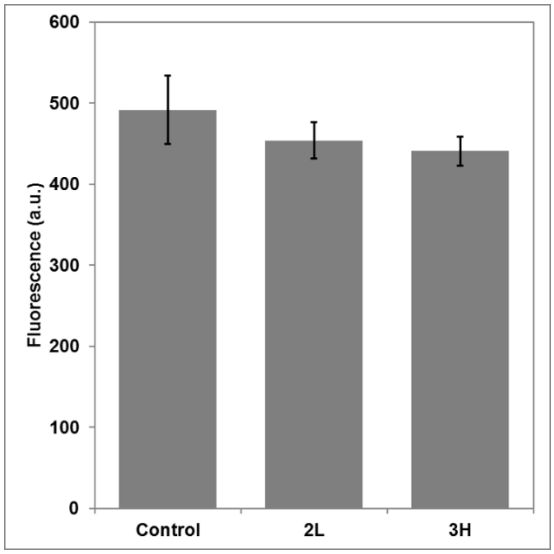

Figure S2. Cell metabolism readings for Saos-2 cells grown on the calcium treated paper alone, without any hydrogel encapsulation. Data shows that there was no statistically significant difference in cell metabolism between samples.

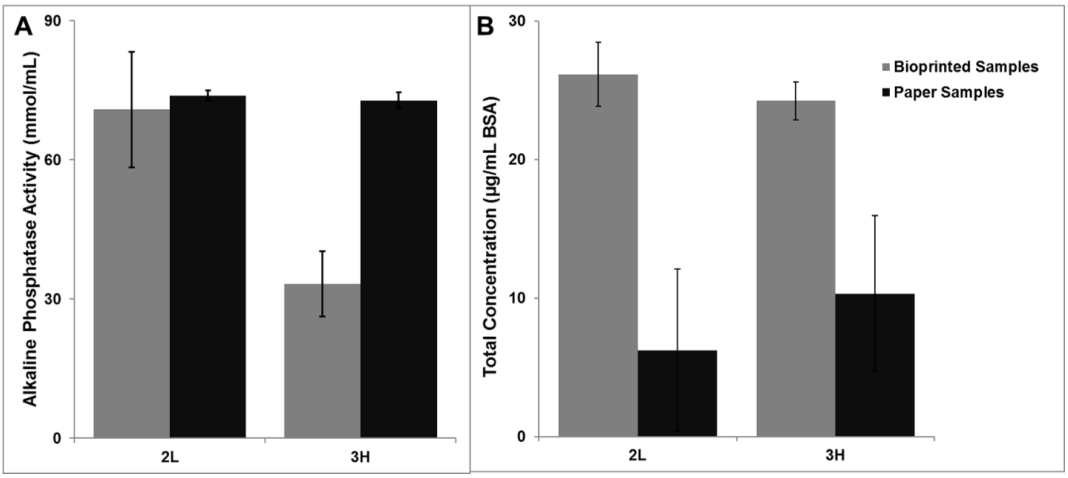

Figure S3. Alkaline phosphatase activity (A) and total protein content (B) of 2L and 3H samples both grown on calcium-treated paper (red) and bioprinted (blue). The ALP activity for bioprinted 3H samples is statistically significantly lower compared to bioprinted 2L samples while total protein content remains statistically the same. There is no significant difference in ALP activity or total protein content for the sample cultured on the paper alone.

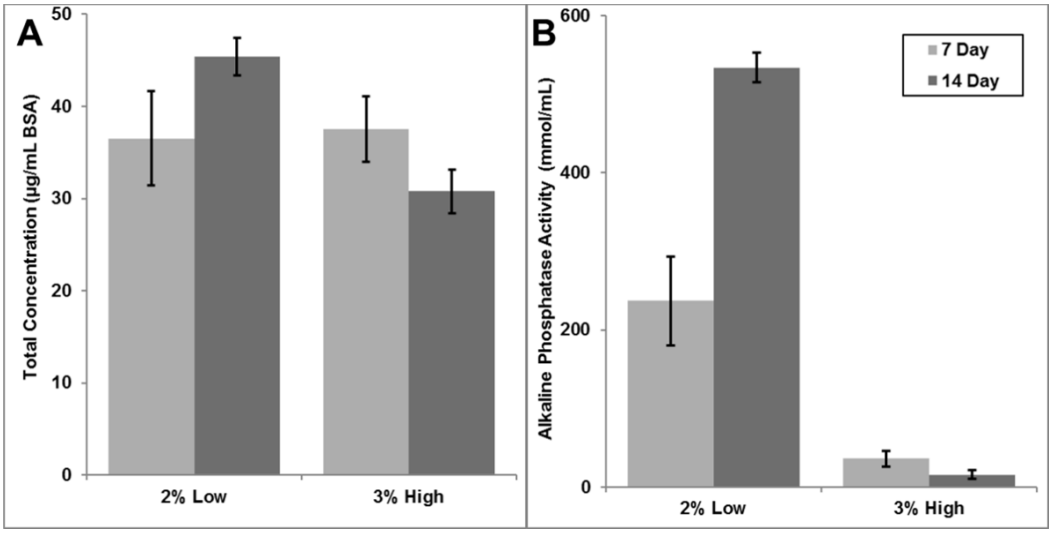

Figure S4. Alkaline phosphatase (ALP) activity (A) and total protein content (B) for 2L and 3H samples after 7 and 14 days of incubation.

Chapter 4: MICRO-MOLDING TECHNIQUE

A Rapid Biofabrication Technique for Self-Assembled Collagen based Multicellular and Heterogeneous 3D Tissue Constructs

Alireza Shahin-Shamsabadi[1], P. Ravi Selvaganapathy [1,2,*]

[1] School of Biomedical Engineering, McMaster University, Canada

[2] Department of Mechanical Engineering, McMaster University, Canada

[*] Corresponding Author: P. Ravi Selvaganapathy, Department of Mechanical Engineering, McMaster University, Canada. selvaga@mcmaster.ca

Status: Published

Full Citation:

Shahin-Shamsabadi, Alireza, and P. Ravi Selvaganapathy. "A rapid biofabrication technique for self-assembled collagen-based multicellular and heterogeneous 3D tissue constructs." Acta biomaterialia 92 (2019): 172-183.

Abstract

Although monolayer cell culture models are considered as gold standard for *in vitro* modeling of pathophysiological events, they cannot reconstruct *in vivo* like gradient of gases and nutrients and lack proper cell-cell and cell-matrix interactions. Spherical cellular aggregates, otherwise known as multicellular spheroids, are widely used as three-dimensional *in vitro* models to mimic natural *in vivo* cellular microenvironment for applications such as drug screening. Although very useful, the previously established techniques are limited to low cell numbers, their processes are usually slow, and sometimes show limitations in terms of the cell type that can be used. Here, a versatile technique based on rapid self-assembly of cells and extracellular matrix material in different shapes using microfabricated molds is introduced to form multicellular tissue constructs. The self-assembly process takes less than 6 hrs and produces a mechanically robust tissue construct that could be handled easily. We demonstrate that a variety of shapes including spherical, cuboidal, dumbbell- and cross-like shapes could be fabricated using this approach. Interestingly, the structures formed with non-spherical shapes were able to retain that shape even after removal from the molds and during long term cell culture. This versatile approach is applicable to a variety of cell types (breast cancer cell lines MCF-7, MDA-MB-321, Hs-578T; osteosarcoma cell line SaOS-2; endothelial cell line HUVEC) as well as a range of cell numbers (10^4-10^6). Furthermore, we also show that the constructs could be spatially patterned to position various cell types in a precisely controlled way. Such heterogeneous constructs that are formed provide physiologically relevant cell densities, 3D structure as well as close positioning of multiple types of cells that are not possible using other fabrication approaches. This fabrication approach will find significant applications in developing 3D cell culture models for drug discovery as well as tissue grafts for implantation.

Keywords: Self-assembly; Tissue constructs; Multicellular aggregates; Collagen; *In vitro* model; Tissue engineering

1. Introduction

Culturing mammalian cells in 3D has a long history. Even though, culturing cells on two-dimensional (2D) surfaces is currently considered to be the gold standard, initial investigations for *in vitro* cell culture were made using three-dimensional (3D) systems [1]. One of the initial attempts at 3D *in vitro* cell culture that used tissue explants of chick embryo was reported in 1912 [2]. Later in 1952 a new technique to form 3D cellular aggregates *in vitro* from disrupted cells of explanted tissues was developed [3]. After this a number of other 3D cell culture techniques were developed, in particular those using collagenous gels [4]. Comparison of these techniques with 2D systems shows their critical differences in terms of their biological behavior. For instance only 3D systems show drug responses that are comparable to *in vivo* systems and the same is true for gene expression patterns [4]. This is because the tissue topography and cell-cell interactions in 3D systems are more biomimetic compared to 2D ones [5].

Multicellular spheroids are one of these 3D *in vitro* models that are formed when cells are cultured in suspension or non-adherent surfaces [6]. These spheroids are cell aggregates containing complex cell-cell and cell-matrix interactions that recapitulate natural microenvironments of cells including natural gradient of nutrients, gasses, and different growth and signaling factors [7] that are physiologically relevant [8]. Microstructure of spheroids can be manipulated to study effect of chemical, physical, physiological, and architectural environment on different cellular function and behavior [7]. Many different techniques have been developed for multicellular spheroid formation which can be classified based on whether they incorporate extracellular matrices (ECM) in their initial construction. Matrix-free methods such as hanging drops, spinner flasks, low adhesion flasks, and external force-driven techniques are more common in which a dispersion of cells initially form loose aggregates and slowly turn into more solid structures over a period of days due

to cell-cell interactions and subsequently through the generation and assembly of their own extracellular matrices [9]. Alternatively, matrix-based techniques start with cells embedded in a hydrogel matrix such as collagen, Matrigel™, or alginate that serves as the scaffold [1, 6, 7, 10] and provides the shape of the construct formed. In addition, such techniques provide means to precisely tailor the cellular microenvironment and well as induce cell-matrix interactions [11].

Matrix-free techniques sometimes form spheroids with uncontrolled morphologies and low structural reproducibility. Aggregation in these systems is also limited to certain types of cells and there is no control over the matrix composition as they secrete their own. Therefore, they are more suited for developmental studies and for use with stem cells. Furthermore, these cell aggregates are limited in the size that they can grow and differentiate as large sizes lead to formation of a necrotic core due to mass transfer limitations [12-14]. Matrix-based techniques have the advantage of high control over cell and ECM source and type, size and shape of the formed structures, and cell density [15] and are more suited to study disease processes and for drug discovery. One of the emerging matrix-based techniques of forming spheroids is the use of micro-fabricated molds to cast bioinks with high cell to ECM composition ratio. Such methods make more efficient use of valuable bioinks, reduce the amount of reagents used and the amount of shear stress applied to the cells during initial deposition. Wells with spherical shapes and other predefined complex geometries like rods and honeycombs can be formed that can be used for high-throughput screening [6, 7]. These molds have been used with collagen [15], Matrigel™ [16], or UV curable hydrogels such as methacrylated hyaluronic acid or poly(ethylene glycol) [17, 18]. These extracellular matrices can provide appropriate microenvironment that will simulate *in vivo* conditions and lead to more physiological cell behavior that can be useful in the study of disease processes or in drug discovery [19]. The use of molds also allows scale up (up to 822 spheroids

can be formed in a single mold with a microwell array) and standardization of spheroid generation [20, 21]. Combinatorial variation of parameters such as cell number, ECM composition, growth factor concentration can also be introduced easily which facilitates drug screening. Despite these advantages, such techniques are time consuming (spheroid formation usually takes a few days), limited in cell type and to low cell density, and show no or limited control over positioning different type of cells in the 3D structure. Furthermore, the spherical shape of most of these constructs ensure that they can only be grown up to a certain size beyond which a necrotic core forms due to transport limitations. A universal technique capable of forming tissue constructs of various 3D shapes from a wide variety of cell types at physiologically relevant cell densities and with the ability to precisely position and integrate different cell types in close proximity to each other would be useful to overcome these limitations and provide a more relevant 3D model.

Here, we combine matrix- and cell-directed self-assembly processes to develop a rapid, scalable, controllable, and simple method to form multicellular tissue constructs. The self-assembly process is rapid and is typically completed in under 6 hrs as opposed to days for other methods. The method is capable of forming constructs in a variety of shapes such as spheres, rods, dumbbells and cuboids, and can be easily parallelized to produce large numbers at the same time. It also has the flexibility to produce both homogeneous multicellular constructs as well as heterogeneous ones where the location of different types of cells can be precisely defined. These constructs can be made at high and physiologically relevant cell densities which makes this method appropriate for creating 3D *in vitro* models for drug discovery applications and biological assays.

2. Fabrication process of the 3D Tissue Construct

A two-step fabrication process was devised so that the process of self-assembly associated with the ECM and the cells occured at different stages. The process begins with the fabrication of molds

with appropriate shapes that are representative of the final shapes of the tissue constructs. The molds were made of Poly dimethyl siloxane (PDMS) casted onto 3D printed features that represent the final shape. 3D printing was used for this purpose rather than other replication techniques such as soft-lithography because they were labor intensive and costly and required specific facilities. PDMS provides a low adhesion surface that is critical for formation of the tissue construct. Next, the bioink, a 1:1 mixture of cell loaded (5×10^4 -1×10^6 cells) culture media and collagen (5 mg/mL), was filled into the PDMS mold (Figure 1a). The pH of the bioink was adjusted to 7.4 by adding 0.1 M NaOH immediately before the filling process to initiate collagen self-assembly. Incubation for 2 hrs completes the crosslinking process and was used to fix the shape of the final tissue construct. Subsequently, extra culture medium was added to provide the cells with sufficient nutrients for the rest of the process. After this addition, a rapid consolidation and shrinkage of the tissue construct to its final state occurred (within 4 hrs) with the 3D shape fixed due to the initial collagen crosslinking, retained (Figure 1b). The rapid consolidation does not happen in the absence of cells and was related to the cell concentration, indicating that the cell-ECM interaction is primarily responsible for this shrinkage. The bioink can be composed of a single cell type or multiple cell types to create homogeneous mono- or co-culture constructs (Figure 1c). The shape of the mold fixes the shape of the initial construct formed due to collagen crosslinking and a variety of 3D shapes including cuboids, dumbbells, and crosses (Figure 1d) can be formed. Heterogeneous constructs can also be formed by depositing various bioinks composed of different cells in specific locations into the mold (Figure 1e). High viscosity of the inks and the hydrophobic nature of the PDMS enable spatial localization of the inks both during the deposition process as well as during the initial collagen crosslinking and construct formation (Figure 1e).

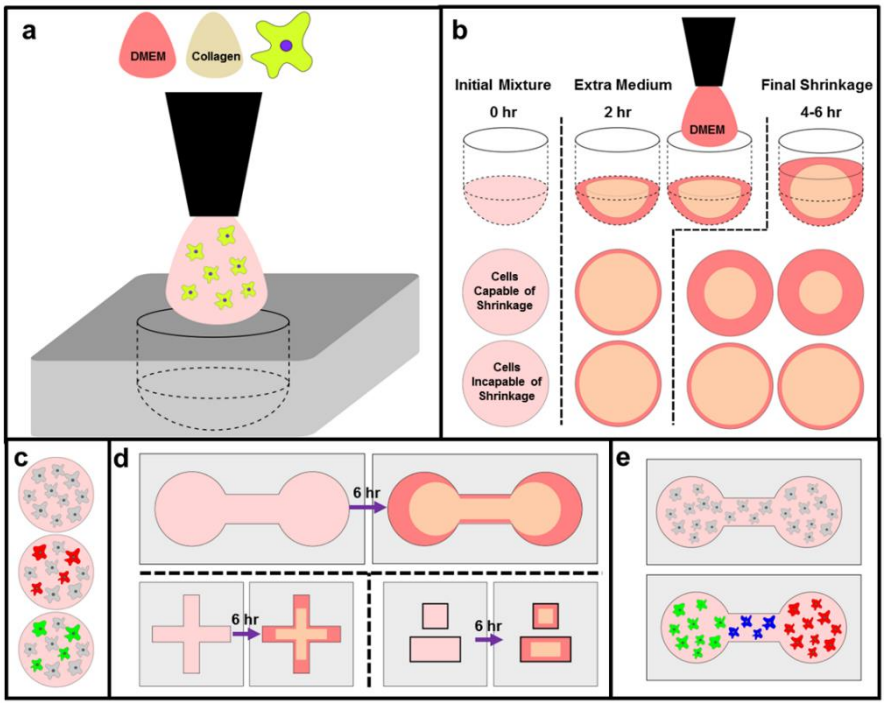

Figure 1. Schematic of the fabrication process; a) Addition of collagen, media (DMEM), and cell mixture to wells; b) Media addition steps and structural changes introduced to the constructs by cells capable and incapable of causing shrinkage; c) Mono- and co-culture of cells in spheroids; d) Various morphologies formed with this technique; e) Precise control over distribution of cells in complex structures.

3. Materials and Methods

3.1. Rapid Formation of Spheroidal Tissue Constructs

In order to form spheroidal tissue constructs, PDMS molds in the form of circular wells with spherical bottom were used. These molds were prepared by mixing PDMS and its curing agent with the ratio of 10:1 and casting it on the poly(lactic acid) (PLA) master mold with negative of the required patterns. Master molds were designed using software Solidworks® and 3D printed using a Stereolithography (SLA) based 3D printer (Objet 24 Desktop 3D printer). Large and small well sizes were created with diameters of 4 and 2.5 mm respectively. MCF-7 (Michigan Cancer Foundation-7, a breast cancer cell line) cells were cultured in Dulbecco's Modified Eagle Media

(DMEM) (Thermofisher, high glucose) supplemented with 10% V/V fetal bovine serum (FBS) (Thermofisher, US origin) and 1% Penicillin-Streptomycin (Thermofisher, 10000 U/mL) until 70% confluent. Cells were trypsinized and detached from tissue culture flasks. Required number of cells (10^5 or 10^6) were aliquoted, precipitated using centrifugation, and resuspended in proper amount of media (5 µL for small wells, 15 µL for large wells). The cell solution then was added to the equal amount of bovine collagen type I (Thermofisher, 5 mg/mL) and mixed to get a uniform distribution of cells. Finally, pH of the solution was adjusted to 7.4 by adding sufficient amount of 0.1 M NaOH solution and the mold was incubated at 37°C with 5% CO_2. Two hrs later, after the collagen was crosslinked, more media (25 µL for large wells and 10 µL for small wells) was added to provide cells with enough nutrients for the reminder of the assembly process. Bright field images of wells were taken using a stereo microscope immediately after filling the wells and after 1, 2, 4, and 6 hrs to measure the shrinkage using ImageJ software. After 6 hrs, spheroids were moved to 96 well plates for further applications or observations. The same process was performed with 5×10^4 cells in small and large wells with 1:1 ratio of collagen to culture media, as well as 5×10^4 cells in large wells with 1:3 ratio of the solutions but the same total volume in order to investigate possibility of using this technique with lower cell number or lower ECM to cell ratios.

3.1.1. Viability and Distribution of the Cells in the Final Spheroids

Effect of cell number and well size on cell viability at the end of the process (after 6 hrs) was studied by staining the spheroids (formed in large well with 10^5 cells and small well with 10^6 cells) with calcein-AM (Thermofisher). Five µL of calcein-AM solution was dissolved in 5 mL PBS and 100 µL of this solution was added to each spheroid. Spheroids were kept with this solution for 1 hr and then washed with PBS. Images were taken using an upright fluorescent microscope using green fluorescent filter with 4X magnification.

Microstructure of the spheroids was compared by studying two set of spheroids created with different cell densities. The high-density spheroid was fabricated in small wells loaded with 10^6 cells, while the low-density spheroids were fabricated in large wells with 10^5 cells. For histological staining, at the end of 6 hr process, spheroids were fixed in 4% wt/V formaldehyde in deionized (DI) water for 1 hr, dehydrated step wise in 40, 60, 80% ethanol in water and after embedding in 1 wt% agarose, paraffin embedding, and sectioning, staining with Hematoxylin and Eosin (H&E) was performed and images were taken using inverted microscope with 10 and 20X magnifications.

3.1.2. Structural and Functional Evaluations

The total amount of protein in the spheroids was measured using Pierce™ BCA Protein Assay Kit (Thermofisher). Crosslinked collagen in each spheroid was broken using 100 µL of collagenase/dispase (Sigma-Aldrich) solution (10 µL of 100 mg/mL collagenase/dispase as the stock solution in DI water, 10 µL of 10 mM $CaCl_2$ as enzyme activator, and 80 µL of DPBS). Half an hour later contents of each well were pipetted vigorously to break the spheroids. To deactivate the enzyme, 25 µL of 10 mM EDTA was added and incubated for 5 min. Eventually 50 µL of this solution was transferred to a new well plate and the same amount of 0.1 %V/V Triton X-100 in PBS solution was added to lyse the cells with 10 min incubation in incubator. The difference between each condition and the control (same solution of enzyme and its deactivator) was reported as the total protein content of each spheroid. The same process was performed on acellular spheroids (the same collagen and medium solution in small and large wells without cells) to measure ECM protein content of each spheroid and eventually cell protein content in each case was defined as BCA reading of spheroid with cells minus BCA reading of acellular constructs. These readings were translated to actual protein amounts using the calibration curve of the kit.

To measure the mass transfer in and out of each spheroid through metabolic activity, Alamar blue assay (ABA) kit (Thermofisher) was used. Spheroids were transferred to 96 well plates and 200 µL of DMEM supplemented with 10 %V/V Alamar blue solution was added to each well and incubated for 90min. After that, 100 µL samples were transferred to a black 96 well plate and reading was performed at excitation and emissions of 560 and 590 nm.

To study the cause of the shrinkage in the spheroids, effects of cells' transmembrane proteins and cytoskeleton were studied. PCR was performed to study expression of cell-cell and cell-ECM junctions. For this purpose, spheroids formed in small wells with 10^6 cells (S-10^6 group, highest cell density) and the ones formed in large wells with 10^5 cells (L-10^5 group, lowest density) were chosen. Spheroids were digested the same as before and solutions were transferred to 0.5 mL DNase free PCR tubes, 250 µL PBS was added to dilute it, cells were centrifuged, and the supernatant was aspirated. As for control, collagenous grafts that didn't show contraction were formed with 10^5 cells in 25 µL of collagen and 5 µL of media and after 6 hrs the same digestion and extraction process was performed. To study gene expression, a one-step qRT-PCR kit (Cells-to-CT™ 1-Step Power SYBR™ Green, ThermoFisher) was used. Primers for E-cadherin (as cell-cell adhesion marker), β1-Integrin (as cell-ECM marker), and β-Actin (as housekeeping gene) were used according to Table 1. The ΔΔCt values for each primer set were calibrated to the average of housekeeping Ct values and then to the Ct values of the L-10^5 group. qRT-PCR was performed for 4 samples in each group in duplicates.

Table 1. Sequence of the used primers for qPCR (5'to 3')

Target Gene	Forward	Reverse
E-Cadherin	TGCCCAGAAAATGAAAAAGG	GTGTATGTGGCAATGCGTTC
β1-Integrin	CATCTGCGAGTGTGGTGTCT	GGGGTAATTTGTCCCGACTT
β-Actin	CATGGAGTCCTGGCATCCACGAAACT	ATCTCCTTCTGCATCCTGTCGGCATA

Effect of cytoskeleton on the contraction was studied by impairing the actin network of the cells. MCF-7 cells were cultured up to 70% confluent and pretreated with medium supplemented with 100 nM Latrunculin A (LAT-A, Abcam) for one hour. Then cells were trypsinized and spheroids were formed with 5×10^5 cells in large wells once without LAT-A in the media (T-nT) used for spheroid formation and another time with media containing the same concentration that was used for pretreatment (T-T). The same spheroids were formed without LAT-A treatment as the control (nT-nT).

3.2. Spheroid Formation Using Other Cell lines

To determine whether the same technique can be used with other cell lines, large wells (4 mm in diameter) and 5×10^5 cells in 30 µL of 1:1 collagen and DMEM solution was used with other cell lines including MDA-MB-231 and Hs-578T (two other breast cancer cell lines), SaOS-2 (osteosarcoma cell line), human umbilical cord endothelial cells (HUVEC), 3T3, L929, and Chinese Hamster ovary (CHO) cell lines (three fibroblastic cell lines), and C2C12 (myoblast cell line). All of the cells were grown in their specified culture media until 80% confluent (HUVECs were grown in EBM-2, CHO cells were grown in F12K supplemented with 10% FBS, SaOS-2 cell were grown in McKoy's medium supplemented with 15% FBS, and C2C12s were grown in DMEM with 10% heat inactivated FBS. All of the other cells were grown in DMEM supplemented with 10% FBS) and trypsinized to prepare the cell suspension that were used to form spheroids. The same procedure as described previously was used to form spheroids. In all cases DMEM supplemented with 10% FBS was used for spheroid fabrication to eliminate effect of media composition on collagen crosslinking and shrinkage pattern. All of the cell lines were acquired from ATCC®, HUVECs were used under passage number 10, and as for the rest of the cells, passage numbers below 30 were used.

Effect of cell type on mechanical properties of the spheroids was studied using a microscale mechanical test system (MicroSquisher, Cell Scale). A 3×3 mm stainless steel platen connected to a 0.4 mm diameter cantilever was pressed on the spheroids at the rate of 10% strain per minute in a displacement-controlled setup. Location of platen was tracked using a camera and a load cell connected to the other end of cantilever was used to measure the force exerted by the spheroids. The force-displacement data were then used to measure stiffness of the spheroids. Eight spheroids (5×10^5 cells in Large wells) were tested for each condition.

3.3. Heterogenous Multi-cellular Spheroid Formation

To determine whether this method is capable of forming heterogeneous spheroids with more than one cell type, spheroids were fabricated using bioinks consisting of MCF-7 cells along with either green fluorescent protein (gfp) tagged 3T3 fibroblasts or red fluorescent protein (rfp) tagged HUVECs in large wells. The total cell population was kept at 5×10^5 with 90% of the cells being MCF-7 and 10% of the second cell type. Bright field images as well as fluorescent ones were taken the same as before to study effect of second cell type on spheroids shrinkage and distribution of different cell types. These results were compared to spheroids formed in the same condition but just with MCF-7 cells.

3.4. Effect of Extracellular Matrix on Spheroid Formation

Effect of the ECM type on the construct formation process and that of the concentration of the ECM was studied in large wells using collagen or Geltrex™ (ThermoFisher) as ECM. Two concentrations of bioinks were prepared by adding either 15 or 30 µL of the ECM, with 15 µL DMEM or without it, respectively, loaded with 5×10^5 MCF-7 cells. The rest of the fabrication process was the same as that described previously.

3.5. Homogeneous Non-spherical Structures Using MCF-7

Versatility of the technique to form non-spheroidal tissue like constructs was shown using molds with different shapes. Molds in the shape of a cross (2(L)×2(W)×2(H) mm), a dumbbell (1.5 mm in radius with 3 mm distance between wells, 2 mm deep), and a series of cuboids (2(L)×2(W)×2(H) and 4(L)×2(W)×2(H) mm) were made in PDMS. Bioink was deposited into the molds and the construct allowed to assemble using the same procedure as described previously. In case of the cross structure, 10^6 cells with total solution of 50 µL were deposited into the mold. Similarly, in the case of the dumbbell, 60 µL of the bioink containing 10^6 cells was deposited while for the cuboid shapes 8 and 16 µL of bioink containing 5×10^5 and 10^6 cells were used. The ratio of collagen to DMEM was 1:1, which was the same as previous experiments. Six hours later, the constructs formed in the shape of cross were transferred to 48 well plates and images were taken 24 hrs, 3 and 7 days later to confirm their ability in maintaining their predefined shape. To show whether constructs will be able to maintain these predefined shapes independent of the mold, constructs with the shape of cross were kept in 48 well plates and images were taken.

3.6. Heterogeneous Multi-cellular Non-Spherical Structure Formation

To demonstrate the capabilities of this method to fabricate heterogeneous tissue constructs molds in the shape of a dumbbell were used. Three different bioinks were loaded into different locations on the mold. Specifically, 25 µL of the bioink with 5×10^5 of gfp-3T3 cells was added to the left well and a similar volume with the same concentration of rfp-HUVECs was added to the right well. The high viscosity of the bioink prevented its spread and spatially confined it to the round chambers into which they were deposited. Finally, 10 µL of bioink with 2×10^5 MCF-7 cells dyed with blue cell tracker (CMF_2HC Dye, ThermoFisher) was added to the connecting channel region. Bright field and fluorescent images of the 3D tissue construct that self-assembled were taken using

a stereo microscope and a ChemiDoc™ MP imaging system (Bio-Rad), respectively. After 4 hrs, close-up images of the interface regions between the different cell types were taken using an upright fluorescent microscope, in order to determine cell distribution and the shape of the tissue structure formed in these regions.

3.7. Data Analysis

Data is reported as Mean ± Standard Deviation (SD), statistical analysis is performed using the two-way student's t-test with an accepted statistical significance of P-value < 0.05.

4. Results and Discussion

4.1. Rapid Formation of Spheroidal Tissue Constructs

In order to determine the speed at which tissue constructs are formed, bioinks were loaded into molds with spheroidal bottom. Bioinks with various population of cells (10^5 and 10^6) were loaded into wells of different sizes (2.5 and 4 mm in diameter) and imaged periodically over 6 hrs (Supplementary Figure 1). For the first 2 hrs after loading, the primary mechanism of assembly was the collagen crosslinking which led to a small amount of consolidation and initial formation of the construct. The change in pH due to the addition of NaOH causes onset of collagen crosslinking that initiates the assembly process. Subsequent addition of the growth medium leads to a more dramatic consolidation with a reduction in volume (~70% when 10^6 cells were used and ~50% in case of 10^5 cells independent of well size) as shown in Figure 2. The second phase of consolidation does not happen in the absence of cells (Supplementary Figure 2) indicating the key role played by the cells in this process. Bioinks loaded into both large and small wells were consolidated (Figure 2b) in a highly repeatable manner with very small variation in the sizes, unlike many of the other spheroid generation methods. The final consolidated volume of the tissue

construct was not dependent on the initial population of cells for small wells while it was significantly different in the case of large wells. It is interesting to note that the trajectory of the consolidation is mostly dependent on the cell population in the wells and not on the well size as shown in Figures 2c. The constructs formed were found to be mechanically robust and easy to handle after 6 hrs unlike other methods where the consolidation process takes several days (up to 7) for similar amount of consolidation [15]. This method is scalable and able to form spheroidal constructs with cell population as low as 50,000 cells in both small and large wells (Supplementary Figure 3). Changing the ratio of the collagen to DMEM loaded with cells (5×10^4 cells in large wells) in the bioink from 1:1 to 1:3 resulted in smaller spheroids (Supplementary Figure 4) demonstrating the role of ECM in determining the final consolidated size.

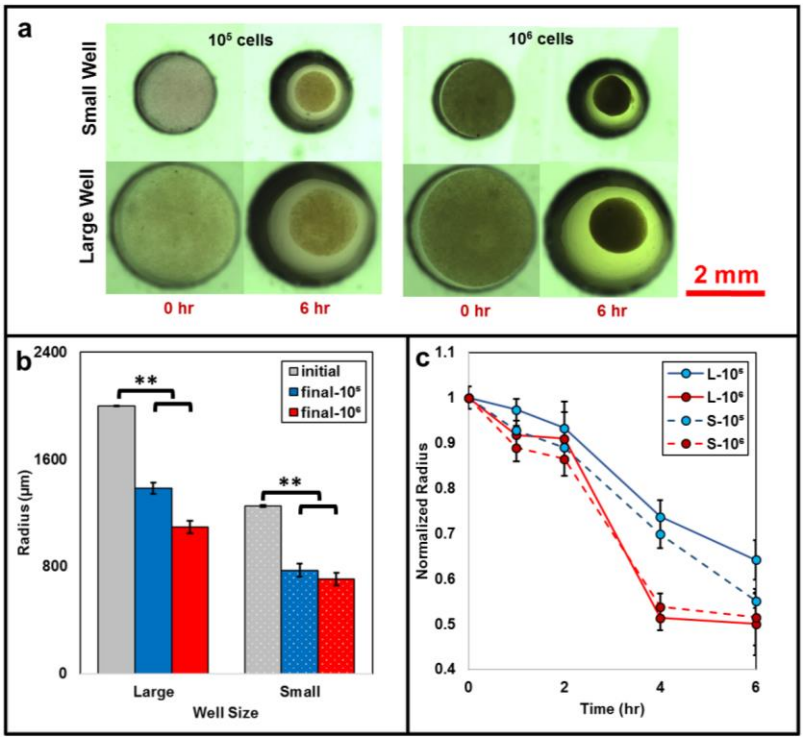

Figure 2. a) Bright field images of constructs at beginning and end of the process; b) Radius of spheroids (blue and red bars) after 6 hrs compared to their initial radius (grey bars) (n=6). All of p-values are <0.001; c) Effect of well size (2.5 and 4 mm in diameter) and cell number (10^5 and 10^6) on shrinkage pattern (amounts are normalized to initial radius of each of them). Data in part b are actual values and in part c are normalized to the initial condition.

The distribution of live cells within the spheroid formed was determined using live cell staining with calcein-AM (Figure 3a). It shows that at the end of the process there was a uniform distribution of live cells in all regions of the spheroids. Spheroids formed in large well with 10^5 cells and small well with 10^6 cells were chosen for live staining as the first one has the largest size with lowest cell density while the latter had the smallest with highest cell density. Interestingly, the cells at the center of the spheroid appear to be alive and with the same density as those at the surface even though the diffusion limit in the spheroids is similar to avascular tissues and is around 150 to 200 µm [22-25]. This is probably due to the fact that the fabrication process is very fast, and viability of the cells is not affected during this time period.

The spheroid fabrication process can also be used to control the primary type of interaction of the cells. A high density of cells in the spheroid will promote a greater cell to cell interaction while a lower density will provide more cell ECM interactions. In order to demonstrate it, the same spheroids as for live staining were used and histological staining was performed using H&E to show the distribution of the cells in each condition (Figure 3b). They show that it is possible to create conditions where the cells are closely packed and cell-cell interaction is substantial by using small wells and high cell numbers. Similarly, for those assays that investigate cell-ECM interactions, large wells with low cell numbers would be suitable.

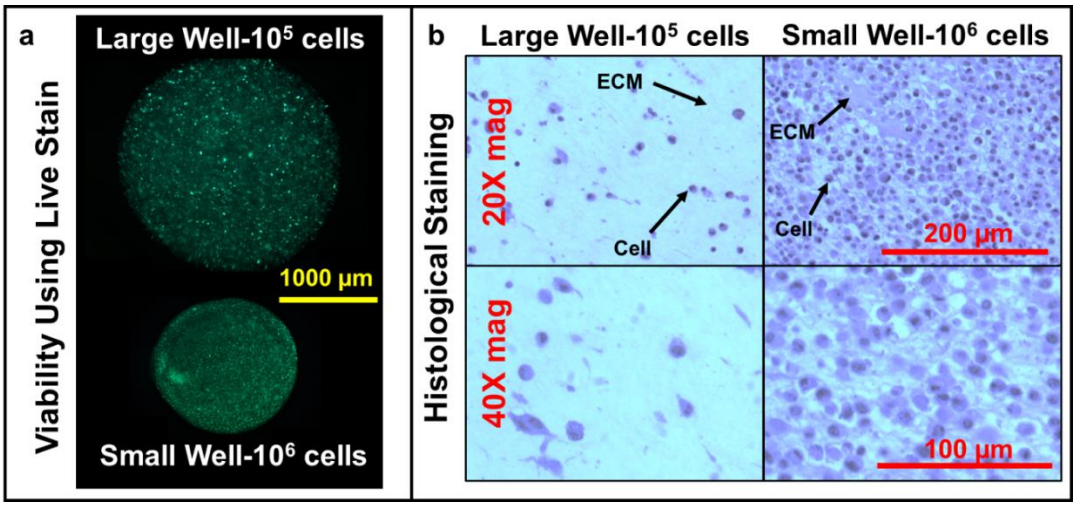

Figure 3. a) Live stained spheroids at the end of the fabrication process (6 hrs after process is started); b) H&E stained sections of different MCF-7 spheroids showing compactness of cells.

Total protein content of each of the spheroids was measured and compared to each other and acellular spheroids using Pierce BCA kit (Figure 4a) and as expected this amount is dependent on both well size which represents the amount of collagen used and the total cell number in each spheroid. Comparing spheroids with the same cell number but different well sizes shows that total protein is significantly dependent on the cell number and less on the well size. Figure 4b represents the total metabolic activity of each of the spheroids using Alamar blue. Interestingly, metabolic activity changed much more significantly with cell numbers in large wells as compared with smaller wells. This may be related to transport dynamics of the resazurin sodium salt and the final product in and out of the spheroids which is related to the compactness of the structure as well as their radii. Spheroids formed in both large and small well sizes show a propotional increase in protein content when loaded with 10^5 and 10^6 cells, as expected. This was in contrast with the metabolic assays (ABA intensity) where the larger wells showed a more dramatic change to changes in the number of cells as compared with the smaller wells. This indicates importance of

spheroid size and composition on mass transport properties which can be used to modify transport dynamics of drugs in and out of the spheroids formed with applications in drug screening [26].

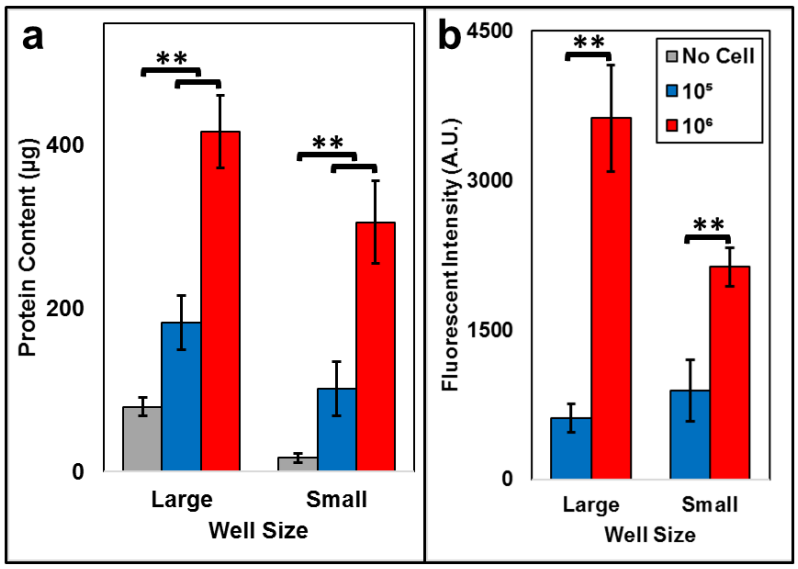

Figure 4. a) Total protein content of spheroids with and without MCF-7 cells in different well sizes. Protein content of the acellular constructs are 16.88±5.65 and 79.78±11.15 µg for small and large wells respectively; b) Total metabolic activity of the spheroids. All of p-values are <0.001. While there is a significant difference between total protein content of samples formed in each well size with different cell numbers (L-10^5 vs. L-10^6 and S-10^5 vs. S-10^6) (p-value<0.001) the difference is not significant for spheroids formed with the same number of cells in different well sizes with p-value being 0.07 for samples with 10^5 cells and 0.23 for samples with 10^6.

The microstructure of the spheroids was also studied. As it is shown in Figure 5a, while there is no meaningful difference between expression of E-cadherin, a cell-cell junction protein, in the two studied groups (spheroids with higher cell density (S-10^6) and spheroids with lowest density (L-10^5)), β-integrins, cell-ECM junctions, are expressed more than 6-fold higher in denser spheroids (S-10^6) which explains the higher amount of shrinkage observed. Samples that didn't show shrinkage were used as control and although they showed slightly lower expression of both E-cadherins and β-integrins compared to L-10^5 group, this difference wasn't significant. It has been shown that formation of multicellular spheroids includes an initial phase of integrin-ECM interaction to form the aggregates which is then followed by the enhanced cell-cell interactions

through cadherins which causes the final compaction. The different timeframe of action between these two phases can be due to the time needed for expression of sufficient amount of E-cadherins on the cell membrane [1, 6]. Formation of a spheroid starts by formation of loose aggregates with initial cell-ECM attachments which later forms a compact solid structure by accumulation of cadherins on cell surface and their hemophilic binding [9, 27].

To study whether cell-cell and cell-ECM adhesions are dominant in spheroid formation or contraction caused by cytoskeleton, MCF-7 cells were treated with actin cytoskeleton influencing drug latrunculin A (LAT-A) that is known to bind to actin monomers and prevent their subsequent reorganization of cytoskeleton in MCF-7 cells [28]. Spheroids were formed with 5×10^5 cells in large wells without pre- or post-treatment (nT-nT), pre-treated cells with 100 nM for 1 hr without post-treatment during spheroid formation (T-nT), and pretreated cells with post-treatment using the same concentration as pretreatment step (T-T). Spheroids were formed in all cases and there was no meaningful difference between their radii after 6 hrs (p-value > 0.05) which combined with increased expression of integrins shows the importance of cell-cell and cell-ECM interactions over cytoskeleton remodeling and reorganization during the first few hours of the shrinkage process. Such multifactorial effects on cell aggregation have also been observed in aggregation of cell types without the ECM present, where cytoskeleton tension and cell-cell adhesion played an opposing role in determine the extent of compaction observed [29].

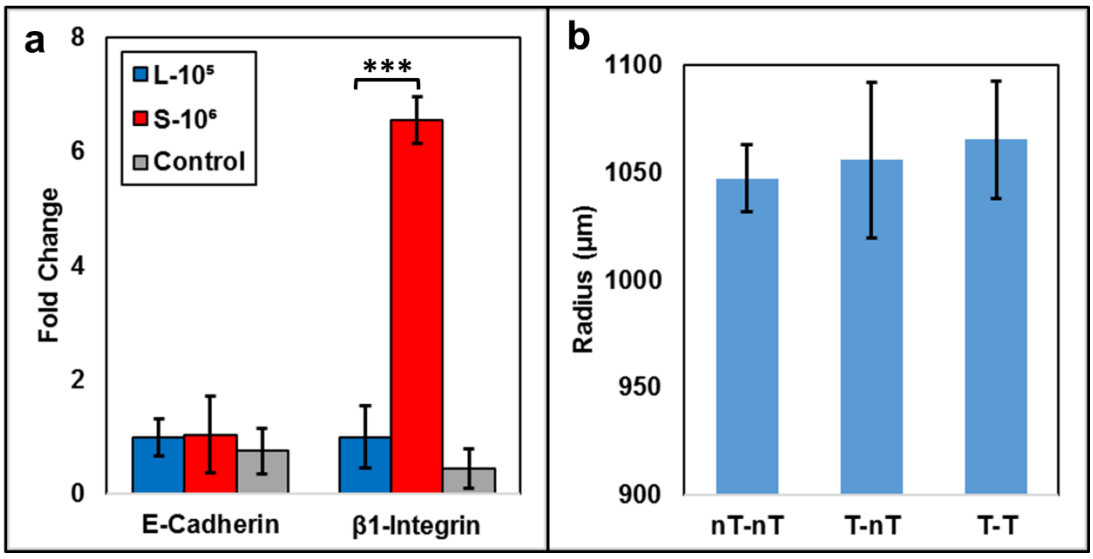

Figure 5. a) Expression of Cadherins and Integrins using PCR (n=4) for L-10^5 and S-10^6 spheroids compared to control (collagenous grafts with no shrinkage). p-value: **<0.0001; b) Final spheroid sizes of cells with and without disrupted actin networks (n=6 with no significant difference between different conditions).

4.2. Homogeneous Multi-cellular Spheroid Formation

The ability of different cell types to rapidly form spheroids was evaluated by using eight other cell lines (in large wells with 5×10^5 cells). Some of the cell types such as HUVEC and HS578T demonstrated a higher propensity for rapid consolidation as compared with MCF-7 cells while others such as SaOS-2 and MDA demonstrated a lower propensity as shown in Figure 6a. For instance, the spheroids made from HUVEC cells consolidated to a radius of 890.23±15.48 μm within 6 hrs from the original well with 2 mm in radius while spheroids made using L929 bioink hardly reduced in size within the given timeframe (Figure 6b) and only had the shrinkage associated with the original collagen crosslinking in the first phase of consolidation. C2C12, 3T3, and CHO cells didn't show any shrinkage either. This propensity may be linked to the differing ability of the cell types to express adhesion molecules such as cadherins or integrin within this short time frame.

Multicellular spheroids and other self-assembled constructs have been used for different applications such as modeling naturally occurring processes, as a model for cancer research and drug discovery, as well as building blocks in tissue engineering. One of the limitations of using these as building blocks for large tissue constructs is diffusion limitations and the need for vascularizing the structure [20].

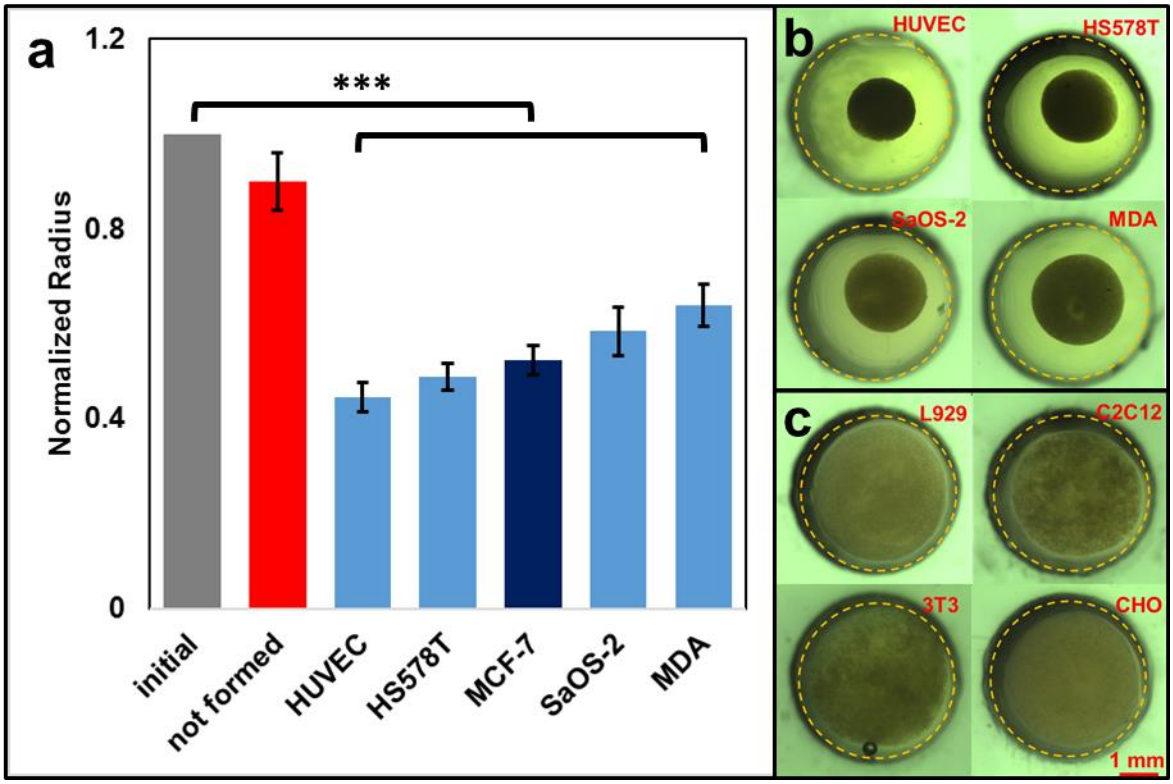

Figure 6. a) Normalized radius of the constructs compared to their initial size for cells that didn't form spheroids and for spheroids formed in large wells with 10^5 Cells after 6 hrs with different cell types (n=6). Final radius is normalized and compared to their initial values. There is a meaningful difference between final size of all of the formed spheroids (p-value<0.0001) and their initial size but not for constructs that didn't show shrinkage; b) Final spheroids of HUVEC, HS578T, SaOS-2, and MDA cell lines that formed spheroids; C) Grafts of cells that didn't form spheroids at 6 hrs (L929, C2C12, 3T3, and CHO cells).

Using MicroSquisher testing machine (setup shown in Figure 8a) spheroids formed above were tested under compression and their compressive stiffness is calculated as the slope of the initial linear region of Force-Displacement diagram (Figure 8b). Based on these results although

spheroids formed with different cells showed different amount of compaction, the final stiffness was the same for most of them once their initial cell density and well size were the same. The only exception was the human carcinosarcoma cell line which was observed to have a significantly higher stiffness as compared with other cell lines. Collagen constructs without cells formed with the same conditions didn't have enough mechanical stability and disintegrated in the process of transferring them from the PDMS wells to the Microsquisher machine. These preliminary results indicate that the cell-ECM interaction is critical for the formation to mechanically stable spheroids.

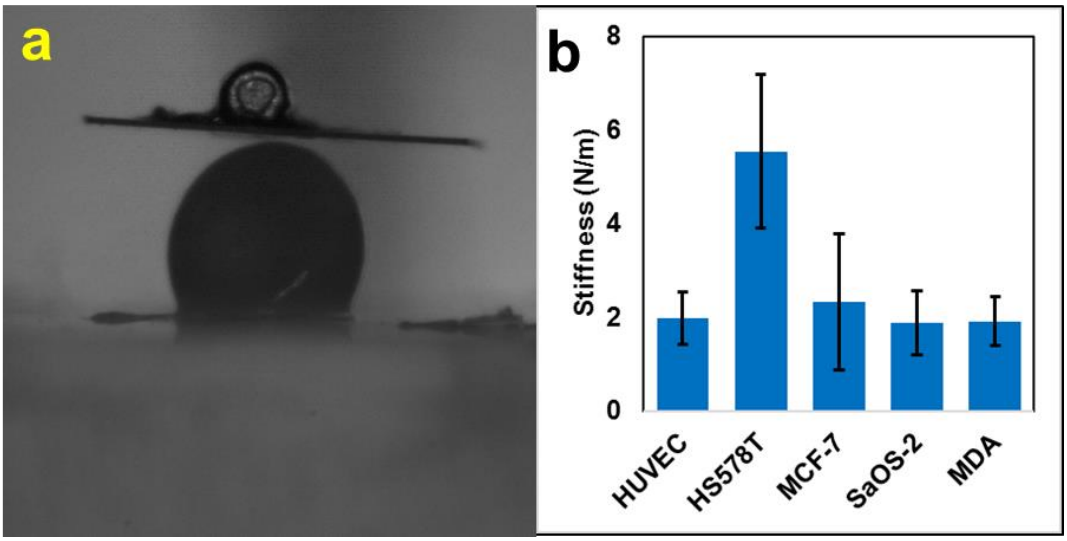

Figure 7. a) Mechanical testing setup; b) Comparison of spheroids in terms of their stiffness (n=8).

4.3. Heterogeneous Multi-cellular Spheroid Formation

Ability of the method to form heterogeneous multi-cellular spheroids was demonstrated by using a bioink that consisted of 90% MCF-7 cells along with 10% of 3T3s or HUVECs. These specific cell types were chosen as interaction of stromal cells such as fibroblasts and endothelial cells with cancer cells is an active area of study and developing 3D models that can recapitulate these interactions is important. For example, 3D spheroidal models that recapitulate fibroblast support

of cancer cell invasion, and their effect on proliferation and ECM expression as well as endothelial effect on tumor evasion and angiogenesis have been shown [30-34].

The total cell population was fixed as 5×10^5 cells and spheroid formation occurred in large wells. All of these bioinks were found to result in spheroid formation as shown in Figure 8. Bright field and fluorescent images shown in Figure 8a also demonstrate that the cells are uniformly distributed within these spheroids. Interestingly, addition of a small percentage of cells of the second type caused additional consolidation of the spheroids even when some of the cell types (3T3s) didn't cause consolidation by themselves within the given timeframe. Bioinks with MCF-7 cells alone consolidated to form spheroids that were 1047.17±15.6 μm in size but replacing of 10% of cell population with HUVECs resulted in further decrease in the final size to 959.30±7.8 μm. Using 3T3s that by themselves did not cause considerable consolidation of the spheroids also produced a spheroid of the size of 947.28±13.3 μm with higher shrinkage compared to MCF-7 ones alone which could be because of the increased expression of E-Cadherins in cancer cells when co-cultured with fibroblasts [35].

Other matrix-based spheroid formation techniques have been developed using different types of ECMs or biofabrication approaches. Harma et al. [36] has formed spheroids of prostate cells by embedding them between two Matrigel® layers. The spheroid formation using this technique is mostly initiated from single cells resulting in different morphologies such as round, stellate, mass, or grape-like structures over the course of a few days. This technique fails to form spheroids in collagen rich ECMs and spheroids with different shapes and sizes can form. Lee et al. [27] has used a fibrinogen-modified poly(ethylene glycol)-diacrylate hydrogel to form spheroids of liver-like cells in a three-week time span. UV polymerization is used to crosslink this hydrogel with a photoinitiator and cells aggregate inside the bulk of hydrogel to form the spheroids with different

sizes with the ones in the edges being bigger compared to the ones in the center parts. Besides from a slow process and spheroids with different sizes, spheroids formed using these two techniques are trapped inside the bulk of hydrogel and there is no direct access to them separately. Microfluidic systems have also been used to form spheroids using droplet-based techniques [37]. Although these techniques can form spheroids in a highly controlled and fast way, the applied shear force and the fast gelation mechanism could have adverse effects on cell viability not to mention the labor-intensive process and high-tech equipment necessary for fabrication of the devices.

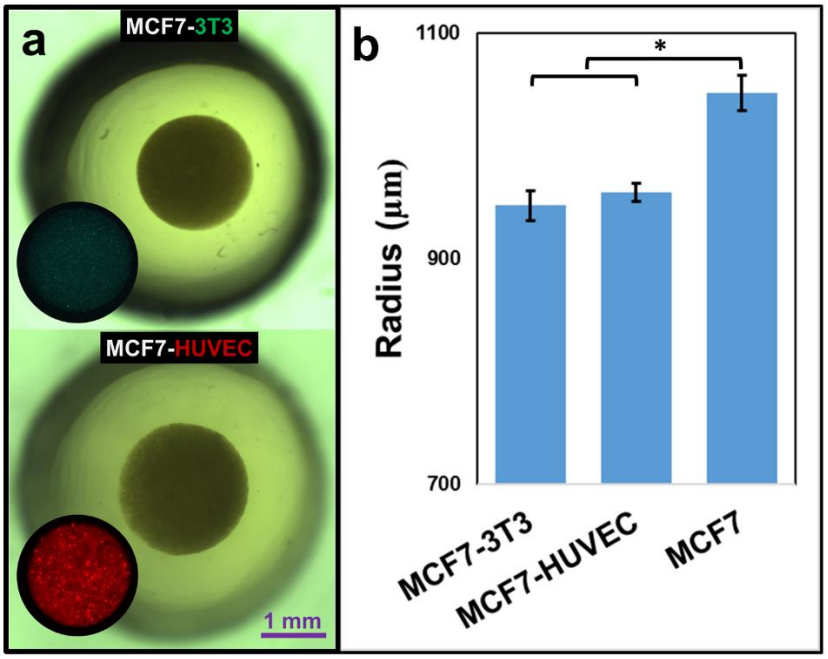

Figure 8. a) Brightfield and fluorescent images of 3T3 and HUVEC (10% of total population) co-culture with MCF-7s in large wells with 10^5 cells after 6hrs. p-values: *<0.01; b) Effect of second cell type on final spheroid radius (n=6).

4.4. Effect of Extracellular Matrix on Spheroid Formation

Previously, we had determined that cells were essential for rapid formation of the tissue constructs. In order to determine other essential conditions, we tested the method with different ECM. Apart

from collagen many other natural ECMs such as laminin, elastin, glycoproteins and proteoglycans [38] are also looked upon as important matrices for 3D cell culture and to recreate the tissue microenvironment. Matrigel® and its reduced growth factor version, Geltrex™ are some of the most widely used examples [39-41]. We evaluated the use of Geltrex™ with this method and impact addition of extra DMEM. Figure 9 shows the grafts formed with collagen and Geltrex™ with and without DMEM. As it can be seen only in the case of collagen with DMEM was the consolidation significant. This experiment indicates that both collagen and DMEM (at least equal volume of collagen) is critical for the consolidation. In all of the scenarios we found that the ECM crosslinked in less than 2 hrs and formed a solid structure (in case of collagen by adjusting its pH to 7.4 and in case of Geltrex™ by increasing the temperature). Once collagen crosslinks it starts to exclude water and self-assemble into crosslinked fibrils forming well connected scaffold. Furthermore, cells have transmembrane adhesion receptors that adhere to Collagen, enabling forces to be transmitted from the cells onto the matrix scaffold. This coupling between the ECM and the cells promotes the consolidation process. The exclusion of water pushes it out of the scaffold and promotes consolidation. Geltrex on the other hand does not precipitate out and therefore will not exclude as much water from the matrix as Collagen does leading to a considerably less consolidation.

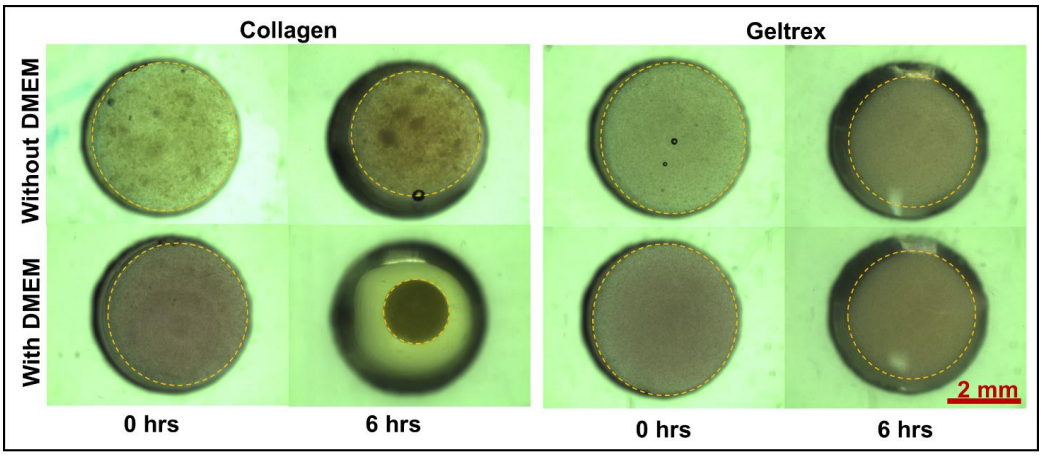

Figure 9. Effect of Collagen vs. Geltrex™ and dispersion in DMEM in fabrication of the spheroids.

4.5. Homogeneous Non-spherical Structures Using MCF-7

Multicellular spheroids are widely used because of their ability in resembling structure of real tissues and conditions such as initial avascular state of tumors [6, 42], but the formation of a necrotic core is not preferable in studying other tissue types and biological systems where use of non-spherical constructs can be used. To this end, molds with different shapes were used with the same process as before in order to determine whether initial shape at which collagen crosslinks defines the final shape or the forces exerted by the cells during the shrinkage process. Figure 10 represents the final shape of these non-spherical aggregates. The tissue constructs consolidated isotopically in all directions after the initial collagen crosslinking phase that fixed the shape of the initial scaffold structure. These structures could be removed after 6 hrs from the molds whereupon they acquire enough structural stiffness and stability to be handled with tweezers. Interestingly, these structures retained their shape even when unconstrained as shown in Supplementary Figure 5 where they were kept in a 48 well plate for a further 24 hrs, 3 and 7 days. Non-spherical cell-embedded collagen aggregates has been prepared before using PDMS molds for different applications [43-45]. These constructs required micro-cantilevers in the molds formed using multistep photolithography process to hold the consolidating construct to the non-spherical shape. In the absence of such constraints they would revert to the spherical shape. Unlike them, our method does not require complex mold fabrication or cantilevers and utilizes the two-step consolidation process to fix the shape of the scaffold and then introduce isotropic consolidation. In addition, our constructs can be physically removed from their molds easily for further processing, while those attached to the cantilevers are fixed in place. Other approaches of tissue construct formation using Collagen [15] using PDMS molds are not rapid (take several days as compared to 6 hrs) and weren’t able to maintain their initial shape once removed from the mold

unlike the constructs formed in our study (supplementary Figure 5). The two step process for consolidation and the use of higher concentration of Collagen (5 mg/mL vs. 3 mg/mL) are critical for the difference in the observed consolidation process. The ability to allow sequence assembly of the collagen into fibrils and then subsequently promote the rapid binding and force exertion of the cells leads to formation of tissue constructs of any shape which is fixed even when unconstrained that opens significant possibilities for engineering them.

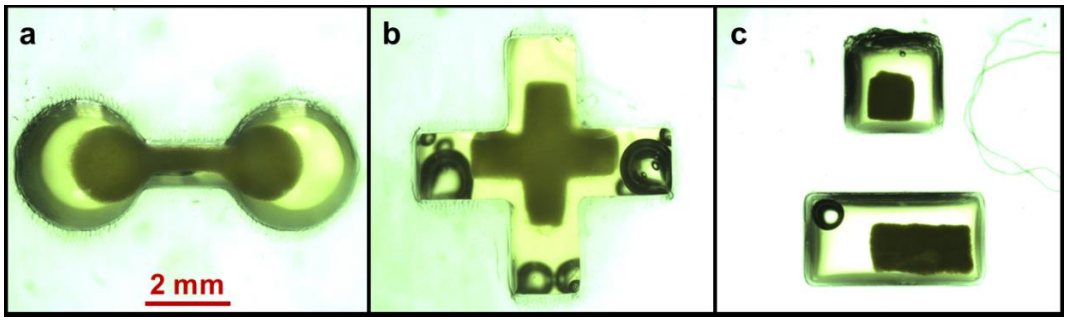

Figure 10. Different morphologies formed with DMEM to collagen ratio of 1:1, a) dumbbell with 10^6 cells in 60 µL bioink, b) cross with 10^6 cells in 50 µL bioink, and c) cuboids with 5×10^5 and 10^6 cells in 8 and 16 µL bioink. Bioink is 1:1 ratio of collagen and DMEM.

4.6. Heterogeneous Multi-cellular Non-Spherical Structure Formation

In natural tissues different cell types are positioned adjacent to each other in close proximity. The signaling from one cell affects the behavior of the neighboring ones and is critical to recreate *in vivo* like microenvironment. The ability of this method to form multicellular structures with predefined positioning of cells was shown by formation of multi-cellular dumbbells. Figure 11 represents the bright field and fluorescent images of the multicellular-dumbbells after 0 and 4 hrs with three different cell types in left, center, and right sections of the structure. Even though the bioinks have been introduced into the different regions of this mold one after the other, the consolidation process is smooth and a single continuous construct is formed (Figure 11a). There

is also not much mixing between the regions and a clear and intimate interface is formed where different cells are positioned at different locations within the same ECM. It is also interesting that due to the different cell types used in different locations the amount of consolidation that occurs varies with position. Nevertheless, that does not cause separation and a smooth continuous construct is formed to accommodate all the different stresses imposed by the cells. Figure 11b shows this continuity and defined distribution of cells according to the initial pattern of the mold even after they have shrunken to their final size and structure. Structures like this can be used to study indirect effect of cells on each other, for example through paracrine activity. Unlike other methods for formation of heterogeneous constructs multiple cells [46] that require restraining features to form non-spherical structures and several days for the different cell types to grow towards each other to achieve intimate contact, our method is rapid and extremely precise in spatial positioning. It is also capable of retaining the established non-spherical geometry even when removed from the mold for further processing.

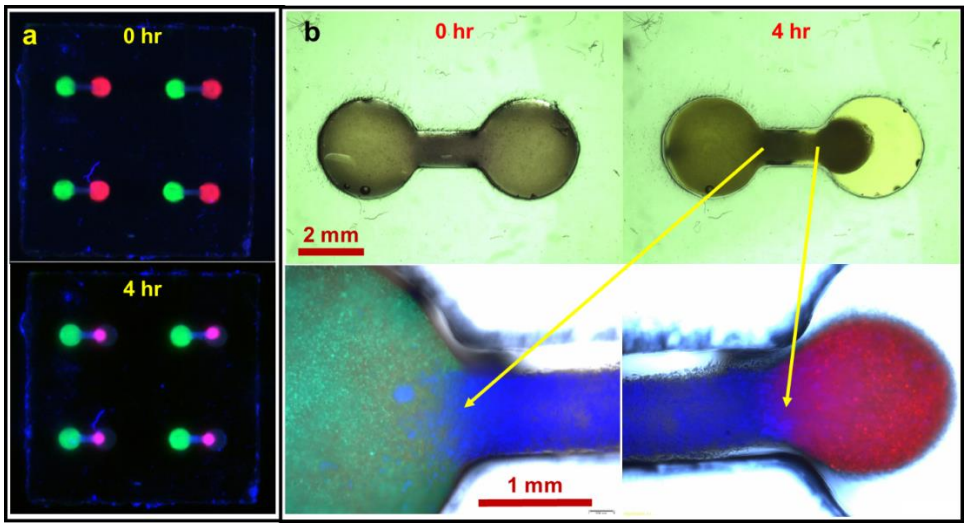

Figure 11. a) Connected wells with gfp-3T3s in left, MCF-7 cells stained with blue tracker in center, and rfp-HUVECs; b) Dumbbell formation with time and defined borders between cell types.

5. Conclusion

In the current study a rapid fabrication method has been developed to form spatially controlled collagen-based tissue constructs through self-assembly process applicable to different cell types in complex shapes with predefined distribution of cells with highly controlled borders between them. The presence of collagen matrix that forms the scaffold and addition of extra volume of growth medium after 2 hrs were found to be critical for this rapid fabrication method. Spherical and non-spherical constructs can be formed which are robust to handle and retain their shape even after removal from the mold. Both homogeneous and heterogeneous multicellular constructs can be constructed which will be useful in many bioassays that investigate the interaction of these cells as realistic *in vitro* model. The heterogeneous constructs not only provide precise positioning but also sharp interfaces which can be important in quantification of migration, or gene and protein expression in these bioassays. Low to very high cell numbers that are physiologically relevant can be used in small or larger structures for different applications such as tissue development or drug screening. Although these constructs can be immediately applied as *in vitro* models for drug discovery, the method can also be adapted for use in regenerative medicine. Despite these advantages, addition of vasculature-like constructs as well as implementation of bioreactors to add different stimuli could add to the potential value of this work. Furthermore, studies are needed to determine the effect of compaction process and the stiffness produced in the tissue constructs thus created on its structural coherence over the long term.

References

1. Benien, P. and A. Swami, *3D tumor models: history, advances and future perspectives.* Future Oncol, 2014. **10**(7): p. 1311-27.
2. Carrel, A., *On the Permanent Life of Tissues Outside of the Organism.* J Exp Med, 1912. **15**(5): p. 516-28.
3. Moscona, A. and H. Moscona, *The dissociation and aggregation of cells from organ rudiments of the early chick embryo.* J Anat, 1952. **86**(3): p. 287-301.
4. Hoffman, R.M., *To do tissue culture in two or three dimensions? That is the question.* Stem Cells, 1993. **11**(2): p. 105-11.
5. Pampaloni, F., E.G. Reynaud, and E.H. Stelzer, *The third dimension bridges the gap between cell culture and live tissue.* Nat Rev Mol Cell Biol, 2007. **8**(10): p. 839-45.
6. Lin, R.Z. and H.Y. Chang, *Recent advances in three-dimensional multicellular spheroid culture for biomedical research.* Biotechnol J, 2008. **3**(9-10): p. 1172-84.
7. Cui, X., Y. Hartanto, and H. Zhang, *Advances in multicellular spheroids formation.* J R Soc Interface, 2017. **14**(127).
8. Vinci, M., S. Gowan, F. Boxall, L. Patterson, M. Zimmermann, W. Court, C. Lomas, M. Mendiola, D. Hardisson, and S.A. Eccles, *Advances in establishment and analysis of three-dimensional tumor spheroid-based functional assays for target validation and drug evaluation.* BMC Biol, 2012. **10**: p. 29.
9. Lin, R.Z., L.F. Chou, C.C. Chien, and H.Y. Chang, *Dynamic analysis of hepatoma spheroid formation: roles of E-cadherin and beta1-integrin.* Cell Tissue Res, 2006. **324**(3): p. 411-22.
10. Haycock, J.W., *3D cell culture: a review of current approaches and techniques.* Methods Mol Biol, 2011. **695**: p. 1-15.
11. Ruedinger, F., A. Lavrentieva, C. Blume, I. Pepelanova, and T. Scheper, *Hydrogels for 3D mammalian cell culture: a starting guide for laboratory practice.* Appl Microbiol Biotechnol, 2015. **99**(2): p. 623-36.
12. Soranzo, C., G. Della Torre, and A. Ingrosso, *Formation, growth and morphology of multicellular tumor spheroids from a human colon carcinoma cell line (LoVo).* Tumori, 1986. **72**(5): p. 459-67.
13. Fukuda, J., A. Khademhosseini, Y. Yeo, X. Yang, J. Yeh, G. Eng, J. Blumling, C.F. Wang, D.S. Kohane, and R. Langer, *Micromolding of photocrosslinkable chitosan hydrogel for spheroid microarray and co-cultures.* Biomaterials, 2006. **27**(30): p. 5259-67.
14. Karp, J.M., J. Yeh, G. Eng, J. Fukuda, J. Blumling, K.Y. Suh, J. Cheng, A. Mahdavi, J. Borenstein, R. Langer, and A. Khademhosseini, *Controlling size, shape and homogeneity of embryoid bodies using poly(ethylene glycol) microwells.* Lab Chip, 2007. **7**(6): p. 786-94.
15. McGuigan, A.P., D.A. Bruzewicz, A. Glavan, M.J. Butte, and G.M. Whitesides, *Cell Encapsulation in Sub-mm Sized Gel Modules Using Replica Molding.* PloS one, 2008. **3**(7).
16. Sodunke, T.R., K.K. Turner, S.A. Caldwell, K.W. McBride, M.J. Reginato, and H.M. Noh, *Micropatterns of Matrigel for three-dimensional epithelial cultures.* Biomaterials, 2007. **28**(27): p. 4006-16.
17. Khademhosseini, A., G. Eng, J. Yeh, J. Fukuda, J. Blumling, 3rd, R. Langer, and J.A. Burdick, *Micromolding of photocrosslinkable hyaluronic acid for cell encapsulation and entrapment.* J Biomed Mater Res A, 2006. **79**(3): p. 522-32.

18. Yeh, J., Y. Ling, J.M. Karp, J. Gantz, A. Chandawarkar, G. Eng, J. Blumling, 3rd, R. Langer, and A. Khademhosseini, *Micromolding of shape-controlled, harvestable cell-laden hydrogels.* Biomaterials, 2006. **27**(31): p. 5391-8.
19. Rijal, G. and W. Li, *3D scaffolds in breast cancer research.* Biomaterials, 2016. **81**: p. 135-156.
20. Achilli, T.M., J. Meyer, and J.R. Morgan, *Advances in the formation, use and understanding of multi-cellular spheroids.* Expert Opin Biol Ther, 2012. **12**(10): p. 1347-60.
21. Napolitano, A.P., P. Chai, D.M. Dean, and J.R. Morgan, *Dynamics of the self-assembly of complex cellular aggregates on micromolded nonadhesive hydrogels.* Tissue Eng, 2007. **13**(8): p. 2087-94.
22. Mueller-Klieser, W., *Method for the determination of oxygen consumption rates and diffusion coefficients in multicellular spheroids.* Biophys J, 1984. **46**(3): p. 343-8.
23. Alvarez-Perez, J., P. Ballesteros, and S. Cerdan, *Microscopic images of intraspheroidal pH by 1H magnetic resonance chemical shift imaging of pH sensitive indicators.* MAGMA, 2005. **18**(6): p. 293-301.
24. Curcio, E., S. Salerno, G. Barbieri, L. De Bartolo, E. Drioli, and A. Bader, *Mass transfer and metabolic reactions in hepatocyte spheroids cultured in rotating wall gas-permeable membrane system.* Biomaterials, 2007. **28**(36): p. 5487-97.
25. Groebe, K. and W. Mueller-Klieser, *On the relation between size of necrosis and diameter of tumor spheroids.* Int J Radiat Oncol Biol Phys, 1996. **34**(2): p. 395-401.
26. Gencoglu, M.F., L.E. Barney, C.L. Hall, E.A. Brooks, A.D. Schwartz, D.C. Corbett, K.R. Stevens, and S.R. Peyton, *Comparative Study of Multicellular Tumor Spheroid Formation Methods and Implications for Drug Screening.* ACS Biomater Sci Eng, 2018. **4**(2): p. 410-420.
27. Lee, B.H., M.H. Kim, J.H. Lee, D. Seliktar, N.J. Cho, and L.P. Tan, *Modulation of Huh7.5 spheroid formation and functionality using modified PEG-based hydrogels of different stiffness.* PLoS One, 2015. **10**(2): p. e0118123.
28. Khanfar, M.A., D.T. Youssef, and K.A. El Sayed, *Semisynthetic latrunculin derivatives as inhibitors of metastatic breast cancer: biological evaluations, preliminary structure-activity relationship and molecular modeling studies.* ChemMedChem, 2010. **5**(2): p. 274-85.
29. Saias, L., A. Gomes, M. Cazales, B. Ducommun, and V. Lobjois, *Cell-Cell Adhesion and Cytoskeleton Tension Oppose Each Other in Regulating Tumor Cell Aggregation.* Cancer Res, 2015. **75**(12): p. 2426-33.
30. Kunz-Schughart, L.A., M. Kreutz, and R. Knuechel, *Multicellular spheroids: a three-dimensional in vitro culture system to study tumour biology.* Int J Exp Pathol, 1998. **79**(1): p. 1-23.
31. Park, J.I., J. Lee, J.L. Kwon, H.B. Park, S.Y. Lee, J.Y. Kim, J. Sung, J.M. Kim, K.S. Song, and K.H. Kim, *Scaffold-Free Coculture Spheroids of Human Colonic Adenocarcinoma Cells and Normal Colonic Fibroblasts Promote Tumorigenicity in Nude Mice.* Transl Oncol, 2016. **9**(1): p. 79-88.
32. Upreti, M., A. Jamshidi-Parsian, N.A. Koonce, J.S. Webber, S.K. Sharma, A.A. Asea, M.J. Mader, and R.J. Griffin, *Tumor-Endothelial Cell Three-dimensional Spheroids: New Aspects to Enhance Radiation and Drug Therapeutics.* Transl Oncol, 2011. **4**(6): p. 365-76.

33. Chiew, G.G.Y., N. Wei, S. Sultania, S. Lim, and K.Q. Luo, *Bioengineered three-dimensional co-culture of cancer cells and endothelial cells: A model system for dual analysis of tumor growth and angiogenesis.* Biotechnol Bioeng, 2017. **114**(8): p. 1865-1877.
34. Noel, P., R. Munoz, G.W. Rogers, A. Neilson, D.D. Von Hoff, and H. Han, *Preparation and Metabolic Assay of 3-dimensional Spheroid Co-cultures of Pancreatic Cancer Cells and Fibroblasts.* J Vis Exp, 2017(126).
35. Angelucci, C., G. Maulucci, G. Lama, G. Proietti, A. Colabianchi, M. Papi, A. Maiorana, M. De Spirito, A. Micera, O.B. Balzamino, A. Di Leone, R. Masetti, and G. Sica, *Epithelial-stromal interactions in human breast cancer: effects on adhesion, plasma membrane fluidity and migration speed and directness.* PLoS One, 2012. **7**(12): p. e50804.
36. Harma, V., J. Virtanen, R. Makela, A. Happonen, J.P. Mpindi, M. Knuuttila, P. Kohonen, J. Lotjonen, O. Kallioniemi, and M. Nees, *A comprehensive panel of three-dimensional models for studies of prostate cancer growth, invasion and drug responses.* PLoS One, 2010. **5**(5): p. e10431.
37. Jang, M., I. Koh, S.J. Lee, J.H. Cheong, and P. Kim, *Droplet-based microtumor model to assess cell-ECM interactions and drug resistance of gastric cancer cells.* Sci Rep, 2017. **7**: p. 41541.
38. Erickson, A.C. and J.R. Couchman, *Still more complexity in mammalian basement membranes.* J Histochem Cytochem, 2000. **48**(10): p. 1291-306.
39. Kleinman, H.K., M.L. McGarvey, L.A. Liotta, P.G. Robey, K. Tryggvason, and G.R. Martin, *Isolation and characterization of type IV procollagen, laminin, and heparan sulfate proteoglycan from the EHS sarcoma.* Biochemistry, 1982. **21**(24): p. 6188-93.
40. Kleinman, H.K. and G.R. Martin, *Matrigel: basement membrane matrix with biological activity.* Semin Cancer Biol, 2005. **15**(5): p. 378-86.
41. Hughes, C.S., L.M. Postovit, and G.A. Lajoie, *Matrigel: a complex protein mixture required for optimal growth of cell culture.* Proteomics, 2010. **10**(9): p. 1886-90.
42. Ishiguro, T., H. Ohata, A. Sato, K. Yamawaki, T. Enomoto, and K. Okamoto, *Tumor-derived spheroids: Relevance to cancer stem cells and clinical applications.* Cancer Sci, 2017. **108**(3): p. 283-289.
43. Legant, W.R., A. Pathak, M.T. Yang, V.S. Deshpande, R.M. McMeeking, and C.S. Chen, *Microfabricated tissue gauges to measure and manipulate forces from 3D microtissues.* Proc Natl Acad Sci U S A, 2009. **106**(25): p. 10097-102.
44. Sakar, M.S., J. Eyckmans, R. Pieters, D. Eberli, B.J. Nelson, and C.S. Chen, *Cellular forces and matrix assembly coordinate fibrous tissue repair.* Nature Communications, 2016. **7**: p. 11036.
45. Turnbull, I.C., I. Karakikes, G.W. Serrao, P. Backeris, J.J. Lee, C. Xie, G. Senyei, R.E. Gordon, R.A. Li, F.G. Akar, R.J. Hajjar, J.S. Hulot, and K.D. Costa, *Advancing functional engineered cardiac tissues toward a preclinical model of human myocardium.* FASEB J, 2014. **28**(2): p. 644-54.
46. Osaki, T., S.G.M. Uzel, and R.D. Kamm, *Microphysiological 3D model of amyotrophic lateral sclerosis (ALS) from human iPS-derived muscle cells and optogenetic motor neurons.* Sci Adv, 2018. **4**(10): p. eaat5847.

Supplementary Information

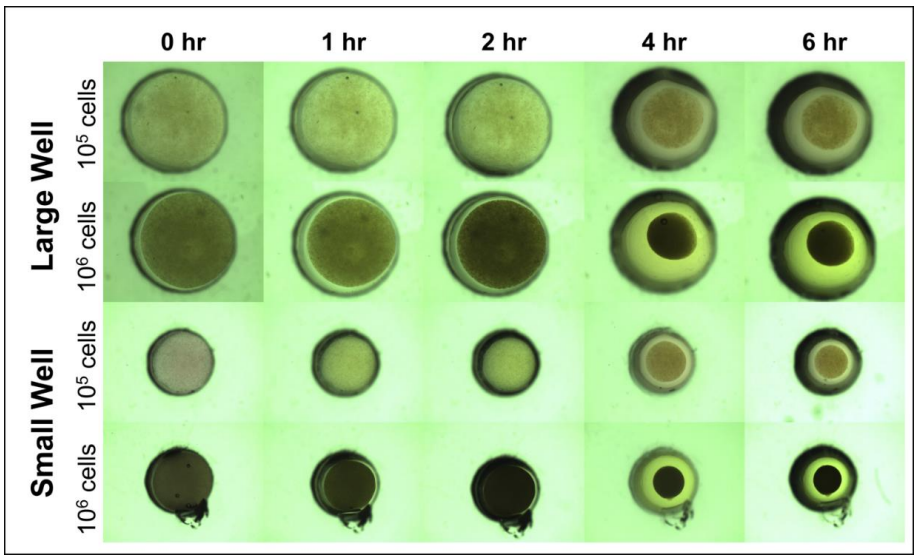

Supplementary Figure 1. Shrinkage of grafts with time for different well sizes and cell numbers

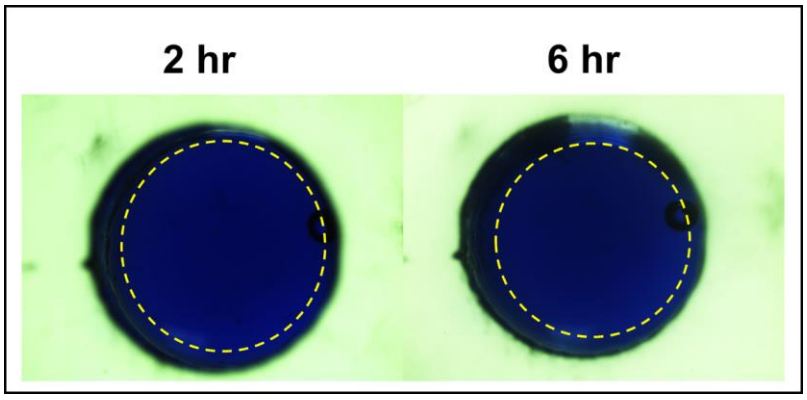

Supplementary Figure 2. Shrinkage of collagen in absence of cells. Methylene blue was added for observation purposes.

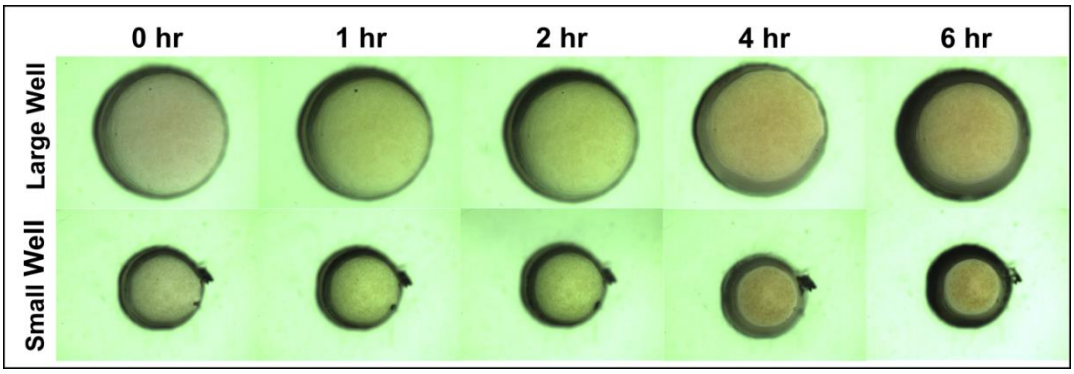

Supplementary Figure 3. Shrinkage pattern of 5×10^4 cells in small and large wells as the lower limit

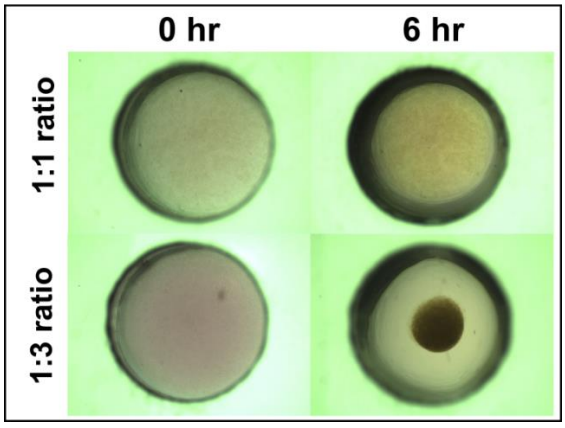

Supplementary Figure 4. Effect of collagen to DMEM ratio on the final spheroid size (1:1 and 1:3 ratio of collagen to DMEM for 5×10^4 cells in large wells)

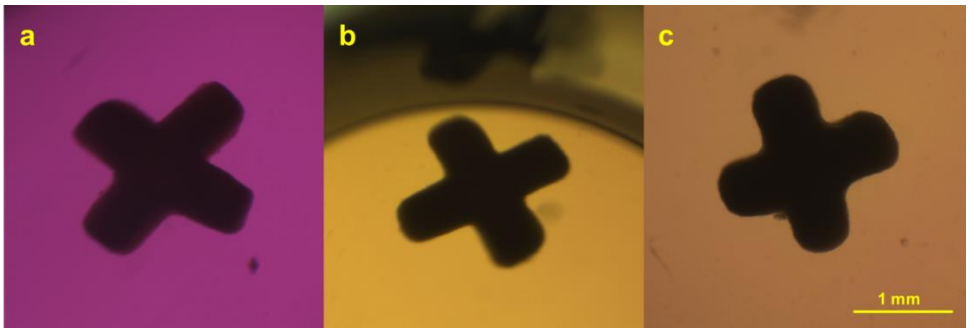

Supplementary Figure 5. Graft in the shape a cross out of PDMS wells after a) 24 hrs, b) 3 days, c) 7 days. Even without constraints of the well they maintained the predefined shape.

Chapter 5: MICRO-MOLDING APPLICATION

A 3D Self-Assembled In Vitro Model to Simulate Direct and Indirect Interactions Between Adipocytes and Skeletal Muscle Cells

Alireza Shahin-Shamsabadi[1], P. Ravi Selvaganapathy [1,2,*]

[1] School of Biomedical Engineering, McMaster University, Canada

[2] Department of Mechanical Engineering, McMaster University, Canada

[*] Corresponding Author: P. Ravi Selvaganapathy, Department of Mechanical Engineering, McMaster University, Canada. selvaga@mcmaster.ca1280 Main Street West, L8S 4L7, Hamilton, Ontario, Canada

Status: Published

Full Citation:

Shahin-Shamsabadi, Alireza, and Ponnambalam Ravi Selvaganapathy. "A 3D Self-Assembled In Vitro Model to Simulate Direct and Indirect Interactions between Adipocytes and Skeletal Muscle Cells." Advanced Biosystems (2020): 2000034.

Abstract

The molecular mechanisms of development and progression of diabetes and obesity involve complex interactions between adipocytes and skeletal muscle cells. Although two-dimensional (2D) *in vitro* models are the gold standard for mechanistic study of such behaviors, they do not recreate the complexity and the dynamics associated with the interactions between the cell types involved. Alternatively, animal models are used but are expensive, difficult to visualize or analyze, are not completely representative of human physiology or genetic background and have associated ethical considerations. Three-dimensional (3D) co-culture systems can be complementary to these approaches. Here we show that using a newly developed 3D biofabrication method, adipocytes and myoblasts can be positioned precisely either in direct physical contact or in close proximity such that the paracrine effects could be systematically studied. We also develop suitable protocols for growth and differentiation of both cells in the co-culture system. Cells showed more restrained lipid and protein production in 3D systems compared to 2D ones and adipocytes showed more lipolysis in indirect contact with myoblasts as response to drug treatment. These findings emphasize importance of physical contact between cells that has been overlooked in co-culture systems such as transwell inserts and can be used in studies for applications such as development of anti-obesity drugs.

Keywords: 3D *in vitro* model; Collagenous tissue construct; Self-assembly; Muscle-fat co-culture; Drug assay

1. Introduction

Interactions between adipocytes and skeletal muscle cells and effect of such interactions on growth and metabolism has been shown to be important in development of various diseases [1]. Obesity, characterized by excessive accumulation of fat mass in white adipose tissue due to increase in number of cells and/or volume of adipose tissue, as well as other metabolic diseases such as diabetes type II can cause muscular pathologies by inducing lipid accumulation and inflammation [1, 2]. Studies have shown that aberrant fat storage either in muscle cells or between them could cause muscle cells to show insulin resistance or abnormal organization of muscle fibers [3-5].

Animal models have been used to study such conditions but because of their different metabolism and physiology, experiments performed on them to study obesity and other metabolic diseases may not be completely representative of the human conditions. In some cases there are no equivalent animal models and therefore transgenic models are used [6, 7]. A complementary approach has been to use *in vitro* models containing human cells. 2D models have been gold standard for *in vitro* modeling but it has been previously shown that for most tissues, 3D models are more representative compared to 2D ones [8, 9]. A case point is the adipose tissue, where it has been shown that adipose-like cells in spheroid format show more differentiated phenotype compared to 2D cultures [10].

The significance of the interaction between adipocytes and myofibers *in vivo* was recognized initially by Jarret et al. [11] when they showed secretion of a paracrine mediator by skeletal muscle cells in insulin treated rats stimulated glycogen synthase and pyruvate dehydrogenase activity in adipocytes [12]. Consequently, various co-culture systems were developed to understand metabolic connections between fat and other tissues such as muscle to provide realistic insight into the pathways that can be exploited for applications such as new pharmacological treatments for

obesity [13]. Most of these systems investigate the role of these cells in inflammation or insulin resistance caused by obesity [14]. Interaction between skeletal muscle cells and adipocytes has been studied previously *in vitro* in different formats including transwells, or by manual transfer of supernatant fluid between isolated wells where the two cell types are cultured and treatment with conditioned media of the other cell type is performed [2, 11, 15-17]. Better understanding of the interaction between these two cells will have important outcomes in treatment of obesity and diabetes [12].

The interaction mediated between the cells through exchange of secrotomes is important in recreating some of the dynamics of cellular behavior *in vivo*. Nevertheless, these formats have significant limitations. The transwell format still cultures cells as a monolayer on an artificial plastic substrate which is different from the *in vivo* condition. Similarly, the transfer of supernatant fluids between wells that contain monoculture of the cells, can mimic paracrine activity but cannot recreate dense packing of multiple cell types and physical contact between the various cell types [12]. Alternatively, cellular spheroids, one of the oldest 3D *in vitro* cell culture techniques [18, 19], have been used to study skeletal muscle cells [20, 21] and adipocytes [10, 22, 23] individually. Although these 3D models better recapitulate complexities of human biology and have a more differentiated phenotype with gene expressions higher than equivalent 2D models, they require a complex and often slow fabrication processes and are limited to low cell numbers. These models also don't provide sufficient spatial positioning capability to fabricate heterogenous tissue constructs containing different cell types.

In this paper, we use a newly developed rapid 3D tissue construct fabrication method as the tool to fabricate co-culture systems with controlled positioning of cells [24] and create the first spatially defined, heterogeneous tissue construct composed of adipocyte and skeletal muscle cells. We study

effect of media type on the behavior of both of cell types in co-culture and integrity of the 3D constructs. The versatility of this method is demonstrated by constructing models that simulate direct (with direct physical contact between cells of different kinds) and indirect (only with paracrine effect of cells on each other without direct physical contact) interactions between these two cell types. We show that these 3D models have significant differences from their 2D counterparts. Finally, we show that the effect of a β-adrenergic drug (isoproterenol hydrochloride) on lipolysis was different between the direct and indirect 3D co-culture models. These findings together show the significance of the 3D co-culture model and the ability to create heterogeneous tissue constructs of multiple cell types that can be a valuable tool in understanding of biological mechanisms behind disease processes and in drug discovery.

2. Experimental Section

Homogeneous and heterogeneous 3D tissue constructs composed of adipocytes and skeletal muscle cells in bovine collagen type I as ECM were fabricated using a newly developed rapid self-assembly process [24]. A poly(lactic acid) master mold shaped in the form of two intersecting cylindrical posts (each of them were 3 mm in diameter and 3 mm in height) with a 0.5 mm overlap was 3D printed using a stereolithography printer (Objet 24 Desktop 3D printer). Polydimethylsiloxane (PDMS) at 10:1 ratio of the polymer to its curing agent was cast onto the master mold to form the microwells (Figure 1a) that were used to form the self-assembled constructs for 3D culture systems. Bioinks were prepared by adding cells dispersed in culture medium to neutralized collagen (5 mg/mL). This bioink was then added to one of the cylindrical chambers in the PDMS microwells. Because of the viscous nature of the ink, it remained in its chamber without spreading to the adjacent one. Next, the adjacent chamber was filled with the bioink of the same or different cell type and incubated for 2 hrs during which, collagen rapidly

gelled forming a dense construct of interconnecting cylinders. At this point, additional culture medium was added to the wells to provide cells with nutrients they needed for their survival.

This system was used to study effect of direct co-culture of these two cell types (equal number of both cell types in each chamber) or their indirect co-culture (only one cell type in each chamber). As control, similar constructs with only one of the cell types were fabricated (the same cell type in both wells) (Figure 1b). These samples were compared with each other in terms of their metabolic activity, and total lipid and protein content. For further comparison, the same set of experiments were performed with cells cultured in 48 well plates in 2D systems (Figure 1b). For 2D indirect co-culture system, each cell was treated with conditioned medium of the other one.

Since cells used in this study have to be differentiated in a different differentiation media to gain their specific phenotype, effect of culture medium on the cells was also studied. For this purpose, a special protocol was designed for the differentiation of the cells (Figure 1c). First cells were cultured in their own growth medium (GM) three days before starting the co-culture experiments (D-3).The following day (D-2) medium was replaced with each cells' differentiation medium (DM) and they were kept in this medium for two days to partially prime them towards their functional phenotype. These partially differentiated cells were trypsinized and used for either 2D or 3D co-cultures (D0). After this point in the process, experiments were separately performed using either fat DM (F-DM) (1st set) or muscle DM (M-DM) (2^{nd} set) for all 4 groups to identify the best choice for the co-culture system based on long-term maintenance of the structural integrity of the tissue constructs and total lipid and protein production. Details of different culture media used in this experiment are included in Supplementary Table 1.

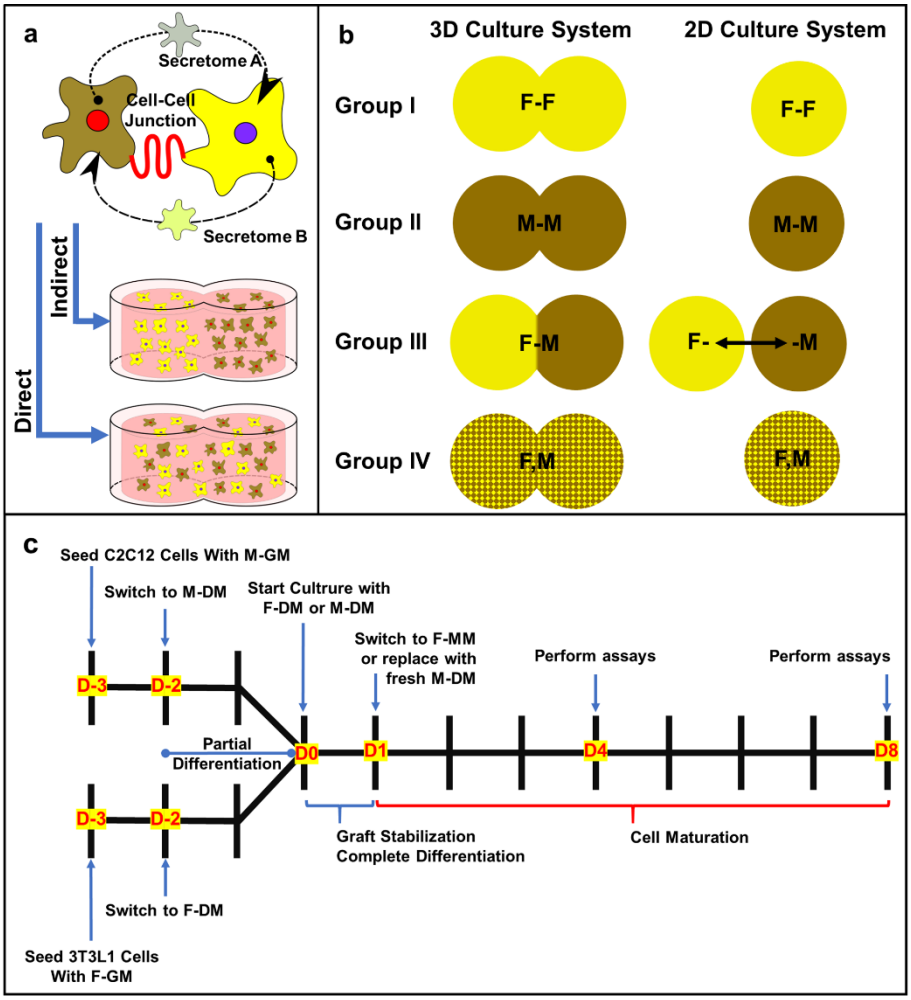

Figure 1. a) Interaction of cells through cell-cell junctions and secretomes. In indirect co-culture cells of different types affect each other only through their secretomes but in direct co-culture both effects are present. **b)** Top view of different groups of cultures (controls: F-F and M-M where only one of the cell types is present, indirect (F-M), and direct (F,M) co-culture) in 3D and 2D culture systems. Culture systems after partial differentiation are started once with F-DM (1st set) and another time with M-DM (2nd set). ↔ indicates switching conditioned media; **c)** Protocol for differentiating cells, forming culture systems, and performing assays.

2.1. Cell culture and Differentiation Protocols

In the current study C2C12 and 3T3-L1 cells are used to study their crosstalk in different 3D and 2D co-culture systems. C2C12 cells were cultured in Dulbecco's Modified Eagle Medium (DMEM) (high glucose, Gibco), supplemented with 10 %V/V of heat inactivated fetal bovine serum (HI-FBS) (US origin, Thermofisher) and 1%V/V Penicillin-Streptomycin (100X,

Thermofisher). This medium was termed as the muscle growth medium (M-GM). For expansion purposes they were cultured up to 70% confluent. For differentiation, they were subcultured with starting confluency of 40-60%, kept in their GM for 1 day and then switched to their differentiation medium (M-DM) (high glucose DMEM supplemented with 2 %V/V horse serum (Thermofisher), 1% Insulin solution (Insulin-Transferrin-Selenium, 100X, Thermofisher) and 1%V/V Penicillin-Streptomycin). They were kept in this medium for 2 days for partial differentiation before they were trypsinized and used for further studies.

3T3-L1 cells were cultured in their growth medium (F-GM) which was Dulbecco's Modified Eagle Medium (DMEM) (low glucose, Gibco), supplemented with 10 %V/V of fetal bovine serum (FBS) (US origin, Thermofisher) and 1%V/V Penicillin-Streptomycin (Thermofisher, 100X) up to 70% confluency. For differentiation, they were subcultured with starting confluency of 40-60%, kept in F-GM for 1 more day and then switched to their differentiation medium (F-DM) (DMEM (high glucose, Gibco), supplemented with 10 %V/V of FBS and 1%V/V Penicillin-Streptomycin, 2 µM Rosiglitazone, 0.25 µM Dexamethasone, 0.5 mM 3-Isobutyl-1-methylxanthine (IBMX), and 1 µg/mL Insulin (from Sigma-Aldrich)). They were in this medium for 2 days for partial differentiation and before they were trypsinized and used for further studies.

2.2. Three-dimensional Culture System

Each microwell consists of two interconnected small cylindrical chambers. Each of these chambers was filled with 16 µL of bioink containing 10^5 cells. The bioink also contained 5 mg/mL bovine collagen type I neutralized with 0.1 M NaOH solution (20% of the volume of the collagen) and DM with 1:2 ratio.

Four different co-culture constructs were formed, namely: Group I, fat cells in both of the wells (F-F); Group II, muscle cells in both wells (M-M); Group III, fat cells in one well and muscle cells in the other (F-M); and Group IV with both fat and muscle cells with equal numbers in each of the wells (F,M). Groups I and II are controls while Groups III and IV represent indirect and direct co-culture, respectively. All of these constructs were cultured in F-DM (1st set) and M-DM (2nd Set) in parallel. Once the bioink was added to each well, samples were incubated for 1 hr for the collagen to gel and then 175 µL of the respective DM was added of that to provide cells with the required nutrients. The next day, the culture medium for all the samples formed with F-DM medium was replaced with F-MM. As for the samples formed with M-DM, the culture medium was changed with fresh M-DM. After first day, it was refreshed every two days (F-MM for the former and M-DM for the latter). Images of samples were taken using a stereo microscope after 1, 4, and 8 days to trace evolution of each of the constructs' morphology with time. Cells were also stained with long-term fluorescent trackers (C2C12 with red DiI and 3T3-L1 with green DiO following the supplier's protocol (Thermofisher)) in order to visualize the spatial distribution of the individual cell types within the constructs. Fluorescent images were taken at the similar time points using a ChemiDoc™ MP imaging system (Bio-Rad) and an inverted fluorescent microscope (Olympus, USA).

2.3. Two-dimensional Culture System

The same partially differentiated cells were used to study direct and indirect co-culture of C2C12 and 3T3-L1 cells in 2D. As for control 0.05×10^6 cells of either C2C12 or 3T3-L1 were dispersed in 0.2 mL of medium and were added into wells of 48 well plates (Groups I and II, F-F and M-M, respectively). For direct co-culture 0.025×10^6 cells of each type was used together (Group IV, F,M). Medium was replaced every two days. As for indirect co-culture (Group III including F- and

M- wells), 0.05×10^6 cells of each type were cultured separately and every day half of the medium was changed with fresh medium and the other half was replaced with conditioned medium of the other group (3T3-L1 to C2C12 and vice versa). The same as before, experiments were repeated once with F-DM (1st set) and another time with M-DM (2^{nd} Set). In the first set of experiments, culture started with F-DM and then switched to F-MM after one day. F-MM was used for the rest of the days and it was refreshed every other day. In the second set, experiments started with M-DM which was used for the rest of the experiments and changed every two days.

2.4. Assessment of Metabolic activity and Lipid/Protein Production

Alamar blue assay kit (Thermofisher) (ABA), Bradford total protein kit (Thermofisher) (BCA), and a customized assay based on Nile red dye (Thermofisher) (NRA) were used to measure metabolic activity, total protein, and total lipid content of the samples, respectively, in each of the conditions.

In the case of 3D co-culture systems, samples were transferred to wells of a 96 well plate after 1, 4, and 8 days. 200 µL of the appropriate medium (F-MM or M-DM) containing 10% alamar blue was added to each well and incubated for 90 min. Then 100 µL aliquots of the supernatant were transferred to 96 black well plates and fluorescent intensity was measured using a plate reader (Infinite® M200, Tecan, Männedorf, Switzerland)) at excitation/emission of 560/590 nm. The same volume of medium containing Alamar blue solution was used as control. After this step, the constructs were digested using enzymatic treatment. Stock solution of collagenase/dispase (Sigma-Aldrich) was prepared by dissolving its powder in DI water to achieve concentration of 100 mg/mL. Working solution was prepared by diluting this stock solution in FBS-free DMEM to get 5% V/V solution. 100 µL of the working solution was added to each well containing the constructs and incubated for 2 hrs. Samples were eventually pipetted gently and 50 µL of 0.1 M EDTA

solution was added to neutralize the enzymes (this solution is called digest solution). Two 25 µL aliquots were transferred to 96 black well plate wells to perform NRA. Nile red dye was dissolved in acetone with the concentration of 10 mg/mL. It was then diluted in FBS-free DMEM to achieve 0.2% V/V staining solution of which 200 µL was added to each of the 25 µL digest samples. Following a 15 min incubation, the fluorescent intensity was measured at excitation/emission of 560/640 nm. As a control, 25 µL samples of digestive working solution mixed with Nile red's working solution was also measured. In parallel, 100 µL of digested samples were mixed with 100 µL of lysis solution (0.5% Triton X-100 in PBS) to lyse the cells. After 15 min incubation with lysis solution, two 25 µL aliquots were transferred to new 96 well plates and 200 µL of BCA solution (50:1 ratio mixture of parts A and B of the kit) was added to each well. Absorbance was measured at 562 nm after 30 min incubation. Digestive solution neutralized with EDTA and mixed with lysis solution was used as control.

The same assays were performed for 2D samples with slight modifications. For ABA, the same volume of the solution (10% alamar blue in either F-MM or M-DM) was added but incubation was performed only for 60 min. For NRA, 200 µL of its working solution was added to each well and after 15 min incubation multiple spots in the well (a 5×5 filled circle) was measured and the sum of fluorescent intensity from these 25 spots reported as the final value. 2D culture samples were lysed using a digestive/lysis solution containing 0.5% V/V Triton X-100 and 0.5% Trypsin-EDTA (25X, Thermofisher) in PBS with 15 min incubation. Two 25 µL aliquots of each of the lysed samples were used for BCA following the same steps as before with digestive/lysis solution as control. In all of the experiments, eight biological replicates with duplicate readings were used.

2.5. Effect of Co-culture System on Responsiveness to Drug Treatment

F-M and F,M co-cultures were cultured with F-DM and at day 4, their medium was replaced with 120 µL of FBS-free DMEM containing 10 µM isoproterenol hydrochloride (SigmaAldrich) (10 mM in DI water as stock solution) and incubated for 4 hours. At the end of incubation time, two 50 µL aliquots of supernatant were used with a free fatty acid quantification kit (Abcam) following its instructions to measure lipolysis in each group. Same samples in FBS-free DMEM but without isoproterenol treatment were used as control. Measured values were normalized to values of non-treated F-M group for comparison.

2.6. Statistical Analysis

Data are reported as Mean ± Standard Deviation (SD) and statistical analysis is performed using two-way ANOVA test in GraphPad Prism with an accepted statistical significance (p-value) less than 0.05. Significant outlier data points were detected using Grubbs' test performed in GraphPad Prism and removed before performing ANOVA test. In all cases n=8 was used except where otherwise mentioned.

3. Results and Discussion

3.1. Integrity and Morphology of Direct and Indirect Co-culture in 3D Constructs

The ability to form 3D homogeneous and heterogeneous constructs with control over positioning of cells [24] using fat and muscle cells allows, for the first time, the study of direct (cell-cell) and indirect (through paracrine activity) interactions between the cell types in 3D, delineate them and understand the mechanisms through which their growth, metabolic activity, and regulation are modulated. Nevertheless, such constructs should have structural integrity despite the morphological changes that will be introduced during the self-assembly process to form the constructs and the remodeling that happens later on, as well as the respective cell differentiation

processes. Since two cell types are involved, an appropriate process that will simultaneously generate the respective cellular phenotypes for both fat and muscle cells must be identified. Parameters such as the ratio of medium to collagen and cell number should also be optimized to control the final size of the grafts and avoid formation of a necrotic core than occurs due to mass transfer limitations when the constructs are larger or denser.

In the current study 3T3-L1 and C2C12 cell lines were used. Among the various adipose cells used for *in vitro* modeling, including primary cells or established cell lines, 3T3-L1 is the most common [25]. This cell line is a preadipocyte line developed from murine Swiss 3T3 cells that under proper conditions will show adipocyte-like phenotype [13, 26]. Advantage of this cell line over isolated primary cells is that it's easier and less expensive to culture them, their population is more homogenous, and they can tolerate higher passage numbers [27]. Despite these advantages, these cells might not exactly represents *in vivo* conditions in terms of metabolic characteristics of the native tissue and its responsiveness to drugs [28]. In the same vein, one of the best myoblast cell lines that suitably mimics *in vivo* differentiation of these cells is C2C12. They proliferate readily in their undifferentiated state in high concentrations of serum and their terminal differentiation can be induced by serum deprivation [29]. It is also possible to use cells from different cell lines for each tissue to establish these *in vitro* models to get complementary results in order to alleviate some of the shortcomings of cell lines as compared to primary cells and *in vivo* conditions.

In order to determine the appropriate conditions to differentiate and yet retain integrity of the constructs, a new protocol, outlined in Figure 1, was developed. It has been previously shown that, using similar cocktails, 3T3-L1 cells show maximal differentiation in the first 48 hrs and after 4 days, start to accumulate lipid droplets [13, 30]. Similarly, C2C12 cells have been shown to form first myotubes after 48-74 hrs of treatment [31]. In the devised protocol in this study, the partial

differentiation before D0 provides the initial impetus to push these cells towards their respective phenotype. The protocol is designed such that the cells are typsinized and released to form the construct before the 3T3-L1s start to accumulate lipid droplets (which would make their plasma membrane fragile) or the C2C12s fuse with each other. The protocol also used high levels of insulin as it has been shown to assist differentiation of C2C12s [32, 33]. Systematic studies were then carried out to determine the suitable common medium that could be used to maintain phenotype of both cell types when they are in co-culture. The behavior of the cells in the co-culture constructs (F-M (Group III) with 10^5 of one cell type in one chamber and 10^5 in the other and F,M (Group IV) with 0.5×10^5 of each cell type homogeneously distributed in each chamber) were compared to constructs fabricated with only one type of cells (Groups I (F-F) and II (M-M) each containing 10^5 cells of the same cell type in each chamber) and differentiated in the appropriate DM. Various assays were performed to measure total lipid and protein production as well as metabolic activity of the constructs after 1, 4, and 8 days to cover the entire differentiation time course of both cell types.

Figure 2 shows bright field images of 3D constructs and their morphology over several days of culture in various media conditions (F-DM vs. M-DM) and containing different combinations of cell types (Groups I-IV). All of samples in 1st set (Figure 2a) showed less shrinkage compared to their respective counterparts in the 2nd set (Figure 2b). During the 8 days in culture, F-F samples maintained their integrity in both sets, but M-M samples started to form satellite aggregates (shown in Figure 2 and with higher magnification in Supplementary Figure 1a). Such formation of satellite aggregates was found to occur only in a limited amount on day 8 for the 1st set while it was observed even on day 4 for the 2nd set. Similar observations were noted in the co-culture groups

(F-M and F,M samples). In general samples in the 1st set were more stable and thus F-DM medium was considered to be more suitable for maintaining integrity of the 3D constructs.

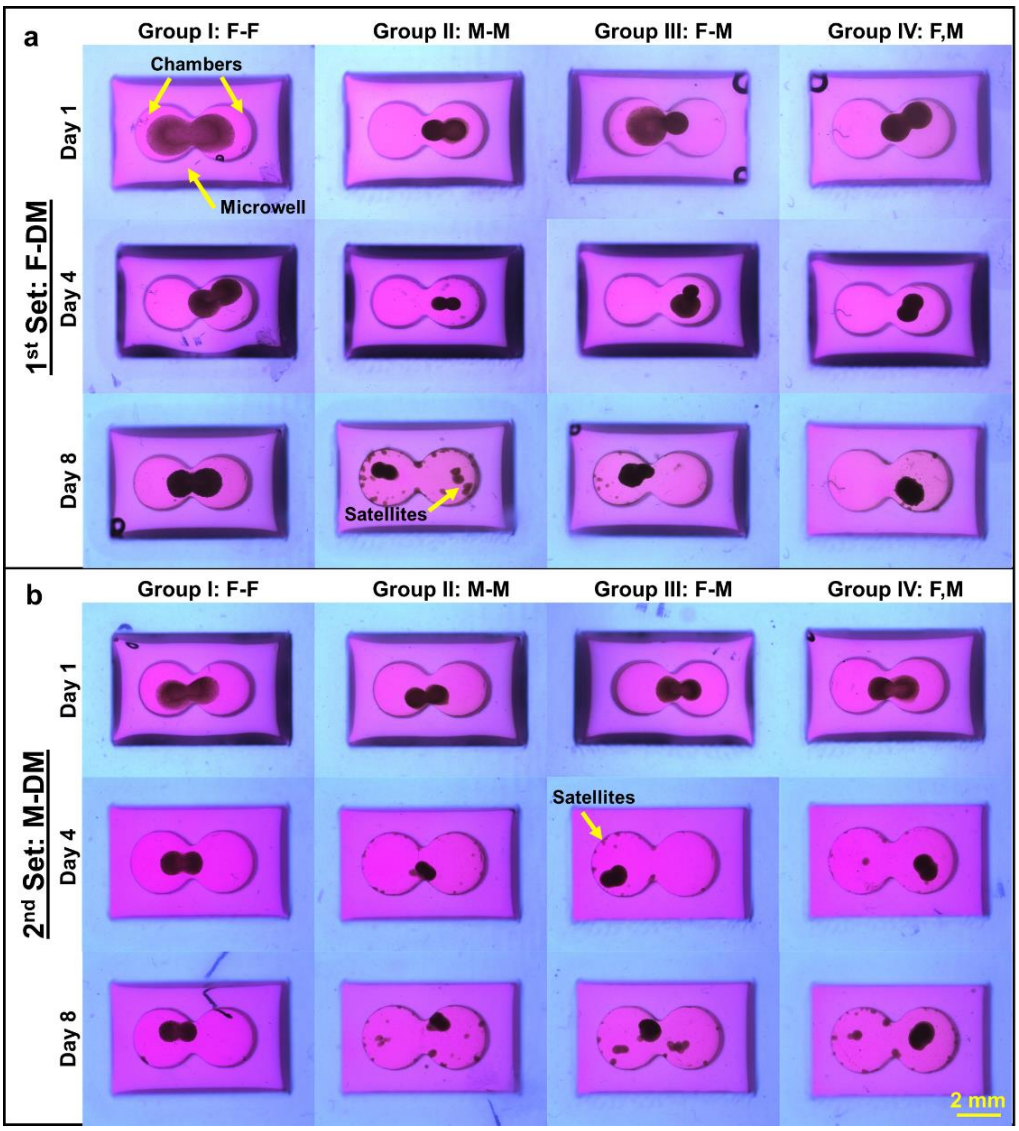

Figure 2. Bright field images of 3D grafts formed with **a)** F-DM and **b)** M-DM over time. Samples had different morphology and stability over time in different sets and 1st set had better outcome in terms of preserving the integrity of the constructs.

The evolution of these constructs was then analyzed by the amount of contraction experienced. In both sets, F-F (Group I) samples showed lowest contraction while M-M samples (Group II) had the highest contraction. F-M samples (Group III) which had heterogenous co-culture of fat cells

on one side and muscle cells on the other showed contraction that is consistent with F-F on the fat side and M-M on the muscle side which shows cells have maintained their initial positioning and didn't mix with each other. This can further be confirmed using fluorescent images (Figure 3). In F,M samples (Group IV) which are homogenous co-culture models where both fat and muscle type cells are mixed and distributed throughout the construct, contraction was identical in both chambers and higher than F-F and lower than M-M samples. This observation is consistent with the fact that both cells are mixed with each other in these wells and the fact that C2C12 cells have a greater ability to initiate the contraction of the ECM. Since there are fewer number of them in each well compare to M-M samples (they are only half of the population) the contraction is also lower. It is later shown that lack of direct physical contact between cells affects ability of muscle cells to mature and adipocytes in maintaining their stored lipids to a significant degree.

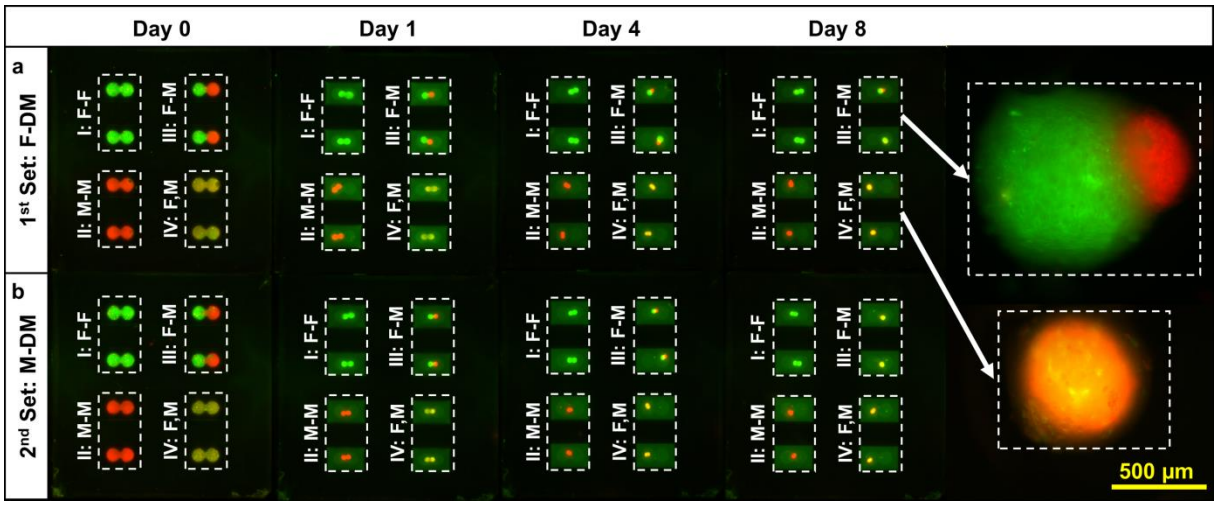

Figure 3. Fluorescent images of 3D grafts formed with **a)** F-DM and **b)** M-DM over time. Different cell types maintained their initially defined positions during the whole period of culture.

3.2. Difference between 2D and 3D Culture Systems on Cellular Behavior

The interaction between 3T3-L1 and C2C12 cells, especially the effect of direct physical contact between the two cells types on this interaction was studied by measuring total lipid and protein

content of the constructs and their metabolic activity with samples containing various combinations of 3T3-L1 or C2C12 cells both in 2D and 3D at different time points (1,4, and 8 days). In order to measure the difference in metabolic activity of different groups, Alamar blue assay was used that incorporates Resazurin, a non-fluorescent dye, as an oxidation-reduction indicator which changes into highly fluorescent Resorufin, in response to cellular metabolic reduction [34]. NRA and BCA were used to measure lipid and protein content of the samples.

Results of these measurements for 3D systems are shown in Figure 4, and it shows a dramatic difference when cultured in F-DM vs. M-DM. In the 1st set (F-DM), all of the groups had higher metabolic activity at day 1 compared to similar constructs in the 2nd set (M-DM). The metabolic activity reduces from day 1 to 4 for both sets but the reduction is more significant for 1st set as compared with the 2nd set. The activity increases slightly from day 4 to 8 for the 1st set while it remains about the same in the 2nd set. The total lipid and protein contents also show a similar trend of initial decrease from day 1 to 4 while it stabilizes between days 4 to 8 for the 1st set and continues to decrease in the 2nd set. F-F samples in both sets are the exception with similar total protein content over time. In the 1st set (cultured using F-DM), F-F samples had the highest amounts of total lipid and protein content while M-M had the lowest amounts between days 4 and 8. This initial decrease can be explained with the first growth arrest that cells experience during the differentiation process [35]. F-M and F,M groups have lipid and protein content in between F-F and M-M groups and are not significantly different from each other. In most of the cases there is no significant difference between M-M and the co-culture groups (F-M and F,M) which shows the ability of skeletal muscle cells to influence adipocyte in co-culture systems. It has been previously shown that fully differentiated myotubes can negatively affect proliferation and differentiation of adipose cells in a transwell setup [17] which is in agreement with our results.

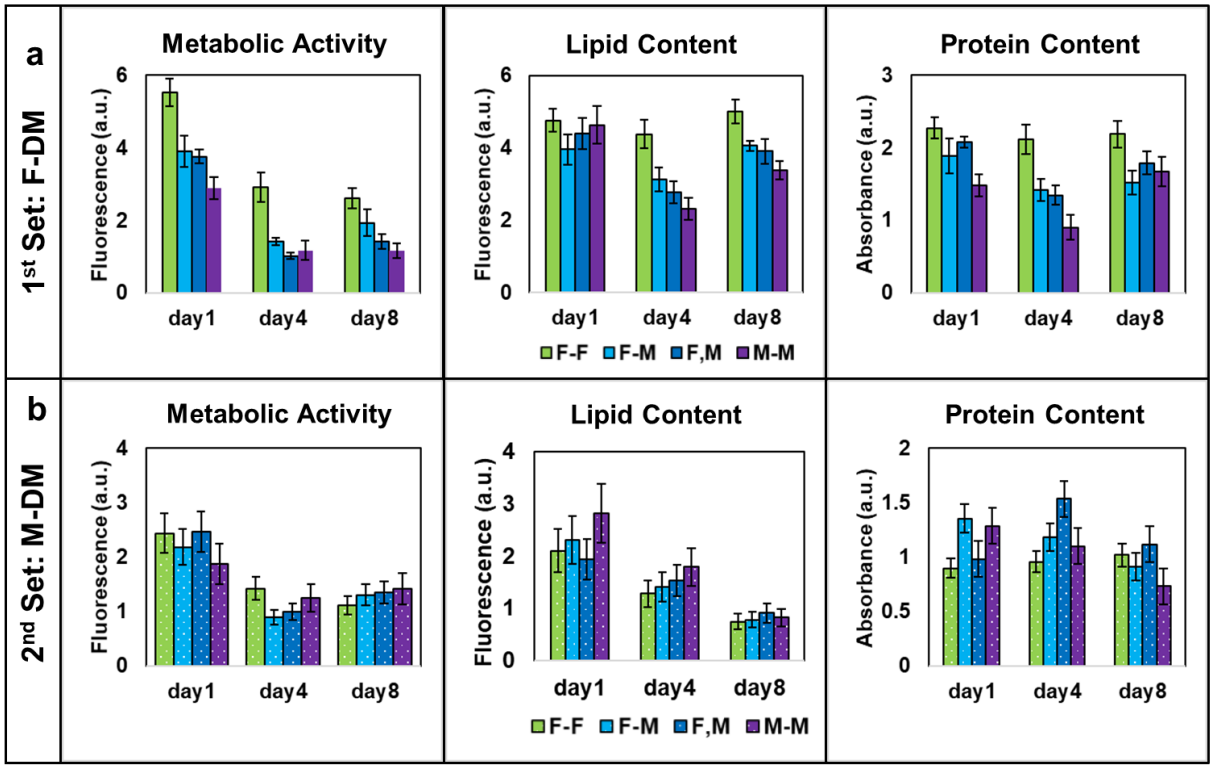

Figure 4. Results of ABA, NRA, and BCA in 3D culture systems to measure metabolic activity, lipid content, and protein content of the samples, respectively, for **a)** 1st set: samples formed with F-DM and **b)** 2nd Set: samples formed with M-DM. Similar groups showed higher amounts in the 1st set on different days compared to 2nd Set. In the 1st set amounts increased after initial decrease unlike 2nd set that either no pattern was observed, or amounts showed continuous decrease. Based on these results, F-DM and F-MM were chosen as the better choice for forming constructs and maintaining them (data are presented as mean±SD for n=8 and absolute measurements from readings are reported).

In the 2nd set (cultured using M-DM), the total lipid content of all of the samples decreased with time which shows that M-DM may not be appropriate for supporting proliferation and differentiation of adipocytes. It is also supported by the observation that among the various groups the F-F had the smallest of lipid content during the entire culture period. Comparison of all three parameters between similar groups in different sets shows overall higher cellular activity in the 1st set indicating that the combination of F-DM and F-MM is the more suitable common culture media. Therefore, based on cellular activity and the stability of the constructs (**Figure 4**), F-DM is the better choice for culturing the cells in the 3D culture system in this study.

Next, cellular activity of these cells in 2D mono- and co-cultures was studied to compare them with 3D systems. For this purpose, the same assays were performed for all of the groups and sets of experiment in 2D (Figure 5). All of the four groups in the 1st set showed stable culture, increase in metabolic activity, fat, and protein production with time. At day 8, F-F group had lower metabolic activity, but higher lipid and protein contents compared to M-M group. This is while in indirect co-culture samples, F- samples had lower lipid and protein contents compared to M- ones. Based on these results, indirect co-culture decreases lipid production of fat cells but increases protein production of muscle cells. In contrast, 2D culture using the M-DM (2nd set) was unsuitable for some groups (M-M monoculture and F,M direct co-culture) which resulted in delamination after 4 days (Supplementary Figure 1b). Similarly, the indirect co-culture using medium exchange was also unstable on the muscle side (M- samples of group III) at day 8. This kind of detachment has been observed before when an improper medium was used for differentiation of L6 cells, another myoblast cell line [36]. These results are consistent with the observation in 3D systems that constructs were unstable when M-DM was used. Similar to 3D experiments, F-DM and F-MM are better choices for these co-culture experiments in maintaining cells in their functional state.

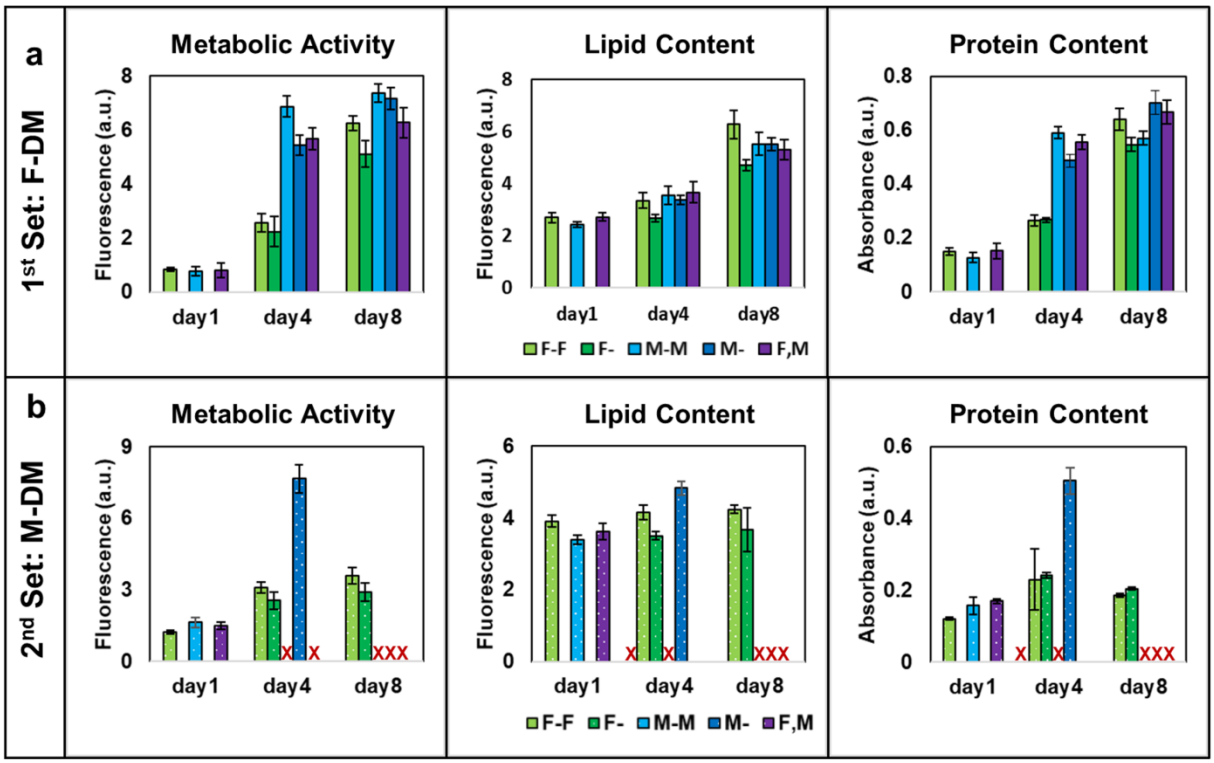

Figure 5. Results of ABA, NRA, and BCA in 2D culture systems to measure metabolic activity, lipid, and protein content of the samples, respectively in samples formed with **a)** F-DM and **b)** M-DM. X indicates samples that delaminated and assays couldn't be performed for them (data are presented as mean±SD for n=8 and absolute measurements from readings are reported).

The cellular activity of the 2D and 3D co-culture systems using F-DM (as the chosen common culture media) were then compared to identify if there are differences due to culture formats as well as determine whether the direct or indirect contact in these culture systems have an effect on cellular behavior. F-M group in 2D system is defined as the average of F- and M- groups. In 2D systems, the metabolic activity, their total lipid and protein content increased with time which indicates that the cells have multiplied, and total number of cells increased while a fraction of the population differentiated and accumulated lipids. In 3D systems however, there is a distinct decrease of these parameters from day 1 to 4 but they stabilize and show slight increase from day 4 to day 8. It was shown using live/dead staining of the constructs at day 1 (Supplementary Figure

2) that majority of these cells are alive, and the 3D self-assembly based fabrication process did not adversely affect cell viability. It has been previously shown that during differentiation process of 3T3-L1 cells, cells first experience growth arrest when they reach confluent stage, and then experience a few more rounds of post-confluent mitosis which is fundamental for their final differentiation [35]. To further investigate the 3D culture system, constructs cultured in F-DM were kept in culture for 12 days (Supplementary Figure 3). Live/dead staining showed that even over the long term there were very few dead cells in these constructs (Supplementary Figure 2). The constructs formed with C2C12 cells spawned a number of satellite aggregates which subsequently grew larger over the long term and similar phenomenon was also observed with the 3T3 cells albeit after a longer time. When the cellular activity assays were performed on constructs (Supplementary Figure 4) without the spawned satellite aggregates, there is a small increase (not significant) in metabolic activity and total protein content of F-F samples from day 8 to day 12 but a dramatic increase in total lipid content which shows that the cells have fully differentiated and lipid accumulation is in progress. Similar trends were observed for other groups (M-M, F-M, and F,M ones) as well but with marginal increase in metabolic activity and a noticeable increase in both total lipid and total protein content. These findings indicate that in 3D systems, cells are more likely to undergo full differentiation and maturation and show more controlled lipid and protein production in a pattern that is consistent with growth arrest phase that happens during these cells differentiation as compared to 2D systems. It is also noticeable that at day 12, total lipid content of F,M group is higher while in F-M group total protein content is higher. As before, it shows direct physical contact between muscle cells with fat cells could influence their differentiation and protein production. Results of the assays for F-M and F,M groups cultured in F-DM are shown in Supplementary Figure 5 for both 2D and 3D systems to better illustrate these findings.

Supplementary Figure 6 shows the statistical differences for each group (F-F, M-M, F-M, or F,M) over time. There is a meaningful increase for all of the parameters in 2D systems from days 1 to 4 and 4 to 8, but each group behaves differently in 3D. Although there is a meaningful decrease for metabolic activity of all of the groups from day 1 to day 12, total lipid content of the groups containing fat cells (F-F, F-M, and F,M) shows a meaningful increase while there is no meaningful difference for M-M samples at this time. On the other hand, while total protein content of M-M and F,M groups shows a meaningful increase from day 1 to 12, the other two groups didn't show a meaningful change.

Statistical differences between different groups at each day were also studied (Supplementary Figure 7). For 2D systems there is no difference in any of the parameters at day 1 while at day 8 differences arise between different groups. For 3D system however, there are statistically meaningful differences between metabolic activities of almost all of the groups at day 1 but the differences become less meaningful by day 12. The differences between lipid and protein contents of the groups become more meaningful from day 1 to 12.

Interaction between skeletal muscle cells and adipocytes has been studied previously *in vitro* in transwell formats or by manual transfer of supernatant media between isolated wells where the two cell types are cultured. It has been shown that treating adipocytes with insulin mediators secreted by skeletal muscle cells stimulate pyruvate dehydrogenase activity in them [11]. In another study, atrophy of skeletal muscle cells was observed when they were treated with conditioned media of adipose cells. It was also shown that atrophy was significantly higher when skeletal muscle cells were treated by conditioned media of visceral adipocyte cells obtained from obese samples compared to subcutaneous adipocytes of lean subjects [2]. Different levels of mRNA expression of genes such as caspases, calpains, and heat shock proteins that are important

in natural behavior of muscle cells and adipocytes, have also been observed in indirect co-culture of fully differentiated adipose and skeletal muscle cells using transwell inserts as compared to their monoculture systems after 48 hrs in co-culture [15]. Furthermore, induction of insulin resistance in muscle cells was observed when cultured with adipocytes in transwell inserts due to paracrine interactions [16]. Finally, co-culture of fully differentiated myotubes with preadipocytes in a transwell setup has been shown to arrest proliferation and differentiation of adipose cells [17].

Although these models have provided good insight on the crosstalk of these cells, they are still considered 2D cultures and in many cases direct physical contact between cells is neglected. The mechanisms involving paracrine activity of cells from different locations (e.g. adipocytes from different locations such as visceral vs. subcutaneous) can be studied using our technique easily compared to current methods as there is no need to transfer conditioned media of samples between different wells. The secretome of one cell aggregate is constantly being exposed to the other while the cells themselves are in their predefined positions, making analysis easier. Here it is also possible to study direct and indirect effect of cells on each other and mimic phenomenon such as marbling. The developed model can also be used to study which proteins are targeted in direct and indirect co-culture systems. It is also possible to make this model more physiologically relevant by adding to its complexity. For example, it has been reported that adipose tissue can affect liver and then liver can induce skeletal muscle defects (portal-visceral hypothesis) [37]. This can be studied by developing an indirect triculture of adipose, liver, and skeletal muscle cells using our technique in an *in vitro* setup.

3.3. Responsiveness of Co-culture Systems to Drug Treatment

Effect of direct and indirect co-culture on cells' responsiveness to drug treatment was studied by treating F-M and F,M constructs at day 4 with isoproterenol hydrochloride, a β-adrenergic agonist

drug that enhances metabolic rate by stimulating uncoupling protein 1 that resides on the mitochondrial membranes [38]. Constructs were treated with FBS-free DMEM containing 10 µM isoproterenol hydrochloride for 4 hours. Control samples were treated with FBS-free DMEM but without isoproterenol. A free fatty acid quantification kit was used to measure lipolysis in each group. Amounts of free fatty acids in the conditioned media of drug treated samples was much higher than in untreated samples as shown in Figure 6a. In control samples (untreated) there was no meaningful difference between the fatty acid release from the direct (F,M) and indirect (F-M) co-culture groups. However, there was a significant difference noted between the same groups for the drug treated samples indicating that the fat cells have higher responsiveness to the drug in indirect co-culture system. The statistical differences between treated and untreated groups as well as comparison between behavior of F-M and F,M groups is shown in Figure 6b.

Responsiveness of 3T3-L1 cells to isoproterenol hydrochloride have been reported before [39, 40] but here it was shown that direct physical contact between these cells and C2C12 cells makes them more resistant to change in their metabolic rate and ability to perform lipolysis which is important in anti-obesity research [41]. These findings in aggregate demonstrate that the spatial positioning of the cells as well as the 3D culture are both important in recreating conditions similar to *in vivo* conditions in order to obtain realistic response from *in vitro* models consisting of fat and muscle cells. Intramuscular fat, accumulated fat within skeletal muscle cells or between muscle fibers, and its effect on muscle cell function and metabolism has been an active area of research and unlike subcutaneous fat that is known to be cardioprotective and negatively correlated to metabolic diseases, intramuscular fat is believed to be responsible, at least partially, for mobility and strength loss of muscle cells *in vivo* [42]. It is also shown that treating skeletal muscle cells with conditioned media of adipose cells causes their atrophy which can be higher when they are treated by

conditioned media of cells obtained from obese samples compared to lean ones [2]. Based on our results direct physical contact between cells could intensify this effect.

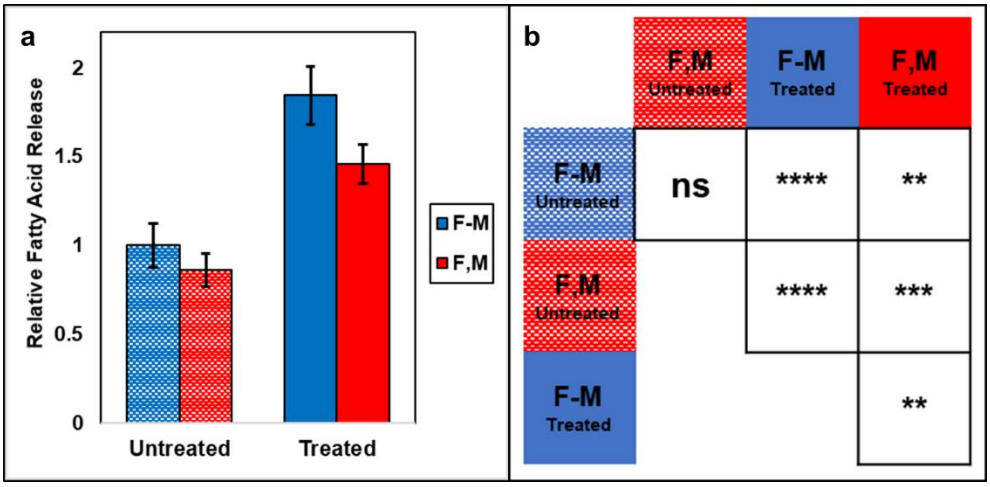

Figure 6. a) Relative amounts of free fatty acids in conditioned media of samples treated with a lipolysis agent (isoproterenol) normalized to untreated group for F-M at day 4 of culture; **b)** Statistical difference between different groups (Two-way ANOVA, n=4). All of the data points are within the first mode of the calibration curve of the kit.

The observed differences in the functions of these cells in direct and indirect co-culture systems were further confirmed by studying gene expression levels of cells in 3D and comparing them with undifferentiated cells in 2D monoculture. For this purpose, PPAR-γ and β-Actin genes were considered. PPAR-γ is a member of PPAR family, ligand-activated transcription factors of nuclear hormone receptor, that is important in adipogenesis by maintaining expression of genes that are necessary to mature adipocyte phenotype [43, 44]. PPAR-γ levels were similar in both direct and indirect co-culture systems at days 1 and 4 (Supplementary Figure 8a) but its levels were decreased during this time which is consistent with observed decreased total lipid content of samples. These findings are similar to other investigations where 2D co-culture of fat and muscle cells in transwell inserts using primary cells obtained from newborn piglets showed that co-culture of adipocytes

with muscle cells doesn't change expression of PPAR-γ during proliferation or differentiation stages compared to monoculture systems [45].

β-Actin is one of the isoforms of actin that is considered to be expressed ubiquitously in most of the cells [46] but it has been suggested that its levels can change with muscle tissue maturation [47]. In this study, mRNA level of β-Actin was studied for co-culture systems and its levels was found to be significantly different between the F-M and F,M co-culture models both in magnitude as well as in the their change over the culture period. The expression level was found to increase with time for F-M while it decreased significantly for the F,M group. This leads to a dramatic change in the expression levels at day 4 between the two groups which suggests direct physical contact of adipocytes and skeletal muscle cells might be an important factor in differentiation and maturation of cells in coculture systems.

4. Conclusions

A new 3D co-culture *in vitro* model has been developed to study the interaction between fat and muscle cells in direct and indirect co-cultures and these results have been compared with 2D environments. Considering the fact that each of the used cell lines (3T3-L1 and C2C12) has their own growth and differentiation medium, a thorough study was performed to find the best growth and differentiation media to support both of cell types, as well as integrity of the 3D constructs and proper adhesion to the culture plate in 2D systems. These media are then used to study differences between 2D and 3D cultures on these cells' behavior including metabolic activity, total protein and lipid content of the structures, and effect of previously overlooked direct physical contact between cells in co-culture systems that cannot be studied using traditional techniques such as transwell inserts. For example, it is shown that cells follow different differentiation process routes in 3D based on the spatial arrangement of the cells. In indirect co-culture where there is

lower physical contact between the two cell types, the muscle cells show more differentiation while in direct culture, fat cells show reduced lipolysis in response to anti-obesity drugs. This cannot be modeled using transwell inserts or when conditioned media is transferred between wells containing different cell types. To further make these results physiologically relevant primary cells can be used instead of using cell lines. Effect of the cell ratio on their behavior can also be important and should be considered in future studies as allosteric scaling has been an important factor in organ-on-a-chip studies. This model can also be used in personalized medicine with subjects' specific cells for applications such as drug discovery and could be used with more cell types to make more complex and realistic models.

Conflict of interest: There is no conflict of interest for both authors.

Acknowledgements: The cells used in this study, C2C12 and 3T3-L1 Cells, were kindly provided by Dr. Sandeep Raha from Department of Pediatrics of McMaster university. The authors acknowledge support from the NSERC Discovery Program for funding support. P.R.S acknowledges support from the Canada Research Chairs Program and the Discovery accelerator supplement award.

References:

1. Wang, Q.A., P.E. Scherer, and R.K. Gupta, *Improved methodologies for the study of adipose biology: insights gained and opportunities ahead.* J Lipid Res, 2014. **55**(4): p. 605-24.
2. Pellegrinelli, V., et al., *Human Adipocytes Induce Inflammation and Atrophy in Muscle Cells During Obesity.* Diabetes, 2015. **64**(9): p. 3121-34.
3. Boettcher, M., et al., *Intermuscular adipose tissue (IMAT): association with other adipose tissue compartments and insulin sensitivity.* J Magn Reson Imaging, 2009. **29**(6): p. 1340-5.
4. Gallagher, D., et al., *Adipose tissue distribution is different in type 2 diabetes.* Am J Clin Nutr, 2009. **89**(3): p. 807-14.
5. Kemp, J.G., et al., *Morphological and biochemical alterations of skeletal muscles from the genetically obese (ob/ob) mouse.* Int J Obes (Lond), 2009. **33**(8): p. 831-41.
6. Kanasaki, K. and D. Koya, *Biology of obesity: lessons from animal models of obesity.* J Biomed Biotechnol, 2011. **2011**: p. 197636.
7. King, A.J., *The use of animal models in diabetes research.* Br J Pharmacol, 2012. **166**(3): p. 877-94.
8. Duval, K., et al., *Modeling Physiological Events in 2D vs. 3D Cell Culture.* Physiology (Bethesda), 2017. **32**(4): p. 266-277.
9. Benien, P. and A. Swami, *3D tumor models: history, advances and future perspectives.* Future Oncol, 2014. **10**(7): p. 1311-27.
10. Turner, P.A., et al., *Three-dimensional spheroid cell model of in vitro adipocyte inflammation.* Tissue Eng Part A, 2015. **21**(11-12): p. 1837-47.
11. Jarett, L., et al., *Insulin mediators from rat skeletal muscle have differential effects on insulin-sensitive pathways of intact adipocytes.* Science, 1985. **227**(4686): p. 533-5.
12. Dodson, M.V., et al., *The development and utility of a defined muscle and fat co-culture system.* Tissue Cell, 1997. **29**(5): p. 517-24.
13. Armani, A., et al., *Cellular models for understanding adipogenesis, adipose dysfunction, and obesity.* J Cell Biochem, 2010. **110**(3): p. 564-72.
14. Ruiz-Ojeda, F.J., et al., *Cell Models and Their Application for Studying Adipogenic Differentiation in Relation to Obesity: A Review.* Int J Mol Sci, 2016. **17**(7).
15. Pandurangan, M., et al., *Co-culture of C2C12 and 3T3-L1 preadipocyte cells alters the gene expression of calpains, caspases and heat shock proteins.* In Vitro Cell Dev Biol Anim, 2012. **48**(9): p. 577-82.
16. Dietze, D., et al., *Impairment of insulin signaling in human skeletal muscle cells by co-culture with human adipocytes.* Diabetes, 2002. **51**(8): p. 2369-76.
17. Chu, W., et al., *C2C12 myotubes inhibit the proliferation and differentiation of 3T3-L1 preadipocytes by reducing the expression of glucocorticoid receptor gene.* Biochem Biophys Res Commun, 2016. **472**(1): p. 68-74.
18. Carrel, A., *On the Permanent Life of Tissues Outside of the Organism.* J Exp Med, 1912. **15**(5): p. 516-28.
19. Moscona, A. and H. Moscona, *The dissociation and aggregation of cells from organ rudiments of the early chick embryo.* J Anat, 1952. **86**(3): p. 287-301.
20. Baek, N., et al., *Monitoring the effects of doxorubicin on 3D-spheroid tumor cells in real-time.* Onco Targets Ther, 2016. **9**: p. 7207-7218.
21. Bosutti, A. and H. Degens, *The impact of resveratrol and hydrogen peroxide on muscle cell plasticity shows a dose-dependent interaction.* Sci Rep, 2015. **5**: p. 8093.
22. Turner, P.A., et al., *Spheroid Culture System Confers Differentiated Transcriptome Profile and Functional Advantage to 3T3-L1 Adipocytes.* Ann Biomed Eng, 2018. **46**(5): p. 772-787.
23. Klingelhutz, A.J., et al., *Scaffold-free generation of uniform adipose spheroids for metabolism research and drug discovery.* Sci Rep, 2018. **8**(1): p. 523.

24. Shahin-Shamsabadi, A. and P.R. Selvaganapathy, *A rapid biofabrication technique for self-assembled collagen-based multicellular and heterogeneous 3D tissue constructs.* Acta Biomater, 2019. **92**: p. 172-183.
25. Morrison, S. and S.L. McGee, *3T3-L1 adipocytes display phenotypic characteristics of multiple adipocyte lineages.* Adipocyte, 2015. **4**(4): p. 295-302.
26. Green, H. and M. Meuth, *An established pre-adipose cell line and its differentiation in culture.* Cell, 1974. **3**(2): p. 127-33.
27. Poulos, S.P., M.V. Dodson, and G.J. Hausman, *Cell line models for differentiation: preadipocytes and adipocytes.* Exp Biol Med (Maywood), 2010. **235**(10): p. 1185-93.
28. Ghorbani, A. and M. Abedinzade *Comparison of in vitro and in situ methods for studying lipolysis*. ISRN endocrinology, 2013. **2013**, 205385 DOI: 10.1155/2013/205385.
29. Yoshida, N., et al., *Cell heterogeneity upon myogenic differentiation: down-regulation of MyoD and Myf-5 generates 'reserve cells'.* J Cell Sci, 1998. **111 (Pt 6)**: p. 769-79.
30. Zebisch, K., et al., *Protocol for effective differentiation of 3T3-L1 cells to adipocytes.* Anal Biochem, 2012. **425**(1): p. 88-90.
31. Janot, M., et al., *Glycogenome expression dynamics during mouse C2C12 myoblast differentiation suggests a sequential reorganization of membrane glycoconjugates.* BMC Genomics, 2009. **10**: p. 483.
32. Conejo, R., et al., *Insulin produces myogenesis in C2C12 myoblasts by induction of NF-kappaB and downregulation of AP-1 activities.* J Cell Physiol, 2001. **186**(1): p. 82-94.
33. Grabiec, K., et al., *The influence of high glucose and high insulin on mechanisms controlling cell cycle progression and arrest in mouse C2C12 myoblasts: the comparison with IGF-I effect.* J Endocrinol Invest, 2014. **37**(3): p. 233-45.
34. Rampersad, S.N., *Multiple applications of Alamar Blue as an indicator of metabolic function and cellular health in cell viability bioassays.* Sensors (Basel), 2012. **12**(9): p. 12347-60.
35. Tang, Q.Q., T.C. Otto, and M.D. Lane, *Mitotic clonal expansion: a synchronous process required for adipogenesis.* Proc Natl Acad Sci U S A, 2003. **100**(1): p. 44-9.
36. Lawson, M.A. and P.P. Purslow, *Differentiation of myoblasts in serum-free media: effects of modified media are cell line-specific.* Cells Tissues Organs, 2000. **167**(2-3): p. 130-7.
37. Cai, D., et al., *Local and systemic insulin resistance resulting from hepatic activation of IKK-beta and NF-kappaB.* Nat Med, 2005. **11**(2): p. 183-90.
38. Azzu, V., et al., *The regulation and turnover of mitochondrial uncoupling proteins.* Biochim Biophys Acta, 2010. **1797**(6-7): p. 785-91.
39. Miller, C.N., et al., *Isoproterenol Increases Uncoupling, Glycolysis, and Markers of Beiging in Mature 3T3-L1 Adipocytes.* PLoS One, 2015. **10**(9): p. e0138344.
40. Aberdein, N., M. Schweizer, and D. Ball, *Sodium acetate decreases phosphorylation of hormone sensitive lipase in isoproterenol-stimulated 3T3-L1 mature adipocytes.* Adipocyte, 2014. **3**(2): p. 121-5.
41. Lidell, M.E., M.J. Betz, and S. Enerback, *Brown adipose tissue and its therapeutic potential.* J Intern Med, 2014. **276**(4): p. 364-77.
42. Addison, O., et al., *Intermuscular fat: a review of the consequences and causes.* Int J Endocrinol, 2014. **2014**: p. 309570.
43. Tyagi, S., et al., *The peroxisome proliferator-activated receptor: A family of nuclear receptors role in various diseases.* J Adv Pharm Technol Res, 2011. **2**(4): p. 236-40.
44. Tamori, Y., et al., *Role of peroxisome proliferator-activated receptor-gamma in maintenance of the characteristics of mature 3T3-L1 adipocytes.* Diabetes, 2002. **51**(7): p. 2045-55.
45. Li, Y., et al., *Myokine IL-15 regulates the crosstalk of co-cultured porcine skeletal muscle satellite cells and preadipocytes.* Mol Biol Rep, 2014. **41**(11): p. 7543-53.
46. Perrin, B.J. and J.M. Ervasti, *The actin gene family: function follows isoform.* Cytoskeleton (Hoboken), 2010. **67**(10): p. 630-4.

47. Dittmer, A. and J. Dittmer, *Beta-actin is not a reliable loading control in Western blot analysis.* Electrophoresis, 2006. **27**(14): p. 2844-5.

Supplementary Information

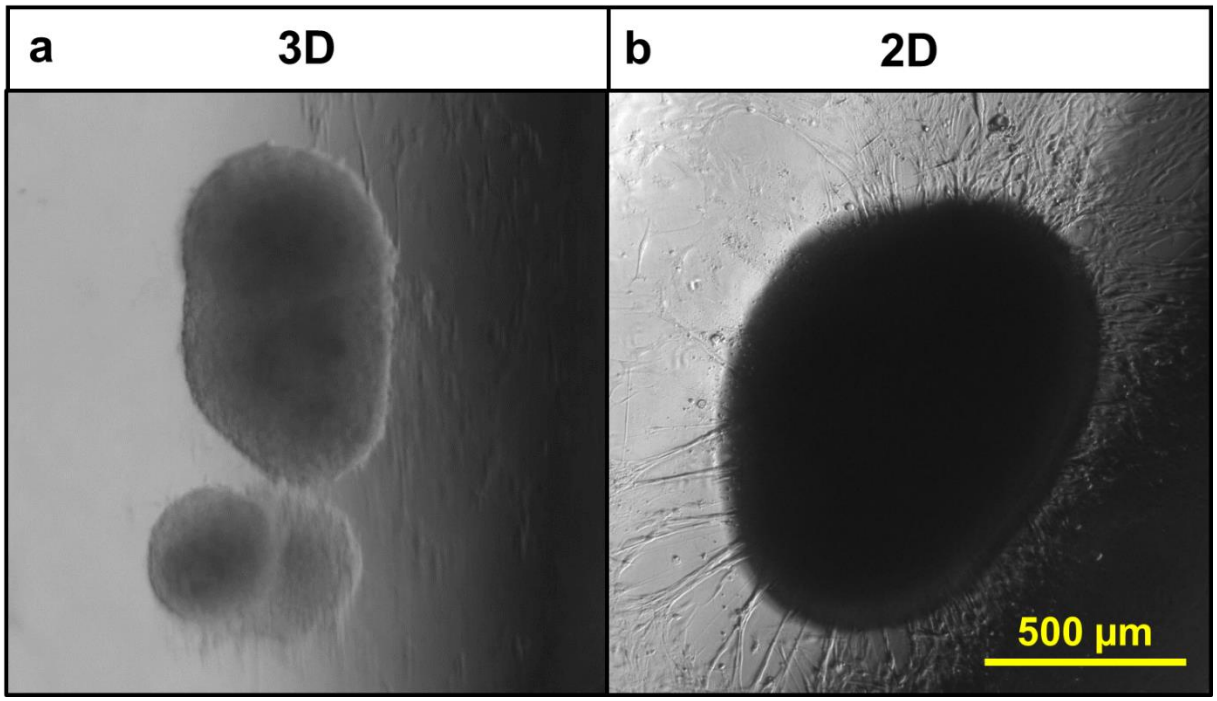

Supplementary Figure 1. a) Islets formed by C2C12 cells escaped from M-M graft formed with M-DM (Group II of 2nd set in 3D). These islets were observed only in M-M samples of 1st set at day 8 but in the 2nd set they were observed at day 4 for all of the groups except for F-F samples. **b)** Clumps formed by delaminated cells in M-M group at day 4 (Group II of the 2nd set in 2D culture). F,M samples (Group IV of this set) of this set showed the same behavior at day 4 and Group III M- (muscle cells in direct co-culture with fat cells) showed this behavior at day 8.

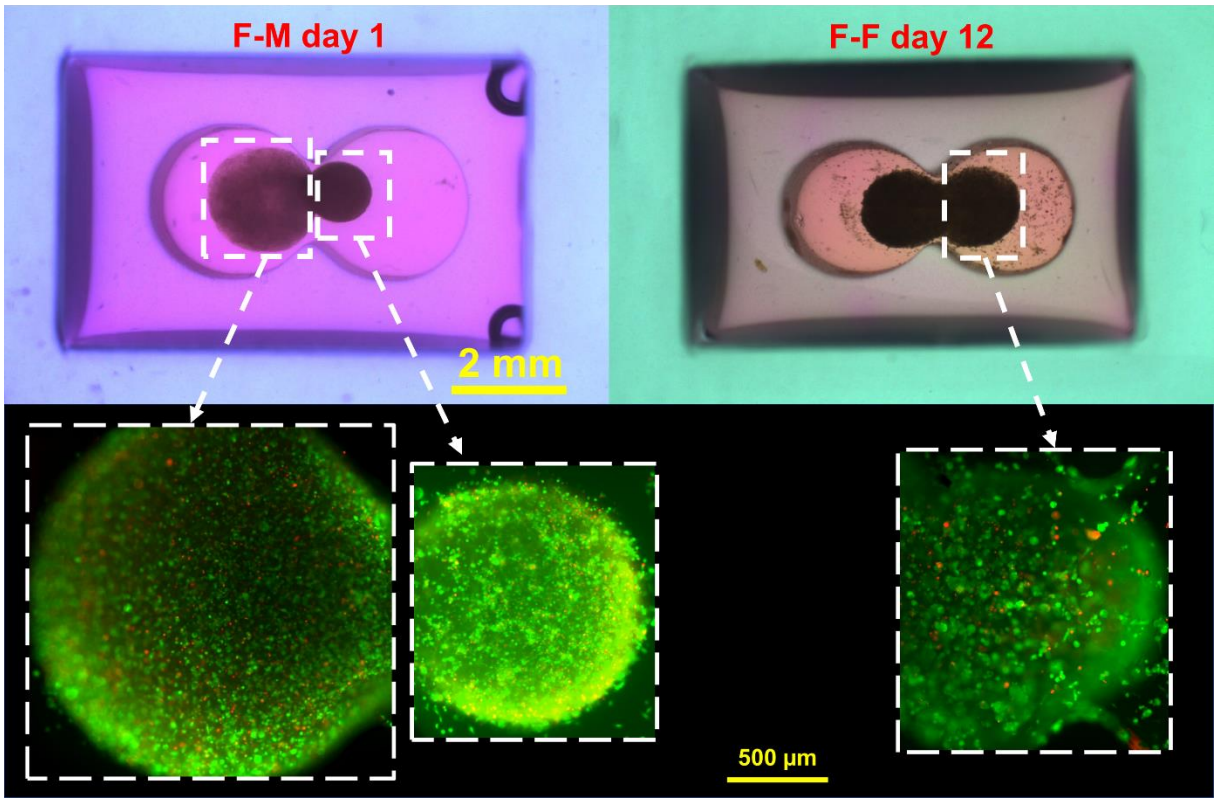

Supplementary Figure 2. Live/Dead stained samples formed with F-DM after 1 (F-M) and 12 days (F-F) from graft fabrication. Groups containing muscle cells showed fusion of cells and higher compaction and staining wasn't feasible for them.

Live/dead staining is performed using the kit from Thermofisher following the instructions. Each graft was incubated with 175 µL of F-MM containing Calcein-AM and Ethidium Homodimer-1 for 45 min. Imaging is performed using an inverted microscope (Olympus, USA) using 475-485/485-536 nm (FITC) and 542-582/582-644 nm (TXRED) filters for the live and dead stains respectively. Staining of the constructs containing C2C12 cells wasn't possible due to higher compaction and fusion of muscle cells to each other that interferes with penetration of dyes to the structure.

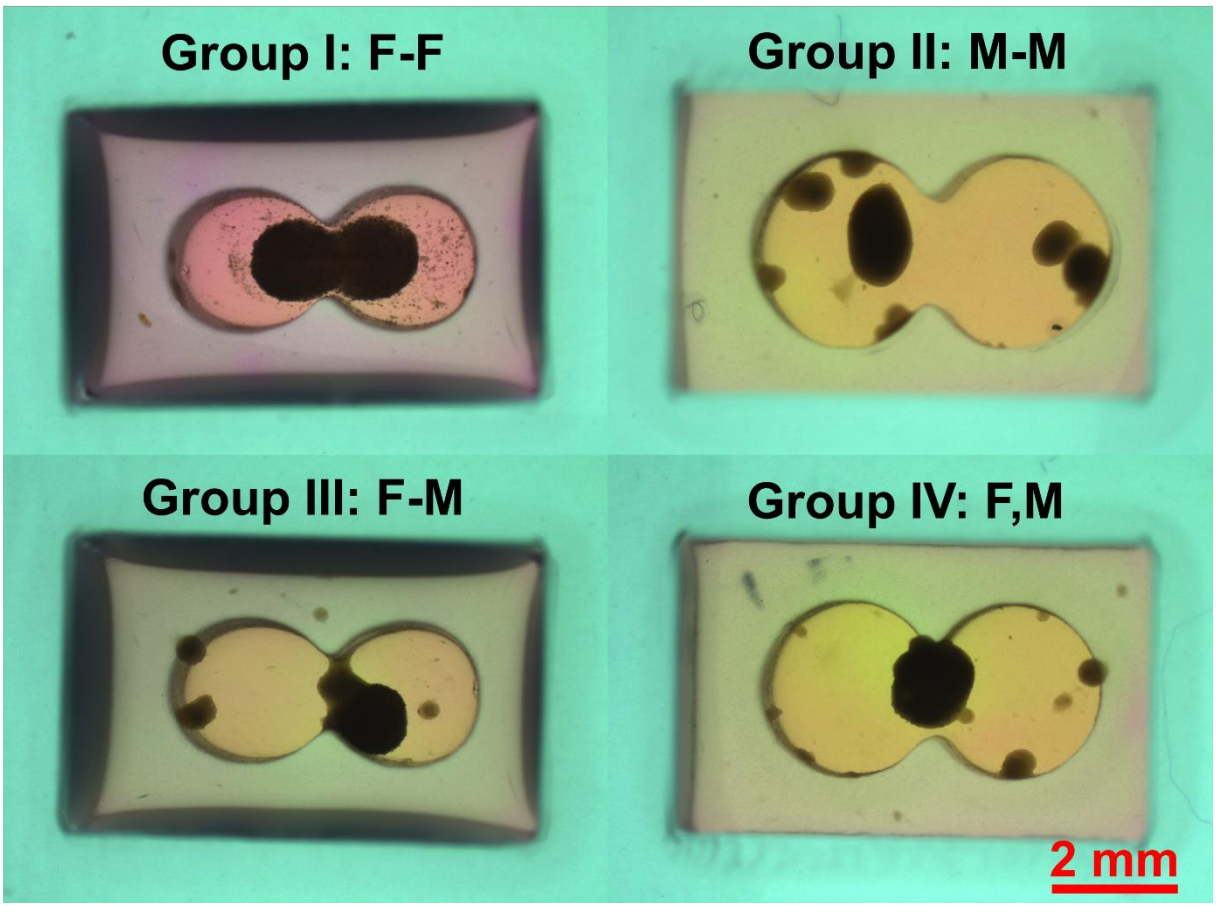

Supplementary Figure 3. Brightfield images of samples formed with F-DM after 12 days in culture. F-F samples started to disintegrate but maintained their predefined morphology. In other groups, islets grew in size compared to day 8.

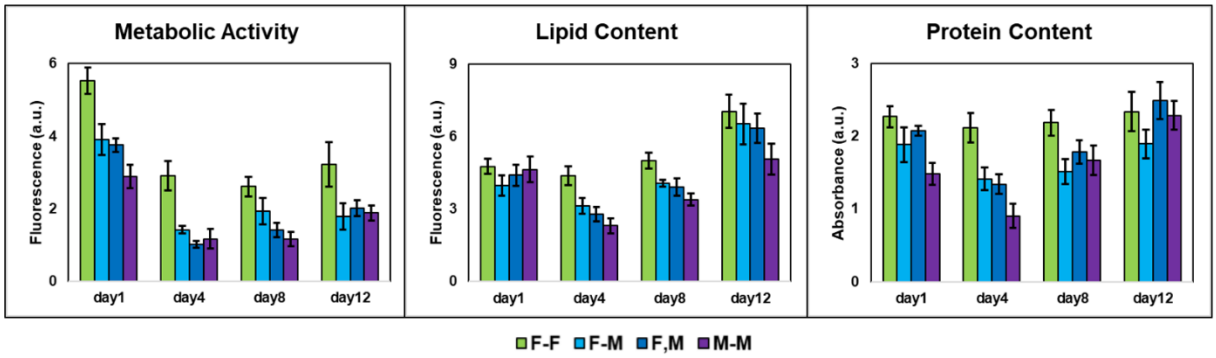

Supplementary Figure 4. Results of ABA, NRA, and BCA in 3D culture systems to measure metabolic activity, lipid content, and protein content of the samples, respectively, for samples formed with F-DM. From day 8 to 12 metabolic activity shows slight increase or no change for samples but their total fat increases for all of the samples. Protein content of F-F samples stayed the same but it increased for the rest of the groups which all of them happened to have muscle cells.

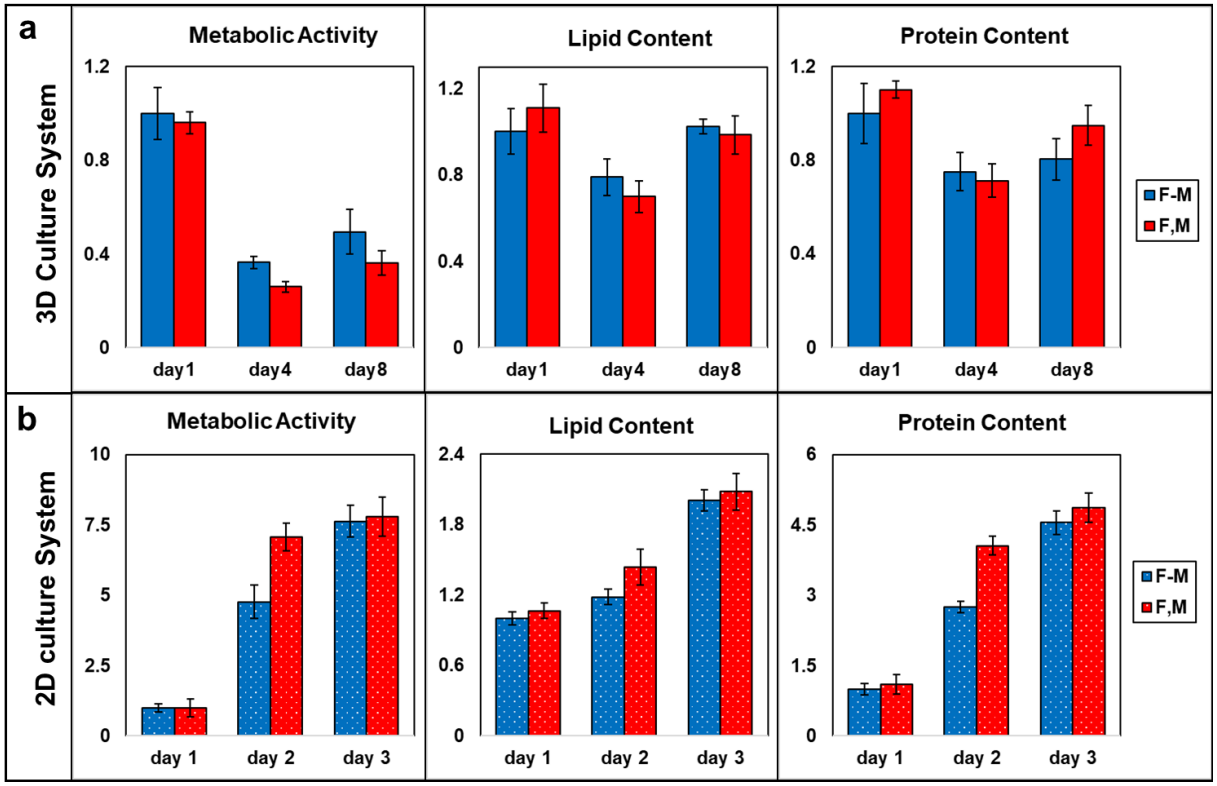

Supplementary Figure 5. Effect of direct and indirect co-culture on measured metabolic activity, lipid and protein content of the direct and indirect co-culture groups in **a)** 3D and **b)** 2D. Samples are normalized to day 1 of F-M group. For 2D systems, F-M is the average of F- and M- groups on that day. Data are presented as mean ± SD and n=8.

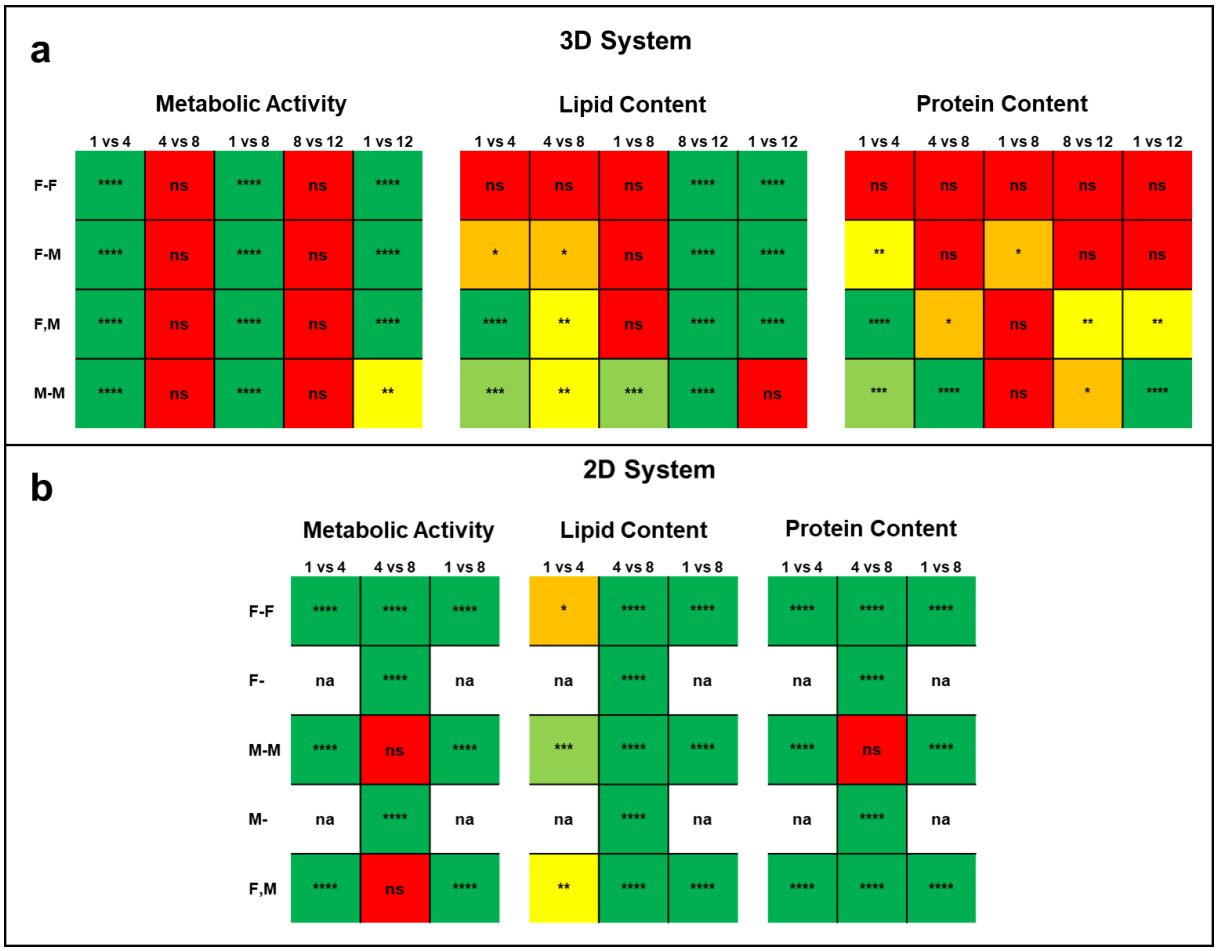

Supplementary Figure 6. Statistical differences of the observed changes in metabolic activity, lipid content, and protein content of each group over time for **a)** 3D and **b)** 2D systems for samples formed with F-DM and F-MM. The change in each group is studied over time. ns: not significant, na: not applicable, *: p-value<0.05, **: p-value<0.01, ***: p-value<0.001, and ****: p-value<0.0001.

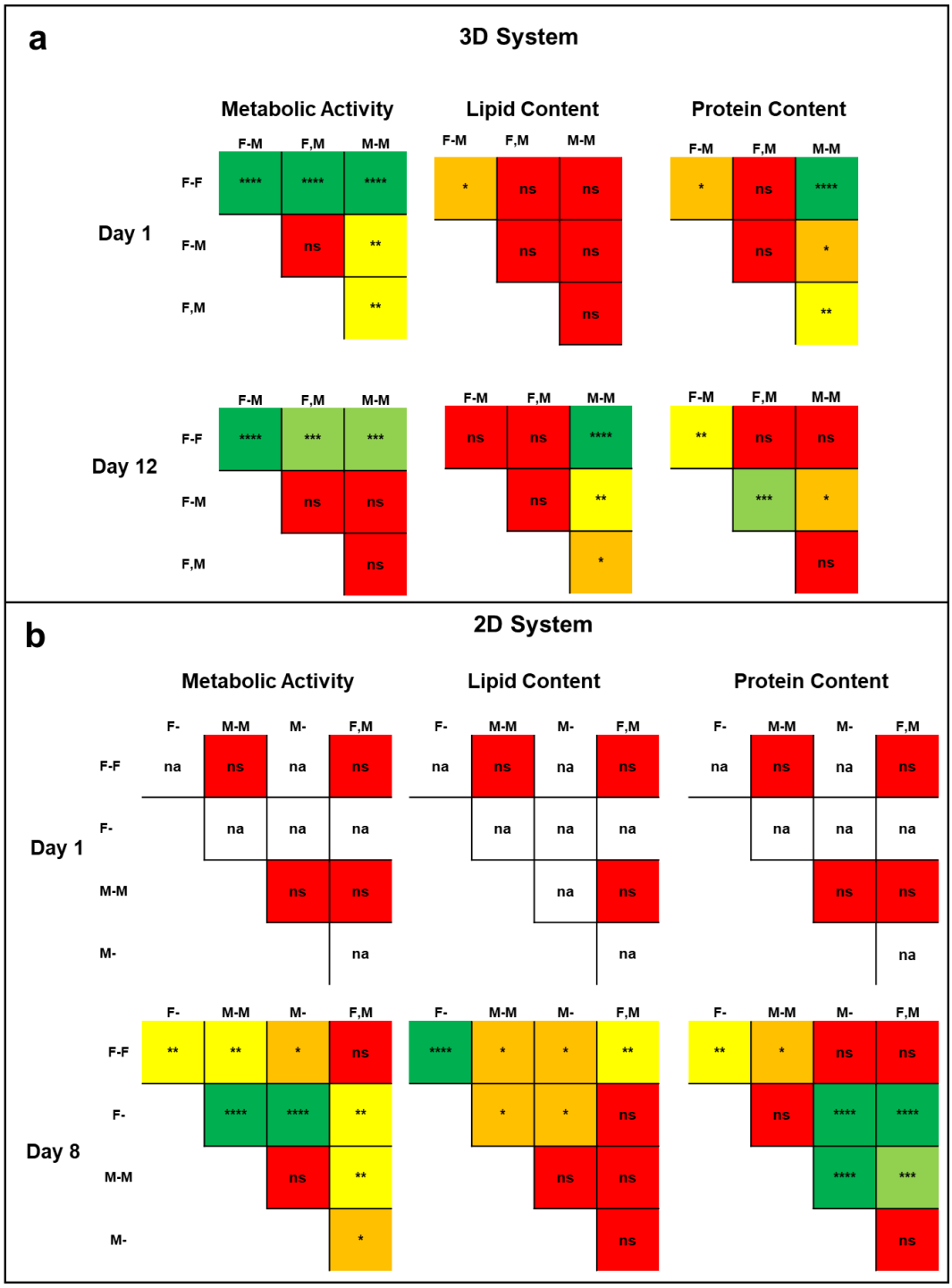

Supplementary Figure 7. Statistical differences of the measured metabolic activity, lipid content, and protein content of different groups at each time point for **a)** 3D and **b)** 2D systems with F-DM and F-MM. At each time point. ns: not significant, na: not applicable, *: p-value<0.05, **: p-value<0.01, ***: p-value<0.001, and ****: p-value<0.0001.

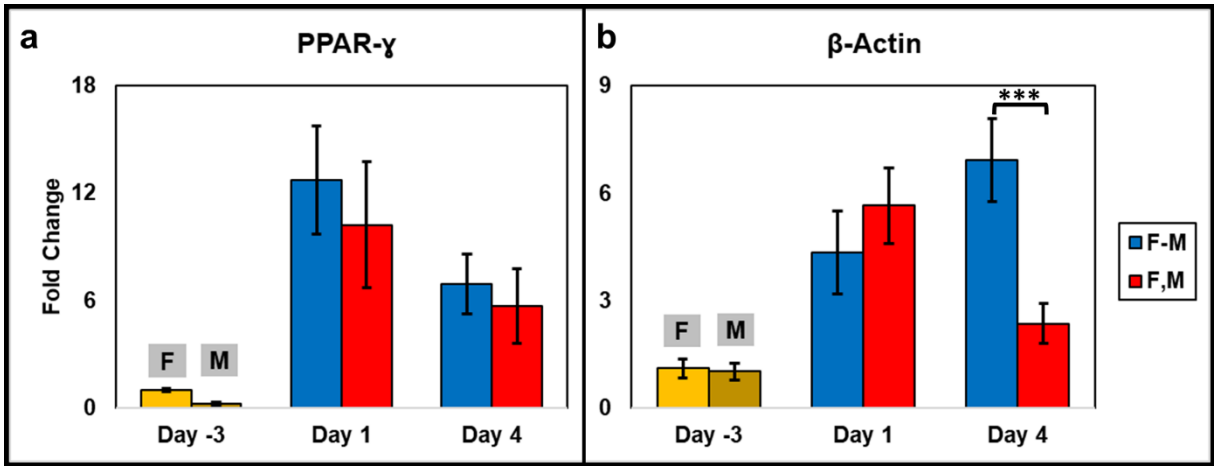

Supplementary Figure 8. mRNA expression levels for F-M and F,M samples in 3D system at days 1 and 4 as compared to undifferentiated cells in 2D for **a)** PPAR-ɣ and **b)** β-Actin. *** P-value<0.001 (n=4). Data are normalized to expression levels of F samples in 2D for PPAR-ɣ group and to M samples in 2D for β-Actin group.

Differentiation of C2C12 and 3T3-L1 cells into their mature states was investigated in 3D co-culture systems using qRT-PCR. Peroxisome proliferator-activated receptors-ɣ (PPAR-γ) and β-Actin were chosen as markers for 3T3-L1 and C2C12 cells respectively and GAPDH was used as house-keeping gene (Supplementary Table 2). F-M and F,M co-cultures in 3D systems formed with F-DM were used for this experiment and PCR was performed for samples after 1 and 4 days. Constructs were digested the same as before and digest solutions were transferred to 0.2 mL DNase free PCR tubes before dilution with 100 µL PBS. Extracted cells were spun down, the supernatant aspirated and cells were flash frozen using liquid nitrogen and stored in -80°C. A one-step qRT-PCR kit (Cells-to-CT™ 1-Step Power SYBR™ Green, ThermoFisher) was used to measure gene expression following the provided instructions. Both cell types grown in 2D without differentiation (cells in GM at D-3) were used as controls. The ΔΔCt values for each primer set were calibrated to Ct values of the housekeeping gene and then to the Ct values of controls (C2C12 (M group) cells for β-Actin group and 3T3-L1 (F group) for PPAR-ɣ group). For each group 4 samples in duplicate readings were used.

Supplementary Table 1. Details of different used for cell culture at different time points of the study *

	C2C12	3T3-L1
Growth Medium (GM)	High Glucose DMEM+10 v/v% HI-FBS	Low Glucose DMEM+10 v/v% FBS
Differentiation Medium (DM)	High Glucose DMEM+2 v/v% horse serum+1 v/v% Insulin	High Glucose DMEM+10 v/v% FBS+1 mg/mL Insulin+ 0.5mM IBMX+0.25 µM Dexamethasone+ 2µM Rosiglitazone
Maintenance Medium (MM)	Same as M-DM	High Glucose DMEM+10 v/v% FBS+1 mg/mL Insulin

* FBS: fetal bovine serum, HI-FBS: heat-inactivated FBS; DMEM: Dulbecco modified eagle medium; IBMX: 3-Isobutyl-1-methylxanthine

Supplementary Table 2. Sequence of the used primers for qRT-PCR (5'to 3')

Target Gene	Forward	Reverse
PPAR-γ	GGA AGA CCA CTC GCA TTC CTT	GTA ATC AGC AAC CAT TGG GTC A
β-Actin	CAT GGA GTC CTG GCA TCC ACG AAA CT	ATC TCC TTC TGC ATC CTG TCG GCA TA
GAPDH	CAC CCT CAA GAT TGT CAG C	TAA GTC CCT CCA CGA TGC

Chapter 6: MICRO-MOLDING IMPROVED TECHNIQUE

Tissue-in-a-Tube: 3D In vitro Tissue Constructs with Integrated Multimodal Environmental Stimulation

Alireza Shahin-Shamsabadi [1], P. Ravi Selvaganapathy [1,2,*]

[1] School of Biomedical Engineering, McMaster University, Canada

[2] Department of Mechanical Engineering, McMaster University, Canada

[*] Corresponding Author: P. Ravi Selvaganapathy, Department of Mechanical Engineering, McMaster University, Canada

Status: Published

Full Citation:

Shahin-Shamsabadi, Alireza, and Ponnambalam Ravi Selvaganapathy. " Tissue-in-a-Tube: 3D In vitro Tissue Constructs with Integrated Multimodal Environmental Stimulation." Materials Today Bio.

Abstract

3D *in vitro* tissue models are superior to 2D cell cultures in replicating natural physiological/pathological conditions by recreating the cellular and cell-matrix interactions more faithfully. Nevertheless, current 3D models lack either the rich multicellular environment or fail to provide appropriate biophysical stimuli both of which are required to properly recapitulate the dynamic *in vivo* microenvironment of tissues and organs. Here, we describe the rapid construction of multicellular, tubular tissue constructs termed Tissue-in-a-Tube using self-assembly process in tubular molds with the ability to incorporate a variety of biophysical stimuli such as electrical field, mechanical deformation, and shear force of the fluid flow. Unlike other approaches, this method is simple, requires only oxygen permeable silicone tubing that molds the tissue construct and thin stainless-steel pins inserted in it to anchor the construct and could be used to provide electrical and mechanical stimuli, simultaneously. The annular region between the tissue construct and the tubing is used for perfusion. Highly stable, macroscale, and robust constructs anchored to the pins form as a result of self-assembly of the ECM and cells in the bioink that is filled into the tubing. We demonstrate patterning of grafts containing cell types in the constructs in axial and radial modes with clear interface and continuity between the layers. Different environmental factors affecting cell behavior such as compactness of the structure and size of the constructs can be controlled through parameters such as initial cell density, ECM content, tubing size, as well as the distance between anchor pins. Using connectors, network of tubing can be assembled to create complex macrostructured tissues (centimeters length) such as fibers that are bifurcated or columns with different axial thicknesses which can then be used as building blocks for biomimetic constructs or tissue regeneration. The method is versatile and compatible with various cell types including endothelial, epithelial, skeletal muscle cells, osteoblast cells, and neuronal cells. As an example,

long mature skeletal muscle and neuronal fibers as well as bone constructs were fabricated with cellular alignment dictated by the applied electrical field. The versatility, speed, and low cost of this method is suited for widespread application in tissue engineering and regenerative medicine.

Keywords: 3D *in vitro* model; Dynamic microenvironment; Perfusion; Mechanical/electrical stimuli; Multiculture system; Cell patterning

1. Introduction

Improved *in vitro* models for human tissues and organs are sought for drug discovery and understanding disease mechanisms as they simulate the *in vivo* conditions better than existing two-dimensional (2D) cell culture systems and can also mimic human physiology better as compared with animal models. Several approaches have been investigated to address these limitations such as organ-on-a-chip devices that recreate tissue and organ interfaces *in vitro* [1, 2] with precise structural, mechanical, electrical, and fluidic control over customized cellular environments [3]. Alternatively, three-dimensional (3D) models that recreate the complex cell-cell and cell-matrix interactions and incorporate transport induced features such as natural gradient of gases, nutrients, and signaling factors have been developed as well in the form of multicellular spheroids [4] and using bioprinting techniques [5].

Organ-on-a-chip systems incorporate the major components of physiological systems that were previously missing from 2D *in vitro* models such as the multicellular patterning and interfaces of organs, presence of flow, and electrical and/or mechanical stimulation [1]. This interface was traditionally created by incorporating plastic porous membranes into microfluidic channels [1] which prevented direct physical contact between cell types. Recognizing this limitation, later versions have been created with much thinner membranes. However, fabricating such devices and integrating thin and fragile membranes to the microfabricated chips requires special expertise and the methods that are expensive and time-consuming. Furthermore, traditional Organ-on-a-chip systems, were capable of recreating a dynamic microenvironment, but were essentially 2D in nature which was non-physiological. Later versions were developed to overcome this limitation by incorporating microtissues, cell laden hydrogels, multi cell layers and living tissue biopsies to make them physiologically relevant, albeit with increased complexity in fabrication [1].

Multicellular spheroid models preserve the interactions between cells and their matrices that are found *in vivo* and attempt to recapitulate gradients in nutrients and signalling molecules that have a strong influence on cellular behavior resulting in gene and protein expression profiles that are closer to *in vivo* conditions [6]. Multicellular spheroids can be formed by incorporation of extracellular matrices (ECM) to embed the cells in the initial construct [4, 7-9] or by matrix-free methods that rely on formation of initial loose cell aggregates that become more compact by subsequent secretion of extracellular matrices by the cells [10]. Matrix-free methods are dependent on the cell type used to efficiently self assemble and the initial conditions as well as settling of the cells can have an effect on the 3D shapes formed. Furthermore, as they need to produce their own ECM, the assembly process takes a long time (several days) and the matrix composition can be variable [11-13]. Matrix based techniques overcome some of these limitations by using a well-defined ECM material that not only creates a controlled environment [14] but also aids in the initial self assembly process and makes assembly less prone to settling [4, 7]. Despite these advantages many of the current techniques are limited in the cell density, fabrication speed, control over positioning of different cell types, and creation of tissue/organ interfaces. More importantly, formation of necrotic cores and the inability to grow them beyond a certain size due to mass transport limitations is one of the key limitations of multicellular spheroid models, especially for applications other than modeling avascular stage of the cancerous tissues. Finally, it is also difficult to incorporate biophysical cues such as electrical and mechanical stimulation that is increasingly being considered important to recreate the *in vivo* environments, due to their form factor.

For this reason, non-spherical 3D constructs have been fabricated to not only avoid formation of necrotic cores but also to introduce biophysical signals (electrical and mechanical, stretch or shear) either during the formation or the testing phase. Most of these techniques form small (millimeter

size) constructs, often made of one cell type, with long assembly time and are capable of introducing one or at most two biophysical signals. For example, 3D constructs solely composed of cardiomyocytes have been converted to functional cardiac tissue using pneumatic methods to apply a periodic stretch over a period of 5 days [15] without the ability to provide other biophysical stimulus. 3D skeletal muscle constructs of a few millimeters in length have also been fabricated using self assembly around anchoring pins but without the ability to introduce different types of cells and ECMs and their precise positioning [16-18]. In addition, the fabrication process takes a few days, and the use of rigid pins [16, 17] restrict the application of external mechanical deformation while the compliant pins [18] were used to measure the self generated traction force and not provide stimulus. Ability to precisely position cells to form neuromuscular interfaces has been demonstrated using a device that required a microfabrication process and a lengthy cell culture period [19, 20]. Annular cardiac tissue constructs of a few millimeters in length have also been fabricated by self-assembly of collagenous bioink around suture wires [21] or hollow fibers [22] over 7 days. External electrodes were then incorporated to impart electrical stimulation to these constructs. A variation of the method using compliant suture wires as anchors was also demonstrated to sense the contractile tension in the tissue construct [23] but with no means to impart external stretch or electrical signals.

In some examples, multiple biophysical stimuli have been combined albeit with simple and small (< 1 cm) 3D constructs with single cell type and no ability to pattern cells. An interesting example, is a device that enabled simultaneous mechanical (static stretch) and electrical stimulation of a 3D construct composed of collagen embedded cardiomyocytes [24]. It took 3 days to form the self assembled construct of 7 mm in length and a complicated pneumatic system was used to impose a static deformation on a microfabricated mold without any perfusion control. Alternatively,

perfusion bioreactors where cells seeded in 3D scaffolds (without any control over their positioning) and incorporating electrodes for stimulation [25, 26] have been used to combine perfusion with electrical stimulation.

In summary, existing methods do not combine all the required features including rapid self-assembly of 3D tissue constructs, ability to precisely position different cell types and pattern them, ability to scale sizes of the constructs, and the ability to incorporate all the three important biophysical stimuli, stretch, shear, and electric. More importantly, they also involve customized molds, tools and equipment that make it difficult to implement without appropriate engineering expertise. In this paper, we develop a method to overcome these limitations. Here, large constructs with cylindrical shape, and uniform and well-defined mass transport properties without necrotic cores are created with high cell density, with multiple cell types positioned in predefined patterns and with clear interfaces, combined with multitude of electrical/mechanical stimulation to create a dynamic environment. The cylindrical format enables scalability and construction of various sizes (mm to cm). The format inherently is suited for perfusion of media to support metabolic needs of cells and create biomimetic shear conditions resulting in a physiologically relevant model that very closely mimics the *in vivo* conditions. This technique is simple (no microfabrication steps required) and fast (only a few hours culture time before stable tissue constructs are formed) without the need for specific fabrication equipment, has the ability to control positioning of multiple cell types/ECM materials with uni- or multi-directional crosstalk between them. It can also be used to fabricate macrostructures with different shapes that can be used as cell vehicles for implantation or as *in vitro* models for applications such as drug screening.

2. Materials and Methods

Collagenous constructs of cells inside a silicone tubing and anchored to the metallic pins were formed using a process of self-assembly that has been used previously for spheroidal and non-spheroidal structures [27]. There, a mixture of cells, medium, and neutralized bovine collagen type I were added to a polydimethylsiloxane (PDMS) mold with the specific form that defined the final shape of the construct. A stable construct forms after rapid gelation of collagen and attachment of cells to it that causes the consolidation of the construct. Replacing PDMS molds with silicone tubing enables production of solid tube-like constructs which are anchored on the stainless-steel pins (Figure 1). The silicone tubing is widely available, do not require any special fabrication process and can be connected using connectors to form complex networks. It is also gas permeable. The pins can be inserted into the tubing without leakage and serve as anchoring points axially to shape the construct formation and to apply axial tension as the construct forms.

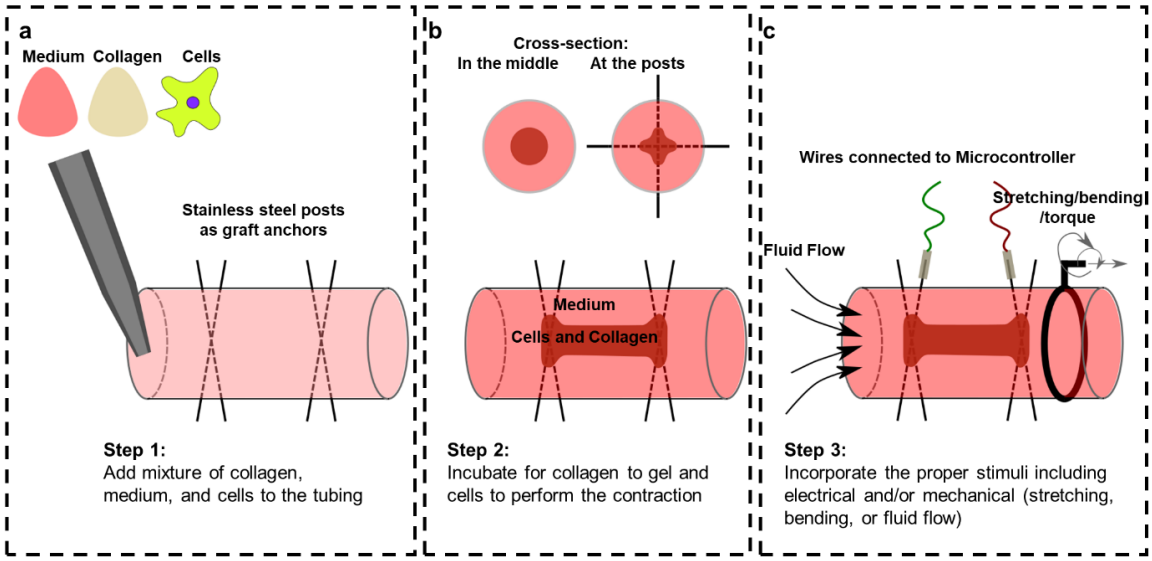

Figure 1. Schematic of the process; **a)** Tubing is filled with neutralized collagen, medium, and cell solution; **b)** After collagen gels and cells adhere to it, collagenous construct is formed within the tubing by clinging to the stainless-steel pins as support; **c)** Fluid flow, electrical stimuli, and deformation of tubing (stretching, bending, and torsion) can be applied to create a 3D dynamic environment for cells. Different volume ratios of collagen to medium, cell densities, and tubing sizes can be used to change the compactness and size of the construct.

Once the self-assembly process is complete an annular gap forms between the construct and the tubing that can be used for perfusion purposes and to apply shear forces on the construct. The inserted pins can be connected to a microcontroller to apply electrical stimulation to the construct, and the tubing itself can be stretched, bent, or torqued to create different types of mechanical deformation in the construct. This setup allows formation of collagenous constructs in a very short process (4-6 hrs) that can be kept and monitored in a true 3D and dynamic environment with different types of stimuli.

2.1. Cell Culture

Different types of cells were used in the current study for different purposes. Michigan Cancer Foundation-7 (MCF-7) breast cancer cells were cultured in Dulbecco's Modified Eagle Medium (DMEM) (with L-glutamine and high glucose, Gibco), supplemented with 10 %V/V fetal bovine serum (FBS) (Canada origin, Thermofisher) and 1%V/V Penicillin-Streptomycin (10,000 U/mL, Thermofisher) until 70% confluent. C2C12 myoblast cells were grown in the same DMEM, supplemented with 10%V/V heat inactivated FBS (HI-FBS) (Canadian origin) and 1%V/V Penicillin-Streptomycin. For differentiation purposes, these cells were cultured in DMEM supplemented with 2%V/V of horse serum (Thermofisher) and 1%V/V Penicillin-Streptomycin and 0.1% Insulin (Insulin-Transferrin-Selenium, 100X, Thermofisher, Catalogue number 41400045). SH-SY5Y neuroblastoma cells were cultured in DMEM/F-12 (Thermofisher, with L-glutamine) medium supplemented with 10% HI-FBS and 1% Penicillin-Streptomycin. For differentiation of these cells DMEM/F12 was supplemented with 1% heat inactivated FBS, 1% N2 supplement, and 1 μM retinoic acid. Red fluorescent protein (rfp)-tagged human umbilical vein endothelial cells (HUVEC) were grown in EBM-2 medium. Osteoblast-like cells from Saos-2

osteosarcoma cell line were cultured in McCoy's medium (Thermofisher, with L-glutamine) supplemented with 15% FBS and 1% Penicillin-Streptomycin.

2.2.Tissue-in-a-Tube: Fabrication and Optimization

MCF-7 cells were used for characterization purposes to study effect of collagen to medium ratio (CMR), cell density, tubing size, and distance between the stainless-steel pins. 1:1, 1:3, and 1:5 ratios were used while other parameters were kept constant at 2×10^6 cells/mL, tubing with 3 mm inner diameter (ID), and pins being 2 cm apart. The 1:1, 1:3 and 1:5 ratios corresponded to ~ 2,5 mg/ml, 1,25 mg/ml and 1 mg/ml of effective collagen concentration in the final solution. Effect of cell density was studied by using bioinks containing 1, 2, and 3×10^6 cells/mL of the bioink with 1:3 CMR and 2 cm wide pins in 3 mm ID tubing. Effect of Tubing size was studied by using tubing with 1, 3, and 7 mm ID, termed as thin, medium, and thick, respectively, while 1:3 CMR, 2×10^6 cells/mL bioink, and 2 cm wide pins were used. In order to study the ability to form constructs with different lengths, tubing with 3 mm ID was used with a bioink with 1:3 CMR and 2×10^6 cells/mL density but pins were kept 2 and 4 cm apart. After filling the tubing with the bioink in each case, incubation at 37°C was performed for 4 more hours until shrinkage of the stable constructs was done. Images of the samples were taken using a dissecting microscope (Infinity Optical Systems). Bioink was prepared by dispersing cells in the required volume of the medium and then addition of neutralized bovine collagen I (Thermofisher, 5 mg/mL). Collagen was neutralized by addition of 0.1 M sodium hydroxide in DI water. Stainless steel 304 wire (McMASTER-CARR) with 0.5 mm diameter were used as pins and at each point two pins perpendicular to each other were inserted in the tubing to provide proper anchorage for the constructs.

Live/dead staining was performed using the kit (ThermoFisher) following the provided protocol. Briefly, calcein-AM and ethidium homodimer-1 were diluted in the medium and added to the samples (formed with 1:3 CMR and 2×10^6 cells/mL density in tubing with medium thickness and with 2 cm apart pins) 4 hrs after process was started followed by 1 hr of incubation. Images of the samples were taken using an inverted fluorescent microscope with 4X magnification and proper filters.

2.3. Controlled Cellular Interfaces

Formation of clear and continuous interface between regions containing different cell types in a contiguous tissue construct was shown in both axial and radial configurations. MCF-7 cells were stained with either green DiO or red DiI fluorescent cell trackers (Thermofisher). For the axial configuration, half of the tubing was filled with the bioink containing green stained cells (1:3 CMR, 2×10^6 cells/mL solution). After half hour incubation when the collagen had gelled but the cells hadn't attached to the ECM to apply significant traction forces, the other half of the tubing was filled with the same bioink but with red stained cells. For radial configuration, the whole tubing was filled with green stained cells' bioink (1:3 CMR, 2×10^6 cells/mL solution). After 2 hrs of incubation that shrinkage was performed, extra medium was extracted and a 1:3 CMR bioink with 1×10^6 cells/mL was added followed by further incubation. Fluorescent images were taken before and after addition of each bioink using a ChemiDoc™ MP imaging system (Bio-Rad).

2.4. Complex Macrostructures

Macrostructures with different patterns including bifurcated patterns and columns with varying axial thicknesses were formed using HUVECs. For bifurcated patterns, three 3 mm ID tubing, each 2 cm in length were connected to each other using a Y-shaped connector. At the end of each tubing

two perpendicular pins were inserted as anchor pins and the entire connection was filled with 1:3 CMR and 2×10^6 cells/mL solution of HUVECs. After 1 hr of incubation that collagen had gelled, and some shrinkage was observed, pins were removed and bifurcated macrostructure was retrieved from the tubing. Columns with descending thicknesses were formed by connecting 2 cm long tubing with 7, 3, and 1 mm IDs using proper connectors, respectively. Perpendicular pins were inserted in the middle of each tubing and the same bioink as before was added. Macrostructure was retrieved after 1 hr of incubation. Fluorescent images were taken using the same ChemiDoc™ MP imaging system, before and after samples were taken out of the connected tubing.

2.5. Dynamic Environment

C2C12 constructs were formed with 1:3 CMR and 2×10^6 cells/mL bioink in tubing with 3 mm ID and 2 cm apart pins in the cells' growth medium. After 24 hrs, the medium was switched to the cells' differentiation medium and at the same time a step electrical signal with peak to peak voltage of 10 V (5 V/cm) and frequency of 50 Hz was applied (5 samples in parallel). An open source microcontroller, Arduino Uno R3, was used to create this signal and to control a motor that was used for perfusion (flow rate of 0.1 mL/min for 1 min every 12 hrs). The code used for programming the microcontroller that controls the bioreactor is included in Supplementary Box 1. This group of samples were named "Dynamic". Samples were kept in this condition for 3 more days. As control groups, samples formed in the tubing for 24 hrs but retrieved from it and kept in 6 well plates in 2 mL differentiation medium ("In Well" group), and samples kept in tubing with differentiation medium but without electrical stimulation ("In Tube" group) were considered. At day 4, samples were taken out of the tubing and images were taken using the dissecting microscope used previously. ImageJ software was used to measure thickness of the constructs before and after releasing them from the anchor pins and were compared to the "In Well" samples.

Three samples for each condition (n=4) were digested using a 0.5 mL of 2 V/V% collagenase/dispase (Sigma-Aldrich) solution in PBS (stock solution was 100 mg/mL collagenase/dispase in DI water). After digestion was done another 0.5 mL of 0.5% Triton X-100 in PBS was added to lyse the samples. Pierce BCA (Thermofisher) kit was used to measure the protein content of each sample by using two 25 µL aliquots of lysate solution in 96 well plates where 200 µL of kit solution (50:1 ratio mixture of parts A and B of the kit) was added to each well. Absorbance was measured at 562 nm after 30 min incubation at 37°C in duplicate reading for each sample. Mixture of Collagenase/dispase and Triton X-100 solutions was used as control and its value was subtracted from the samples.

Three more samples for each condition were fixed in 2% formaldehyde solution in DI water for 1 hr. After fixation was done, samples were washed with warm PBS two times and 1 mL of PBS containing 25 µL of Alexa Fluor™ 488 Phalloidin (Thermofisher) stock solution (300 units dissolved in 1.5 mL methanol) and 0.2% Tween-20 as permeabilizing agent was added with 1 hr incubation at room temperature. After washing with PBS, samples were counterstained with 1 mL PBS containing 1 µL of DAPI (4',6-Diamidino-2-Phenylindole, Dihydrochloride, Thermofisher) stock solution (10 mg/mL in DI water) for 30 min. Imaging was performed using an inverted fluorescent microscope (Olympus, USA) with DAPI and FITC filters with Ex/Em of 381-392/417-477 and 475-495/512-536, respectively. Live/dead staining and imaging was performed as before on the “Dynamic” and “In Tube” groups after samples were taken out of the tubing at day 4.

Constructs were also formed with SH-SY5Y and Saos-2 cells in 3 mm ID tubing with 1:3 CMR and 2 cm apart pins while cell density was 4×10^6 cells/mL for SH-SY5Y cells and 2×10^6 cells/mL for Saos-2 cells. Differentiation of SH-SY5Y was started at day 1 by switching to their

differentiation medium and in both cases electrical stimulation was started after 1 day and continued for 5 days with 10 V peak to peak and 50 Hz frequency.

2.6. Statistical Analysis

Data are reported as Mean ± Standard Deviation (SD) and statistical analysis was performed using one-way ANOVA test in GraphPad Prism with an accepted statistical significance (p-value) less than 0.05. Significant outlier data points were detected using Grubbs' test.

3. Results and Discussion

3.1. Tissue-in-a-Tube: Fabrication and Optimization

A new biofabrication approach termed as Tissue-in-a-Tube has been developed to form highly dense multicellular cylindrical constructs, rapidly with the ability to incorporate electrical and/or mechanical stimuli to cells in a 3D environment along with continuous medium perfusion (Figure 1). Silicone tubing with stainless steel pins inserted in it were used as the molds for the assembly of 3D collagenous constructs. These pins, inserted at specific locations, act as anchors and direct the self-assembly of the constructs between them when appropriate bioinks are injected into the silicone tubing (Figure 1a). They also allow application of electric field axially over the construct during or after its formation process. The self-assembly process leads to shrinkage of the collagenous bioink into a dense construct at the center of the tubing leaving a uniform concentric gap around it that can be used for perfusion of nutrients, removal of waste, and to apply shear stimulus (Figure 1b). The silicone tubing is also gas permeable and thus allows gas exchange to support long term tissue culture. It is also flexible and mechanical deformation of it such as stretching, bending, or torsion can induce similar effect on the anchored tissue constructs (Figure 1c). Single or multiple stimuli can be applied to the constructs in a time dependent manner

depending on the cell types used in the biofabrication process. The technique is simple, low-cost, rapid, and can be used with a variety of cell types including epithelial (such as MCF-7 breast cancer cells) and endothelial (such as HUVECs) cells, skeletal muscle cells (such as C2C12 cells), neuronal cells (such as SH-S5Y5 cells), and bone cells (such as Saos-2 cells), either alone or in co-culture as shown in detail in the following sections. It can also form larger constructs with multitude of stimuli applied simultaneously.

Different parameters such as cell density, initial collagen to medium ratio (CMR), and tubing size (inner diameter (ID)) can affect the dimensions of the formed construct as well as its compactness which was characterized using MCF-7 cells with the epithelial phenotype characteristic. Increasing the cell density and CMR, or decreasing the tubing ID, decreased the thickness of the construct (Figure 2a-c). For instance, increasing the cell density from 1 to 2 and 3×10^6 cells/mL while the CMR and tubing ID were kept at 1:3 and 3 mm, decreased the diameter of the tubular graft from 1854±45 to 1375±41 and 1028±51 μm, respectively (n=4). It should be noted that the formation of the construct and the contraction leads to a dramatic increase in its cell density (final densities of ~0.28×10^7, ~1.06×10^7, and ~2.54×10^7 cells/mL for initial densities of 1, 2, and 3×10^6 cells/mL, respectively, when CMR and tubing ID of at 1:3 and 3 mm were used). Starting with a higher cell density will also result in a higher relative increase in the final construct as more shrinkage happens due to higher cell-cell interactions. For example, the total increase in the final density of constructs with seeding densities of 1, 2, and 3×10^6 cells/mL was 2.8, 5.3, and 8.5, respectively.

Increase in cell density leads to increase in cell-cell and cell-ECM interactions that facilitate higher traction forces and increased consolidation of the construct [27]. Longer constructs were formed by increasing the distance between the anchor pins while maintaining the diameter of the tubular structure (Figure 2d). The rate of contraction due to self assembly is dramatic in the first 4 hrs and

decreases over the next 20 hrs after which the size of the construct stabilizes (Supplementary Figure 1).

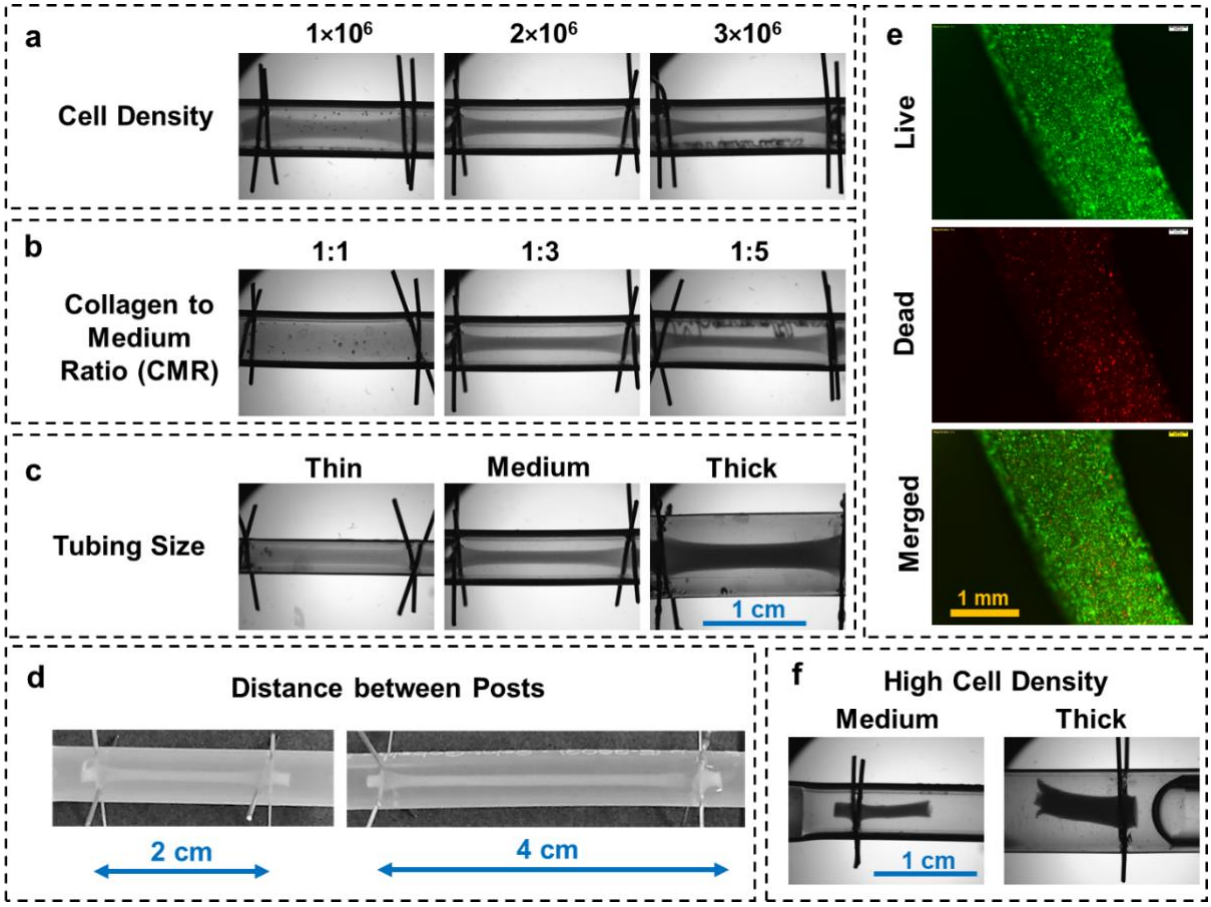

Figure 2. Characterization of parameters effective on the tissue-in-a-tube process using MCF-7 cells; Effect of **a)** cell density (with 1:3 CMR and medium thickness tubing); **b)** CMR (with density of 2×10^6 cells/mL and medium thickness tubing); **c)** Tubing thickness (with 1:3 CMR and density of 2×10^6 cells/mL). **d)** Effect of distance between anchor pins, longer constructs can be formed by increasing the length of the tubing (with 1:3 CMR and density of 1×10^6 cells/mL); **e)** Live/dead stained samples 4 hrs after process was started. **f)** Increasing the cell density would increase the contraction which leads into developing a tear in the structure. All images are taken 4 hrs after assembly. In each case n=3 was used to ensure the process is repeatable.

Bioinks with CMR of 1:3 and cell density 2×10^6 cells/mL seeded into tubing with anchor pin spacing of 2 cm and 4 cm produced correspondingly long constructs with minimal change in their diameter (1375±41 vs. 1320±89 μm for 2 and 4 cm apart pins, respectively). Since construct

formation process is fast (~4 hrs), the cells were viable and only a small number of dead cells can be observed with uniform distribution rather than formation of necrotic regions (Figure 2e). Interestingly, the number of dead cells close to the anchoring pins was slightly higher than in the rest of the construct which could be due to higher traction forces in those regions (Supplementary Figure 1). Increasing the cell density increased the amount of internal strain generated in the construct resulting in excessive contraction which led to its catastrophic failure (Figure 2f).

3.2. Controlled Cellular Interfaces/Complex Macrostructures

Multilayered and multi-material tissue engineered constructs better mimic function and architecture of natural tissues [28]. Such constructs can be used to study the interaction between different cells in a tissue that happens through paracrine or contact-dependent cell signaling which significantly influences their individual function [29]. The rapid self-assembly process used in this method enables formation of constructs that can be axially or radially patterned with different cell types (demonstrated here with MCF-7 cells stained with different colors) while maintaining its structural continuity and integrity (Figure 3a). In order to be able to produce axial patterns, a portion of the tubing was initially filled with the first bioink and allowed to self-assemble for 30 min which was long enough to allow the collagen to gel and solidify but not sufficient for the cells to adhere to the ECM and initiate substantial shrinkage. Next, the second bioink was introduced into the rest of the tubing which then subsequently also self-assembled forming an axially patterned construct. The interface between the two cell regions in the tissue construct formed after shrinkage induced by the cell attachment to the ECM was found to be precise and capable of withstanding high internal tension. Delay in addition of second phase resulted in two separate unfused regions that due to high contractile force were positioned distant from each other (Figure 3b). Concentric or radial patterning of cells was formed by initially filling the entire space between

the pins with the first bioink followed by a longer incubation time (~2 hrs) so that the construct shrank to nearly half of the final stable size. At this point the excess medium was extracted and replaced with the second bioink containing a different cell type and/or ECM combination (Figure 3a) which then proceeded to self-assemble around the partially assembled first layer in an annular fashion. Formation of second layer around the first layer at the anchor pins is shown in Figure 3c. In radial mode, by decreasing the cell number and increasing the CMR single layer cell coverage can be potentially made to cover the inner cell construct for example to mimic blood-brain barrier. These patterning can also be used to create constructs with different types of ECMs in different locations. While presence of collagen is necessary for formation of stable structures, other types of ECM can be mixed with it to provide more favorable environment for different cells in each region or for example to study migration of cells from one region with one type of ECM to the other. Such constructs allow direct contact between different cell types at the interface and paracrine interactions for the rest of the cells in different layers. The paracrine interactions can also be modeled in a unilateral direction by forming the constructs in two separate tubing and connecting them using interconnects. Applying a small fluid flow will allow exposure of the downstream construct to the paracrine signaling while preventing it in the upstream construct. Such cell patterning can also be useful in applications such as controlled release of pharmaceuticals [30].

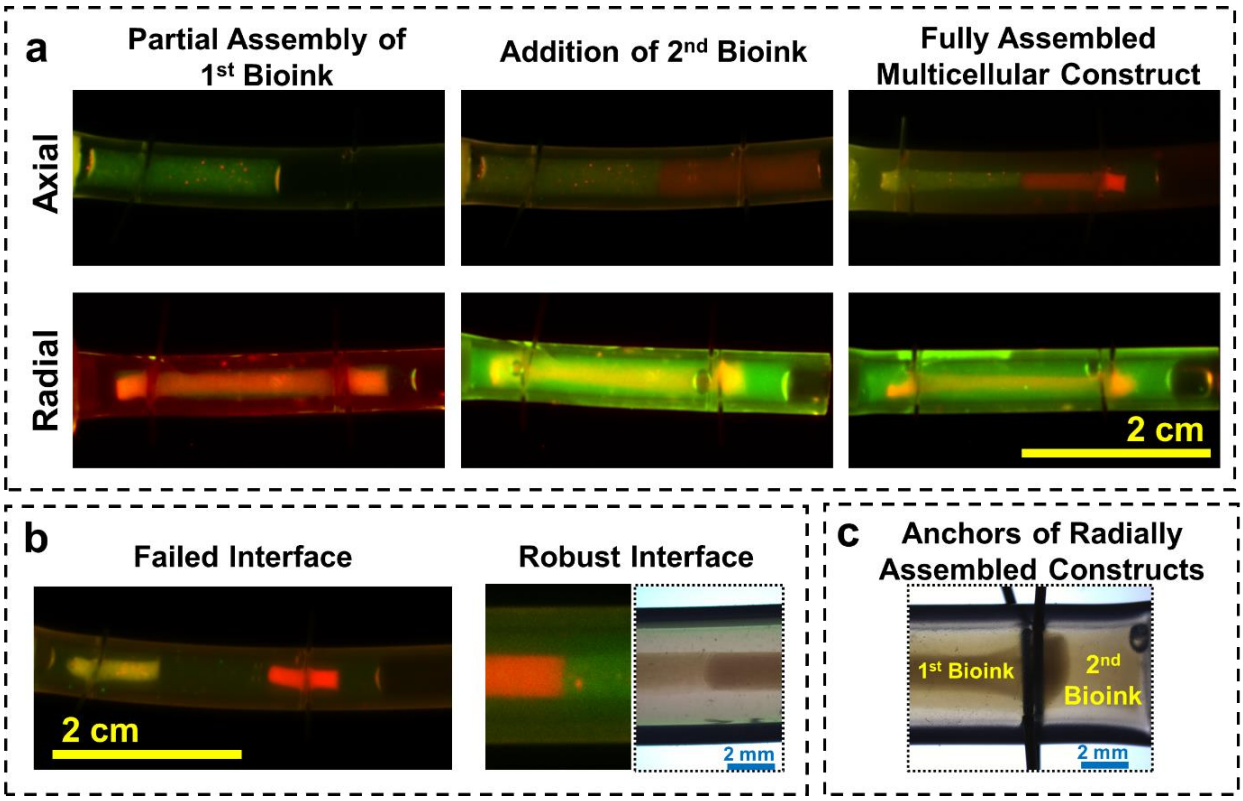

Figure 3. a) Controlled graft interfaces containing different cells in tissue-in-a-tube constructs in Axial and Radial configurations with clear continuity and interfaces; **b)** Failed and robust interfaces in constructs with Axial configuration; **c)** Anchor point formed with two cells in Radial configuration. Addition of second bioink in the Axial configuration should be done right after completion of gelation process for the first bioink. If it is added earlier, a well-defined border between two regions won't be formed and if it is added long after this point, a firm junction won't be formed and due to force exerted by shrinkage of the constructs they will tear apart. All the images in panels b and c are taken after 8 hrs of starting the process.

Spherical constructs have been widely used, for example in the case of spheroids, mostly due to ease of fabrication for applications such as modeling the initial avascular state of cancerous tissues [7], but this format can lead to formation of necrotic core that is not favorable for other applications including modeling physiological conditions of different tissues. An alternative and elegant tissue structure would be cylindrical or tubular structures that can be extended along their axial dimension to have a larger volume without increase in the radial direction in order to avoid formation of necrotic cores. Control over the radial dimensions of such structures affect the mass

transport fluxes within the construct and could be used to create unique biochemical environments. Here such long tubular macrostructures with different thicknesses in different regions were fabricated (Figure 4a) by connecting silicone tubing with different IDs, using appropriate connectors, inserting anchor pins in each of them and then filling the entire construct with the bioink. In under an hour, the cells and ECM rapidly assembled to form constructs that are several centimeters in length but have different diameters in the various sections. The constructs were robust enough that they can be retrieved from the tubing using tweezers and were strong enough to support their own weight. These types of constructs provide different mass transfer conditions in different sections and can be used as *in vitro* models or as cell delivery vehicles for *in vivo* implantation. Extrusion printing of bioinks containing hydrogels and cells can be used to form long tubular constructs but they typically have low cell density (less than a few million cells/mL [31-33]). Newer extrusion techniques with lower speed can produce high density constructs with radial and axial patterning [34, 35] , but have difficulty in creating branching networks and require specialized equipment. Alternatively, the hanging drop method has been modified with patterned substrates in rectangularly designed hydrophilic regions to confine cells in a semi-cylindrical fashion in order to assemble ECM-free fibers [36]. This interesting approach is an advancement over the traditional hanging drop method but is still limited in its ability to form multicellular patterns radially or axially. Furthermore, it requires specialized substrates and long assembly times. Our approach presented here, represents a simple yet robust method that can be adapted easily to produce macro tissues of almost any length from multiple cell types with the ability to create branching structures (Figure 4b) very easily (single step) without the use of expensive equipment or complicated operations.

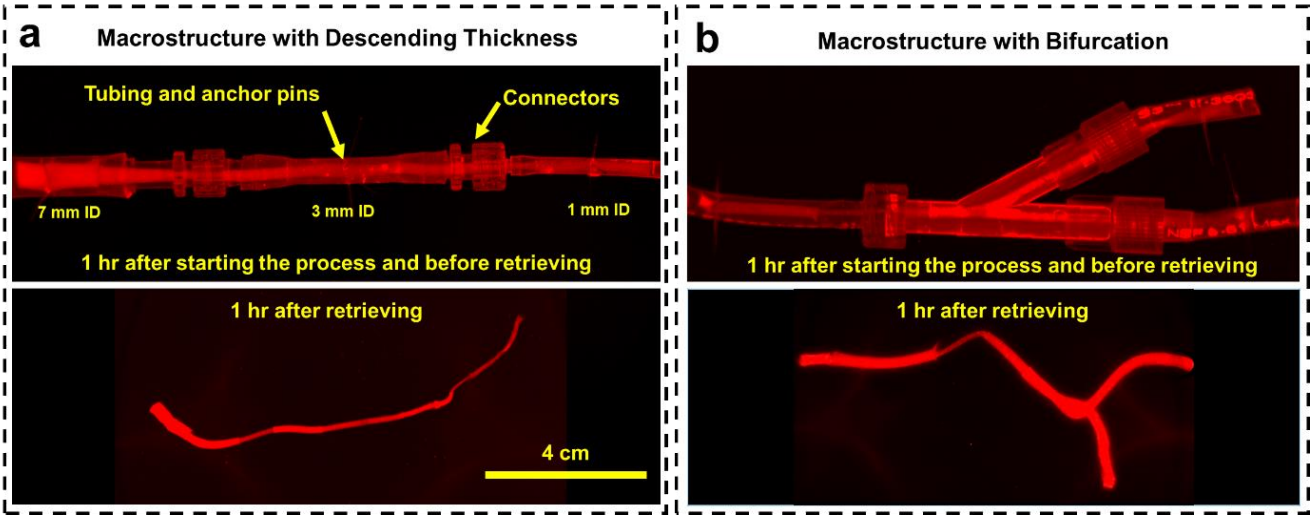

Figure 4. Formation of macrostructures with complex patterns using tissue-in-a-tube technique; **a)** long column with descending thickness and **b)** with bifurcation. Constructs are formed with HUVECs (with density of 2×10^6 cells/mL and 1:3 CMR) and are stable outside the tubing. After retrieving from the tubing, a noticeable shrinkage happens but they will preserve their premeditated morphology.

The branching structures shown here (Figure 4b) are particularly important as complex interactions between different tissues can be simulated by fabricating each tissue separately in a tubing and then simply connecting them using appropriate Y-shaped connectors. These conformations allow more complex interactions where the paracrine signalling of two different tissues can be simultaneously exposed to a common down stream tissue or inversely the signaling from a common upstream tissue could provide exposure to several downstream tissues while they don't affect each other. By repeating these connections, a more complex fluidic network can be developed that can provide physiologically relevant paracrine interactions between multiple tissue types in a simple and robust way without the use of any complex microfabrication processes. By using different cell densities in each tubing in the branched network or connecting different number of tubing containing each cell type a more accurate model of interaction between different tissues and organs can be created using proper allosteric scaling [37, 38].

3.3. Dynamic Environment

In addition to 3D cell-cell and cell-ECM interactions and paracrine activities, biophysical signals such as mechanical or electrical stimulation play an important role in recreating the *in vivo*-like microenvironments that determine the functioning of tissues [39, 40]. The use of metal pins as anchors provided the ability to apply electrical stimulus to the tissue construct during different assembly and development phases. In addition, due to the self assembly and the contraction of the forming tissue construct that are constrained by the rigid pins, a time varying and auto-regulating mechanical stimuli is also applied on the construct. Similarly, the flexibility of the silicone tubing as well as the ability to perfuse the annular region between the tube and the tissue provided the ability to introduce active and dynamic mechanical stimulus and perfusion of fluids. A bioreactor (Supplementary Figure 2) was designed to apply electrical field (up to 5 V/cm with 50 Hz frequency) to the constructs through the anchor pins and to perfuse the growth medium to avoid waste accumulation and apply shear force. Using a microcontroller and additional pins in different locations, a range of different electrical signals can be applied at different locations and multiple assays can be conducted while continuity of the tissue construct and its exposure to nutrients and drugs are preserved.

Importance of dynamic environment on cell function was studied by studying effect of electric field on differentiation and maturation of myoblast cells as well as their ECM deposition. For this purpose, muscle tissue constructs (formed using C2C12 cells, 1:3 CMR, 2×10^6 cells/mL, and 2 cm apart pins) that were formed in their growth medium and subsequently their differentiation into mature skeletal muscle cells in the form of multinucleated myofibers, in three different conditions were compared. Cellular behavior in samples formed in the tubular constructs without subsequent confinement to the anchor pins was studied by transferring the formed tubular constructs to 6 well

plates containing differentiation medium ("In Well" group), 24 hrs after the process started. Effect of being confined to anchor pins on cell behavior was studied by keeping the formed tissue samples in the tubing ("In Tube" group) and switching to differentiation medium. Effect of electrical stimulation on this process was studied by applying electric field to the anchored samples in the tubing while they were exposed to differentiation medium ("Dynamic" group). Grafts in these conditions were compared 3 days later (4 days in culture in total) (Figure 5). Bright field images of samples at day 4 (Figure 5a) showed that "In Tube" group samples had significantly higher thicknesses (1563±105 μm) compared to "Dynamic" and "In Well" samples which weren't significantly different from each other (1047±55 and 1042±31 μm respectively) (Figure 5b). Measurement of total protein content of the constructs using Pierce BCA assay showed that both "Dynamic" and "In Tube" samples were similar to each other in protein content (Figure 5c) which was significantly higher as compared to "In Well" samples (~1.4 times higher). At day 4 "In Tube" and "Dynamic" samples were retrieved from the tubing and were kept in 6 well plate in differentiation medium for 3 more days. Immediately after retrieval, "Dynamic" samples showed a detectable shrinkage while it was much lower for "In Tube" ones. After 3 more days in culture, more shrinkage was observed for "Dynamic" samples while "In Tube" ones showed a small amount of shrinkage. Higher magnification imaging during the first 3 days of differentiation showed that a high number of cells disaggregated from "In Well" group and proliferated on the well surface (Figure 5a) while such disaggregation was not seen in the case of "In Tube" and "Dynamic" constructs during the 3 days of culture after being retrieved from tubing. Staining for F-actin in the constructs using phalloidin at day 4 (Figure 5d), revealed that although samples in all three groups were treated with the same differentiation medium, cells in the "In Well" group didn't fuse and didn't form multinucleated fibers unlike samples in the "Dynamic" group that

showed formation of fibers aligned in the direction of electric field (perpendicular to the anchor pins). Samples in the "In Tube" group, which were exposed to mechanical constriction, had a few fibers formed which were very short compared to the ones in the "Dynamic" group. Presence of electrical stimulation in "Dynamic" group didn't affect the protein content and therefore ECM production in those samples as compared with the "In Tube" group where there was no electrical stimulation (Figure 5c), but it did induce more extensive fiber formation and maturation of skeletal muscle cells. This shows that various stimulation that are important to obtain morphological features seen in natural tissues can be induced in this method easily. Presence of anchor pins provided a continuous mechanical strain to the developing construct which stabilized the construct and prevented cells from disaggregating. Live/dead staining of the "In Tube" and "Dynamic" samples right after retrieval from the tubing at day 4 showed fewer dead cells in the "Dynamic" condition (Figure 5e) which shows not only the "Dynamic" environment promoted the differentiation and maturation of cells, it also preserved their viability as well. Although electrical stimulation and perfusion have been applied previously to skeletal muscle cells to study myofiber formation [41-44], our method allows simultaneous application of all three stimuli – perfusion, electrical and mechanical along with control over tissue interfaces, environmental factors such as construct size and compactness, as well as a fast process with little to no effect on cell viability.

Other tissue constructs including neural (formed using SH-SY5Y neuroblastoma cells) and osseous (formed from Saos-2 osteosarcoma cells) also demonstrated cellular alignment with the electrical stimulus in our tissue formation method (Figure 5f). These constructs were kept in culture for 8 days and were able to maintain their integrity despite observation of further shrinkage. Although the effect of electrical field on bone cells have been previously studied in 2D cultures [45], cells cultured on scaffolds or substrates [46, 47], here we have shown *in situ* cellular

alignment of osteoblast-like cells in a truly 3D culture system composed only of cells and ECM. Such alignment can potentially be used to mimic the anisotropic microstructure of bone [48] that influences its behavior resulting in anisotropic viscoelastic properties [49]. Similarly, alignment of neuronal cells along with electric field lines have been demonstrated previously in 2D culture systems or on scaffolds [50, 51] as well as in loosely packed hydrogel based constructs [52, 53]. However, our method demonstrates the ability to create highly dense and aligned neuronal tissue constructs without pre-fabricated scaffolds which can be used to form neural tube bundles for the use in regenerative medicine applications.

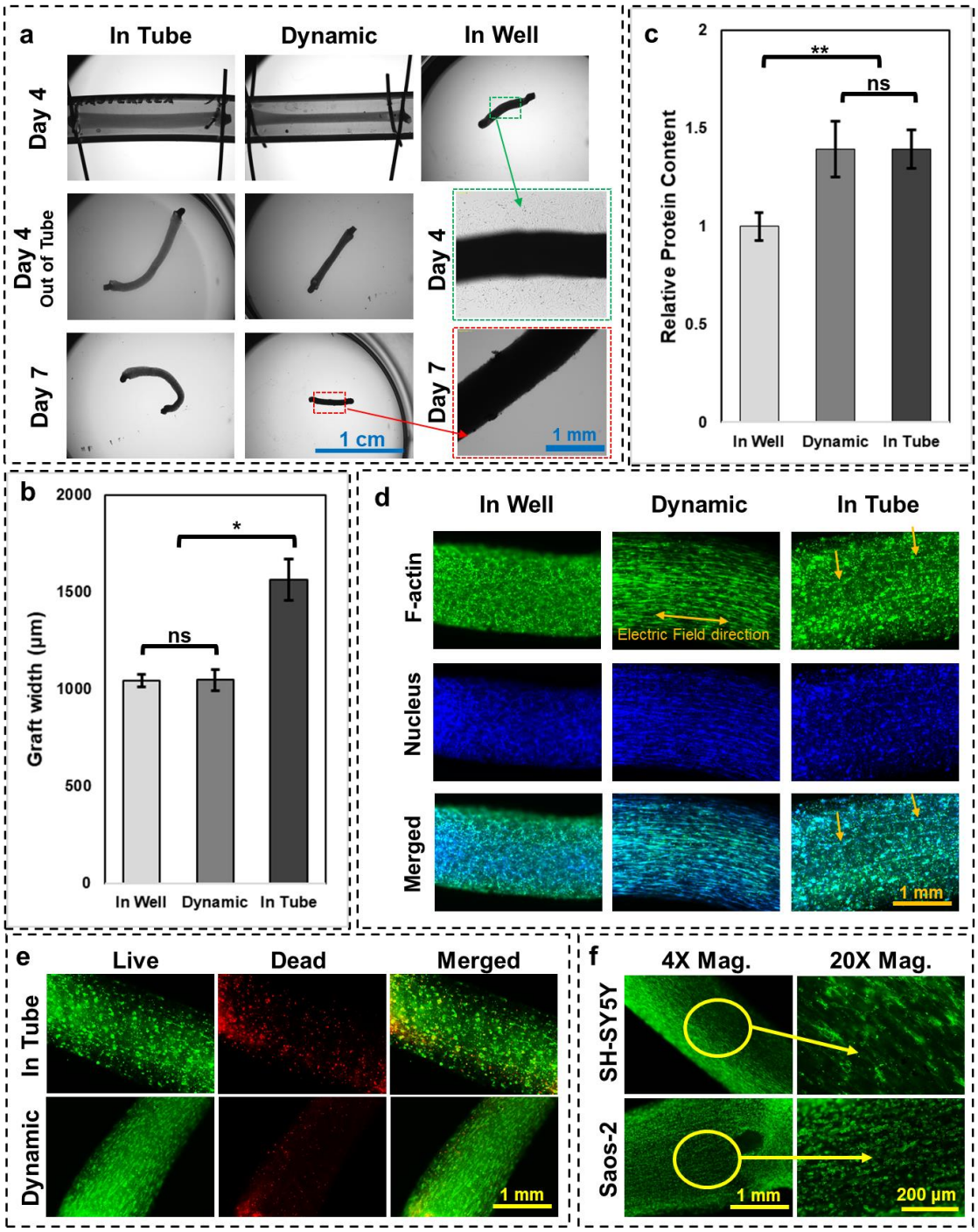

Figure 5. Effect of dynamic microenvironment on cellular constructs. **a)** Constructs were formed with undifferentiated myoblast C2C12s and differentiation was performed in three different conditions: "In Well" with no constrictions, "In Tube", constricted between anchor points, and in "Dynamic" condition anchored to the pins and facing electrical stimuli; **b)** Effect of culture condition on thickness of the constructs, * P-value<0.01 (n=4); **c)** Total protein content of differentiated C2C12s in three culture conditions, ** P-value<0.001 (n=4); **d)** Effect of culture condition on formation of multinucleated muscle fibers and their alignment. Electrical stimulation while greatly affected the cell alignment and fiber formation, didn't influence the protein content

of samples. Constructs kept shrinking over time outside the constriction of tubing and its anchors, cells didn't show fusion and some of the cells even escaped the fiber on to the culture plate. Samples exposed only to the anchor pins showed some fiber formation and didn't show much shrinkage and cell escape after retrieving from the tubing. Samples in "Dynamic" environment showed full fiber formation, had more shrinkage after retrieving from the tubing and no cell break out was observed. **e)** Live/dead stained images of "In Tube" and "Dynamic" samples at day 4 right after retrieving from the tubing. There are slightly more dead cells in the "In Tube" group. **f)** Effect of electric field on alignment of SH-SY5Y and Saos-2 cells.

In addition to electrical stimulation, additional biophysical stimulation can also be applied in this system. For instance, other types of stimuli including the perfusion of medium that generates shear force of the fluid flow on the cells on the outer layer of the tubular construct and the mechanical bending of the tubing that translates to the mechanical deformation of the constructs including stretching or compression can be performed. A wave-like mechanical deformation can be created through induction of in the tissue graft by controlling the flow rate of the medium as well as. Effect of this mechanical deformation on maturation of skeletal muscle cells was studied by forming the C2C12 constructs and creating the dynamic environment by applying mechanical stimulation by bending the tubing for 2 hr every day for 3 days. Mechanical deformation was started one day after grafts were formed and transferred to differentiation medium. More fibers were observed in those constructs exposed to mechanical deformation (Supplementary Figure 4) as compared to those without stimulation. However, fewer fibers were formed under this mechanical stimulation compared with electrical stimulation (Figure 5d), which could be because of the shorter (only 2 hr of mechanical stimulation was done every day) duration of stimulation compared with electrical one (applied continuously). Details of the mechanical deformation are included in the Supplementary information. Similar effect of mechanical deformation on cellular alignment and fiber formation of skeletal muscle cells and their maturation in 3D culture systems have been previously observed [43, 54] but independent of stimulation mode (chemical, mechanical, or

electrical) or ECM type, it has been shown that once such mature skeletal muscle cell constructs that show dense and highly organized fibers are formed, the constructs can be actuated and will exert forces that can be used for applications such as soft biorobotics and bioactuators [55-58].

This technique is also compatible with high throughput screening applications. For example a large number of constructs can be formed in the same tubing by inserting more than just two anchor pins or by connecting different construct containing tubing to each other in series. This could increase the nutrient consumption and by-product accumulation rate and adjustments to the flow rate of the medium or size of the tubing needs to be done to properly support cellular behavior. Alternatively, connections in parallel can be also used in case perfusion is not desired. This will isolate the metabolic impact of one tissue type on the other. A combination of series and parallel connections can be introduced to replicate the ratio of metabolic outputs of different tissue types in the body.

4. Conclusions

A new and simple biofabrication technique for rapid formation of collagenous, tubular, macroscale tissue constructs has been developed. The method allows for formation of complex tubular shapes and branching networks while providing the flexibility to control positioning of different cell types in predefined patterns, at high densities and with clear interfaces that can mimic *in vivo* like environments. The fabrication process is low cost, simple, and easy to adapt to create various tissue geometries and allosteric scaling. It can also be used to apply various biophysical stimuli such as mechanical deformation, fluid shear, and electric field separately or in conjunction to create a dynamic environment as well. We have demonstrated that a variety of cell types including endothelial, epithelial, skeletal muscle cells, bone cells, and neuronal cells are amenable to this method and multicellular structures can be created by radial or axial patterning. To demonstrate the efficacy of this method, aligned muscle, neural, and bone tissues were constructed.

Macrostructures (several centimeters in length) with complex patterns such as the columns with different thicknesses in different regions and bifurcated constructs which can be used as cellular constructs or *in vitro* models were rapidly constructed. By providing both the biochemical and the biophysical environment and the ability to direct complex paracrine interactions between different segments using fluid flow, these systems can serve as a versatile tool for biomedical researchers understanding disease mechanisms and discovering new drugs.

Acknowledgements:

The authors would like to acknowledge the support of the Natural Sciences and Engineering Research Council of Canada (NSERC) and the Canadian Institute for Health Research (CIHR). *In vitro* studies were performed at the Biointerfaces Institute at McMaster University. C2C12 cells were kindly provided by Dr. Sandeep Raha from Department of Pediatrics of McMaster university, Saos-2 cells from Dr Kathryne Grandfield from Department of Materials Engineering McMaster university, and SH-SY5Y cells from Dr Margaret Fahnestock from Department of Psychiatry and Behavioural Neurosciences McMaster university.

Data Availability: The data that support the findings of this study are available from the corresponding author upon reasonable request.

References:

1. Zhang, B., et al., *Advances in organ-on-a-chip engineering.* Nature Reviews Materials, 2018. **3**(8): p. 257-278.
2. Sung, J.H., *Chapter 10 - Pharmacokinetic-based multi-organ chip for recapitulating organ interactions*, in *Methods in Cell Biology*, J. Doh, D. Fletcher, and M. Piel, Editors. 2018, Academic Press. p. 183-197.
3. El-Ali, J., P.K. Sorger, and K.F. Jensen, *Cells on chips.* Nature, 2006. **442**(7101): p. 403-411.
4. Cui, X., Y. Hartanto, and H. Zhang, *Advances in multicellular spheroids formation.* J R Soc Interface, 2017. **14**(127).
5. Peng, W., D. Unutmaz, and I.T. Ozbolat, *Bioprinting towards Physiologically Relevant Tissue Models for Pharmaceutics.* Trends in Biotechnology, 2016. **34**(9): p. 722-732.
6. Katt, M.E., et al., *In Vitro Tumor Models: Advantages, Disadvantages, Variables, and Selecting the Right Platform.* Front Bioeng Biotechnol, 2016. **4**: p. 12.
7. Lin, R.Z. and H.Y. Chang, *Recent advances in three-dimensional multicellular spheroid culture for biomedical research.* Biotechnol J, 2008. **3**(9-10): p. 1172-84.
8. Haycock, J.W., *3D cell culture: a review of current approaches and techniques.* Methods Mol Biol, 2011. **695**: p. 1-15.
9. Benien, P. and A. Swami, *3D tumor models: history, advances and future perspectives.* Future Oncol, 2014. **10**(7): p. 1311-27.
10. Lin, R.Z., et al., *Dynamic analysis of hepatoma spheroid formation: roles of E-cadherin and beta1-integrin.* Cell Tissue Res, 2006. **324**(3): p. 411-22.
11. Soranzo, C., G. Della Torre, and A. Ingrosso, *Formation, growth and morphology of multicellular tumor spheroids from a human colon carcinoma cell line (LoVo).* Tumori, 1986. **72**(5): p. 459-67.
12. Fukuda, J., et al., *Micromolding of photocrosslinkable chitosan hydrogel for spheroid microarray and co-cultures.* Biomaterials, 2006. **27**(30): p. 5259-67.
13. Karp, J.M., et al., *Controlling size, shape and homogeneity of embryoid bodies using poly(ethylene glycol) microwells.* Lab Chip, 2007. **7**(6): p. 786-94.
14. Rijal, G. and W. Li, *3D scaffolds in breast cancer research.* Biomaterials, 2016. **81**: p. 135-156.
15. Rogers, A.J., et al., *Hemodynamic Stimulation Using the Biomimetic Cardiac Tissue Model (BCTM) Enhances Maturation of Human Induced Pluripotent Stem Cell-Derived Cardiomyocytes.* Cells Tissues Organs, 2018. **206**(1-2): p. 82-94.
16. Snyman, C., et al., *Simple silicone chamber system for in vitro three-dimensional skeletal muscle tissue formation.* Front Physiol, 2013. **4**: p. 349.
17. Agrawal, G., A. Aung, and S. Varghese, *Skeletal muscle-on-a-chip: an in vitro model to evaluate tissue formation and injury.* Lab Chip, 2017. **17**(20): p. 3447-3461.
18. Vandenburgh, H., et al., *Drug-screening platform based on the contractility of tissue-engineered muscle.* Muscle Nerve, 2008. **37**(4): p. 438-47.
19. Uzel, S.G., et al., *Microfluidic device for the formation of optically excitable, three-dimensional, compartmentalized motor units.* Sci Adv, 2016. **2**(8): p. e1501429.
20. Osaki, T., S.G.M. Uzel, and R.D. Kamm, *Microphysiological 3D model of amyotrophic lateral sclerosis (ALS) from human iPS-derived muscle cells and optogenetic motor neurons.* Sci Adv, 2018. **4**(10): p. eaat5847.
21. Nunes, S.S., et al., *Biowire: a platform for maturation of human pluripotent stem cell-derived cardiomyocytes.* Nat Methods, 2013. **10**(8): p. 781-7.
22. Xiao, Y., et al., *Microfabricated perfusable cardiac biowire: a platform that mimics native cardiac bundle.* Lab Chip, 2014. **14**(5): p. 869-82.
23. Wang, E.Y., et al., *Biowire Model of Interstitial and Focal Cardiac Fibrosis.* ACS Cent Sci, 2019. **5**(7): p. 1146-1158.

24. Miklas, J.W., et al., *Bioreactor for modulation of cardiac microtissue phenotype by combined static stretch and electrical stimulation.* Biofabrication, 2014. **6**(2): p. 024113.
25. Barash, Y., et al., *Electric field stimulation integrated into perfusion bioreactor for cardiac tissue engineering.* Tissue Eng Part C Methods, 2010. **16**(6): p. 1417-26.
26. Maidhof, R., et al., *Biomimetic perfusion and electrical stimulation applied in concert improved the assembly of engineered cardiac tissue.* J Tissue Eng Regen Med, 2012. **6**(10): p. e12-23.
27. Shahin-Shamsabadi, A. and P.R. Selvaganapathy, *A rapid biofabrication technique for self-assembled collagen-based multicellular and heterogeneous 3D tissue constructs.* Acta Biomater, 2019. **92**: p. 172-183.
28. Lind, J.U., et al., *Instrumented cardiac microphysiological devices via multimaterial three-dimensional printing.* Nat Mater, 2017. **16**(3): p. 303-308.
29. Alberts, B., et al., *Essential Cell Biology*. 2013: CRC Press.
30. Fang, Y. and R.M. Eglen, *Three-Dimensional Cell Cultures in Drug Discovery and Development.* SLAS Discov, 2017. **22**(5): p. 456-472.
31. Lee, J.M. and W.Y. Yeong, *Design and Printing Strategies in 3D Bioprinting of Cell-Hydrogels: A Review.* Adv Healthc Mater, 2016. **5**(22): p. 2856-2865.
32. Liu, W., et al., *Rapid Continuous Multimaterial Extrusion Bioprinting.* Adv Mater, 2017. **29**(3).
33. Holzl, K., et al., *Bioink properties before, during and after 3D bioprinting.* Biofabrication, 2016. **8**(3): p. 032002.
34. Goyanes, A., et al., *3D Printing of Medicines: Engineering Novel Oral Devices with Unique Design and Drug Release Characteristics.* Mol Pharm, 2015. **12**(11): p. 4077-84.
35. Trujillo-de Santiago, G., et al., *Chaotic printing: using chaos to fabricate densely packed micro- and nanostructures at high resolution and speed.* Materials Horizons, 2018. **5**(5): p. 813-822.
36. Sousa, A.R., et al., *One-Step Rapid Fabrication of Cell-Only Living Fibers.* Adv Mater, 2020. **32**(2): p. e1906305.
37. Wikswo, J.P., et al., *Scaling and systems biology for integrating multiple organs-on-a-chip.* Lab Chip, 2013. **13**(18): p. 3496-511.
38. Moraes, C., et al., *On being the right size: scaling effects in designing a human-on-a-chip.* Integr Biol (Camb), 2013. **5**(9): p. 1149-61.
39. Caddeo, S., M. Boffito, and S. Sartori, *Tissue Engineering Approaches in the Design of Healthy and Pathological In Vitro Tissue Models.* Front Bioeng Biotechnol, 2017. **5**: p. 40.
40. Wiesmann, H.P., et al., *Biophysical Stimulation of Cells and Tissues in Bioreactors*, in *Fundamentals of Tissue Engineering and Regenerative Medicine*, U. Meyer, et al., Editors. 2009, Springer Berlin Heidelberg: Berlin, Heidelberg. p. 633-646.
41. Hosseini, V., et al., *Engineered contractile skeletal muscle tissue on a microgrooved methacrylated gelatin substrate.* Tissue Eng Part A, 2012. **18**(23-24): p. 2453-65.
42. Takahashi, H., T. Shimizu, and T. Okano, *Engineered Human Contractile Myofiber Sheets as a Platform for Studies of Skeletal Muscle Physiology.* Sci Rep, 2018. **8**(1): p. 13932.
43. Kim, H., M.C. Kim, and H.H. Asada, *Extracellular matrix remodelling induced by alternating electrical and mechanical stimulations increases the contraction of engineered skeletal muscle tissues.* Sci Rep, 2019. **9**(1): p. 2732.
44. Nagamine, K., et al., *Contractile Skeletal Muscle Cells Cultured with a Conducting Soft Wire for Effective, Selective Stimulation.* Sci Rep, 2018. **8**(1): p. 2253.
45. Qi, Z., et al., *Combined treatment with electrical stimulation and insulin-like growth factor-1 promotes bone regeneration in vitro.* PLoS One, 2018. **13**(5): p. e0197006.
46. Portan, D.V., et al., *Combined Optimized Effect of a Highly Self-Organized Nanosubstrate and an Electric Field on Osteoblast Bone Cells Activity.* Biomed Res Int, 2019. **2019**: p. 7574635.
47. Matsugaki, A., et al., *Quantitative regulation of bone-mimetic, oriented collagen/apatite matrix structure depends on the degree of osteoblast alignment on oriented collagen substrates.* J Biomed Mater Res A, 2015. **103**(2): p. 489-99.
48. Burr, D.B. and M.R. Allen, *Basic and applied bone biology*. 2019: Academic Press.

49. Iyo, T., et al., *Anisotropic viscoelastic properties of cortical bone.* J Biomech, 2004. **37**(9): p. 1433-7.
50. Koppes, A.N., et al., *Neurite outgrowth on electrospun PLLA fibers is enhanced by exogenous electrical stimulation.* J Neural Eng, 2014. **11**(4): p. 046002.
51. Yan, L., et al., *Aligned Nanofibers from Polypyrrole/Graphene as Electrodes for Regeneration of Optic Nerve via Electrical Stimulation.* ACS Appl Mater Interfaces, 2016. **8**(11): p. 6834-40.
52. Wu, C., et al., *Cell-Laden Electroconductive Hydrogel Simulating Nerve Matrix To Deliver Electrical Cues and Promote Neurogenesis.* ACS Appl Mater Interfaces, 2019. **11**(25): p. 22152-22163.
53. Koppes, A.N., et al., *Robust neurite extension following exogenous electrical stimulation within single walled carbon nanotube-composite hydrogels.* Acta Biomater, 2016. **39**: p. 34-43.
54. Bansai, S., et al., *Effect of Cyclic Stretch on Tissue Maturation in Myoblast-Laden Hydrogel Fibers.* Micromachines (Basel), 2019. **10**(6).
55. Sakar, M.S., et al., *Formation and optogenetic control of engineered 3D skeletal muscle bioactuators.* Lab Chip, 2012. **12**(23): p. 4976-85.
56. Cvetkovic, C., et al., *Three-dimensionally printed biological machines powered by skeletal muscle.* Proc Natl Acad Sci U S A, 2014. **111**(28): p. 10125-30.
57. Morimoto, Y., H. Onoe, and S. Takeuchi, *Biohybrid robot with skeletal muscle tissue covered with a collagen structure for moving in air.* APL Bioeng, 2020. **4**(2): p. 026101.
58. Ikeda, K., et al., *In vitro drug testing based on contractile activity of C2C12 cells in an epigenetic drug model.* Scientific Reports, 2017. **7**(1): p. 44570.

Supplementary Information

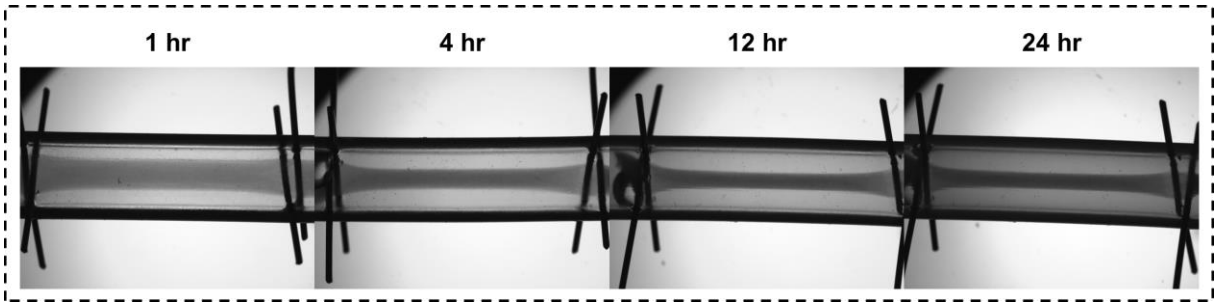

Supplementary Figure 1. Shrinkage pattern of the constructs over time for samples formed with MCF-7 cells with 2×10^6 cells/mL and 1:3 ratio. A dramatic decrease in size is observed in the first 6 hrs followed by a much lower shrinkage in the next 20 hrs.

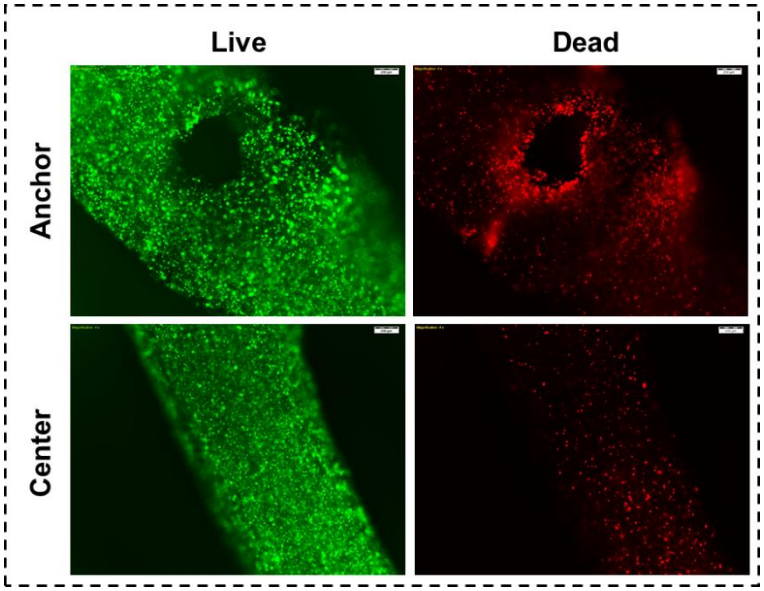

Supplementary Figure 2. Distribution of live and dead cells in the middle of the construct vs. close to anchor points. In the locations close to the pins number of dead cells was higher while in the other regions of the construct a uniform distribution of live cells with only low number of dead cells was observed. Staining and imaging were done 4 hrs after the fabrication process started.

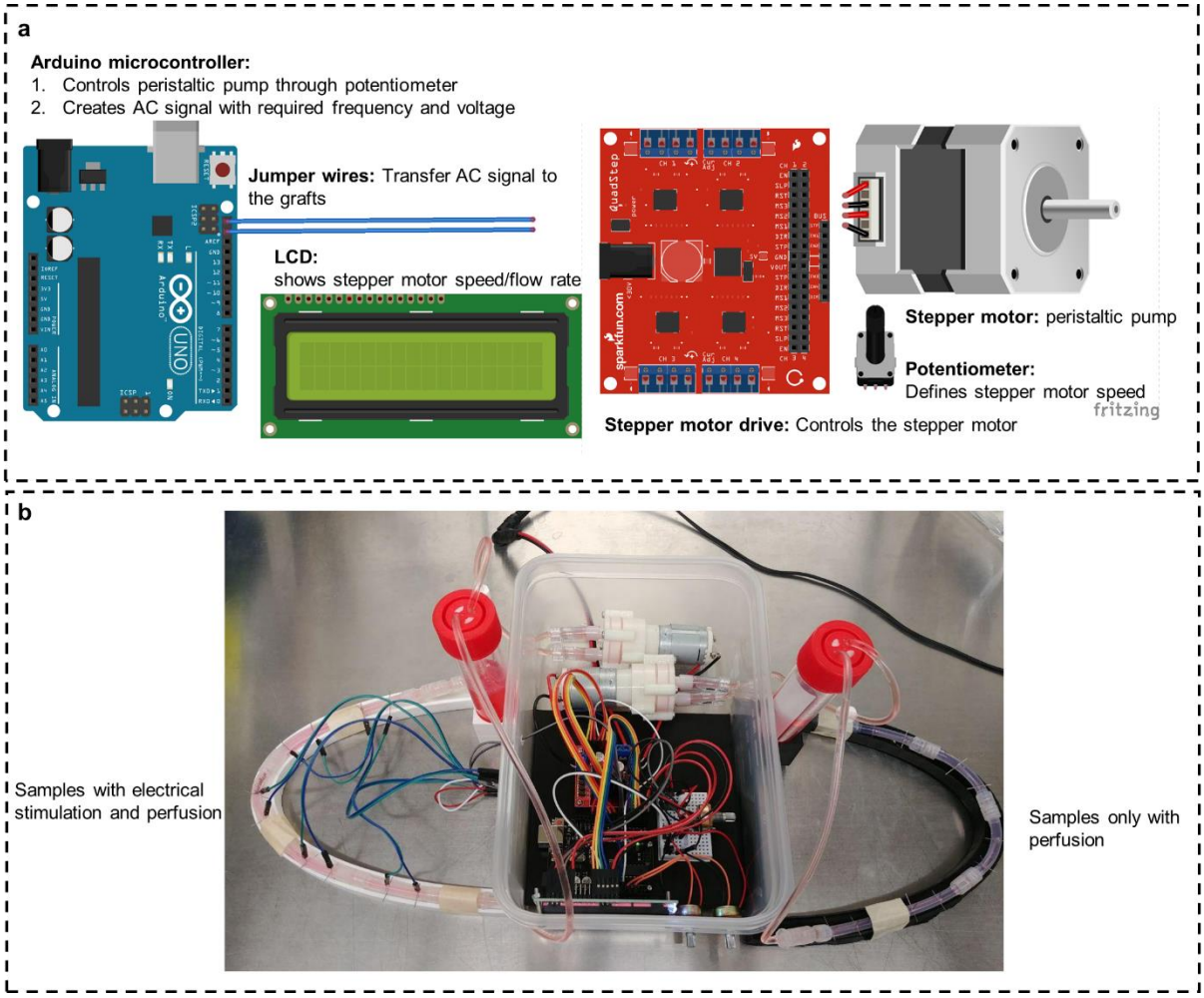

Supplementary Figure 3. a) Components of the bioreactor. Arduino microcontroller creates the AC step signal (50 Hz and -5 to +5 V). It also controls the flow rate through the speed of the motor that can be defined using the potentiometer and is shown on the LCD. **b)** Assembled bioreactor.

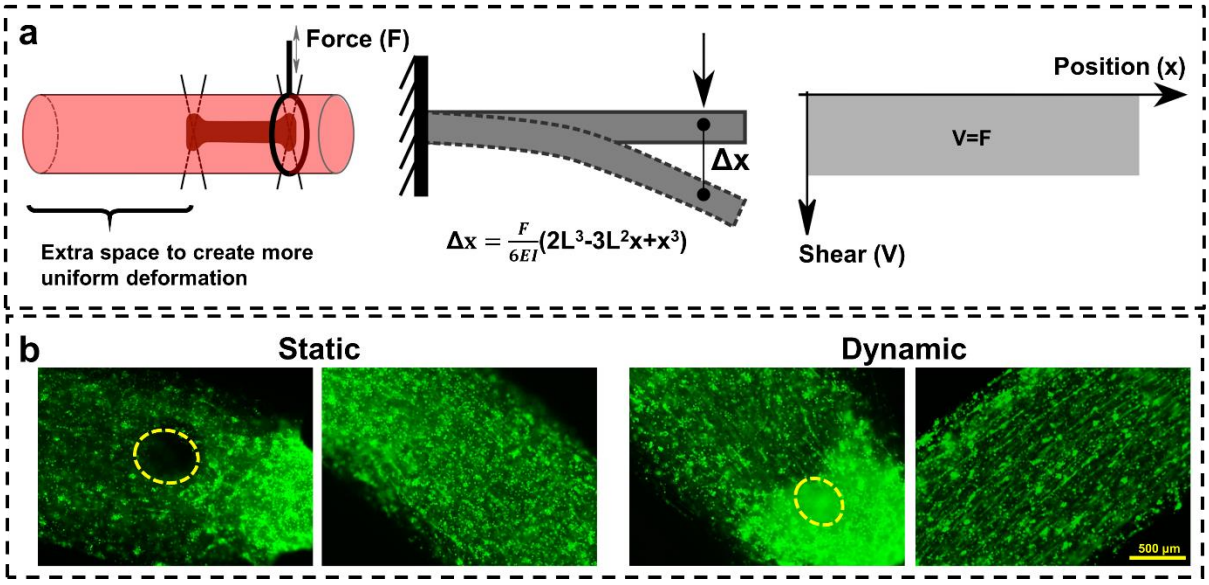

Supplementary Figure 4. a) Schematic of the mechanical deformation imposed to C2C12 grafts to create a dynamic microenvironment, **b)** effect of mechanical deformation on fiber formation of skeletal muscle grafts in dynamic environment as compared to static condition. The tubing and graft inside it can be treated as a beam that is fixed on one side and is deflected using a concentrated force on the other end. There is a uniform shear force applied to all cross-sections of the sample across the length of the graft and while there is a cubic relation between deformation and position. In order to create more uniform deformation in the graft, a 3 cm extra space between the left fixed side of the tubing and the graft was allowed. Formation of fibers was observed both in the middle for the sample as well as at the endpoint where connection to the pins. Stimulation was started one day after grafts were formed and a dynamic environment was created by deforming the tubing with amplitude of 2 cm and frequency of 0.5 Hz for 2 hr every day for three days.

Supplementary Box 1. Code used for programming the microcontroller that controls the bioreactor.

```
//define pins for the peristaltic pumps
int EnA=10; //yellow wire
int in1=9; //orange wire
int in2=8; //red wire
int EnB=11;
int in4=12;
int in3=13;
//output voltage for 1st pump
int potValue1=0;
long pwmOutput1=0;
int VoltOutput1=0;
int potValue2=0;
long pwmOutput2=0;
int VoltOutput2=0;


//using potentiometers to define speed of peristaltic pumps
int pot1=A1;
int pot2=A2;

// a step wave between pins 6 and 7 (-5 to +5V) with a frequency of 50Hz
int PinP = 6; //
int PinN = 7; //
int counter=0;


void setup() {
 //controling 1st pump
 pinMode(EnA, OUTPUT);
 pinMode(in1, OUTPUT);
 pinMode(in2, OUTPUT);
 //controling 2nd pump
 pinMode(EnB, OUTPUT);
 pinMode(in3, OUTPUT);
 pinMode(in4, OUTPUT);

 pinMode(pot1, INPUT);
 pinMode(pot2, INPUT);

 //defining outputs for the Sin wave
 pinMode(PinP1, OUTPUT);
 pinMode(PinN1, OUTPUT);
 pinMode(PinP2, OUTPUT);
 pinMode(PinN2, OUTPUT);
}

void loop() {
 //reading the potentiometer and defining the speed of 1st peristaltic pump
 potValue1 = analogRead(pot1); // Read potentiometer value
 pwmOutput1 = map(potValue1, 0, 1023, 0 , 255); // Map the potentiometer value from 0 to 255
 analogWrite(EnA, pwmOutput1); // Send PWM signal to L298N Enable pin
 digitalWrite(in1, LOW);
 digitalWrite(in2, HIGH);
```

```
 potValue2 = analogRead(pot2); // Read potentiometer value
 pwmOutput2 = map(potValue2, 0, 1023, 0 , 255); // Map the potentiometer value from 0 to 255
 analogWrite(EnB, pwmOutput2); // Send PWM signal to L298N Enable pin
 digitalWrite(in3, LOW);
 digitalWrite(in4, HIGH);

 //creating AC signal
 switcher();
}

void switcher(){
 counter=counter+1;
 if (counter%2==0){
 digitalWrite(PinP, HIGH);
 digitalWrite(PinN,LOW);
 delay (20);
 }else{
 digitalWrite(PinN, HIGH);
 digitalWrite(PinP,LOW);
 delay (20);
 }
}
```

Chapter 4: CONCLUSIONS AND FUTURE DIRECTIONS

1. Conclusions

This doctoral thesis was inspired by the need for biofabrication-based techniques that could be used to create more anatomically- and physiologically-relevant 3D dynamic *in vitro* models of different tissues to improve our understanding of biological phenomena compared to what is achievable by using classical approaches. Since different tissues have different structural and biological requirements, there is no one-size-fits-all technique that meets all of them and therefore after extensive investigation, three unique techniques were developed and comprehensively characterized to be used for such different requirements. These techniques were then used to recreate certain features of microphysiological environments of a few select tissues. Comparison of these techniques with previously available tools showed promises in creating more robust and faithful models which was further confirmed by comparing the biological behaviors that were modeled with previous studies in their similarities to *in vivo* conditions. It was proven possible to either model certain phenomena in better ways or model certain cellular behaviors for the first time. It was finally concluded that initial objectives were supported by the results that were provided.

The primary intention was to provide biologists with the tools that they needed to recreate *in vitro* models and integrate the elements of *in vivo* conditions that had been shown to be intrinsic in defining cellular behavior and function but had been overlooked in the previous studies. These included being easy to implement and having fast processes that were compatible with different cell types resulting in models with high cell densities and clear tissue interfaces, as well as high cell viabilities in any shape and morphology. The models were prepared in ways that were highly reproducible, suitable for high throughput screening applications, and allowed easy and direct access to cells for biological evaluations.

This was first partially achieved with development of a novel bioprinting technique that printed cell embedded hydrogels on paper as a scaffolding material followed by stacking these impregnated layers. The printing had acceptable resolution (features < 1 mm were printed) for *in vitro* modeling applications, the extrusion bioprinting that was chosen as the delivery method allowed high cell densities to be used with a combination of different hydrogels, paper as scaffolding material created mechanically stable structures in much larger sizes with proper perfusion channels created using xurography and cutting patterns on the paper. Eventually these layers were delaminated, and biological assays were performed on each layer separately. This technique has improved upon many of the shortcomings of other bioprinting techniques including added possibility of direct access to cells in different locations of the model, having higher mechanical stability and the ability to create much thicker constructs by implementing paper as supporting scaffolding material, and the ability to create blood vessel like constructs and perfusion of these channels through the use of xurography cut papers. Some of the strengths of this technique over other 3D culture systems were highlighted where for the first time an *in vitro* model was developed to decipher the relationship between mechanical properties of the environment of bone tissue and the hypothesized trans-differentiation of osteoblasts to osteocytes during the bone formation. To the best of our knowledge this is the first time that a truly 3D *in vitro* model has been developed for this biological phenomenon. Similar models can be developed for other biological phenomena that require control over mechanical properties of the environment, while integrity of the delicate thin hydrogel layers need to be preserved.

The bioprinting technique while suitable for many applications similar to what was show-cased, may not be appropriate for certain other applications, for example where smaller size models could be used to shift time and energy from vascularization and perfusion of large bioprinted constructs

to forming constructs with much higher cell densities. Other reasons that bioprinting might not be suitable for certain applications importance of using certain ECM materials that are not compatible with bioprinting but are necessary for inducing proper cell function, and the difficulties of implementing a variety of stimuli in the bioprinted models to create dynamic environments that better recreate the requirements of certain tissue types. These motivated the development of a second technique based on bioassembly of cells and collagen as ECM in PDMS molds resulting in formation of structures with precise control over positioning of cells in predefined patterns that had higher resolution (as high as 100 μm) and tissue relevant densities (more than a few tens of million cells/mL). This technique was further improved by adding the ability to implement different stimuli simultaneously in an improved version compared to the first idea. Compared to similar techniques, this method has much higher ability to control microstructure of the models including precise control over cell density and ECM content, it is much faster and can form constructs in a few hours rather than a few days which results in much higher cell viabilities, and the constructs with complicated forms can maintain their predefined shape and cell positioning independent of their molds which could be important for certain applications. Application of this technique in modeling the cross-talk between skeletal muscle cells and adipocytes showed the importance of physical contact and presence of cell-cell junctions on cell behavior that was previously ignored in many other studies. An improved version of this technique made it possible to simultaneous implementation of different dynamic features including perfusion, electrical and mechanical stimulation in the *in vitro* models that wasn't feasible before. The improved version of this technique has still superior to similar techniques in its ability to position cells with high resolution and its faster process results in much higher cell viabilities.

In conclusion, our techniques empower biologists with new and sophisticated tools to develop i*n vitro* models and include a variety of different feature of *in vivo* tissues that are known to be imperative for a model to faithfully represent those target tissues. Such accurate replications weren't previously possible to be performed to increase the complexity of the models while maintaining their practicality and interpretability. Besides from *in vitro* modeling, with certain modifications, these techniques can be adapted for creating functional tissues and organs for regenerative medicine purposes. This will further create the opportunity to understand the requirements of different tissues in more depth that can be beneficial for both *in vitro* modeling and *in vivo* implantation purposes.

2. Future directions

Despite the achievements of the current thesis and contributions that are made to the field, there exists a question that is yet to be fully understood and answered. What characteristics of a tissue, organ, or a pathological condition need to be recreated in *in vitro* models to obtain a full picture of that process, eliminate the need to use animal models, and decrease the chances of drug failure in clinical trials to zero? This question can only be answered by adding more *in vivo* like features to our *in vitro* models in order to understand if these additions make meaningful impacts. This requires powerful tools capable of recreating different features of the human tissues and the ability to interpret the responses observed from such constructs. The tools provided in the current study are much better fitted as compared to previously developed methods for this purpose but they need to be used for modeling different tissues and organs in order to shed light on whether there are certain features that they cannot recreate. So, the first and foremost future consideration should be using these techniques for such applications to understand their shortcomings. Then efforts should be made to address them by either improving these techniques or creating newer ones. Besides

from such possible refinements, there are certain improvements that can be considered for each of these techniques.

The ExCeL technique can be further improved by considering the following elements:

1. The resolution of the printing can be improved to reach the tissue- and organ- level requirements (down to < 20 μm).
2. It can be improved to be compatible with different hydrogels.
3. The paper scaffold can be replaced with a transparent membrane to allow better microscopy. Alternatively, a custom multimaterial scaffold can be used with different cells or ECMs printed on each material type.
4. Xurography can be replaced with other techniques with higher cutting resolutions, such as laser cutting, to make smaller channels.
5. The bioprinter setup can be replaced with an automated all-in-one system capable of printing multiple bioinks and stacking impregnated layers in a faster and more accurate way.

The micro-molding technique and its improved version, tissue-in-a-tube, can be further improved by considering the following elements:

1. Collagen can be replaced with other hydrogels capable of showing the same self-assembly property that are better suited to certain cellular behaviors and even synthetic hydrogels with more control over their chemical structure. The choice of ECM should be based in similarities with *in vivo* conditions.
2. The possibility of innervation and formation of blood vessel networks should be considered in these modules in order to create larger tissue-like constructs that possess more

biologically-relevant features such that these models can be used with more confidence as replacements for animal models.

3. Sensors and imaging systems can be added to tissue-in-a-tube setup to better evaluate cellular behavior.
4. The pipetting and bioink transfer can be performed using an automated setup to increase repeatability and decrease bioink waste.
5. Resolution can be further improved, especially in the case of tissue-in-the-tube technique.
6. In the tissue-in-the-tube, proper conditions for connecting different tissue types and creating more sophisticated models needs to be established.

Although the main objective of the current thesis was to develop techniques solely for modeling purposes, their capabilities often outreaches the requirements of *in vitro* modeling, for example the resolution of cell patterning and creation of clear tissue interfaces in the micro-molding technique. Therefore, these techniques can be used for organ-fabrication and regenerative medicine as well with certain considerations:

1. Replacing paper with a biodegradable and biocompatible scaffold in the ExCeL technique and using proper cell sources such as induced pluripotent stem cells.
2. In the micro-molding technique, defining proper assembly techniques and conditions so that different shape modules that are fabricated can be used as building blocks for organ fabrication.
3. Replacing bovine collagen with synthetic or natural hydrogels that do not cause unwanted immune responses while are capable of showing the same self-assembly behavior.
4. Increasing the fabrication resolution, especially in the case of bioprinting technique, to meet the requirements of different organs.

5. Implement proper bioreactors to pre-condition cells for their proper function once implantation is performed.

Overall, this thesis initiated a few new lines of projects in our group and there is no limit to how advanced these techniques can become or what applications they can be used for.

Appendix 1: CELL SHEET ENGINEERING TECHNIQUE

π-SACS: pH Induced Self-Assembled Cell Sheets Without the Need for Modified Surfaces

Alireza Shahin-Shamsabadi[1], P. Ravi Selvaganapathy [1,2,*]

[1] School of Biomedical Engineering, McMaster University, Canada

[2] Department of Mechanical Engineering, McMaster University, Canada

[*] Corresponding Author: P. Ravi Selvaganapathy, Department of Mechanical Engineering, McMaster University, Canada

Status: Under Review

Abstract

The ability to form tissue-like constructs that have high cell density with proper cell-cell contacts in addition to cell-ECM interactions is critical for many applications including tissue models for drug discovery and tissue regeneration. Newly emerging bioprinting methods sometimes lack high cellular density needed to provide biophysical cues to orchestrate cellular behavior to recreate tissue architecture and function. Alternate methods using self-assembly can be used to create tissue like constructs with high cellular density and well-defined microstructure in the form of spheroids, organoids, or cell sheets. Cell sheets have a particularly interesting architecture in the context of tissue regeneration and repair as they can be applied as patches to integrate with surrounding tissues. Till now, the preparation of these sheets has involved culturing on specialized substrates that can be triggered by temperature or phase change (hydrophobic to hydrophilic) to release cells growing on them and form sheets. Here a new technique is proposed that allows delamination of cells and secreted ECM and rapid self-assembly into a cell sheet using a simple pH trigger and without the need to use responsive surfaces or applying external stimuli such as electrical and magnetic fields, only with routine tissue culture plates. This technique can be used with cells that are capable of syncytialization and fusion such as skeletal muscle cells and placenta cells. Using C2C12 myoblast cells we show that the pH trigger induces a rapid delamination of the cells as a continuous layer that self-assembles into a thick dense sheet. The delamination process has little effect on cell viability and maturation and preserves the ECM components that allow sheets to adhere to each other within a short incubation time enabling formation of thicker constructs when multiple sheets are stacked (double- and quadruple-layer constructs are formed here as supposed to single-layer constructs). These thick grafts can be used for regeneration purposes or as *in vitro* models.

Keywords: Cell Sheet Engineering, Syncytialization, Tissue regeneration, *In vitro* modeling, 3D culture

1. Introduction

Regenerative medicine holds the promise to repair damaged and diseased organs or tissues through the implantation of externally cultivated tissue like constructs. Direct injection of bioinks consisting of stem cells have been widely investigated due to their ease of use but have not shown efficacy. An alternative is to incorporate the cells in a synthetic or biodegradable scaffold to prevent cell loss and facilitate better integration with existing tissue. A more recent approach has been to form sheets of cells using self-assembly approaches that dispense away the need for synthetic scaffolds by preserving extracellular matrix (ECM) secreted by cells to form tissue constructs that are ideally suited for integration with host tissue or organ [1]. This cell sheet engineering approach allows non-invasive and non-enzymatic harvest of cells, their deposited ECM, and cell-cell and cell-ECM junctions as a continuous layer [2]. If transplanted *in vivo*, cells within these sheets will be regulated according to host environment to secrete appropriate growth factors and cytokines. It could also be used as means for protein delivery to the body [1].

Cell sheet engineering was first introduced in 1990s using cell culture dishes that were grafted with N-isopropylacrylamide (PIPAAm) which enabled detachment of cells and their secreted proteins without enzymatic treatment in an intact format just by decreasing the temperature and changing the hydrophilicity of the grafted polymer [2]. The cells in these constructs show higher viability as the secreted proteins, such as E-cadherin and Laminin 5 [3] are preserved and the continuous sheets have adhesive properties such that they can be stacked on top of each other or other tissues without using glue or suture [4]. Alternatively, special surfaces created by layer-by-layer deposition of cationic and anionic polyelectrolytes on indium tin oxide have also been used to trigger delamination of cell sheets as these layers become unstable at low pH [5]. In this technique pH of the medium needs to be around 4 for cell detachment process to start (detachment

starts after 2-3 min) which may affect cell viability. Other techniques for formation of continuous cell sheets include growing cells on a feeder layer and detaching the cell sheet using dispase that digests some of the ECM proteins and not cell-cell junctions, growing cells on amniotic membrane as a carrier and then using them with this membrane, or initiating the delamination through application of external stimuli such as light, electrochemical polarization, ionic solution, and magnetic force [6]. Delamination process for some of these techniques can be very long, for example in case of PIPAAm-grafted surfaces a 40-80 min incubation time at 20°C might be necessary [7] which could have adverse effect on cell viability. These methods involve either specialized surfaces for culture, use of enzyme digestion, sacrificial materials or carriers which makes them complex and expensive processes. In addition, current techniques require customized equipment to maintain the delaminated sheets flat as they spontaneously agglomerate into a crumpled 3D rounded shapes due to traction forces [8-10].

Here, we develop a simple technique that allows formation of cell sheets composed of cells capable of syncytialization without the need for any modified surfaces or enzyme treatments. In this method, cells are cultured on normal tissue culture polystyrene surfaces and upon confluence and fusion, a stepwise treatment with slightly acidic medium followed by slightly basic medium is performed that triggers the delamination of the cell sheet from the culture surface and enables it to remain as free standing flat sheet. Different assays are performed to show cytotoxic effects on cells are minimal during the process. The sheets formed using this technique are robust, can be transferred from one plate or well to another using standard pipettes or tweezers and will immediately unfurl and flatten after transfer. These sheets can also be simply stacked on each other to form multilayer composites by placing them on each other and sliding into position. After

stacking, the cells in the sheets form cohesive linkages with each other and form mechanically robust constructs.

2. Materials and Methods

2.1. Cell Sheet Formation Process

C2C12 cells were cultured in their growth medium (GM), DMEM (high glucose, with glutamine, Gibco) supplemented with 10% heat inactivated fetal bovine serum (FBS) (US origin, Gibco) and 1% penicillin-streptomycin (10K U/mL, Gibco), in 10 cm dishes until 90% confluent. At this stage (D-3, three days before process of sheet starts) cells were subcultured to new 10 cm dishes in their GM with an initial 40-50% confluency. Next day (D-2) medium was switched to C2C12's differentiation medium (DM), DMEM supplemented with 2% horse serum (US origin, Gibco), 1% penicillin-streptomycin, and 1% Insulin-Transferrin-Selenium (100X, ThermoFisher). Cells were in this medium for 2 days and then were trypsinized and used to start forming the self-assembled cell sheets (D0). For this purpose, 0.235×10^6 cells were plated in 24 well plates with 0.5 mL of DM. Medium was refreshed next day (D1) and the day after that (D2) delamination process was performed (Figure 1A).

In order to start the delamination process DM was replaced with acidic medium (medium A) (DM with 0.1% V/V acetic acid, final pH of ~6) and samples were incubated for 5-10 min at 37°C. At this point that sheets started to delaminate the process was accelerated by gentle shaking of the well plate. Process could be accelerated by applying shear force using gentle pipetting of medium to the edges of the wells. Immediately after delamination was completed, medium A was replaced with basic medium (medium B, final pH of ~8, DM with 0.1% V/V 0.1 M sodium hydroxide in

deionized water) in order to prevent samples from forming clumps. After 5 min of treatment with medium B, samples were transferred to neutral medium (medium N, pH of 7.4, DM without any pH adjustment). In case of stacks required number of sheets, either 2 (double-layer constructs) or 4 layers (quadruple-layer constructs), were stacked on top of each other by simply dragging them using a tweezer and placing them on each other. This process was also performed in abundant amounts of medium B and after stacking was done, most of the media was aspirated to let the sheets settle down because of their weight for 5 more minutes and then medium N was added (Figure 1B). Images of sheets were taken 1 hr after delamination/stacking and 24 hrs later using a stereomicroscope (Infinity Optical Systems). Diameter of the sheets was measured using ImageJ at these time points to study effect of number of layers on shrinkage pattern of the constructs.

2.2. Cell Sheet Microstructure

Nile red and DAPI (4′,6-diamidino-2-phenylindole), live/dead, histological, and immunofluorescence staining was used to study microstructure of the sheets and their cell distribution. At D2 and without delamination cells were fixed in 2% paraformaldehyde solution for 1 hr and staining was performed by Nile red (Thermofisher) and DAPI in PBS. One hour after delamination and stacking, single sheets or their stacks were fixed and the same staining was performed as well. Stock solutions were prepared by dissolving 25 mg Nile red in 1 mL acetone and 10 mg of DAPI in 1 mL PBS. For staining, 10 μL of Nile red and 5 μL of DAPI were dispersed in PBS. One hour after delamination live/dead staining was performed on sheets using the kit (ThermoFisher) by diluting calcein-AM and ethidium homodimer-1 in DM and incubating the sheets for 30 min with this solution. For histological staining samples were fixed, stepwise dehydration and wax embedding was performed followed by sectioning and staining with hematoxylin and eosin (H&E). Immunofluorescence staining was performed for samples grown

in GM and DM before delamination at D2 as well as sheets right after delamination for desmin. After fixing, permeabilization was done using 0.2% Triton X-100 in 1% bovine serum albumin (BSA, SigmaAldrich) in PBS for 15 min followed by blocking in 5% BSA for 30 min at room temperature. Treatment with anti-Desmin primary antibody (Abcam, ab8976) was performed with a 1:500 dilution of the stock solution for 24 hrs at 4°C followed by 2 hr treatment with 1:1000 dilution of goat anti-mouse secondary antibody (Abcam, Alexa Fluor® 488, ab150113). Images of the samples were taken using an inverted fluorescent microscope (Olympus) using proper filters.

2.3. Assessment of Cell Behavior in Sheets

Cellular behavior for undifferentiated and differentiated cells in monolayer format (cells grown in GM and cells undergone the devised protocol) one day before delamination (D1), and cell sheet constructs (single-, double-, and quadruple-layer) one day after delamination (D3) was assessed using Alamar blue assay (ABA) for metabolic activity, CyQUANT™ LDH assay to measure cytotoxicity of the process, Pierce™ BCA Protein assay for total protein content, and a 1-Step qRT-PCR (quantitative reverse transcription polymerase chain reaction) to evaluate differentiation of the cells, all using Thermofisher kits.

Cytotoxicity of the process was evaluated by measuring the lactate dehydrogenase (LDH) levels in the conditioned medium. Fresh medium (500 µL) was added to samples the day before LDH assay was performed. Working solution of the assay was prepared according to the instructions on the day of experiment and 50 µL of it was added to a 50 µL sample of the conditioned medium. After 30 min incubation at room temperature, 50 µL of stop solution was added and reading was done immediately using a plate-reader (Tecan Infinite M200 Pro) in absorbance mode at wavelength of 490 nm with absorbance at 680 nm as reference. Four samples in duplicates were used. For ABA, constructs' medium was replaced with 400 µL of proper medium (GM for

undifferentiated cells and DM for differentiated cells and sheets) containing 10% Alamar blue solution followed by 90 min incubation in dark at 37°C. Two 100 μL aliquots for each sample were read using the plate-reader at excitation/emission of 560/590 nm. Alamar blue containing media of each case was used as control (n=4 with duplicate reading). Samples were then lysed in 500 μL of lysis solution (0.5% Triton X-100 in PBS) and BCA was performed according to the instructions in duplicates with lysis solution as control. In case of LDH and BCA calibration curve of the kit was prepared to confirm the readings from samples were in the linear range of the kit. For all of these assays data were normalized to that of cells grown in GM. ABA and LDH assays were performed on single- and quadruple-layer samples 2 days after delamination (D4) as well to study long-term effects of delamination and stacking on cell viability.

qRT-PCR was performed on C2C12 cells in differentiation process the day before delamination (D1) and were compared to cells plated at the same day as these cells but in GM (control group). Myogen, MyoD, and β-Actin were chosen as markers and GAPDH was used as house-keeping gene (Supplementary Table 1). Samples were lysed using lysis solution of the kit and one-step qRT-PCR kit (Cells-to-CT™ 1-Step Power SYBR™ Green, ThermoFisher) was performed following the instructions. The ΔΔCt values for each primer set were calibrated to Ct values of the housekeeping gene and then to the Ct values of control group (n=4 with duplicate readings).

Difference in cytoskeleton reorganization of differentiated cells vs. undifferentiated ones was studied by treating cells with Latrunculin-B (Lat-B) (Abcam, ab144291). C2C12 cells grown in GM and the partially differentiated ones in DM were treated with 100 nM Lat-B in GM and DM, respectively, for 1 hr at D1 and microscopy was performed using inverted microscope in brightfield mode. Effect of cytoskeleton reorganization on detachment of the sheets was also

studied by treating the cells with 50 and 100 nM of Lat-B in DM during the 24 hrs before delamination. Lat-B stock solution was prepared by dissolving 100 μg in 1 mL DMSO.

2.4. Sheets with Multiple Cells in Co-culture

Heterogenous sheets were formed using co-culture of partially differentiated C2C12 cells and cells from different cell lines including red fluorescent protein tagged human umbilical vein endothelial (HUVEC), green fluorescent protein tagged NIH/3T3 fibroblasts, SH-SY5Y neuroblastoma cells, or 3T3-L1 preadipocytes. These cells were grown in their own media up to 90% confluent (EBM-2 Endothelial Cell Growth Basal Medium for HUVEC, High glucose DMEM supplemented with 10% FBS and 1% pen-strep for NIH/3T3, DMEM/F-12 supplemented with 10% heat-inactivated FBS and 1% pen-strep for SH-SY5Y, and low glucose DMEM supplemented with 10% FBS and 1% pen-strep for 3T3-L1). SH-SY5Ys were stained with DiO fluorescent cell tracker (Thermofisher) for imaging purposes. Partial differentiation of C2C12 was performed the same as before and at the D0, all of the cells were trypsinized and a 5:1 ratio of C2C12 to either HUVEC, NIH/3T3, or SH-SY5Y cells or 1:3 ratio of C2C12s to 3T3-L1s were used to start the coculture. At D2 imaging was done using brightfield and fluorescent modes of the inverted microscope.

2.5. Cell Sheets formed with Alternative Fusing Cells

Similar sheet formation and delamination process was performed for placenta choriocarcinoma BeWo cells. Cells were cultured in Ham's F-12K medium containing 10% FBS and 1% pen-strep to 80% confluent. Cells were trypsinized and plated at 0.2×10^6 cells per well in 24 well plates. One day later medium was switched to cells' fusion medium (DMEM/F12 containing 10% FBS, 1% penicillin-streptomycin, and 20 μM forskolin (Abcam, ab120058)). Forskolin's stock solution was prepared by dissolving 10 mg in 1.22 mL DMSO. Cells were kept in the fusion medium for 3 more

days with refreshing every other day. At day 4, cells were treated with medium A and B the same as before and images of delaminated layers were taken using the stereomicroscope and inverted microscopes.

2.6. Statistical Analysis

Data are reported as Mean ± Standard Deviation (SD) and statistical analysis was performed using student's t-test with an accepted statistical significance (p-value) less than 0.05.

3. Results and Discussion

3.1. Cell Sheet Formation Process

A new technique that uses a simple pH trigger to rapidly forms cell sheets using traditional cell culture plates has been developed (Figure 1A). For this purpose, C2C12 myoblast cells that can differentiate into multinucleated myotubes were used with a defined differentiation protocol. In this protocol, culture initially started in growth medium (GM) at 40-50% confluency (D-3). Medium was changed to differentiation medium (DM) the next day (D-2) and the cells were kept in this medium for two days to prime them towards their final mature and differentiated stage. At this stage (D0) that cells were almost confluent and ready to fuse to each other, they were trypsinized and replated at 0.235×10^6 cells per well in 24 well plates in DM. In this condition the cells were about 90% confluent and slowly proliferated and fused to each other at the same time. Due to high cell number and metabolic activity of cells, medium was refreshed the next day (D1, one day before delamination) in order to sustain their metabolic needs and prevent medium to become acidic. At this point the cells fused to form a continuous sheet that applied traction force evident from delamination and curling at the edges of the wells (Supplementary Figure 1a). This traction could lead to formation of ill-defined agglomerated structures (Supplementary Figure 1b)

in case no intervention was done to delaminate the sheets in a controlled manner. Treating cells with a slightly acidic medium (medium A) at D2 (2 days after replating and 5 day starting the whole process) accelerated the delamination and allowed the cells to rapidly delaminate as a continuous layer. After delamination, if the sheets were kept in the same acidic medium, they would fold upon themselves and form undefined 3D constructs (Supplementary Figure 1c). In order to prevent this, medium A was switched to a slightly basic medium (medium B) which arrested the traction force in the cell sheets and kept them flat. Eventually sheets were transferred to a neutral medium (medium N) as single-layers or double/quadruple-layer constructs (Figure 1B). Images of these sheets were taken after 1 and 24 hrs (Figure 2A) and their diameter was measured using ImageJ to study effect of stacking layers on their shrinkage patterns (Figure 2B). Single and multiple-layer constructs shrank but the extent of shrinkage was higher when number of layers was lower (single-layer constructs showed 91.94±1.11% shrinkage while quadruple constructs showed 87.06±0.81% shrinkage). Once cells are detached, contractile forces applied by their cytoskeleton was not compensated by the adhesion force from the surface and as a result shrinkage occurs [11, 12]. The lateral shrinkage of the sheet also thickened it and formed a dense 3D-like construct. However, when multiple such layers were stacked on each other immediately upon delamination, the cells formed interlayer attachments that acted as anchorage sites transmitting and compensating the traction forces within each of the layers and as a result, less shrinkage was observed. If this agglomeration was allowed to continue, it could lead to formation of 3D spheroid-like crumpled structures [13]. During this process significant degradation of the sheets was also observed (Supplementary Figure 1c). It was also more likely for single-layer constructs to fold on themselves due to the high traction force toward the center of the sheet as they lacked the anchorage sites and were less stable compared to double- or quadruple-layer

constructs (Supplementary Figure 2). Sheets were also formed in wells of a 12 well plate to show the ability of the technique in making larger sheets using 0.48×10^6 cells per well and their shrinkage over time was compared to sheets formed in 24 wells (Supplementary Figure 3). It is also possible to form sheets using 10 cm dishes and 1.15×10^6 cells (data not shown). Suitable pH of media A and B as well as proper timing for the treatment were optimized to be as close as possible to neutral culture and physiological conditions and as short as possible to have the least adverse effect on cell viability. Treating samples with these media for shorter times wouldn't cause the intended effect, while treating them for longer times would lower the cell viability dramatically. For instance, lowering the pH of medium A below 5 and increasing pH of medium B above 8 resulted in cell death and degradation of the sheets respectively.

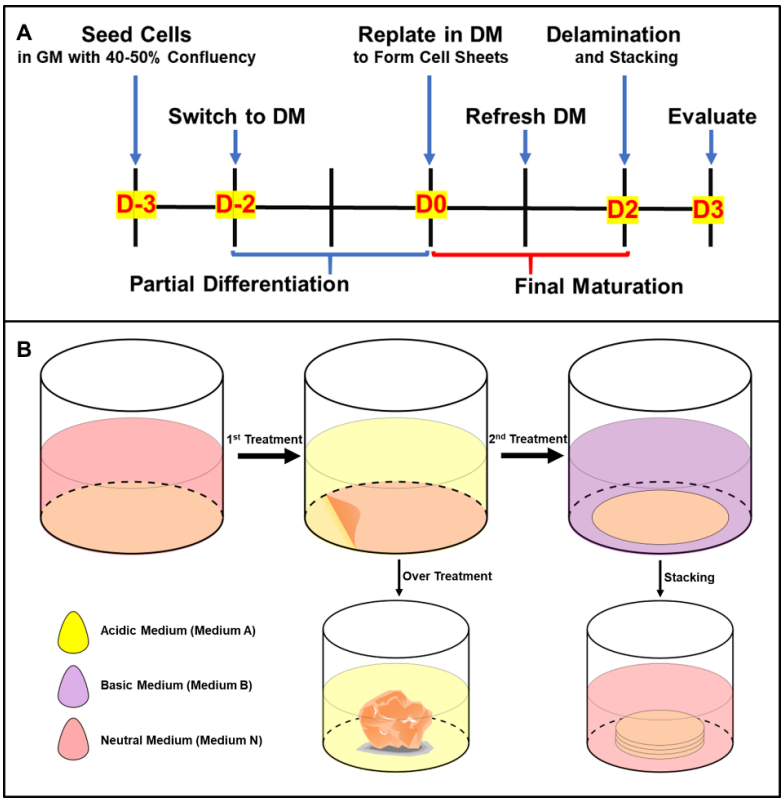

Figure 1. A) Differentiation, maturation, and sheet formation protocol; **B)** Delamination process. Cells are partially differentiated and replated to perform fusion. Once cells are fused and show traction on the edges, stepwise treatment with basic, acidic, and neutral media is performed to form flat sheets.

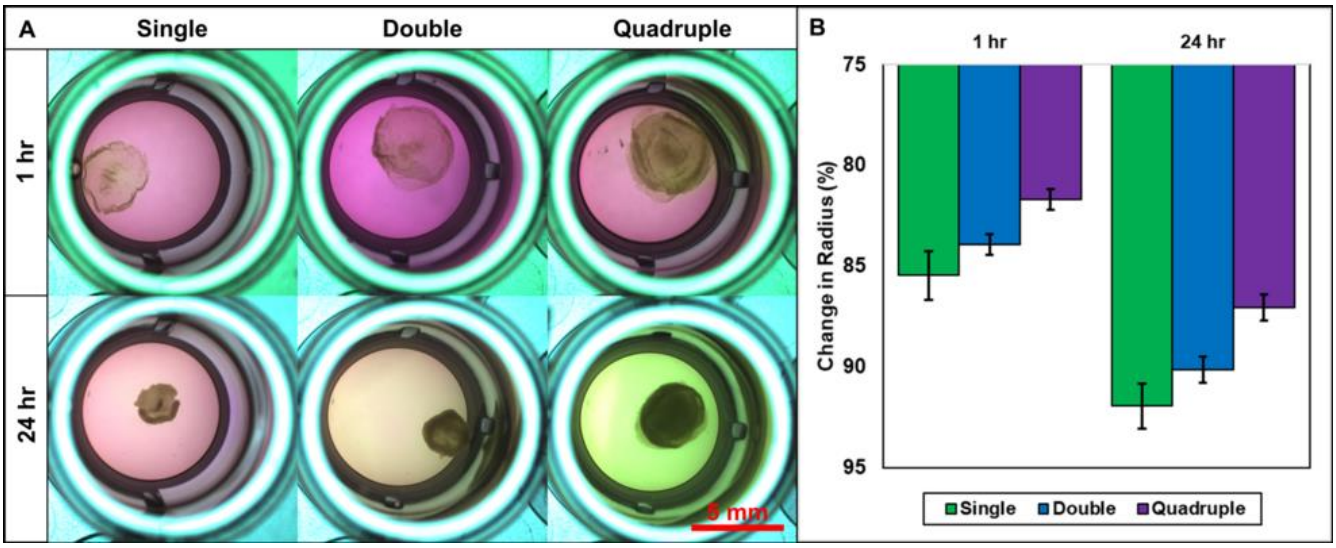

Figure 2. A) Single-, double-, and quadruple-layer constructs 1 and 24 hrs after delamination; **B)** Shrinkage pattern of single- and multiple-layer sheets with time. Samples are kept in 48 well plates after delamination from 24 well plates is performed.

It has been shown that serum depravation by replacing high amounts of FBS with low levels of horse serum can be used for differentiation of C2C12 myoblasts [14]. High levels of insulin (hyperinsulinemia) could help with this process as well [15, 16] and by using such protocols, C2C12 cells have been induced to form the first myotubes after 48-72 hrs [17]. The differentiation medium in this study was devised accordingly. Grabowska et al. reported that in their study C2C12 differentiation in 2D had three different stages, proliferation at day 2, fusion at day 4, and formation of multinucleated myotubes at day 7 [18]. Here in this study, cells that are ready for fusion are trypsinized (partially differentiated cells trypsinized right before fusion) and replated at an almost confluent density. This way they were primed towards their fusing phenotype, but they also showed some degree of proliferation that helped with distribution of the cells to have slightly more cells in the center of the well. This distribution caused the traction force to be radial and resulted in the initial traction and delamination from the edges (Supplementary Figure 1a). This technique can be further improved by aligning cells in the wells before performing the

delamination. Lam et al. has shown that prealignment of the cells is necessary to get a better fiber formation during myogenesis and to mimic physiological conditions [19]. This technique is valuable in different fields such as skeletal muscle tissue engineering and regenerative medicine where different applications require implantable muscle grafts, or where muscle constructs could be used for biomechanical actuators, lab-grown meat, and drug development [20, 21].

An interesting aspect of this method is that it does not require any specialized surfaces. Alternate cell sheet engineering methods require either temperature responsive surfaces [2], or dissolving polyelectrolyte sacrificial layers [5]. Similarly, enzymatic methods to sever the attachment of the cells to the surface can also damage the cell-cell linkages and lead to fragile sheets. Finally, many of the alternate methods require stimuli such as light, electrochemical polarization, ionic solution, or magnetic forces [6] to cause delamination and need specialized equipment. Furthermore, the cell sheets delaminated have to be handled by custom built tools to maintain their flatness as otherwise they would crumple and agglomerate. Our method on the other hand, is simple and requires only a quick change of media. Furthermore, it can arrest the traction force on demand and hence maintain the flatness of the sheets. The sheets formed in this way are also mechanically robust and can be easily handled with pipettes or tweezers as opposed to sheets formed using other methods.

3.2. Cell Sheet Microstructure

Differentiation and delamination protocols that have been developed can have an impact on viability of the cells and microstructure of the sheets. For this purpose, different types of staining were performed and imaged using brightfield and fluorescent microscopy. First, Nile red and DAPI staining was performed on cells both before they were formed into cell sheets (D2) and after were delaminated as sheets (Figure 3A). Consistent with the observed shrinkage of the sheets, cells are

more densely packed after delamination (Supplementary Figure 4). It is also noticeable that at D1 the whole surface is not covered with cells (confirmed by void spaces in Figure 3A) while in the sheets there is a continuous and uniform distribution of cells. This is because culture started at 90% confluent at D0 and although they were exposed to serum starvation, they slowly proliferated and formed a completely confluent layer by D2 when delamination was performed. Sheets in stacked layers showed robust adherence to each other such that handling them by suction into wide orifice pipette tips with large openings, transferring between plates, and resuspension in the medium didn't cause them to fall apart and they maintained their integrity and attachment to each other. Brightfield and fluorescent images of quadruple-layer constructs are shown in Figure 3B demonstrate the scalability of this approach to obtain multilayered sheet like constructs. Even though they are attached to each other the cells from different layers did not fuse with each other and the attachment can be attributed to cell-cell, cell-ECM, or ECM-ECM adherence between different sheets. Images of cross-section of H&E stained single-layer constructs after 1 day (Figure 3C) show that each sheet consists of densely packed cells with thickness of 40-60 μm. Live/dead staining of sheets 1 hr after delamination (Figure 3D) shows very few dead cells present indicating that the delamination process didn't adversely affect cell viability.

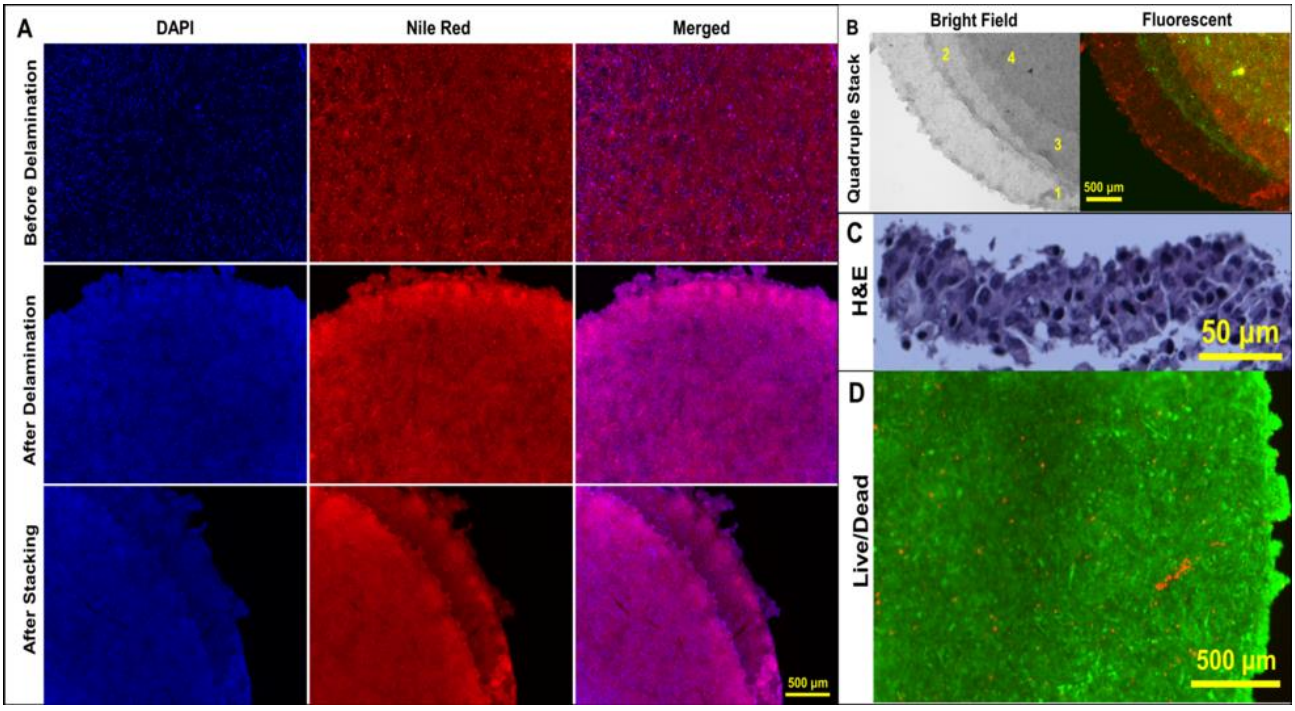

Figure 3. A) DAPI and Nile Red stained constructs before and after delamination as well as after stacking. Staining is performed on monolayer cell culture 1 hr before delamination and on sheets 1 hr after. DAPI stains the nuclei while Nile red stains the cellular lipid; **B)** Fluorescent and brightfield images of quadruple-layer constructs formed with cells stained with DiO and DiI. Layers are numbered from bottom to top; **C)** H&E stained section of a single-layer constructs; **D)** Live/dead stained samples immediately after delamination (top view). Consistent with shrinkage pattern, thickness of sheets increases while cells stay viable during the process.

3.3. Assessment of Cell Behavior in Sheets

Cell sheet formation and delamination process could potentially have an effect on the cells' function and viability. In order to understand this effect in greater detail, assays for metabolic activity, total protein content, as well as the cytotoxicity were performed. These results were compared with similar assays performed on conventional tissue culture plate based monolayer culture of the same number of cells in GM without any delamination (Figure 4A-C) as the first control group. These control samples were prepared by culturing cells in GM and replating at 0.235×10^6 cell/well into 24 well plates in GM (the same process that was performed for partial differentiation of cells except the cells were replated in GM instead of DM). The assays were

performed one day after culture started (equivalent to D1 of partially differentiated cells). Assays were also performed on cells that underwent differentiation process one day before delamination (D1) as a second control group. Metabolic activity of cells in the two control groups at D1 was similar to each other but a dramatic decrease was observed (~80% decrease) in the case of single-layer sheets (Figure 4A). The reduction in metabolic activity of the sheet as compared with the monolayer controls has previously been shown [22]. It can be due to the change in the morphology of the cells and loss of anchorage as well as the change in the form factor of these layers. The surface to volume ratio of the monolayer control is large and the cells in such 2D cultures have sufficient access to nutrients. When the cells are delaminated, they shrink by ~80-90% and increase in thickness in order to conserve volume. Therefore, their surface to volume ratio dramatically decreases while the cell density increases affecting transport of nutrients and oxygen that can affect metabolism in the cells. In thicker multilayer constructs one can envision presence of necrotic regions if the cell sheets are tightly adhered to each other which can further reduce their overall metabolic activity per unit volume as manifested in the less than proportional increase of activity in double and quadruple layer constructs and causing cells to enter quiescent state. Total metabolic activity of double- and quadruple-layer constructs was significantly higher than single sheets but this increase wasn't proportional to the number of sheets.

Cells in the second control group (monolayer cells in DM) had similar and very low levels of LDH in their conditioned medium compared to first control group (monolayer cells in GM) which shows the designed protocol to partially differentiate cells had no adverse effect on cell viability. However, these levels were significantly higher for single sheets 24 hrs after delamination. This increase in cytotoxicity could be caused by the damage caused during the delamination process (treatment with media A and B) as well as change in cell morphology, and loss of their anchorage

points. The total LDH content of the conditioned medium increased once multiple layers were stacked (Figure 4B) to ~1.70 and ~2.50 times of that of a single-layer construct, very similar to the respective increases of their metabolic activities, ~1.65 and ~2.59. This increase for both metabolic activity and LDH content is not proportional to the number of sheets in each case. The average LDH released from each sheet and metabolic activity of double- and quadruple-layer constructs is 0.85 and 0.63 for LDH and 0.82 and 0.64 for metabolic activity of that of a sheet in the single-layer format, respectively. The change in both LDH and metabolic activity is completely proportional and if cytotoxicity due to creating thicker structures was the only phenomenon, the metabolic activity should have decreased and LDH increased by increasing the number of layers but both of these values have changed similarly that shows favorable effect of better anchorage and negative effect of thicker constructs (lower mass transfer) co-exist.

Total protein content of control groups and single-layer constructs are very close to each other which shows preservation of ECM content of the samples during the delamination process and it increases for double- and quadruple-layer constructs (~1.95 and ~3.12 times of single-layer) proportional to the number of cells (Figure 4C). Preservation of ECM as well as preserved cell morphology and structure shown in the following sections shows that such single-layer or few layer cell sheets are viable and could be used to mimic *in vivo* conditions with high cell density and cellular crowding much better than 2D cultures. These constructs are of significant interest in regenerative tissue engineering or for use as tissue-analogue models for studying physiological/pathological conditions for example in drug discovery applications as well [23].

Long-term effect of stacking multiple layers and formation of thicker constructs was studied by keeping single- and quadruple-layer constructs in culture for one extra day (Supplementary Figure 5). Although metabolic activity of both constructs remained the same (Supplementary Figure 5a),

LDH levels only showed significant increase for quadruple constructs (Supplementary Figure 5b). It shows the formed sheets are capable of maintaining their integrity and cell function but stacking multiple layers and increasing the thickness to above mass transfer limits can create cytotoxic environment for cells.

Genetic assays were also conducted to probe for the expression of differentiation/maturation factors. In the process of differentiation of myoblasts, myogenic regulatory markers such as MyoD and Myogenenin are expressed that are indicative of differentiation of the cells from myoblasts into myocytes, myotubes and eventually formation of myofibers [24]. It has been shown that in several cell types including skeletal muscle cells, apoptotic signaling is an important contributing factor [25] and MyoD controls this signaling [26]. The expression of Myogenin and MyoD genes was found to be dramatically increased for partially differentiated cells at D1 (the day before delamination) compared to cells in growth medium without any differentiation, as shown in Figure 4D. β-Actin, an isoform of actin, is sometimes used as house-keeping gene as it is expressed ubiquitously in most cell types [27] but its levels can be impacted by the maturation of skeletal muscle cells [28]. During the partial differentiation of the cells however no significant difference was observed between expression levels of partially differentiated cells at D1 and cells in growth medium. Effect of differentiation and delamination protocols on maturation of cells and microstructure of sheets was also studied by staining for desmin, a muscle specific intermediate filament (Figure 4E). Cells in monoculture with GM showed little expression of this protein while cells in monoculture with DM showed higher expression of the protein as well as formation of thick multinucleated myofibers that are preserved in the cell sheets after delamination. Comparing morphology of cells using bright field images and fluorescent images of samples stained with phalloidin for F-actin (Supplementary Figure 6) at D3 before delamination shows that cells in DM

were elongated and formed myotube-like constructs further supporting gene expression results that the devised protocol is appropriate for differentiation and maturation of these cells.

Effect of differentiation on cytoskeleton reorganization of cells was also studied by treating undifferentiated cells and partially differentiated cells at D1 with Lat-B, an agent that interferes with actin remodeling. Cells were treated with 100 nM Lat-B for 1 hr. Morphology of partially differentiated cells changed very fast to round cells and eventually they formed clumps of cells. Undifferentiated cells however weren't affected by this treatment as much and only became slightly round (Figure 4F). This shows that during the differentiation and fusion process of C2C12 cells, cytoskeleton becomes more active in remodeling and therefore more sensitive to Lat-B.

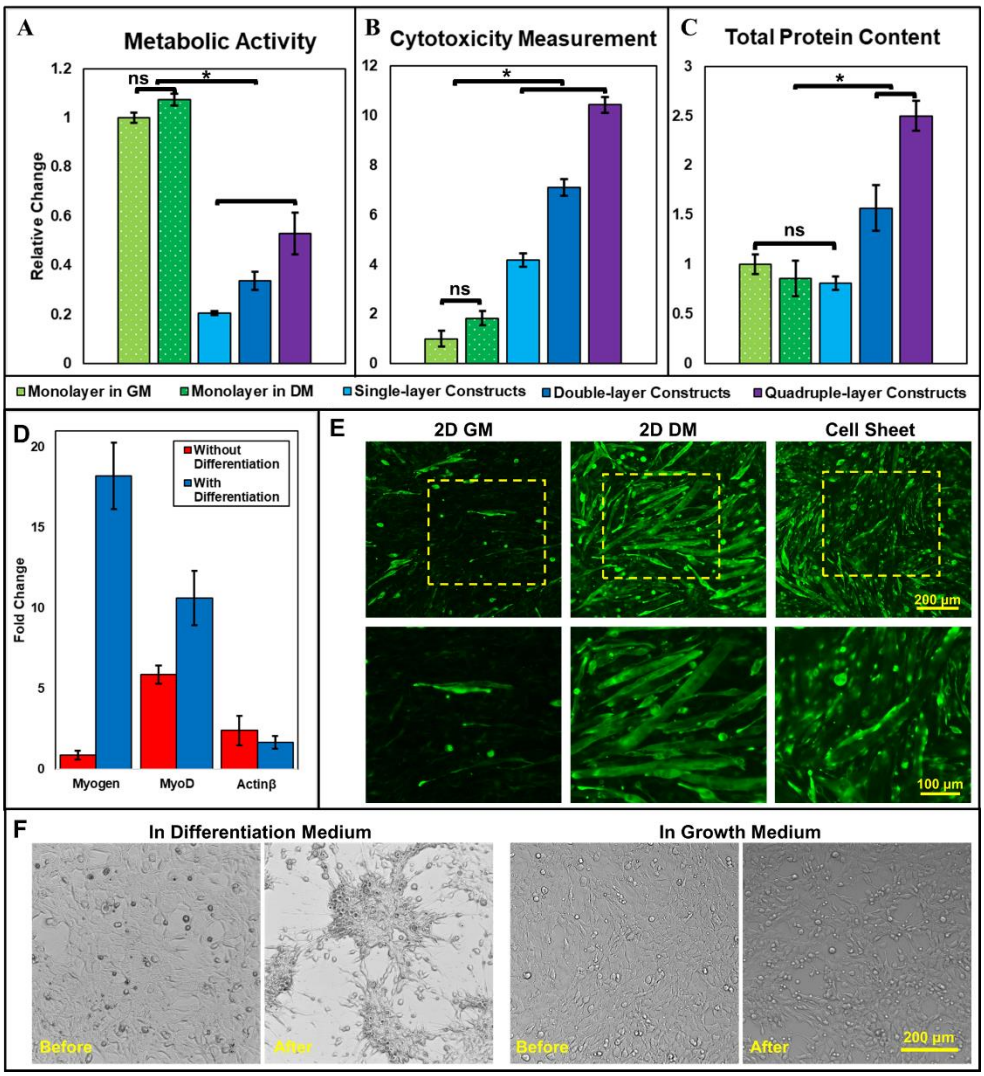

Figure 4. Assays performed on the day before delamination (D1, monolayer cultures in GM and DM) and the day after delamination (D3, single-, double-, and quadruple-layer constructs), **A)** metabolic activity using ABA, **B)** cytotoxicity of the process using LDH levels in the conditioned medium, **C)** total protein content of each construct using BCA. Amounts are normalized to GM group and monolayer cultures on plastic surfaces at D1 are shown in patterned fill while cell sheet samples at D3 are depicted in solid fill. **D)** Expression of skeletal muscle cell maturation markers in cells grown in GM and cells undergone differentiation and maturation protocol at the day before delamination (D1). P-value<0.01 for n=4. **E)** Immunofluorescence images of control groups (formed in GM and DM) at D3 before delamination and cell sheets after delamination using anti-desmin antibody. Samples grown in DM showed higher expression of desmin and formation of thick and multinucleated myofibers that are preserved after delamination. **F)** Effect of treatment by cytoskeleton-disruptive drug latrunculin B (100 nM) on partially differentiated cells in DM and undifferentiated cells in GM. Treatment is performed at D1 for 1 hr.

Importance of cytoskeleton reorganization on sheet formation was studied by treating cells 24 hrs before delamination (From D1 to D2) with DM containing either 50 nM or 100 nM Lat-B. Cells treated with 50 nM Lat-B didn't show significant changes in their morphology during the first few hours (data not shown) but after 24 hr of treatment were slightly round (Supplementary Figure 7). Cells treated with 100 nM solution after initial dramatic changes, regained their stretched morphology after 24 hrs of treatment but were still rounder compared to untreated cells. Treatment with medium A was performed for both of these conditions, 50 nM treated cells started to delaminate, but the sheets were fragile and broke to smaller pieces. 100 nM treated samples on the other hand didn't form sheets at all (Supplementary Figure 7). This shows importance of cytoskeleton reorganization on effective delamination of sheets. It is previously shown that treating C2C12 cells with Lat-B causes a decrease in filopodia and lamellipodia extensions during the differentiation process by inhibiting reorganization of cytoskeleton and actin polymerization and therefore reduction in fusion of myotubes [29]. Nowak et al. reported that C2C12 cells in DM treated with 100 nM had similar morphologies to untreated cells after 1 and 2 days, similar to our observations, but they reported that these cells, although still capable of differentiating, won't fuse to each other [29].

The mechanism by which the cell sheets delaminate by acidic medium treatment might be related to loose attachment of differentiated cells to the surface and effect of lower pH on the conformation of ECM proteins. Partial delamination during differentiation has been observed before for other skeletal muscle cell lines such as L6 cells but was considered undesirable for further studies and attributed to incompatible differentiation medium [14]. However, here using staining for actin cytoskeleton and more specific markers of skeletal muscle cells, desmin, we have shown that the cells differentiated properly in the current protocol and fused with each other to form

multinucleated fibers that are preserved in continuous layers after delamination (Figure 4E and Supplementary Figure 6b). It has been previously shown that during differentiation process of skeletal muscle cells, muscle-specific myosin II will be expressed and replace the non-muscle myosin II that already exists in these cells. These will assemble with F-actin into sarcomers and form branched myotube networks with uncontrolled adhesion that could result in their uncontrolled detachment [30]. On the other hand, cells adhere to the matrix through focal adhesions mediated by transmembrane integrins which are in turn connected to the internal cytoskeleton [31]. Various studies have shown that by decreasing the pH, cell adhesion to matrix strengthens [32]. It has been suggested that this could be because of the fact that extracellular acidic conditions promote integrin activation by causing the opening of its headpieces creating a stronger adhesion and attachment to the ECM [33]. At the same time, it has been shown that in lower pH, cells can show more spread and elongated morphologies [33] and form more stress fibers [34]. This elongation in differentiated C2C12 cells that are fused to each other could result in an internal stress in the cell sheet that combined with loosened attachment can result in delamination from the underlying substrate. This could be the reason for delamination initiated at the edges of the plates where the accumulated extensionary forces are the strongest. The importance of cytoskeleton is further shown when disrupting its structure prevented the delamination or resulted in formation of fragile sheets.

3.4. Versatility of Technique in Patterning, Co-culture, and Alternative Fusing Cells

The cell sheets can be patterned and shaped by controlling the location of the initial cell seeding. To illustrate this point, a small circular (15 mm diameter) Teflon mask was affixed to the bottom of the tissue culture plate (60 cm dish) which prevented the attachment of cells in those regions. A total of 2×10^6 partially differentiated C2C12 cells in 4 mL of DM were added to plate and next

delamination was performed following the same protocol. Continuous sheets were formed, and delamination happened as expected. The delaminated sheets had an annular ring shape instead of the circular shape due to this patterning (Figure 5A). Such patterned sheets can be stacked on top of each other to form constructs with channels embedded in their structure that can allow perfusion of media through the dense constructs and maintain the viability of cells within. Details of the formation process of such patterned sheets are included in Supplementary Figure 8.

Skeletal muscle cells *in vivo* have symbiotic interactions with other cell and tissues including vascular tissue, connective tissue, and nervous tissue that may have significance in disease models and in modulating their function [20], for example fibroblasts are important in providing the stability for the skeletal muscle tissue through secretion of ECM components [35]. Presence of endothelial cells and neuronal cells is also important for vasculogenesis and formation of neuromuscular junctions, respectively. To show the suitability of our technique to recapitulate such interactions, cell sheets of C2C12 and HUVEC were cocultured and delamination was performed the same as before (Figure 5B). The co-cultured sheets also delaminated cleanly using this technique and can be formed into robust sheets that can be handled. It has previously shown that co-cultured endothelial cells in cell sheets will reorganize the constructs and migrate towards vascular bed upon implantation to connect the new capillaries and create perfusion networks [8, 36]. C2C12 cells co-cultured with NIH/3T3 fibroblasts and SH-SY5Y neuron-like cells are also shown in Supplementary Figure 9a. The ability of technique to form sheets with very low numbers of C2C12 cells was also shown by forming sheets where 75% of initial population in the coculture was consisted of 3T3-L1 preadipocytes. These cells differentiated to adipocytes and accumulated lipid droplets that were preserved during the delamination process (Supplementary Figure 9b). Although fusion of C2C12 cells to each other to form multinucleated fibers is pertinent to the

proposed technique, the ability of the co-cultured sheets to delaminate even with low C2C12 numbers shows that the establishment of firm junctions with these fusing cells is sufficient to form robust sheets. Replacing more C2C12s with second cell type could result in formation of sheets that are not as uniform and flat due to the difference between morphology of the two cell types since C2C12s has already fused and formed elongated myofibers while the second cell type still has a round morphology.

This delamination method for cell sheets is also applicable to other cells that are capable of fusion. Cytotrophoblast cells fuse with each other and form syncytiotrophoblasts in human placenta. BeWo cells, cells from choriocarcinoma and a placenta cell line, show this syncytialization phenomenon and formation of syncytiotrophoblast when exposed to forskolin [37, 38]. Unlike C2C12 cells that show complete fusion, BeWo cells although capable, don't show complete fusion which has been confirmed using different techniques such as measuring the decrease in E-cadherins and measuring their fusion index, tagging cells to express different fluorescent proteins with different colors and tracking their fusion using fluorescent microscopy [37, 39, 40]. BeWo cells were cultured in wells of 24 well plates and after 72 hrs of treatment with Forskolin, a fusogenic agent, similar delamination process was performed on them. These cells also form cell sheets (Figure 5C) and delaminated in a faster time period as compared with C2C12 cell sheets. However, the sheets formed were not homogeneous and had small holes in them. This is due to the inability to form a confluent monolayer with 100% cellular coverage and fusion. Nevertheless, this experiment demonstrated that sheets even with non-continuous cell layers and with patterns embedded in them can be delaminated. These sheets didn't show much contraction which could be a result of this incomplete fusion or their lower ability in cytoskeleton reorganization as compared to contractile skeletal muscle cells.

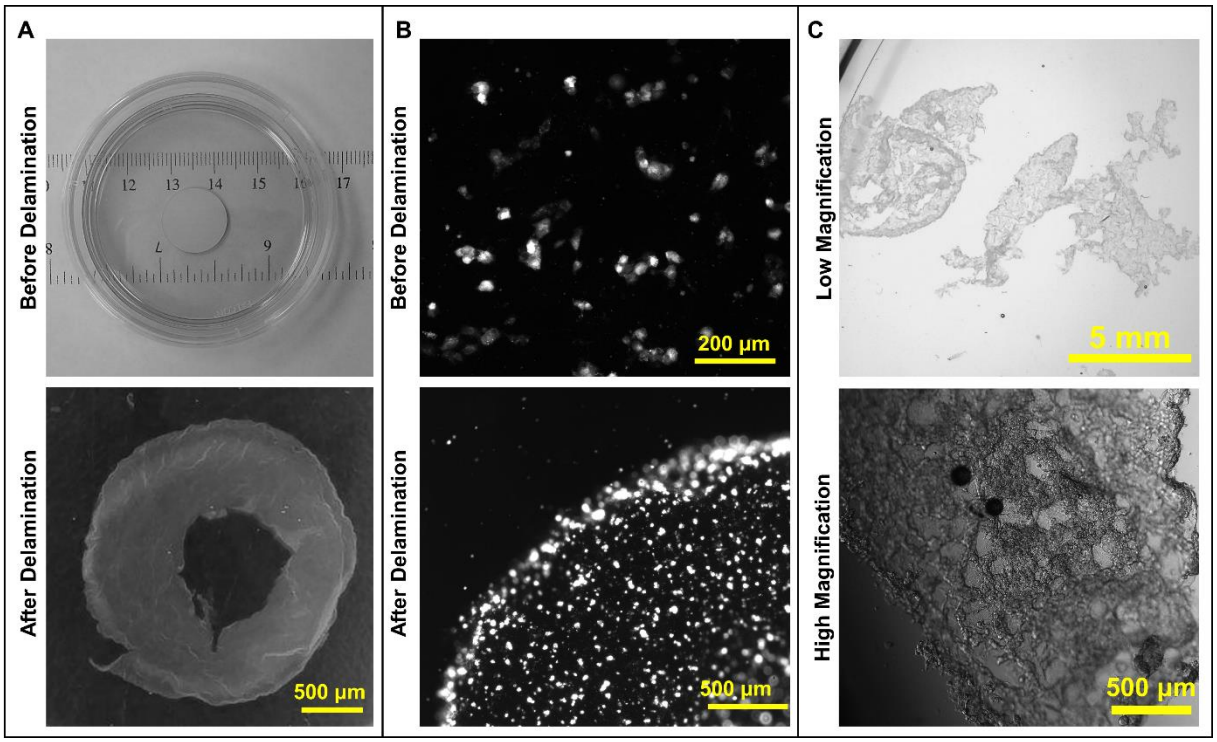

Figure 5. A) Forming sheets with annular distribution of cells. **B)** Formation of heterogenous constructs by co-culture of C2C12s and HUVECs with the ratio of 5:1. **C)** Delaminated sheets of BeWo cells. Since 100% fusion of cells didn't happen, they didn't delaminate as a continuous sheet.

4. Conclusion

In the current study a pH-induced cell sheet engineering technique that doesn't need any modified surfaces or electrical/mechanical stimuli to form the sheets has been developed which can be used for cells that fuse to each other. After cells are grown to confluence and induced to show the fusion, a stepwise treatment with their media that is slightly acidic, basic, and eventually neutral will induce delamination as continuous sheets and stop them from agglomeration. These sheets can be stacked to form thicker structures, they can be formed with co-culture of cells that show fusion property with cells that don't show this behavior, and sheets with hollow patterns in them can be formed to make channel-like structures when they are stacked. Different assays are performed to compare viability, function, and maturation of cells in sheets with cells cultured on plastic surfaces

in 2D monolayers and based on these results this technique has minimal effect on cell viability and allows proper function and maturation of cells. Proof of concept with this technique is performed using C2C12 myoblast cell line as well as BeWo placenta cell line but it can be used with other cell types with similar behavior. It could be used with 2D cell patterning techniques to prepare sheets with different cell types on the same layer. Although here, most commonly used tissue culture vessels made of polystyrene are employed, other materials such as glass or polymeric membranes suitable for cell culture such as polycarbonate can also be tested to evaluate their compatibility with this technique. Compared to other techniques it is cheap, easy to perform, and does not need modified surfaces and any other specific equipment and can be used for applications such as tissue engineering and regenerative medicine and as an *in vitro* models for applications such as drug discovery.

Acknowledgements:

The cells used in this study, C2C12 and BeWo Cells, were kindly provided from Dr. Sandeep Raha from Department of Pediatrics of McMaster university. The authors would like to acknowledge the support of the Natural Sciences and Engineering Research Council of Canada (NSERC). *In vitro* studies were performed at the Biointerfaces Institute at McMaster University.

References

1. Matsuura, K., et al., *Cell sheet approach for tissue engineering and regenerative medicine.* J Control Release, 2014. **190**: p. 228-39.
2. Yamada, N., et al., *Thermo-responsive polymeric surfaces; control of attachment and detachment of cultured cells.* Die Makromolekulare Chemie, Rapid Communications, 1990. **11**(11): p. 571-576.
3. Yamato, M., et al., *Thermo-responsive culture dishes allow the intact harvest of multilayered keratinocyte sheets without dispase by reducing temperature.* Tissue Eng, 2001. **7**(4): p. 473-80.
4. Iwata, T., M. Yamato, and T. Okano, *Chapter 29 - Intelligent Surfaces for Cell-Sheet Engineering*, in *Principles of Regenerative Medicine (Second Edition)*, A. Atala, et al., Editors. 2011, Academic Press: San Diego. p. 517-527.
5. Guillaume-Gentil, O., et al., *pH-controlled recovery of placenta-derived mesenchymal stem cell sheets.* Biomaterials, 2011. **32**(19): p. 4376-84.
6. Owaki, T., et al., *Cell sheet engineering for regenerative medicine: current challenges and strategies.* Biotechnol J, 2014. **9**(7): p. 904-14.
7. Tang, Z., Y. Akiyama, and T. Okano, *Temperature-Responsive Polymer Modified Surface for Cell Sheet Engineering.* Polymers, 2012. **4**(3): p. 1478-1498.
8. Haraguchi, Y., et al., *Fabrication of functional three-dimensional tissues by stacking cell sheets in vitro.* Nat Protoc, 2012. **7**(5): p. 850-8.
9. Tadakuma, K., et al., *A device for the rapid transfer/transplantation of living cell sheets with the absence of cell damage.* Biomaterials, 2013. **34**(36): p. 9018-25.
10. Hirose, M., et al., *Creation of designed shape cell sheets that are noninvasively harvested and moved onto another surface.* Biomacromolecules, 2000. **1**(3): p. 377-81.
11. Shimizu, T., et al., *Two-dimensional manipulation of cardiac myocyte sheets utilizing temperature-responsive culture dishes augments the pulsatile amplitude.* Tissue Eng, 2001. **7**(2): p. 141-51.
12. da Silva, R.M., J.F. Mano, and R.L. Reis, *Smart thermoresponsive coatings and surfaces for tissue engineering: switching cell-material boundaries.* Trends Biotechnol, 2007. **25**(12): p. 577-83.
13. Takezawa, T., Y. Mori, and K. Yoshizato, *Cell culture on a thermo-responsive polymer surface.* Biotechnology (N Y), 1990. **8**(9): p. 854-6.
14. Lawson, M.A. and P.P. Purslow, *Differentiation of myoblasts in serum-free media: effects of modified media are cell line-specific.* Cells Tissues Organs, 2000. **167**(2-3): p. 130-7.
15. Conejo, R., et al., *Insulin produces myogenesis in C2C12 myoblasts by induction of NF-kappaB and downregulation of AP-1 activities.* J Cell Physiol, 2001. **186**(1): p. 82-94.
16. Grabiec, K., et al., *The influence of high glucose and high insulin on mechanisms controlling cell cycle progression and arrest in mouse C2C12 myoblasts: the comparison with IGF-I effect.* J Endocrinol Invest, 2014. **37**(3): p. 233-45.
17. Janot, M., et al., *Glycogenome expression dynamics during mouse C2C12 myoblast differentiation suggests a sequential reorganization of membrane glycoconjugates.* BMC Genomics, 2009. **10**: p. 483.
18. Grabowska, I., et al., *Comparison of satellite cell-derived myoblasts and C2C12 differentiation in two- and three-dimensional cultures: changes in adhesion protein expression.* Cell Biol Int, 2011. **35**(2): p. 125-33.
19. Lam, M.T., et al., *Microfeature guided skeletal muscle tissue engineering for highly organized 3-dimensional free-standing constructs.* Biomaterials, 2009. **30**(6): p. 1150-5.
20. Ostrovidov, S., et al., *Skeletal muscle tissue engineering: methods to form skeletal myotubes and their applications.* Tissue Eng Part B Rev, 2014. **20**(5): p. 403-36.
21. Qazi, T.H., et al., *Biomaterials based strategies for skeletal muscle tissue engineering: existing technologies and future trends.* Biomaterials, 2015. **53**: p. 502-21.

22. Takezawa, T., et al., *Characterization of morphology and cellular metabolism during the spheroid formation by fibroblasts.* Exp Cell Res, 1993. **208**(2): p. 430-41.
23. Sakaguchi, K., et al., *In vitro engineering of vascularized tissue surrogates.* Sci Rep, 2013. **3**: p. 1316.
24. Bentzinger, C.F., Y.X. Wang, and M.A. Rudnicki, *Building muscle: molecular regulation of myogenesis.* Cold Spring Harb Perspect Biol, 2012. **4**(2).
25. Garrido, C. and G. Kroemer, *Life's smile, death's grin: vital functions of apoptosis-executing proteins.* Curr Opin Cell Biol, 2004. **16**(6): p. 639-46.
26. Hirai, H., et al., *MyoD regulates apoptosis of myoblasts through microRNA-mediated down-regulation of Pax3.* J Cell Biol, 2010. **191**(2): p. 347-65.
27. Perrin, B.J. and J.M. Ervasti, *The actin gene family: function follows isoform.* Cytoskeleton (Hoboken), 2010. **67**(10): p. 630-4.
28. Dittmer, A. and J. Dittmer, *Beta-actin is not a reliable loading control in Western blot analysis.* Electrophoresis, 2006. **27**(14): p. 2844-5.
29. Nowak, S.J., et al., *Nap1-mediated actin remodeling is essential for mammalian myoblast fusion.* J Cell Sci, 2009. **122**(Pt 18): p. 3282-93.
30. Griffin, M.A., et al., *Adhesion-contractile balance in myocyte differentiation.* J Cell Sci, 2004. **117**(Pt 24): p. 5855-63.
31. Khalili, A.A. and M.R. Ahmad, *A Review of Cell Adhesion Studies for Biomedical and Biological Applications.* Int J Mol Sci, 2015. **16**(8): p. 18149-84.
32. Stock, C., et al., *Migration of human melanoma cells depends on extracellular pH and Na+/H+ exchange.* J Physiol, 2005. **567**(Pt 1): p. 225-38.
33. Paradise, R.K., D.A. Lauffenburger, and K.J. Van Vliet, *Acidic extracellular pH promotes activation of integrin alpha(v)beta(3).* PLoS One, 2011. **6**(1): p. e15746.
34. Faff, L. and C. Nolte, *Extracellular acidification decreases the basal motility of cultured mouse microglia via the rearrangement of the actin cytoskeleton.* Brain Res, 2000. **853**(1): p. 22-31.
35. Chapman, M.A., R. Meza, and R.L. Lieber, *Skeletal muscle fibroblasts in health and disease.* Differentiation, 2016. **92**(3): p. 108-115.
36. Sekine, H., et al., *In vitro fabrication of functional three-dimensional tissues with perfusable blood vessels.* Nat Commun, 2013. **4**: p. 1399.
37. Douglas, G.C. and B.F. King, *Differentiation of human trophoblast cells in vitro as revealed by immunocytochemical staining of desmoplakin and nuclei.* J Cell Sci, 1990. **96 (Pt 1)**: p. 131-41.
38. Ringler, G.E. and J.F. Strauss, 3rd, *In vitro systems for the study of human placental endocrine function.* Endocr Rev, 1990. **11**(1): p. 105-23.
39. Kudo, Y., et al., *Quantifying the syncytialisation of human placental trophoblast BeWo cells grown in vitro.* Biochim Biophys Acta, 2003. **1640**(1): p. 25-31.
40. Wang, R., et al., *Live cell imaging of in vitro human trophoblast syncytialization.* Biol Reprod, 2014. **90**(6): p. 117.

Supplementary Information

Supplementary Table 1. Sequence of the used primers for qRT-PCR (5'to 3')

Target Gene	Forward	Reverse
Myogen	GCA ATG CAC TGG AGT TCG	ACG ATG GAC GTA AGG GAG TG
MyoD	GCC TGA GCA AAG TGA ATG AG	GCA GAC CTT CGA TGT AGC G
β-Actin	CAT GGA GTC CTG GCA TCC ACG AAA CT	ATC TCC TTC TGC ATC CTG TCG GCA TA
GAPDH	ATG TTT GTG ATG GGT GTG AA	ATG CCA AAG TTG TCA TGG AT

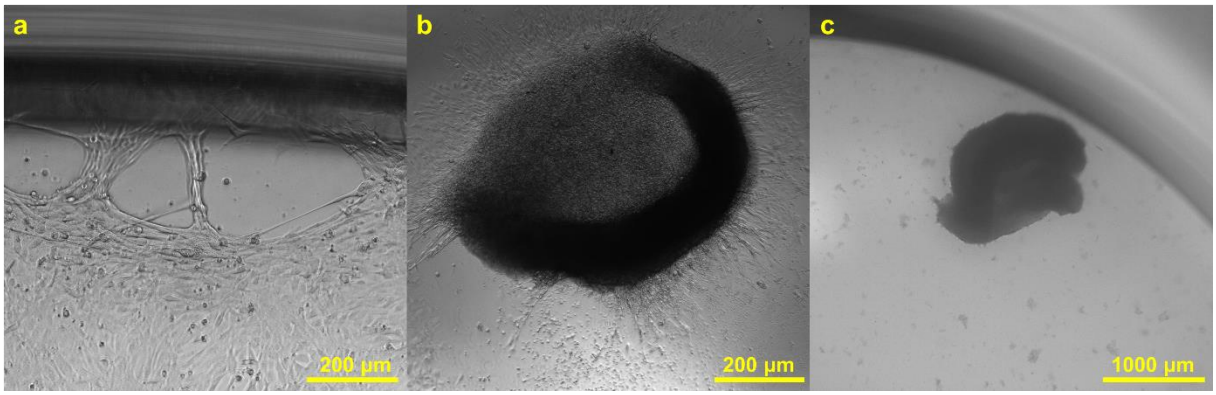

Supplementary Figure 1. a) Cell traction force exerted at the edges of the wells; **b)** Advancement of traction to form undefined agglomerated structures that could lead to spheroid-like structures; **c)** Advancement of folding in case sheets are kept in medium A after delamination is completed.

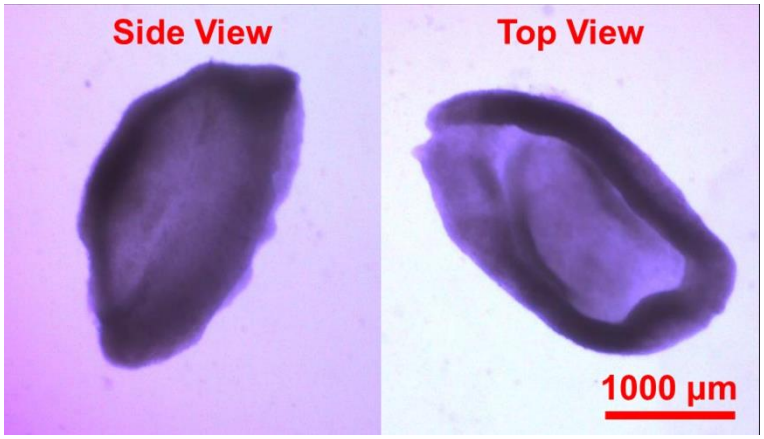

Supplementary Figure 2. Deformed single-layer construct after 1 day from side and top views. Single-layer construct are more prone to unintended deformation

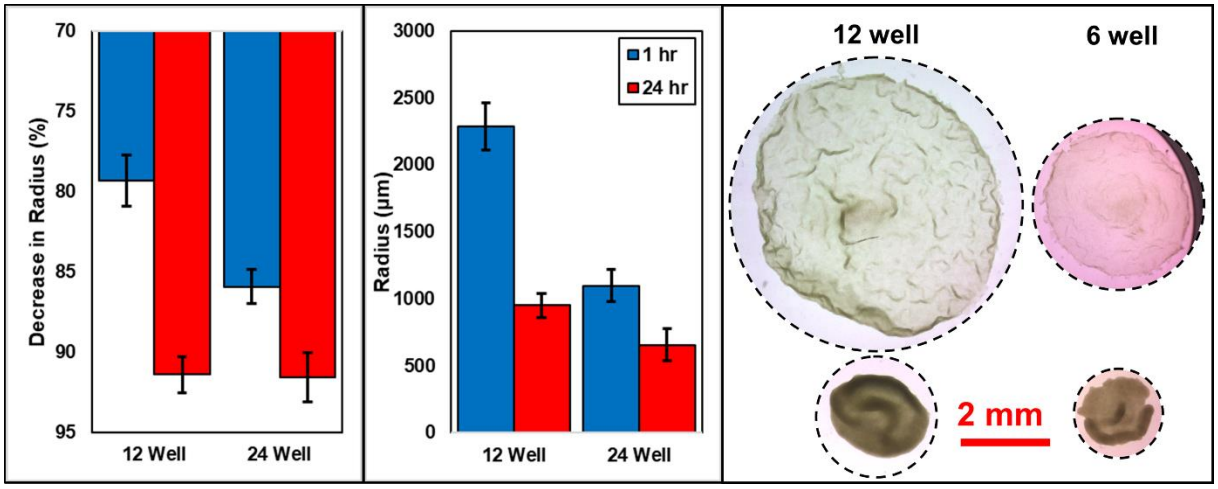

Supplementary Figure 3. Difference between shrinkage of sheets formed with 0.235×10^6 cells in a 24 well plate and 0.480×10^6 cells in a 12 well plate.

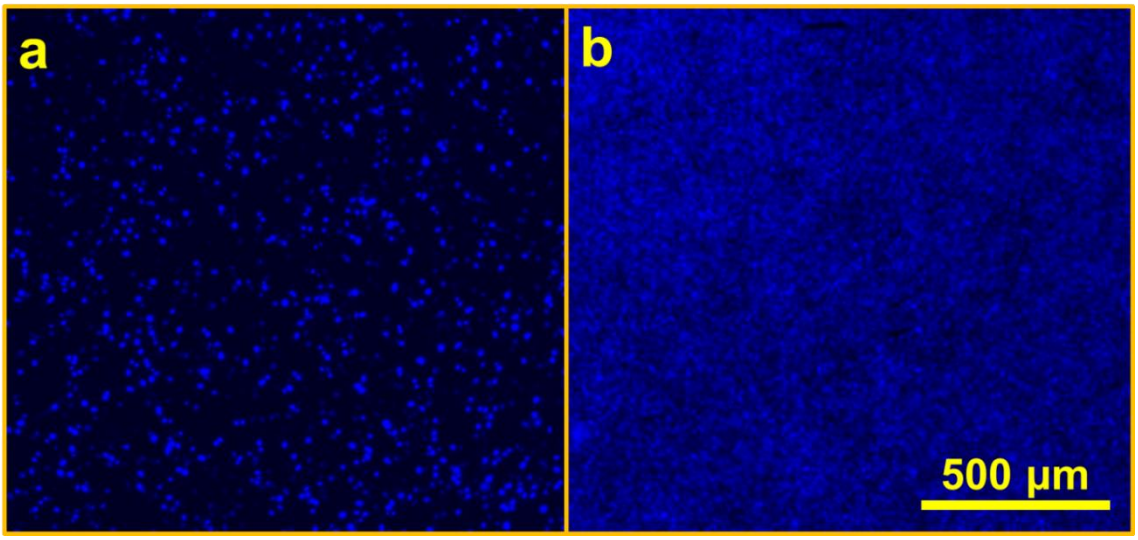

Supplementary Figure 4. Difference between compactness of cells **a)** before and **b)** after delamination. In accordance with decrease in sheet size, cell compactness increases.

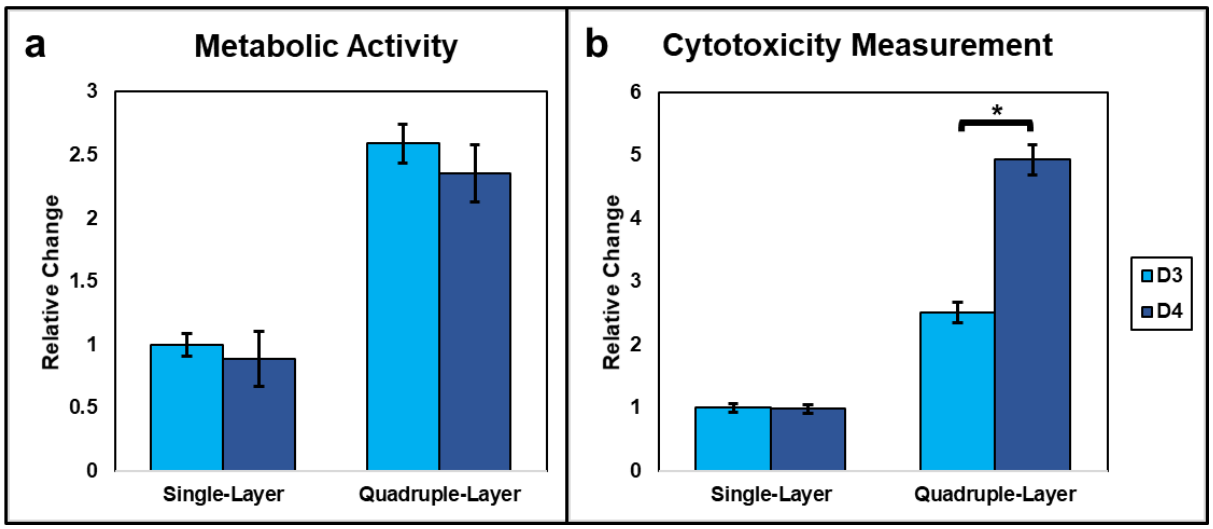

Supplementary Figure 5. Long-term effect of delamination and stacking multiple layers on cell **a)** viability and **b)** cytotoxicity. Assays are performed one day after delamination (D3 in the whole process) and two days after (D4 of the process). P-value<0.01 for n=4.

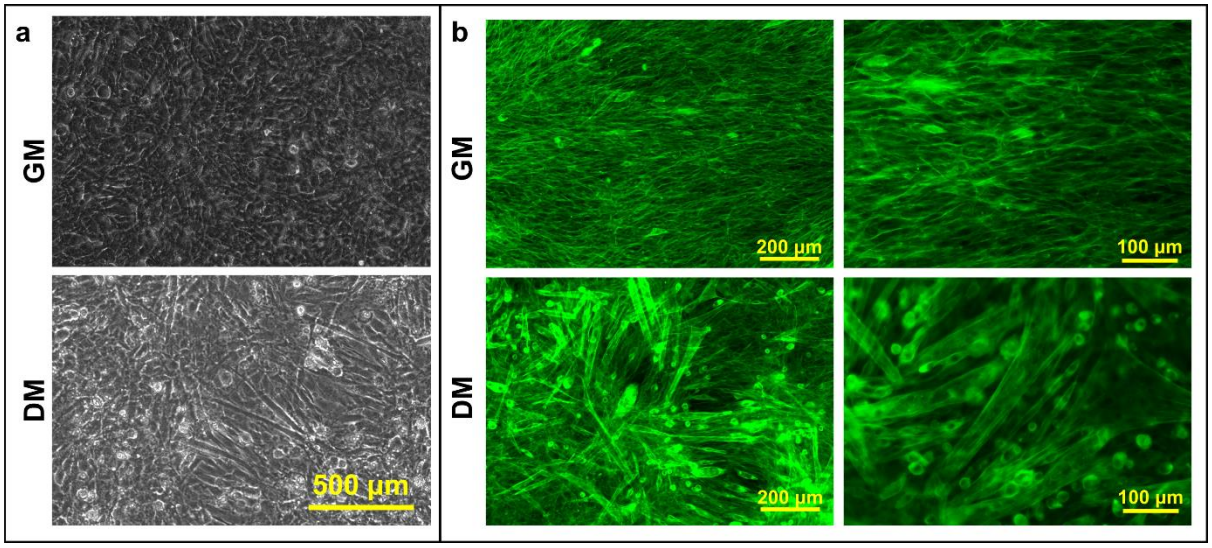

Supplementary Figure 6. a) Phase contrast and **b)** fluorescent stained F-actin (using phalloidin) images of cells without differentiation (in GM), and with differentiation (in DM). Images are taken at D3 before delamination using 10X and/or 20X magnifications. Cells in differentiated state are elongated and has formed thick myofibers. For staining with phalloidin samples were fixed with 2% paraformaldehyde and after washing with PBS, staining was performed using 1:40 dilution of phalloidin (Alexa Fluor™ 488 Phalloidin, Thermofisher, A12379) stock solution (300 units in 1 mL methanol) in PBS with 1 hr incubation at room temperature.

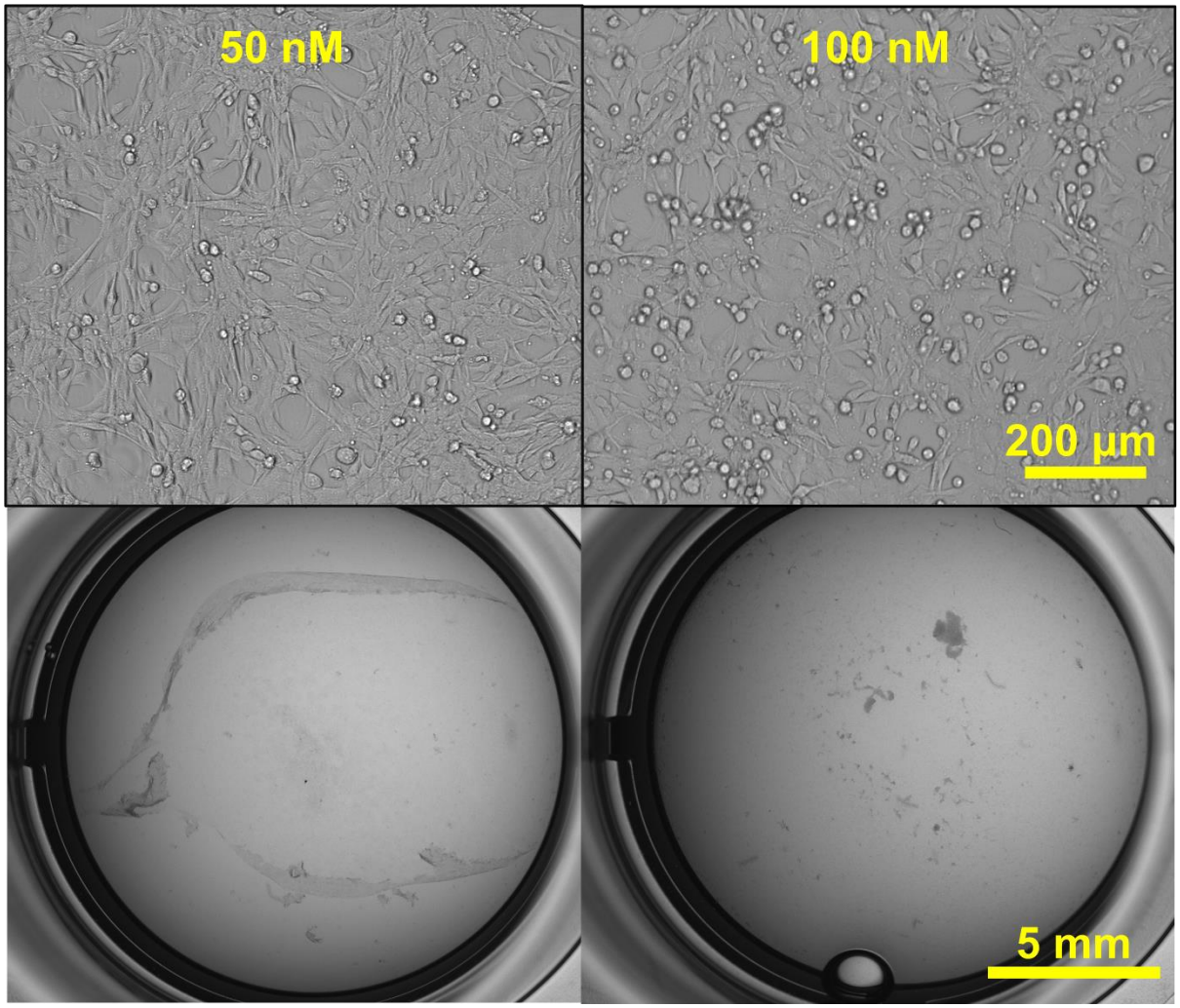

Supplementary Figure 7. Delamination of layers after 24 hr of treatment with 50 and 100 nM solution of Latrunculin-B. 50 nM treated groups delaminated but were fragile, 100 nM treated ones didn't form continuous sheets.

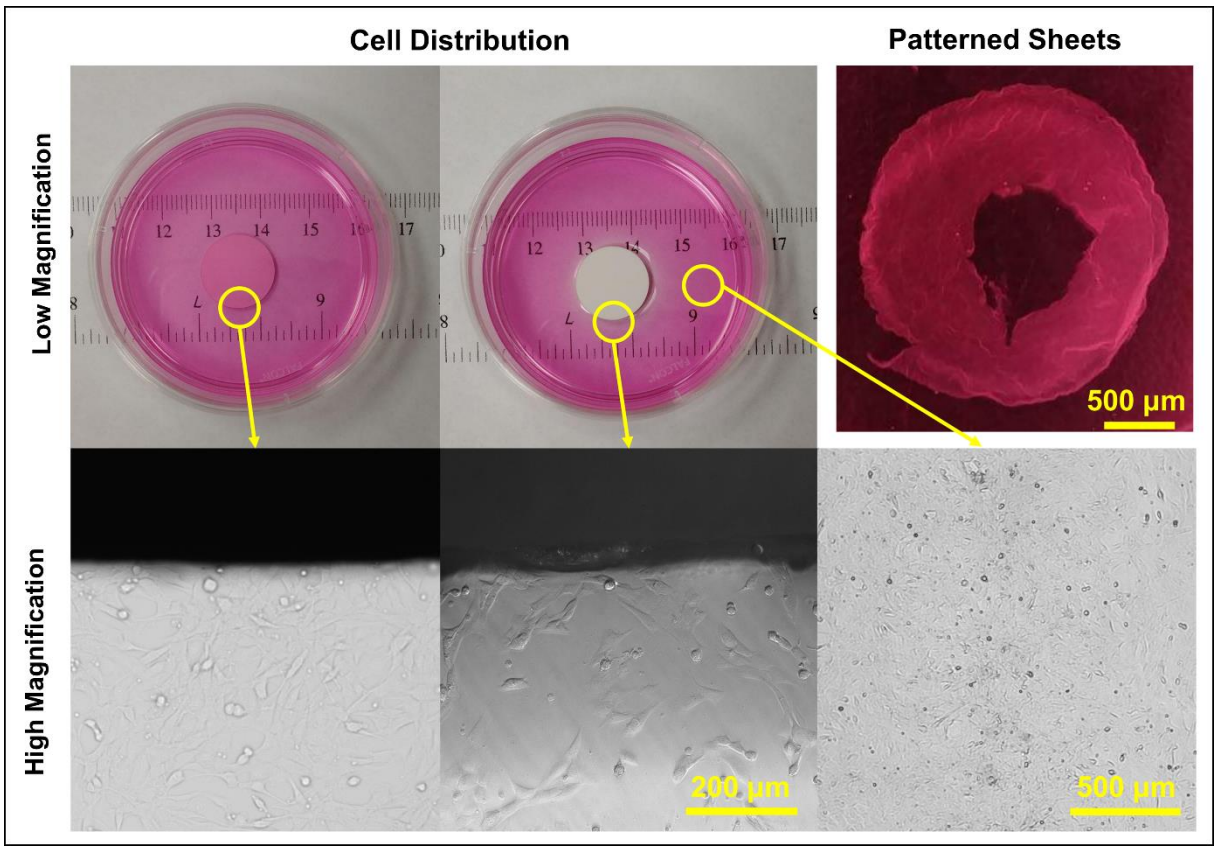

Supplementary Figure 8. Forming sheets with blocked regions using Teflon tape. Teflon is highly hydrophobic and allows spaces devoid of medium and cells. If this void region is not formed, simply by shaking the dish, the surface on top of tape will be covered with media but cells won't stick to it. This will cause different coverage of cells on the non-blocked area and a better distribution is achieved when there is no void area. Sheets can only be formed in the latter case.

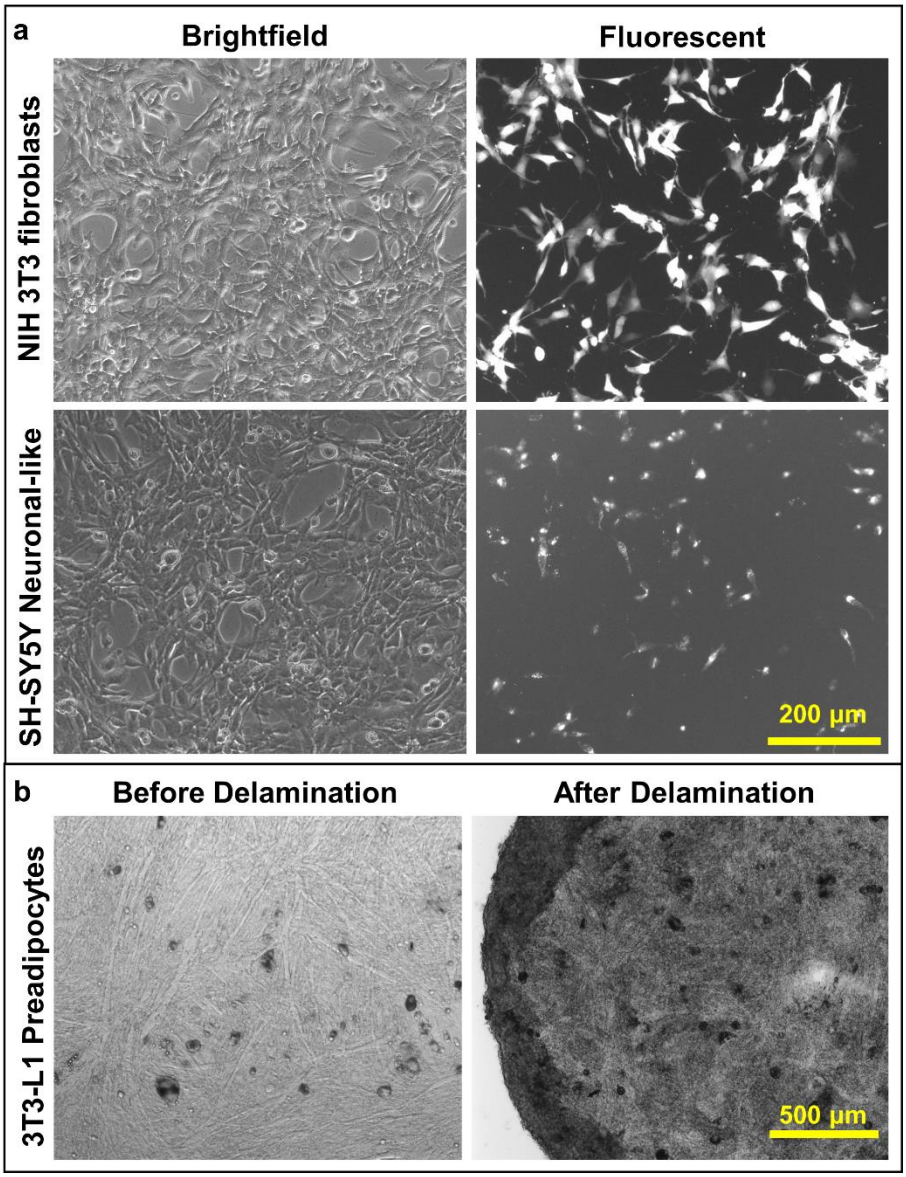

Supplementary Figure 9. a) Co-culture of C2C12 cells with NIH-3T3 fibroblasts and SH-SY5Y neuronal-like cells with 5:1 ratio. **b)** Co-culture of C2C12 myoblasts and 3T3-L1 preadipocytes before and after delamination. Starting culture with C2C12 having as low as 25% of the initial population is still enough to form continuous sheets with proper integrity.

Appendix 2: CELL SHEET ENGINEERING APPLICATION

Engineering Lipid and Protein Content in Meat-like Tissue by Self Assembly-Based Layer by Layer Biofabrication

Alireza Shahin-Shamsabadi [1], P. Ravi Selvaganapathy [1,2,*]

[1] School of Biomedical Engineering, McMaster University, Canada

[2] Department of Mechanical Engineering, McMaster University, Canada

[*] Corresponding Author: P. Ravi Selvaganapathy, Department of Mechanical Engineering, McMaster University, Canada. selvaga@mcmaster.ca

Status: Under Review

Abstract

Global meat consumption has been growing on a per capita basis over the past 20 years resulting in ever increasing devotion of resources in the form of arable land and potable water to animal husbandry which is unsustainable and inefficient. One approach to meet this insatiable demand is to cultivate meat-like tissues, using methods similar to those used in tissue engineering. Here we demonstrate such a method to produce meat-like tissues consisting of both adipocytes and skeletal muscle cells using a layer by layer self-assembly and stacking process, with the ability to tune fat and protein content, in a fast and scalable fashion. Samples with only myoblasts were equivalent to lean meat with comparable protein and fat contents, and incorporating adipocyte cells in different ratios to myoblasts and/or treatment with different media cocktails resulted in a 5% (low fat meat) to 35% (high fat meat) increase in the fat content.

Keywords: lab-grown meat, protein and lipid tunability, layer by layer biofabrication, meat texture and taste

Meat is a food staple that is consumed and enjoyed worldwide. Global meat consumption has grown by 58% in the past 20 years with population growth and growth in per person consumption accounting equally for that increase. Further economic development in Asia along with increased consumption in North America and Europe [1-3] is expected to further increase demand for meat and meat products. Livestock production to meet this demand is unsustainable due to high water consumption, greenhouse gas emission (15% of global greenhouse gas emissions and 37% of methane emissions [2]), accelerated soil erosion, and pollution of waterbodies [4]. The industry accounts for significant use of our resources including 70% of land suitable for agriculture (30% of total land) and almost one-third of agricultural water consumption [5]. Although solutions such as promoting low-meat diet style or switching to plant-based proteins has been suggested, their implementation hasn't been widespread [6, 7] and additives incorporated are a source for concern. Lab-grown meat is an environment friendly and ethically appealing [2] alternative to traditional meat. It has been estimated that once lab-grown meat hits the market it will result up to 45% decrease in energy use, 78-96% fewer greenhouse gas emissions, 99% lower land use, and 82-96% lower water consumption [8]. Furthermore, issues with pathogenic contamination can be easily prevented, beneficial nutrients including minerals, vitamins, and fibers that normally don't exist in meat can be introduced, and production time can be reduced to weeks from years [2].

Recently, tissue culture methods, developed originally for regenerative medicine, have been repurposed for growing meat aggregates (minced meat type granules) in the lab as a way to address this environmental challenge and has been primarily driven by startup companies such as Mosa Meat, Memphis Meat, Aleph Farms and Super Meat [9]. Nevertheless, research in this area is in its infancy [10], standards are non-existent, and a number of challenges including ability to produce at scale, dense tissues that are thick and fibrous with the full complement of cell types

present in animal tissues have not been addressed [11]. The focus has so far been on growing meat aggregates as opposed to meat-like tissue due to difficulties in co-culture and differentiation of fat and muscle progenitor cells as well as in vascularization needed for growing large tissue constructs [9, 10]. Other approaches have used scaffolds made of natural or synthetic biomaterials or even extracellular matrix (ECM) derived from explants of animal tissues in order to culture and grow purely muscle cells [12-15]. Such additives are not ideal as they do not achieve tissue like cell densities, may be difficult to completely remove after culture, and can introduce food safety concerns. Furthermore, incorporation of fat cells is critical to derive the taste that is associated with meat.

Results

Cell sheet formation and assembly: Here, we take a new approach to rapidly assemble thick slabs of meat tissue from densely packed cell sheets composed of differentiated adipocyte and muscle cells as shown in Figure 1a. The process starts with the formation of individual cell sheets. In order to produce adipocyte and muscle co-culture, the progenitor cells (myoblasts and preadipocytes) are grown separately and partially differentiated in their specific differentiation media. Then they are typsinized (before the myoblasts start to fuse) and the appropriate ratio of the partially differentiated adipocyte and muscle cells (corresponding to the desired lipid content in the meat) are plated onto another tissue culture plate at high confluency. The trypsinization and replating does not affect the subsequent full differentiation of them into mature adipocytes and skeletal muscle cells. Upon reaching full confluency, the skeletal muscle cells fuse with each other forming a contiguous sheet which exerts a traction force. They also produce their own ECM that provides additional structure and texture to the sheet. Exposure of this cell sheet to a slightly acidic medium (medium A) leads to its rapid delamination from the culture plate and contraction. The

sheet is then exposed to slightly basic medium (medium B) to preserve its flat profile and then transferred into neutral medium (medium N) (Figure 1a). Finally, several individual sheets are assembled on top of one another whereupon they adhere forming a thick meat-like tissue. This layer by layer process allows formation of highly dense, multicellular, textured tissues that are difficult to produce in other ways. Since the final step can be composed of a large number of sheets assembled in parallel, this process is scalable for fabrication of tissues of any thickness.

Myoblast (C2C12) and preadipocyte (3T3-L1) cell lines were used in this study to demonstrate the feasibility of this approach. Different protocols were devised and compared (Figure 1b) in order to identify conditions that will allow production of different amounts of protein and lipid in the constructs. Different ratios of initial number of cells (C2C12 to 3T3-L1 ratios of 1:0, 1:1, and 1:3) were also used with each of these protocols to eventually produce varying lipid content in the tissues formed. In the 1st protocol (P1) these cells were cultured in muscle differentiation medium (M-DM) for 2 days and delamination was performed at day 3. In the 2nd protocol (P2), cells were treated with fat differentiation and maintenance media (F-DM and F-MM), respectively, for 1 and 4 days before delamination was performed at day 5. In the last protocol (P3) after treating with F-DM and F-MM for a total of 5 days, cells were treated with M-DM for 2 more days and then delamination was performed.

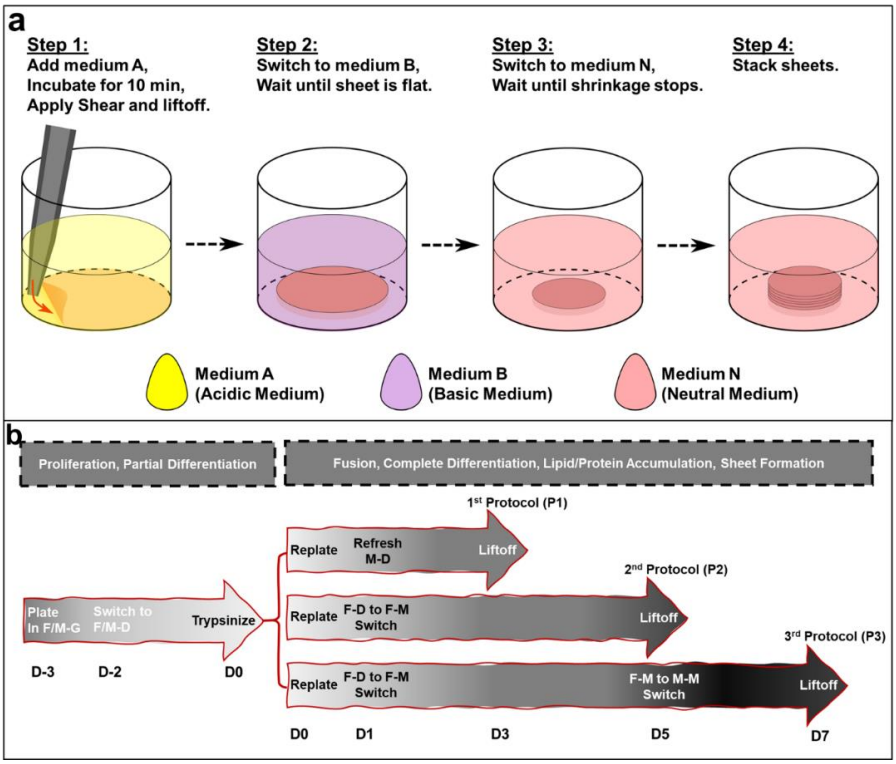

Figure 1. a) Various steps of the proposed process to form cell sheets as building blocks of the lab-grown meat; **b)** Various protocols tried for differentiation and maturation of both myoblasts and preadipocytes. Different amounts of cells or different treatment protocols can be used to tune protein and lipid content of the samples.

Structural characterization: The microstructure of the cell sheets was studied by scanning electron microscopy (SEM) and light microscopy. SEM images for 1:0 and 1:3 ratios in P3 (Figure 2a) show the difference between the morphology of cells in each group. In the 1:0 group where only C2C12 cells are present, all of the cells have elongated morphology while in 1:3 group, 3T3-L1 cells that had accumulated lipid are round and bulky. Hematoxylin and Eosin (H&E) staining of the cross-section of the 1:0 group shows the highly dense and compact microstructure of the sheets (Figure 2a inset) with thicknesses (~50-100 μm) which is much higher than a single layer of cells in two-dimensional culture. Fluorescent staining of the C2C12s with red and 3T3-L1s with green fluorescent dye in a 1:3 ratio sample cultured using P3 shows the presence of both muscle

fibers and lipid droplets after delamination which is important to achieve the meat texture and its taste (Figure 2b). The cellular density and packing also increases significantly after delamination as the sheets shrink and become more compact. Nevertheless, the shrinking process does not damage the fibers or the accumulated fat globules (Figure 2b). Several cell sheets can be stacked on top of each other simultaneously whereupon the adhere to each other to form thicker structures that better resemble meat structure. Stacked structures resist the traction force induced by the cytoskeleton reorganization which occurs when the sheets are delaminated resulting in lesser shrinkage of the overall structure as compared with individual sheets. Total protein and lipid content of two-layer stacked sheets with various ratios of C2C12 and 3T3-L1 cells were analysed a day after stacking. Samples with highest number of initial 3T3-L1 cells and cultured using P3 protocol had the highest lipid and protein content as shown in Figure 2c. It was interesting to find that the protein and lipid content of the tissues can be controlled by changing the differentiation protocol as well as the ratio of cells samples. Weight percentage of fat in different types of meat could range from 2-45% depending on the type of meat and its source. In case of beef, lean round can have as low as 6% fat while this amount for lean T-bone is 10% and could go up to 20% for regular beef [16]. In order to compare these samples with actual meat, fresh extra lean beef meat was purchased from local market and samples with similar weight to 1:0 in P1 (~5 mg) were separated (no fat tissue was observable using naked eye) and the same assays were performed on them. These meat sample had protein and lipid contents that were similar (1.5 and 0.9 times, respectively) to that of 1:0 in P1 sheets. The lower protein content of sheets could be due to the fact that cells secrete less ECM once cultured in 2D and proper stimulation could increase the protein content of the sheets. Figure 2e shows the increase of lipid content in 1:1 and 1:3 groups compared to 1:0 group in each protocol. Using only M-DM (P1) a ~18% increase was observed

for both groups. With F-DM (P2), ~15 and ~35% increase was observed for 1:1 and 1:3 groups, respectively. With P3 these increases were ~5 and ~20%. Based on these results it can be shown that lipid content of samples is completely tunable compared to samples with only muscle cells in a wide range (5-35%). Note that the lipid measurement is from both cell membrane and lipid droplets in adipocyte cells. The measurement from muscle only cell sheet represents the lipid content of bilipid membrane of the cells while the increases in co-culture with adipocytes can be attributed largely to the stored lipids in adipocytes. From the perspective of manufacturing, the ability to rapidly produce high protein and lipid content as well as the ease of delamination of single sheets to assemble them further, is of importance. Different protocols used in the final growth step and the ratio of cells used in the culture has a significant effect on all of these parameters as shown in Figure 2d. When M-DM (P1) was used, higher adipocyte number made it more difficult to delaminate the sheets while in the other two protocols, the opposite was observed. The increase in adipocytes lead to an increase in lipid content and the lipid droplets produced were robust and did not break out upon delamination. These lipid droplets don't exist in the muscle only sheets (1:0) while are clearly abundant and are preserved after delamination and digestion of 1:3 groups of P3 (Figure 2f).

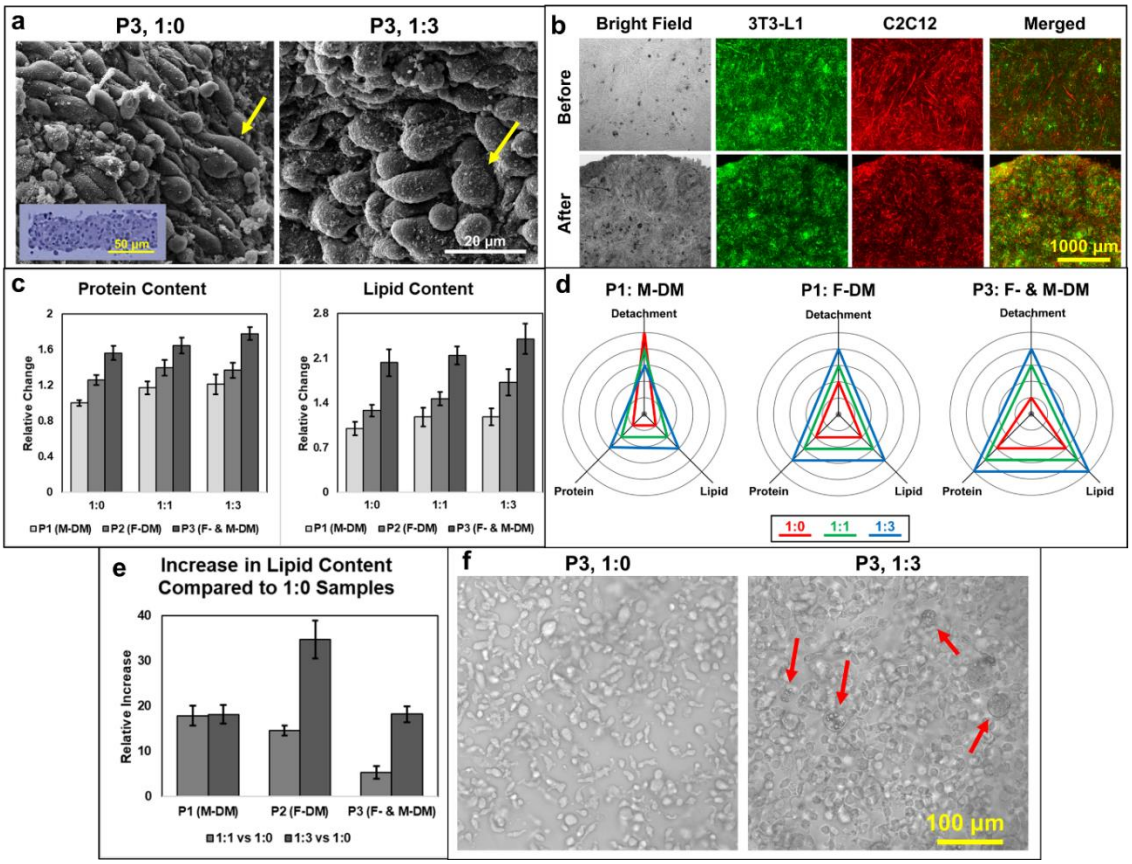

Figure 2. a) SEM images of 1:0 and 1:3 samples in P3, inset shows the Hematoxylin and Eosin stained cross-section of 1:0 in P3, arrow in 1:0 sample shows the elongated muscle cells while the arrow in 1:3 sample shows the adipocyte that has accumulated lipid droplets; **b)** Brightfield and fluorescent images of samples 1:3 ratio in P3 before and after delamination, C2C12s are red and 3T3-L1s are green; **c)** Protein and lipid content of samples with different initial ratios of partially differentiated myoblasts to preadipocytes undergone different differentiation protocols; **d)** Comparison of different conditions in terms of protein and lipid contents as well as ease of sheet formation (delamination); **e)** Increase in lipid content of different groups compared to 1:0 samples in P1; **f)** Brightfield images of 1:0 and 1:3 samples in P3 after digestion with collagenase, lipid droplets (red arrows) that were preserved during sheet formation process are observable.

Scale-up process: This manufacturing process is scalable and can be used to make large meat-like tissues in 24 well plates, 6 well plates, or 10 cm dishes (Figure 3). The ability to form thick and meat-like structures was shown by forming sheets in 6 well plates (1:0 ratio and P1) and stacking 18 layers of them. A multistep assembly process was used wherein three constructs each containing 6 individual cell sheets were formed with 1 hr incubation and later these three constructs were

assembled on top of each other and incubated further for 24 hrs (Figure 3b) (thickness of 1-2 mm can be achieved using this number of layers). Scalability of the technique to form larger structures was further shown by making the cell sheets in 10 cm dishes (1:0 ratio and P1) (Figure 3c). Individual cell sheets show a significant shrinkage immediately after delamination (from 10 cm to 3.5 cm in case of 10 cm dishes) which helps with creating thicker and stable structures. Once assembled into multilayer constructs the amount of shrinkage is dramatically lower even over longer incubation times (a 6-layer stack shrank from 3.5 cm to 2.5 cm after 24 hrs of incubation) which is important to create stable structures.

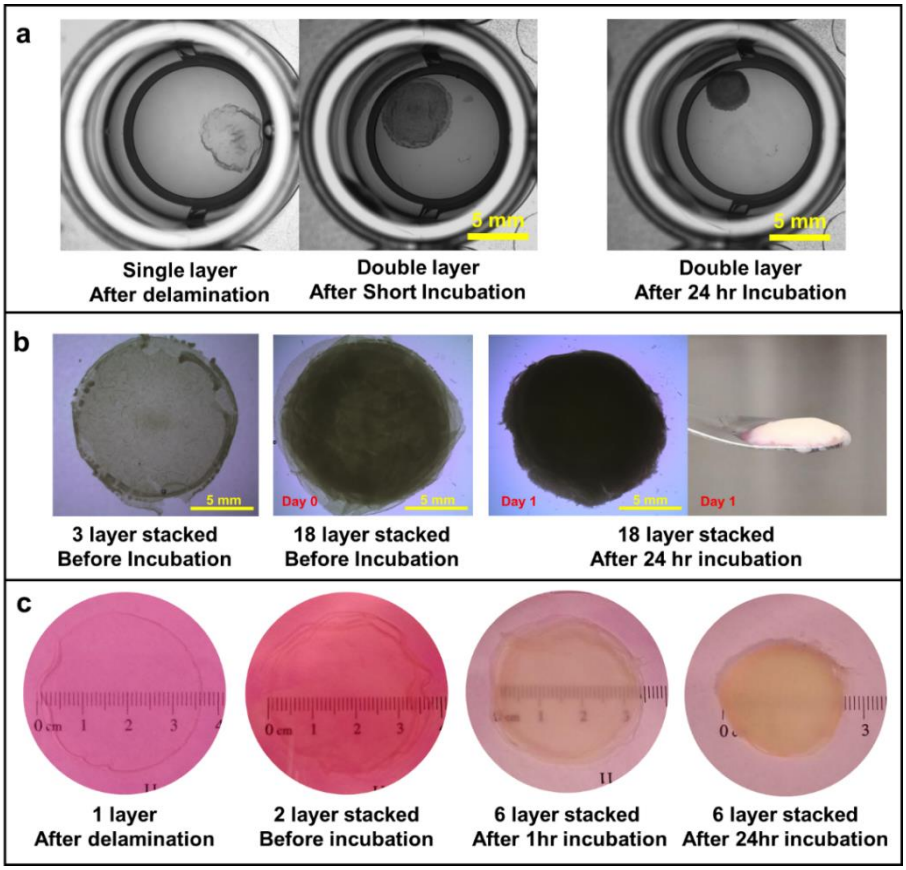

Figure 3. Sheets formed in **a)** 24 well plates, **b)** 6 well plates, and **c)** 10 cm dishes using 1:0 ratio in P1 were delaminated and stacked to form meat-like structure. This technique is scalable to make sheets with different sizes. The more layers are stacked, the less shrinkage happens afterwards. 18-layer stack of sheets formed in 6 well plate showed a low shrinkage after 24 hrs of incubation but a 2 layer stack formed in 24 well plate showed more than 50% shrinkage.

Discussion

Layer by layer assembly of sheet like tissue constructs is a new scalable approach that can be used to build meat-like tissues of any size and thickness. It can avoid the use of scaffolds that are required in other lab-grown meat technologies as the cultured cells themselves produce complex ECM that is preserved and makes robust sheet structures with texture. The growth and construction of these as individual sheets and their subsequent parallel assembly into thicker structures elegantly avoids mass transfer induced growth limitations and the need for integrated vasculature Finally, the complex ECM produced in these sheets during growth include biomolecules such as E-cadherin and Laminin 5 [17] which then lend adhesive properties to the individual sheets and enable them to be stacked to form continuous thick constructs [18]. Unlike current technologies that focus on production of minced meat [10] the constructs produced here better resembles natural structure of meat and thicker pieces of lab grown meat with natural texture can be produced. The process described in this paper for manufacture of meat-like tissue is scalable and amenable for automation, which is an important criteria for economic production [11]. The process produces robust individual sheets that can handle significant mechanical forces such as pipetting from one vessel to another or handled with tweezers which are crucial for automated robotic handling. It does not require any specialized equipment and is the first demonstration, to our knowledge, of incorporating both adipocytes and skeletal muscle cells in meat without the use of any other exogenous scaffolding material or ECM. Nevertheless, other advances are required to transform it into a viable product. Of particular importance is creation of stable cell sources. Primary animal cells including satellite cells (muscle stem cells), mesenchymal, embryonic, or induced pluripotent stem cells can be considered for the muscle progenitor cells, while adipose tissue derived stem cells or mesenchymal stem cells can be considered for the fat progenitor cells. Cell lines for both

of these two main cell types in meat as well as other cell types, including endothelial cells comprising blood vessels and cell types forming the connective tissue, can be created through genetic or chemical induction and are probably a better option to reduce variability and contamination risks associated with primary cell harvest [19]. In the design and development of media to be used with the technique introduced here, growth and differentiation of preadipocytes to adipocytes in coculture with myoblasts should be considered. It is also suggested that by establishing cell lines that are less dependent on exogenous growth factors, cost of the media and dependency on such factors could be decreased [20]. Serum components are not compatible with food safety standards and they can be source of contaminations. The dependence of the process on such components makes it difficult to bring it to market [20] and therefore development of suitable animal- and xeno-free media that is low cost and can be produced at high volume should be considered. Electrical and mechanical stimuli can also be provided to the assembling tissue to mimic the highly complex structure of the native tissue and accelerate its growth and maturation [21, 22]. Visual appearance of the tissues formed can be adjusted from its current yellowish pink tinge which is due to the absence of blood and reduced myoglobin production in the culture condition with high oxygen levels [23] to a natural pinkish tone by culturing cells in low oxygen conditions [24] or by using plant based heme or by addition of extra iron [2]. This approach provides the improvements suggested herein as a viable approach for scalable production of meat tissues with texture and complexity.

Methods

Cell culture: C2C12 and 3T3-L1 cells were culture in their growth medium up to 80% confluent. For partial differentiation, culture started with confluency of 40-60% in each cells growth medium which was then switched to the differentiation medium. Cells were kept in this medium for 2 days

before they were trypsinized and used for sheet formation. A total cell number of 0.235×10^6 was used in 24 well plates, 1.15×10^6 cells in 6 well plates, and 6.25×10^6 cells in 10 cm dishes. C2C12s were cultured in high glucose DMEM supplemented with 10 v/v% heat inactivated (HI) fetal bovine serum (FBS). In their differentiation medium FBS was replaced with 2% horse serum and 1% insulin. 3T3-L1 cells were cultured in low glucose DMEM with 10 v/v% FBS. Their differentiation medium was high Glucose DMEM with 10 v/v% FBS, 1 mg/mL Insulin, 0.5mM IBMX, 0.25 µM Dexamethasone, and 2µM Rosiglitazone while their maintenance medium was high Glucose DMEM with 10 v/v% FBS and 1 mg/mL Insulin. All media had 1% penicillin streptomycin and were bought from Thermofisher.

Imaging: Cells were stained with long-term fluorescent trackers (C2C12 with red DiI and 3T3-L1 with green DiO following the supplier's protocol (Thermofisher, catalogue numbers D282 and D275, respectively)) before being partially differentiated. Fluorescent images were taken using an inverted fluorescent microscope (Olympus, USA) using FITC (475-485/485-536 nm) and TXRED (542-582/582-644 nm) filters. For SEM purposes samples were fixed with 2% formaldehyde for 30 min and were critically point dried (Leica Microsystems, Wetzlar, Germany), cut in half, coated with gold and imaged in cross-section and images using TESCAN VP. SEM at 10kV. For histological staining, fixed samples were dehydrated step wise in 40, 60, 80% ethanol in water and after paraffin embedding and sectioning, staining was done with Hematoxylin and Eosin and images were taken using inverted microscope with 10X magnification.

Cell sheet formation: Partially differentiated cells were replated at specified number for each well size and maturated using any of the three defined protocols (P1, P2, or P3). Delamination process started by treating cells with acidic medium (differentiation medium containing 0.1% V/V acetic acid, final pH of ~6). This starts the delamination of sheets which can be accelerated by gentle

shaking of the well plate or by applying shear force using gentle pipetting of medium to the edges of the wells. after delamination was completed, acidic medium was replaced with basic medium (DM with 0.1% V/V 0.1 M sodium hydroxide in deionized water, final pH of ~8) in order to prevent samples from forming clumps. After 5 min of treatment with medium B, samples were transferred to neutral medium (differentiation medium, pH of 7.4).

Protein and lipid measurement: Sheets were digested using 500 µL of 2 mg/mL collagenase/dispase (Sigma-Aldrich, catalogue number 10269638001) in PBS for 2 hrs. Lipid content was measured using two 25 µL aliquots of this digest solution in 96 black well plate by addition of 200 µL 0.2% V/V Nile red dye (10 mg/mL in acetone, Thermofisher, catalogue number N-1142) in PBS, following a 15 min incubation, the fluorescent intensity was measured at excitation/emission of 560/640 nm using a platereader (Infinite® M200, Tecan, Männedorf, Switzerland). In parallel, 100 µL of digest solution was lysed using 100 µL of lysis solution (0.5% Triton X-100 in PBS). After 15 min incubation with lysis solution, two 25 µL aliquots were transferred to new 96 well plates and 200 µL of Pierce™ BCA Protein assay (Thermofisher, catalogue number 23227) kit solution (50:1 ratio mixture of solutions A and B of the kit) was added to each well. Absorbance was measured at 562 nm after 30 min incubation. A total of 5 samples were used for each assay (n=5).

Acknowledgment: The authors would like to acknowledge the support of the Natural Sciences and Engineering Research Council of Canada (NSERC).

References

1. Lynch, J. and R. Pierrehumbert, Climate Impacts of Cultured Meat and Beef Cattle. Frontiers in Sustainable Food Systems, 2019. **3**(5).
2. Bhat, Z.F., et al., Technological, Regulatory, and Ethical Aspects of in Vitro Meat: A Future Slaughter-Free Harvest. Comprehensive Reviews in Food Science and Food Safety, 2019. **18**(4): p. 1192-1208.
3. Apostolidis, C. and F. McLeay, Should We Stop Meating Like This? Reducing Meat Consumption through Substitution. Food Policy, 2016. **65**: p. 74-89.
4. Bhat, Z.F., S. Kumar, and H.F. Bhat, In Vitro Meat: A Future Animal-Free Harvest. Crit Rev Food Sci Nutr, 2017. **57**(4): p. 782-789.
5. Stoll-Kleemann, S. and T. O'Riordan, The Sustainability Challenges of Our Meat and Dairy Diets. Environment: Science and Policy for Sustainable Development, 2015. **57**(3): p. 34-48.
6. Macdiarmid, J.I., F. Douglas, and J. Campbell, Eating Like There's No Tomorrow: Public Awareness of the Environmental Impact of Food and Reluctance to Eat Less Meat as Part of a Sustainable Diet. Appetite, 2016. **96**: p. 487-493.
7. Graca, J., M.M. Calheiros, and A. Oliveira, Attached to Meat? (Un)Willingness and Intentions to Adopt a More Plant-Based Diet. Appetite, 2015. **95**: p. 113-25.
8. Tuomisto, H.L. and M.J. de Mattos, Environmental Impacts of Cultured Meat Production. Environ Sci Technol, 2011. **45**(14): p. 6117-23.
9. Post, M., *Lab-Based Meat Production: Science Fiction or Reality*. 2017, eCommons open scholarship at Cornell.
10. Dolgin, E., Sizzling Interest in Lab-Grown Meat Belies Lack of Basic Research. Nature, 2019. **566**(7743): p. 161-162.
11. Allan, S.J., P.A. De Bank, and M.J. Ellis, Bioprocess Design Considerations for Cultured Meat Production with a Focus on the Expansion Bioreactor. Frontiers in Sustainable Food Systems, 2019. **3**(44).
12. Van Eelen, W., W. van Kooten, and W. Westerhof, *Industrial Production of Meat from in Vitro Cell Cultures*. 1999, Patent Description
13. Vein, J., *Method for Producing Tissue Engineered Meat for Consumption*. 2004, Google Patents.
14. Benjaminson, M.A., J.A. Gilchriest, and M. Lorenz, In Vitro Edible Muscle Protein Production System (Mpps): Stage 1, Fish. Acta Astronaut, 2002. **51**(12): p. 879-89.
15. MacQueen, L.A., et al., Muscle Tissue Engineering in Fibrous Gelatin: Implications for Meat Analogs. NPJ Sci Food, 2019. **3**: p. 20.
16. Gotto, A.M., Jr., L.W. Scott, and J.P. Foreyt, Diet and Health. West J Med, 1984. **141**(6): p. 872-7.
17. Yamato, M., et al., Thermo-Responsive Culture Dishes Allow the Intact Harvest of Multilayered Keratinocyte Sheets without Dispase by Reducing Temperature. Tissue Eng, 2001. **7**(4): p. 473-80.
18. Iwata, T., M. Yamato, and T. Okano, *Chapter 29 - Intelligent Surfaces for Cell-Sheet Engineering*, in *Principles of Regenerative Medicine (Second Edition)*, A. Atala, R. Lanza, J.A. Thomson, and R. Nerem, Editors. 2011, Academic Press: San Diego. p. 517-527.
19. Specht, E.A., D.R. Welch, E.M. Rees Clayton, and C.D. Lagally, Opportunities for Applying Biomedical Production and Manufacturing Methods to the Development of the Clean Meat Industry. Biochemical Engineering Journal, 2018. **132**: p. 161-168.
20. Sinacore, M.S., D. Drapeau, and S.R. Adamson, Adaptation of Mammalian Cells to Growth in Serum-Free Media. Mol Biotechnol, 2000. **15**(3): p. 249-57.
21. Maleiner, B., et al., The Importance of Biophysical and Biochemical Stimuli in Dynamic Skeletal Muscle Models. Front Physiol, 2018. **9**: p. 1130.
22. Rangarajan, S., L. Madden, and N. Bursac, Use of Flow, Electrical, and Mechanical Stimulation to Promote Engineering of Striated Muscles. Ann Biomed Eng, 2014. **42**(7): p. 1391-405.

23. Post, M.J. and J.F. Hocquette, *New Sources of Animal Proteins: Cultured Meat*, in *New Aspects of Meat Quality: From Genes to Ethics*, P.P. Purslow, Editor. 2017, Woodhead Publishing: UK.
24. Kanatous, S.B. and P.P. Mammen, Regulation of Myoglobin Expression. J Exp Biol, 2010. **213**(Pt 16): p. 2741-7.